Textron Aviation
Raytheon Missile Systems
AIAA Foundation

The 2018 AIAA/Textron Aviation/Raytheon Missile Systems Design/Build/Fly Competition Flyoff was held at Cessna East Field in Wichita, KS on the weekend of April 19-22, 2018. This was the 22nd year for the competition. A total of 134 entries were received along with proposals with each entry. The 134 proposals were judged and 101 teams were invited to submit a formal report for the next phase of the competition. 91 teams submitted design reports to be judged, and 77 teams attended the flyoff (16 international), a new DBF record! About 750 students, faculty, and guests were present. The cold and rainy weather reduced the number of flying hours on Saturday, but we still had 245 flight attempts over the weekend. Of the 245 official flight attempts, 153 resulted in a successful score with 50 teams achieving at least one successful flight score and 24 teams successfully completing all three missions. The quality of the teams, their readiness to compete, and the execution of the flights continues to improve each year.

The contest theme this year was a Regional and Business Aircraft. The aircraft was required to fly a combination of passengers and payload as well as demonstrate the ability to conduct LRU replacement in the field. The first mission was a Staging Flight with no payload for three laps. Prior to attempting the second mission, each team was required to successfully complete the first mission and the ground mission. The ground mission consisted of replacing a randomly selected simple LRU followed by a complex LRU all within 8 minutes. The second mission was a Short Haul of Max Passengers with the passengers being a randomly selected distribution of five different sizes of bouncy balls and the score based on the # of passengers selected by each team divided by the time to fly three laps. The third mission was a Long Haul of Passengers and Payload where each team selected the number of passengers with at least 50% of the number carried in Mission 2 as well as payload blocks with the score being the product of the number of passengers times the total payload weight times the number of laps flown. The total score is the product of the total mission score and design report score divided by the RAC, which was empty weight times the wingspan. More details on the mission requirements can be found at the competition website: http://www.aiaadbf.org .

First Place went to the Clarkson University, Second Place went to Virginia Polytechnic Institute and State University and Third Place went to Georgia Institute of Technology. A full listing of the results is included below. The Best Paper Award, sponsored by the Design Engineering TC for the highest report score, went to University of Southern California with a score of 93.20.

We owe our thanks for the success of the DBF competition to the efforts of many volunteers from Textron Aviation, Raytheon Missile Systems, and the AIAA sponsoring technical committees: Applied Aerodynamics, Aircraft Design, Flight Test, and Design Engineering. These volunteers collectively set the rules for the contest, publicize the event, gather entries, judge the written reports, and organize the flyoff. Thanks also go to the Premier Sponsors: Raytheon Missile Systems and Textron Aviation, and also to the AIAA Foundation for their financial support as well as our Gold sponsors this year – Airbus, Aerovironment, Aurora Flight Sciences, General Atomics, Lockheed Martin, and MathWorks. Special thanks go to Textron Aviation for hosting the flyoff this year.

Finally, this event would not be nearly as successful without the hard work and enthusiasm from all the students and advisors. If it weren't for you, we wouldn't keep doing it.

Brian Richardet
For the DBF Organizing Committee

SCKYWALKER

UNIVERSITY OF SOUTHERN CALIFORNIA

AIAA DESIGN/BUILD/FLY 2017-2018 DESIGN REPORT

Table of Contents

ACRONYMS, ABBREVIATIONS, AND SYMBOLS 3

1.0 EXECUTIVE SUMMARY 4

1.0 MANAGEMENT SUMMARY 5

2.1 Team Organization 5
2.2 Milestone Chart 6

3.0 CONCEPTUAL DESIGN 7

3.1 Mission Requirements 7
3.2 Design Requirements 11
3.3 Configuration Selection 15
3.4 Aircraft Components Selection, Processes and Results 17
3.5 Final Conceptual Design 18

4.0 PRELIMINARY DESIGN 19

4.1 Design Methodology 19
4.2 Mission Model 20
4.3 Design Trade Studies 21
4.4 Aerodynamics 23
4.5 Stability and Control 28
4.6 Predicted Aircraft Performance 29

5.0 DETAIL DESIGN 30

5.1 Dimensional Parameters Table 30
5.2 Structural Characteristics and Capabilities 31
5.3 Sub-system Design 32
5.4 Weight and Mass Balance 37
5.5 Flight and Mission Performance 38
5.6 Drawing Package 39

6.0 MANUFACTURING PLAN 43

6.1 Manufacturing Processes Investigated 43
6.2 Manufacturing Processes Selected 43
6.3 Manufacturing Milestones 46

7.0 TESTING PLAN 47

7.1 Test Objectives 47
7.2 Subsystem Testing 48
7.3 Flight Test Schedule and Flight Plan 52
7.4 Flight Checklists 53

8.0 PERFORMANCE RESULTS 54

8.1 Demonstrated Performance of Key Subsystems 54
8.2 Demonstrated Flight Performance of Completed Aircraft 58

9.0 BIBLIOGRAPHY 60

ACRONYMS, ABBREVIATIONS, AND SYMBOLS

α	Aircraft angle of attack
ω_n	Natural frequency (rad/s)
ζ	Damping coefficient
AIAA	American Institute of Aeronautics and Astronautics
AR	Aspect Ratio
AR_{eff}	Efficient Aspect Ratio
AVL	Athena Vortex Lattice
b	Wingspan
c	Wing chord
C_d, C_D	Drag coefficient (2D, 3D)
CD_0	3D zero-lift coefficient of drag
CD_i	3D induced drag coefficient
CFD	Computational fluid dynamics
C_l, C_L	Coefficient of lift (2D, 3D)
$C_{L_{cruise}}$	3D lift coefficient at cruise
$C_{L_{max}}$	3D maximum lift coefficient
C_{m_α}	3D moment coefficient
C_P	Coefficient of power
C_T	Coefficient of thrust
CG	Center of Gravity
DBF	Design/Build/Fly
e	Oswald efficiency factor
ESC	Electronic Speed Controller
EW	Empty weight of the aircraft
FEA	Finite Element Analysis
FoM	Figures of Merit
h	End plate height
I_{cruise}	Electrical current at cruise
I_{max}	Max. static current
Kv	RPM Constant (RPM/V)
L/D	Lift to drag ratio
$(L/D)_{cruise}$	Lift to drag ratio at cruise
$(L/D)_{max}$	Maximum lift-to-drag ratio
LRU	Line Replaceable Units
M_1	Mission 1 Flight Score
M_2	Mission 2 Flight Score
M_3	Mission 3 Flight Score
MDO	Multidisciplinary design optimization
NiCd	Nickel-Cadmium
NiMH	Nickel-Metal Hydride
N_{Laps}	Number of laps
$N_{PAX,M2}$	Number of passengers; Mission 2
$N_{PAX,M3}$	Number of passengers; Mission 3
N_{PAX}	Number of passengers
$P_{battery}$	Power supplied by battery pack
PAX	Passenger
PF	Payload Fraction
RAC	Rated Aircraft Cost
Re	Reynolds number
Re_{cruise}	Reynolds number at cruise
RPM	Revolutions per Minute
S	Wing planform area
S_h	Horizontal tail planform area
S_v	Vertical tail planform area
T	Time
T_{USC}	USC Time
TOFL	Take Off Field Length
USC	University of Southern California
V	Voltage
V_{cruise}	Cruise velocity
V_h	Horizontal tail volume
V_{launch}	Launch velocity
V_{stall}	Stall velocity
V_v	Vertical tail volume
W_{cargo}	Cargo weight
$W_{payload}$	Payload weight
WS	Max. distance between wingtips
W/S	Wing loading

1.0 EXECUTIVE SUMMARY

The objective of the 2017-18 American Institute of Aeronautics and Astronautics (AIAA) Design/Build/Fly (DBF) competition is to simulate the design of a dual-purpose regional and business aircraft with line replaceable units (LRUs) for easy serviceability. The competition aircraft must be able to complete three flight missions as well as a ground mission of LRU removal and replacement. The payloads for this year's contest are randomly selected Super Balls (passengers) and team-built payload blocks (cargo).

The first flight mission, a demonstration flight, consists of flying three laps without payloads in 5 minutes or less. The second flight mission, a short-haul of passengers, requires the plane to complete three competition laps carrying a team-specified number of passengers as fast as possible. The third flight mission, a long-haul of passengers and payload, consists of flying as many laps as possible within ten minutes while carrying a team-specified number of passengers and weight of cargo. The ground mission consists of two stages of timed LRU removal and replacement. Although the ground mission does not directly affect the total score, it must be passed before attempting Mission 2.

After analyzing the flight mission scoring and the rated aircraft cost (RAC), it was determined that minimizing the wingspan and empty weight, even at the cost of flight performance, was critical to this year's design. Performance trade studies indicated that flying the minimum number of passengers (1) and a single, lightweight cargo block would score the highest due to the effect of empty weight on the RAC.

A monoplane configuration was identified as the optimum configuration due to its low weight, build simplicity, and favorable stability characteristics compared to other configurations. In order to decrease the RAC, endplates were utilized to increase lift without increasing wingspan. Wing and tail loads were carried through spars constructed of a balsa shear web with carbon spar caps. The wire tail dragger landing gear minimized weight and enabled ground handling over long takeoff field lengths (150 ft). The fuselage was a lightweight, balsa structure with plywood bulkheads to transfer flight and landing loads. The single passenger was secured in place using a twisted wire restraint. The light, fiberglass cargo block was restrained at the back of the aircraft to the surrounding bulkheads. Additionally, all necessary components on the aircraft were designed for quick removal to ensure a successful ground mission.

University of Southern California's aircraft, *SCkywalker* (Figure 1), is designed to maximize score by exchanging flight performance for a low empty weight and small wingspan. *SCkywalker* will take off at 36 ft/s (11 m/s) before climbing to cruise altitude and velocity. With a top flight speed of 59 ft/s (18 m/s), *SCkywalker* will complete three laps for Mission 2 while carrying one passenger in 180 s. With one passenger, a single 0.11 oz. 4.25" x 2.75" x 2" payload block, *SCkywalker* will complete 6 laps in ten minutes. At an empty weight of 0.71 lbs. with an 11.4" wingspan, *SCkywalker* yields an RAC of 8.07.

Figure 1: The USC 2017-2018 DBF entry, *SCkywalker*

2.0 Management Summary

The 2017-18 AeroDesign Team of USC consists of 30 students that participate on an extracurricular basis. One member of the team is a graduate student, five are seniors, and the remainder are underclassmen. The team is entirely student-led but receives guidance and suggestions from industry advisors, USC alumni and faculty members at weekly meetings and design reviews.

2.1 Team Organization

The AeroDesign Team of USC employs a matrix structure of leadership, similar to the management hierarchy of most aerospace firms. The team leadership for the 2017-18 competition is shown in Figure 2.

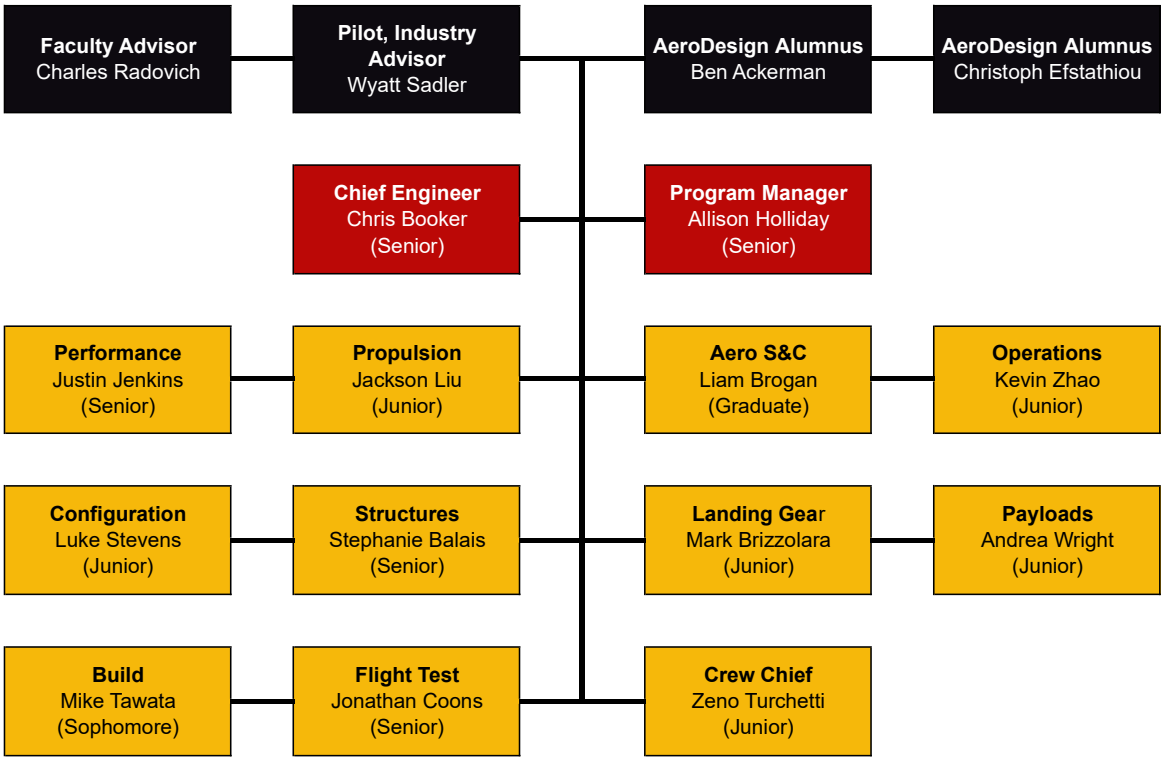

Figure 2: Organization chart of the USC AeroDesign Team

Team leaders, as shown in **red**, receive suggestions from team advisors (**black**) and coordinate the design effort among sub-team leaders (**gold**). The Chief Engineer and Program Manager divide tasks such that the Chief Engineer supervises design, build and test efforts while the Program Manager sets major milestones, ensures adherence to the master schedule and works with the Operations Manager to obtain funding and manage team logistics.

2.2 Milestone Chart

The Program Manager maintains a schedule, shown in Figure 3, that is used to plan workflow, determine required resources, and track tasks to completion. In December and January, an unplanned task (indicated by ***) was required due to issues procuring batteries for the aircraft. The manufacturing schedule set at the beginning of the year was adjusted accordingly as shown by “Actual Timing”. Note that actual timing is not shown for future tasks.

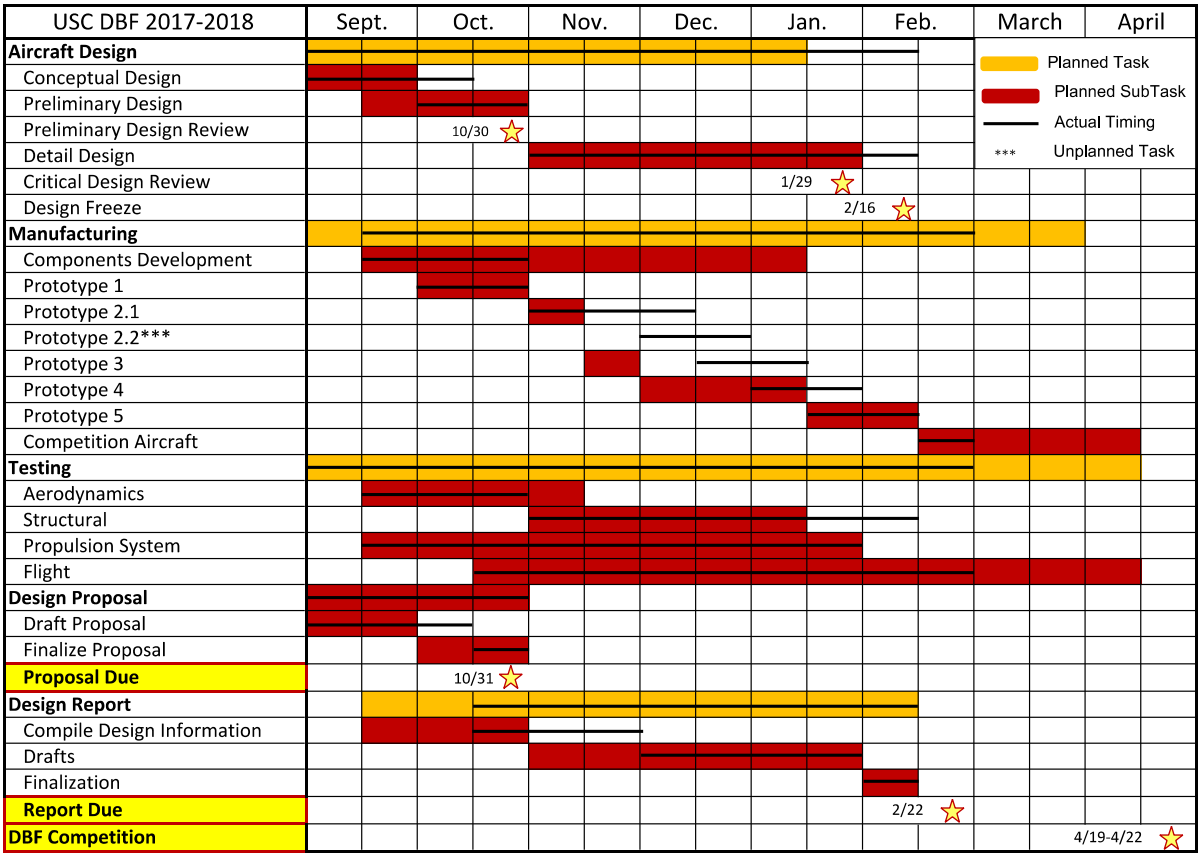

Figure 3: Master schedule showing the planned and actual timing for team tasks

3.0 Conceptual Design

In the conceptual design phase, the team analyzed the competition requirements and scoring equation to set design objectives for the competition year. Numerous aircraft configurations were evaluated to identify the highest scoring configuration. The final conceptual design is presented in Section 3.5.

3.1 Mission Requirements

The rules for the 2017-2018 American Institute of Aeronautics and Astronautics (AIAA) Design/Build/Fly (DBF) contest simulate the design of a dual-purpose regional and business aircraft. The contest consists of three flight missions and a ground mission. The aircraft will be designed to complete flight missions and a ground mission, which does not factor into scoring but must be completed before attempting Mission 2.

Each flight mission requires the aircraft to takeoff upwind within the takeoff field length of 150 ft and then fly competition laps, consisting of two 1,000 ft (300 m) straightaways, two 180° turns, and one 360° turn in the opposite direction of the 180° turns. The competition lap requires that the aircraft make right-hand and left-hand turns and land within the bounds of the runway, thereby demonstrating flight stability and handling characteristics of the aircraft. A schematic of a competition lap is shown in Figure 4. Prior to

each flight, the flight crew will have five minutes to load and secure the passengers at the flight line.

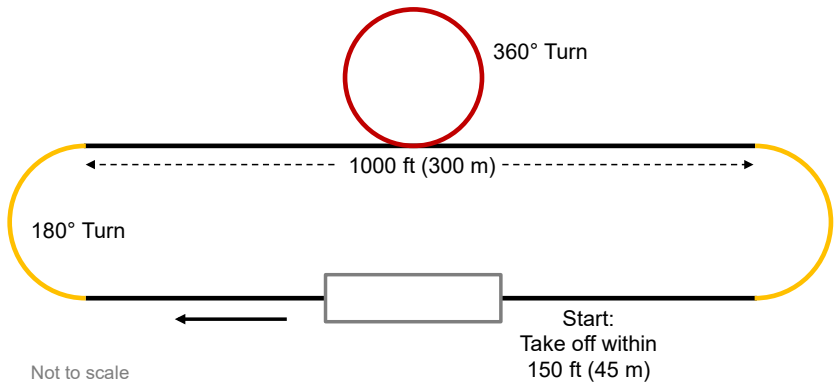

Figure 4: AIAA Competition Lap Layout

3.1.1 Scoring Summary

The overall score for the 2017-2018 AIAA DBF contest is given by Eq. 1.

$$Score = \frac{Written\ Report\ Score \cdot Total\ Mission\ Score}{Rated\ Aircraft\ Cost} \qquad \text{Eq. 1}$$

The $Written\ Report\ Score$ is based on the quality of the design report, and the $Total\ Mission\ Score$ is the sum of the scores of each flight mission given by Eq. 2.

$$Total\ Mission\ Score = M_1 + M_2 + M_3 \qquad \text{Eq. 2}$$

M_1, M_2, and M_3 denote the scores for Mission 1, Mission 2, and Mission 3, respectively. The Rated Aircraft Cost (RAC) is given by Eq. 3.

$$RAC = EW * WS \qquad \text{Eq. 3}$$

The individual components of the RAC are defined as follows:

- $Empty\ Weight\ (EW)$: Maximum aircraft empty weight recorded after each successful mission
- $Wingspan\ (WS)$: Longest distance between wingtips measured perpendicular to the fuselage axis

3.1.2 Mission Scoring

Flight Mission 1 – Aircraft Mission Staging

The objective of Mission 1 is to successfully complete 3 competition laps within a 5-minute flight window without any payloads. Timing starts when the throttle is initiated for takeoff. The score for this mission is binary with $M_1 = 1$ for a successful mission and $M_1 = 0$ for an unsuccessful mission.

Flight Mission 2 – Short Haul of Passengers

The objective of the Mission 2 is to complete 3 laps as quickly as possible with a team-determined number of passengers. Timing starts when the throttle is initiated for takeoff. The score for this mission

(M_2) is given by Eq. 4,

$$M_2 = 2.0 * \frac{\left(N_{PAX,M2}/T\right)_{USC}}{\left(N_{PAX,M2}/T\right)_{BEST}} \qquad \text{Eq. 4}$$

where $\left(N_{PAX,M2}/T\right)_{USC}$ is the number of passengers carried divided by the time for USC to complete Mission 2 and $\left(N_{PAX,M2}/T\right)_{BEST}$ is the maximum ratio of number of passengers carried to time to for any team to complete Mission 2.

Flight Mission 3 – Long Haul of Passengers and Payload

The objective of the Mission 3 is to complete as many laps as possible within a 10-minute flight window with passengers and cargo. The number of passengers carried in Mission 3 must be at least half of the number of passengers carried in Mission 2. The score for this mission (M_3) is given by Eq. 5,

$$M_3 = 4.0 * \frac{\left(N_{PAX,M3} W_{Cargo} N_{Laps}\right)_{USC}}{\left(N_{PAX,M3} W_{Cargo} N_{Laps}\right)_{BEST}} + 2.0 \qquad \text{Eq. 5}$$

where $\left(N_{PAX,M3} W_{Cargo} N_{Laps}\right)_{USC}$ is the product of the number of passengers carried, weight of payload blocks carried, and number of laps flown by USC; $\left(N_{PAX,M3} W_{Cargo} N_{Laps}\right)_{BEST}$ is the maximum product of number of passengers carried, weight of payload blocks carried, and number of laps flown by any team.

Ground Mission – Field and Depot LRU Replacement

The Ground Mission is a pass/fail mission that must be completed prior to attempting Mission 2. The objective of the ground mission is to successfully complete two stages of LRU (Line Replaceable Unit) removal and replacement. The allotted time for the first stage is 3 minutes and the second stage is 5 minutes with any additional time left over from the first stage. For Stage 1, all LRUs and any tools needed for the ground mission must be stored in the payload bay of the aircraft; however, there is no such restriction for Stage 2. In Table 1 the LRU components for each stage are shown. Note that for the control surface, main landing gear, and motor the dice must be rolled again to determine the specific component to be replaced, since there are multiple occurrences of those components on the aircraft.

Table 1: Ground Mission LRU selection table

Dice Roll	Stage 1	Stage 2
1	Servo	ESC
2	Rx Battery	Control Surface
3	Main Propulsion Battery	Receiver
4	Control Pushrod	Main Landing Gear
5	Landing Gear Wheel	Motor
6	Propeller	Roll Again

Once both stages are complete judges will validate that the aircraft is flight-ready and that the replaced components are fully functional.

3.1.3 Aircraft Constraints

In addition to the flight missions described above, the aircraft must meet the following requirements:

Propulsion

- Batteries must be Nickel-Cadmium (NiCd) or Nickel-Metal Hydride (NiMH).

Payloads

- Passengers (Super Balls) will be provided at the flight line and randomly selected from a pool with a distribution as seen in Figure 5.
- Team-manufactured payload (cargo) blocks must be a rectangular cuboid with the sum of length, width, and height greater than or equal to 9”. Each side must be at least 2” and each bock must weigh less than 8 oz. Teams may carry more than one block, but each must be the same size within a 0.25” tolerance per side.
- Each passenger must have an individual seat and restraint system. Both seats and restraints must be able to accommodate passengers of all sizes.

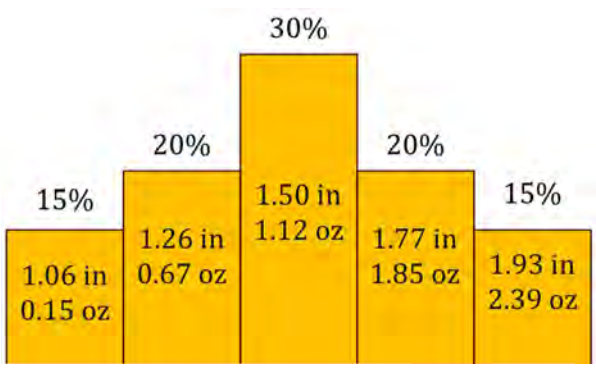

Figure 5: Passenger diameter and weight distribution

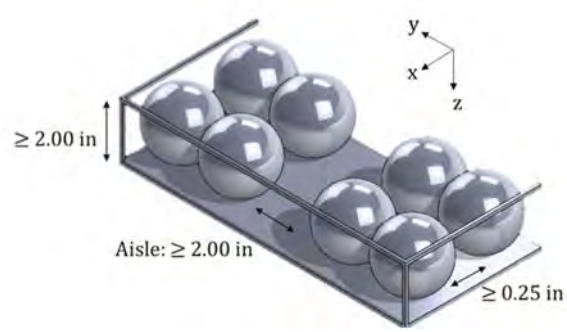

Figure 6: Diagram of spatial constraints in passenger compartment

Passenger Compartment

- All seats must exist on a level, planar surface. Additional spatial constraints are shown in Figure 6. The aisle runs through the fuselage, along the x-axis. The rows, parallel to the y-axis, can consist of a maximum of 4 seats, with no more than 2 on either side of the aisle.

Payload Bay

- Cargo blocks must be carried in a separate compartment below and/or behind the passenger compartment, with a physical divider between the sections.

3.2 Design Requirements

Design requirements were developed from the 2017-2018 DBF scoring equations and competition guidelines in order to guide the design process. By analyzing the scoring equations, an aircraft configuration and competition approach was selected to maximize total score. Mission requirements and score equations were translated into design parameters, as shown in Table 2.

Table 2: Design parameters

Missions and RAC	Objective	Design Parameter
2 – Short Haul	Balance flight speed and payload to maximize the value of the number of passengers carried divided by the flight time to complete three laps	$(N_{PAX,M2}/T)_{USC}$
3 – Long Haul	Balance flight speed and payload (passengers and cargo) to maximize the product of the number of laps, number of passengers, and weight of cargo flown	$(N_{Laps}N_{PAX,M3}W_{Cargo})_{USC}$
RAC	Minimize EW to minimize RAC	EW
RAC	Minimize wingspan to minimize RAC	WS

3.2.1 Flight Score Sensitivity Analysis

The scoring equations, Eq. 1 - Eq. 5, were analyzed to set design objectives by identifying the design parameters that were most important in maximizing score. Analysis began by estimating the top mission performance of any competitor in each of the three missions and performance for a baseline USC competition aircraft shown in Table 3. The assumptions guiding these estimates are detailed in the following paragraphs.

Table 3: Preliminary assumptions for top-performing (competitors) and baseline aircraft (USC) parameters

Top Mission Performance	Assumption
$(N_{PAX,M2}/T)_{BEST}$	0.36
$(N_{PAX,M3}W_{Cargo}N_{Laps})_{BEST}$	12800
Top Mission Performance	**Assumption**
$(N_{PAX,M2}/T)_{USC}$	0.13
$(N_{PAX,M3}W_{Cargo}N_{Laps})_{USC}$	808
EW	1.25 lb (0.57 kg)
WS	23.9 in (0.61 m)

Competitor (BEST) Assumptions

Assumptions for the top mission performance of any competitor were based on aircraft performance in previous competitions with similar requirements for geometric constraints, such as those imposed on the wingspan and passenger compartment. In the 2017 AIAA DBF competition, 93 s was the fastest time to complete 3 laps carrying a payload of 1.5 lb. This was accomplished with a plane that was similar in

dimensions to the baseline plane detailed in Table 3. As another point of comparison, another competitor at the 2013 AIAA DBF competition ferried 3.5 lb internally for 3 laps in a total of 90 s. Using these competitor performances, a plane that optimized for M_2 could feasibly carry 32 passengers (totaling ~2.5 lb based on an average passenger weight of 0.079 lbs) in 90 s. The quantity $\left(N_{PAX,M2}/T\right)_{BEST}$ is then 0.36. Similar research on large-payload competitors returns a competitor of the 2017 AIAA DBF competition, which flew 7 laps in 5 min. with an internal payload of 4.5 lbs. Given the longer (10 min) time constraint on M_3 in the 2017-2018 AIAA DBF competition, it was estimated that a competitor aircraft which was optimized for M_3 could carry 32 passengers and 40.3 oz. of cargo for 10 laps. The quantity $\left(N_{PAX,M3}W_{Cargo}N_{Laps}\right)_{BEST}$ is then 12,800.

Baseline (USC) Assumptions

The baseline assumptions for the aircraft design parameters shown in Table 3 are estimates of the team's capability based on performance in previous competitions. For example, the USC entrant to the 2017 AIAA DBF contest, *Starscream,* completed 6 laps in 5 minutes carrying 1.5 lbs of internal payload [1]. The baseline performance for M_3 is a plane that is a capable of carrying 8 passengers and 10.1 oz of cargo for 10 laps within the 10-minute time limit. The quantity $\left(N_{PAX,M3}W_{Cargo}N_{Laps}\right)_{USC}$ is thus 808. Interpolating from similarly-sized aircraft in USC contest history, the same plane would then be capable of flying 16 passengers in 120 s for M_2, a reasonable increase in lap speed given the lower capacity required to fly 3 laps [1]. The quantity $\left(N_{PAX,M2}/T\right)_{USC}$ is thus 0.13. The empty weight, EW, of the baseline plane was determined based on a payload fraction (PF) of 50% according to Eq. 6

$$PF = W_{Payload}/\,EW \qquad \text{Eq. 6}$$

$PF = 50\%$ is a realistic estimate based on past USC aircraft with similar volumetric requirements as those for the passenger compartment and cargo bay [2,3]. The wingspan, WS, assumptions for the baseline aircraft are driven by Eq. 7, which is an approximate empirical formula based upon similarly-sized USC aircraft and the average linear density of USC-constructed balsa wings [1].

$$WS = EW * 0.11 * 0.675\ in/lb \qquad \text{Eq. 7}$$

Using Eq. 7 and EW of 1.26 lb, the baseline WS is 23.9 in. With these values, each design parameter of the baseline aircraft was varied independently, keeping all remaining variables constant, in order to determine each individual parameter's sensitivity on the overall score; the results are plotted in Figure 7.

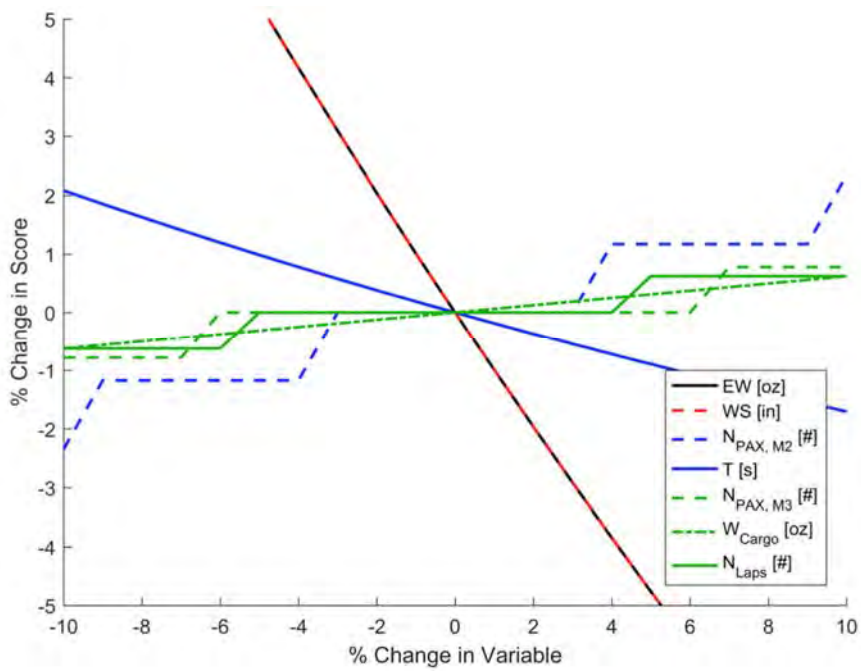

Figure 7: Score analysis representing the impact of score parameters

This preliminary score analysis indicated that minimizing EW and WS have the greatest impact on the total competition score. The positive trend in score with decreasing time (T) and increasing N_{PAX}, W_{Cargo}, and N_{Laps} required further analysis of the coupled effects of those parameters on the EW and WS.

3.2.2 Integrated Performance Analysis

In order to determine the highest scoring aircraft, based on this sensitivity analysis, a simulated contest was developed in order to explore the effect of the competitor assumptions. The team chose to explore four cases, each representing a plane that was optimized towards a different score component: M_2, M_3, RAC, and a balance of the three elements. These four simulated planes were then cycled through an iteration of the design loop performed by PlaneTools, a team-developed MATLAB simulation module for model aircraft (further described in Section 4.2). This design loop resulted in 4 aircraft with unique aerodynamic and structural characteristics designed to score the highest in their assigned role. This solution is more representative of competitor aircraft than the empirical set of equations used for the first-order analysis presented in Figure 7 because of the unique attention devoted to each simulated competitor. Each simulation's final competition score was calculated and compared in Table 4 to the baseline configuration in Table 3.

Table 4: Case optimization study showing aircraft optimized for either M_2, M_3 or RAC

	Baseline	M_2	M_3	RAC
$N_{PAX,M2}$	16	32	48	1
T	120 s	90 s	160 s	200 s
$N_{PAX,M3}$	8	16	24	1
W_{Cargo}	10.1 oz	20.6 oz	52.0 oz	0.1 oz
N_{laps}	10	11	10	3
EW	1.25 lbf	1.96 lbf	3.92 lbf	0.71 lbf
WS	23.9 in.	40.1 in.	81.6 in.	11.38 in.
% Change Total Score	**0%**	**-55%**	**-34%**	**+150%**

This optimization study supports the previous analysis that suggests that minimizing the RAC is most effective to maximizing the total score. Given the apparent benefits of a minimal-passenger aircraft – due primarily to the decreased RAC – the team selected this RAC-optimized design as the basis for the configuration downselect. Because of the sensitivity of the scoring variables, the decisions governing the preliminary and detailed design of the aircraft prioritize the RAC over individual mission performance.

Although EW and WS are the driving parameters in the score, selecting the exact number of passengers and the weight of the cargo block required additional detailed analysis. Even with a minimal-passenger aircraft, the goal remains to optimize W_{Cargo} for the best score, while keeping the total weight of the plane consistent between M_2 and M_3 to keep the wing area from being driven by the cargo. Assuming constant PF, a trend for the score as a function of W_{cargo} is presented in Figure 8.

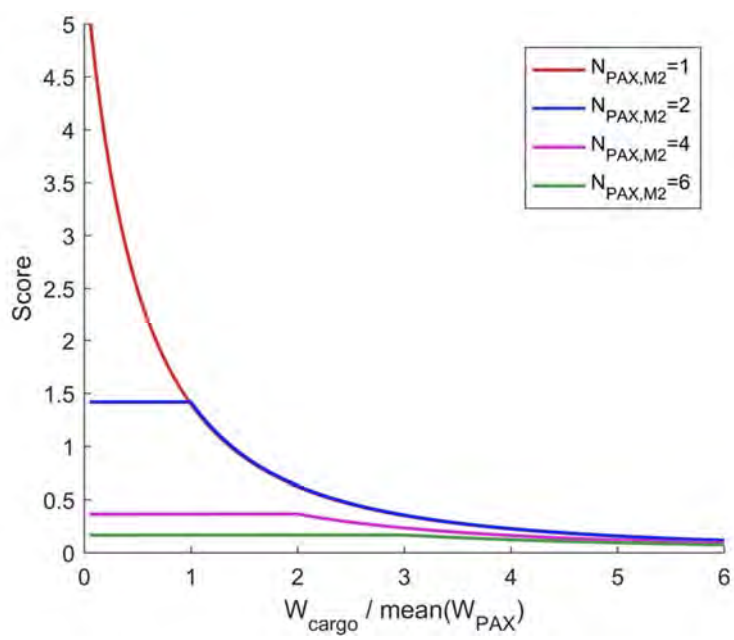

Figure 8: Score sensitivity to cargo weight, represented as a fraction of an average passenger weight. Even passenger numbers chosen to simplify using half of the M_2 passengers for M_3

This analysis further demonstrated that the fewer passengers carried, the higher the score. Additionally, for any given number of passengers, carrying less cargo weight improves the score until W_{Cargo} equals the weight of the passengers lost between M_2 and M_3. For a single-passenger aircraft, this limit does not exist because the rules specify that at least 1 passenger must be carried for M_3, in which case, minimizing W_{Cargo} is beneficial to the overall score.

3.2.3 Ground Mission Analysis

Although the Ground Mission does not directly affect the scoring equation, the added weight of the LRU integration and the volume required to store their tools for Stage 1 affects the aircraft EW, which is a component of the RAC. Additionally, the ground mission must be completed successfully in order to attempt M_2 and M_3.

3.3 Configuration Selection

Once the design requirements were determined, a configuration downselect process was used to select a preliminary aircraft configuration. After the aircraft configuration was selected, concepts for each individual component were selected.

3.3.1 Aircraft Configuration

The configuration downselect method uses a series of estimates and assumptions that quantitatively compare a set of configurations across a range of design parameters. Figures of Merit (FoM) were derived from the design parameters as shown in Table 5. Each FoM was assigned a score factor and was used to identify the most competitive aircraft configuration.

Table 5: Figures of Merit (FoM) and corresponding design parameters for aircraft configuration selection

Figures of Merit	Design Parameters	Score Factor
Flight Speed	T_{USC}	0.10
WS/S	EW_{Plane}	0.25
Stability and Control	T_{USC}, N_{Laps}	0.15
Build Complexity	EW_{Plane}	0.25
Internal Volume	EW_{Plane}	0.25

The score factor for each FoM was derived qualitatively by looking at the comprehensive impact of the FoM on the overall score when compared to the other FoMs. The score factors were weighted such that the sum of the score factors equaled one and are shown in the third column of Table 5. The next step was determining how each configuration scored for each FoM (independent of the other FoMs). As a result of the team's extensive experience with building lightweight monoplanes, a monoplane was used as the baseline to which all other configurations were compared. Each FoM was assigned a value from -1 to 1 indicating the expected performance of that particular aircraft configuration. Therefore, a value of 0 implied that the configuration scored as well as a monoplane for the given FoM. A value of -1 indicates

the design configuration (represented by the column) scored poorly for the FoM (represented by the row), while 1 meant it would be expected to perform well. The final step was to multiply each configuration evaluation with the corresponding FoM Score Factor, and then sum the values for each configuration. The Total Score for each configuration, shown at the bottom of Table 6, provides the basis for the quantitative comparison, with the highest score being most favorable.

Table 6: Aircraft configuration downselect

		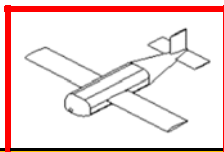	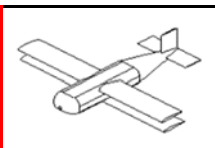	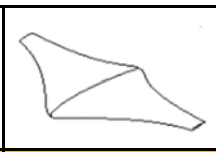	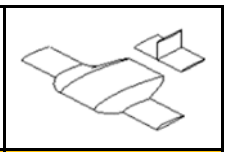
Figures of Merit (FoM)	**Score Factor**	**Monoplane**	**Biplane**	**BWB**	**Lifting Body**
WS/S	0.25	0	1	1	1
Build Complexity	0.25	0	-1	-1	0
Internal Volume	0.25	0	0	-1	-1
Stability and Control	0.15	0	-1	-1	0
Flight Speed	0.10	0	-1	-1	0
	Total Score	**0**	**-0.25**	**-0.5**	**0**

As shown in Table 6, despite the reductions in wingspan, there were significant disadvantages to the biplane and blended wing body (BWB) configurations that would result in a heavier plane and lower total score when compared to the other configurations. Since a lifting body scored as well as a monoplane, both configurations were designed and tested at the December 10th test flight discussed in Section 7.3. The lifting body configuration was unable to meet the TOFL requirement at a competitive EW; the additional propulsion weight or wing area to decrease TOFL made the monoplane preferable.

3.3.2 Tail Configuration

As a result of the aircraft configuration selected, an empennage was required to maintain longitudinal stability. The main factors governing empennage selection were minimizing weight, maximizing stability, and minimizing drag. Due to the team's experience with conventional tails, the conventional configuration was set as the baseline with regards to the Figures of Merit. The following designs were compared, and a configuration downselect is shown in Table 7.

- **Conventional:** The conventional design is simple to design and implement, allowing for a minimized RAC while providing necessary stability and control requirements.
- **T-Tail:** This design locates the horizontal stabilizer further outside of the wing wake than a conventional tail, but requires additional structural support. The additional structure gives rise to weight concerns.

- **V-Tail:** Two lifting surfaces form a V-shape and, through mixed servo action, provide both pitch and yaw control, which can contribute to less pitch and yaw authority [4].

Table 7: Empennage downselect

		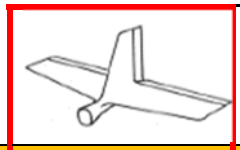		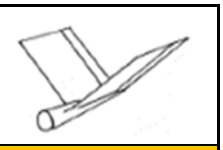
Figures of Merit (FoM)	**Score Factor**	**Conventional**	**T-Tail**	**V-Tail**
Weight (RAC)	0.35	0	-1	0
Stability & Control	0.25	0	1	-1
Drag	0.20	0	0	1
Design & Manufacture	0.10	0	-1	-1
Assembly	0.10	0	-1	0
	Total Score	**0**	**-0.3**	**-0.15**

As a result of the downselect, the conventional empennage design was chosen. Its ease of construction, low weight, and effective control made it the favorable tail configuration for this aircraft.

3.4 Aircraft Components Selection, Processes and Results

Following the aircraft and tail configuration selection, individual propulsion and landing gear components were chosen. Each configuration choice was quantified using downselects similar to those detailed in Sections 3.3.1 and 3.3.2. The highest scoring components were selected for preliminary design.

3.4.1 Propulsion

The propulsion team was responsible for designing a motor configuration that was lightweight, powerful, and efficient, while minimally interfering with other aircraft components. The tractor configuration was set as the neutral-zero baseline with regards to the Figures of Merit. The following motor configurations were compared and a downselect is shown in Table 8.

- **Pusher:** Single motor aft of the fuselage
- **Tractor:** Single motor located at the front of the aircraft
- **Wing-Mounted:** Twin motors mounted on the wings
- **Pull/Push:** Twin motors mounted in-line, fore and aft of the fuselage

Table 8: Motor configuration downselect

Figures of Merit (FoM)	Score Factor	Tractor	Pusher	Wing-Mounted	Pull/Push
Weight	0.4	0	0	-1	-1
Efficiency	0.4	0	-1	0	0
Landing Gear Interference	0.2	0	-1	1	-1
	Total Score	**0**	**-0.6**	**-0.2**	**-0.6**

The tractor configuration yielded the simplest, most-efficient motor configuration that did not interfere with the landing gear. Thus, the tractor configuration was identified as the motor configuration to fulfill the design objectives.

3.4.2 Landing Gear

The landing gear team was responsible for designing a gear to meet takeoff and landing requirements while minimizing weight and drag. Sufficient ground handling was considered an important factor in meeting the TOFL requirement. Five configurations were selected for initial comparison and are shown in Table 9. The tricycle configuration was set as the baseline for the Figures of Merit.

Table 9: Landing gear downselect

Figures of Merit (FoM)	Score Factor	Tricycle	Tip Tricycle	Bicycle	Tail Dragger	Tip Tail Dragger
Weight	0.4	0	0	1	1	0
Ground Handling	0.3	0	0	-1	0	0
Removability/ Integration	0.15	0	0	-1	1	1
Durability	0.1	0	0	-1	1	1
Drag	0.05	0	0	0	0	0
	Total Score	**0**	**0**	**-0.15**	**0.65**	**0.25**

After evaluating the configurations given above, a conventional tail dragger was chosen, which features two main wheels forward of the center of gravity (CG) and a tail wheel. This configuration was chosen for its strong ground handling, ease of removal as an LRU, and the ability to absorb landing loads.

3.5 Final Conceptual Design

The final aircraft configuration is a high wing, conventional tail monoplane designed to carry one passenger and one 4.25” x 2.75” x 2” payload block. The aircraft has a tail-dragger landing gear for reduced weight and ground handling.

4.0 Preliminary Design

The team collaborated to design all aircraft components to meet the two design objectives: minimize empty weight and minimize wingspan. Numerous trade studies were conducted using software simulations and models to develop the optimum sizing for all components of the aircraft. Computer models and prototypes allowed for further development of the structural elements of the team’s design.

4.1 Design Methodology

The preliminary design was developed through an iterative and collaborative process that required the input of numerous captains and team members across multiple disciplines. The critical components in the preliminary design phase and their corresponding design requirements are described as follows:

Wing

- Wing planform area (S): The wing area produces all of the lift required to support the aircraft and payload. This year’s wing area must meet the 150 ft TOFL.
- Aspect Ratio (AR): Although higher aspect ratios offer better takeoff and turning performance, lower aspect ratio wings improve the score; wingspan must be as small as possible to minimize the RAC. A small span could still have low vortex drag with endplates. Therefore, the lowest aspect ratio wing whose performance met required conditions was sized. This would also reduce the structural weight, which is proportional to AR, thus increasing overall score.
- Airfoil: The team utilized a custom airfoil that was designed to operate efficiently at low Reynolds numbers ($Re \leq 200{,}000$). The airfoil is designed to generate the required lift at takeoff and then optimized for the lift to drag ratio at cruise $(L/D)_{cruise}$ to improve the lifting efficiency and minimize power required at cruise.

Structures

- Wing Spars: The wing spars were designed to be lightweight and withstand the maximum in-flight and landing loads (5g) expected for the wing.
- Fuselage: The fuselage connects all the aircraft components, thus requiring efficient load paths from internal components to the ground. The fuselage must also have both minimal weight and drag contributions.

Propulsion

- Motor, propeller, and battery pack: The components were selected to meet the performance goals of the aircraft while minimizing overall package weight.

Line Replaceable Units (LRUs)

- Ground Mission: The LRUs are designed to complete the ground mission and integrate with the aircraft with minimal weight in order to maintain a low RAC.

4.2 Mission Model

The Performance sub-team used multidisciplinary design optimization (MDO) software to determine the highest scoring design. MDO was implemented via PlaneTools, a package of simulation modules written by the team in MATLAB. PlaneTools simulated a full mission of the input aircraft by modeling four phases of the competition course: Takeoff, Climb, Cruise, and Turn [5], as shown in Figure 9 and detailed below:

1. Takeoff – Assumed to be performed by ramping up to maximum throttle using no high-lift devices. Testing was performed to determine the rolling friction coefficient of the landing gear to be 0.1.

2. Climb – The aircraft was assumed to climb to 25 ft (7.6 m) above the 1300 ft (400 m) altitude (ground level) of Wichita, KS. The rate of climb was calculated via the difference in thrust and drag on takeoff and multiplied by the proportion of the takeoff speed to the plane's weight.

3. Cruise – This phase of flight was assumed to be level, constant speed flight with thrust equal to drag. For each mission, an optimum cruise throttle setting was selected so the aircraft did not exceed its nominal battery capacity before the end of the mission.

4. Turn – A coordinated level turn with constant speed and radius was assumed for both types of turning maneuvers (two 180° turns and one 360° turn). The load factor on the aircraft structure was calculated based on predicted turn radius.

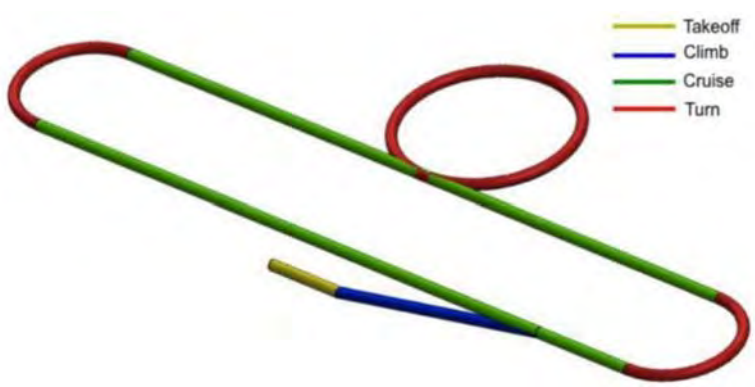

Figure 9: Flight model used in PlaneTools, indicating all phases of flight.

Fundamental aircraft and aerodynamic equations were used to calculate output parameters such as rate of climb, cruise conditions, and turn radius. The mission model also included the following uncertainties and assumptions:

- **Winds** – A headwind of 19 $\pm$ 3 ft/s (5.8 $\pm$ 0.9 m/s) was assumed for cruise based on historical weather patterns during competition weekend in Wichita, KS [6]. For takeoff, a headwind of 17 ft/s

(5.2 m/s) was assumed based on boundary layer calculations.

- **Battery performance** – Battery resistance and capacity were based on in-lab bench tests and flight tests rather than manufacturer specs. Battery voltage was assumed to be constant throughout each flight.
- **Propeller performance** – The coefficients of thrust (C_T) and power (C_p) used in thrust calculations were based on values provided by the manufacturer and verified via static and dynamic testing [5].

The mission model neglected interference drag and compressibility. The propulsion model takes into account variations in internal temperature, which affect the resistance and voltage of the system. From in-lab testing, it was determined that these parameters were very small perturbations on the overall mission. Additionally, these parameters were further verified from flight test data.

The mission model is programmed within PlaneTools as a class with several operations to simulate missions on any user-defined aircraft. The role of the mission model in PlaneTools is represented in Figure 10. The simulations help determine the initial design parameters for the aircraft by selecting those that result in a higher flight score.

This object-oriented approach allowed the team to isolate each component of the aircraft and perform trade studies more effectively. Uncertainty values, which were quantified from laboratory and flight tests, were propagated throughout the mission model. Figure 10 depicts a simplified order of operations that PlaneTools utilizes in order to simulate the entire mission. While this figure shows a linear progression to output values, iteration is used within the tool to ensure convergence.

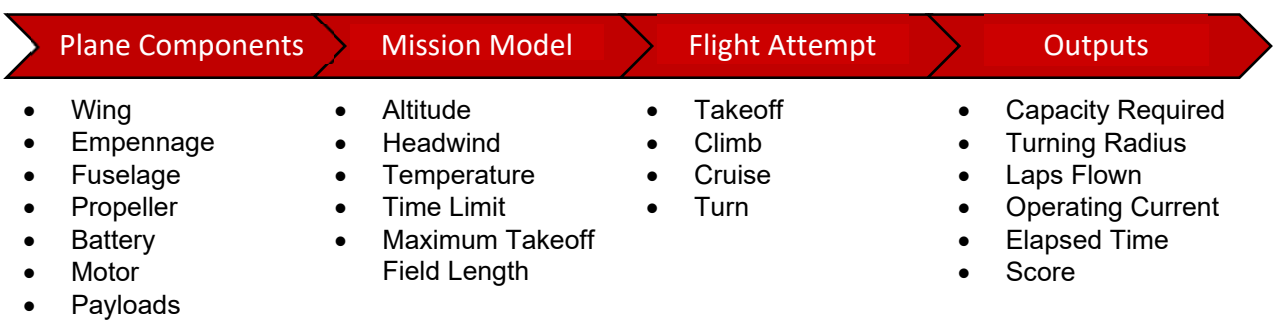

Figure 10: PlaneTools object model

4.3 Design Trade Studies

4.3.1 Wing Geometry

A trade study was implemented to determine the effect of variations in AR, b, and S on score. This was performed for multiple propulsion packages, consisting of different motors, battery cells (type and count), and propeller sizes. Results of this trade study for the final propulsion package are shown in Figure 11,

which presents the score as a function of wing geometry.

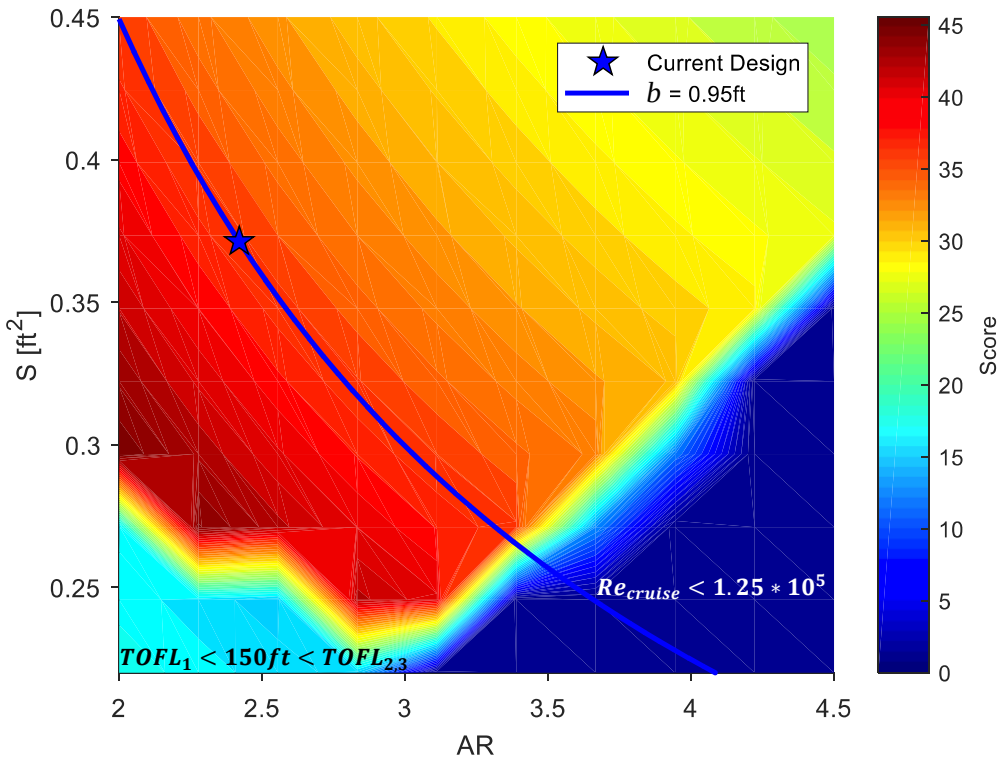

Figure 11: Colormap of scores from variations in *S* and *AR*

In Figure 11, the color gradation represented score and the star denoted the selected design for competition. A line of constant b (0.95 ft) was shown to contextualize the minimal effect on score when constraining b, but varying both S and AR. The optimum wing geometry was bounded by the conditions of $Re < 125{,}000$ at cruise and 150 ft maximum takeoff field length. Those conditions produced two regions in the lower right and left corners in Figure 11, respectively. The design was selected away from the boundaries in the lower left corner to allow for environmental uncertainties in Wichita.

4.3.2 Propulsion Sizing

Preliminary sizing for the propulsion system for the production aircraft was focused on minimizing weight and completing all missions. Mission 2 was the limiting case for sizing due to the increased payload weight of the passenger and the 3-lap requirement for the mission. Along with completing the missions, the propulsion system must also produce enough thrust to satisfy the 150 ft TOFL requirement.

NiMH cells were chosen over NiCd cells due to their higher energy density and lack of memory effect. For preliminary sizing, 2/3 AA 650s cells were chosen for their promising performance during static testing and lighter weight compared to the Elite 1500 2/3A cells [1]. From prior propulsion analysis, a well-sized propulsion package can achieve a maximum of 80% efficiency from the power supplied by the battery pack, which is calculated by Eq. 8 [7].

$$P_{battery} = V * I \qquad \text{Eq. 8}$$

As mission performance was shown to be secondary to weight from score analysis, a target power loading of 50 W/lb was determined to satisfy all requirements [1]. Thus, by sizing for the heaviest passenger for M_2, a minimum power requirement of 35.5 W was calculated using Eq. 9.

$$0.71\ lbs * \frac{50\ W}{1\ lb} = 35.5\ W \qquad \text{Eq. 9}$$

The power that must be generated can then be calculated using the result from Eq. 9 in Eq. 10.

$$P_{battery} = \frac{35.5\ W}{0.8} = 44.4\ W \qquad \text{Eq. 10}$$

The 2/3 AA 650s have a nominal voltage of 1.2 Volts per cell, and a target pack size of 8 cells was chosen. With these parameters, a maximum static current can be calculated using Eq. 11.

$$I_{max} = \frac{44.4\ W}{1.2\frac{V}{cell} * 8\ cells} = 4.6\ A \qquad \text{Eq. 11}$$

The Hacker A10-9L (1700 KV) out-runner motor was chosen as it fulfilled the power requirement from Eq. 11 for completing all missions and achieved the highest score with PlaneTools analysis. PlaneTools was also used to select the preliminary propeller that would produce enough thrust to satisfy the TOFL requirement. The preliminary propulsion package is shown in Table 10.

Table 10: Preliminary propulsion package

Motor	Battery Pack	Propeller
Hacker A10-9L (1700 KV)	8 x 2/3 AA 650s	APC 6 x 5.5 E

4.4 Aerodynamics

The aerodynamic configuration was designed and analyzed using XFLR5, AVL, and STAR-CCM+. XFLR5 is a graphically-oriented analysis program operating on XFOIL's panel method airfoil analysis capabilities. Athena Vortex Lattice (AVL) is a vortex-lattice tool used to analyze the aerodynamic characteristics of the full aircraft configuration, as well as static and dynamic stability derivatives. STAR-CCM+ is a computational fluid dynamics (CFD) tool utilized to further the team's understanding of endplates and buried wing area around the fuselage, as well as identify aircraft regions that might promote flow separation.

4.4.1 Airfoil Selection

Using XFLR5, numerous airfoils were analyzed for takeoff and cruise conditions at Reynolds numbers of 120,000 and 170,000, respectively. Figure 12 shows the lift properties at takeoff and the drag polar at cruise for the best-performing airfoils in this study: SG6043, SD5060, and the team-designed BA527ls.

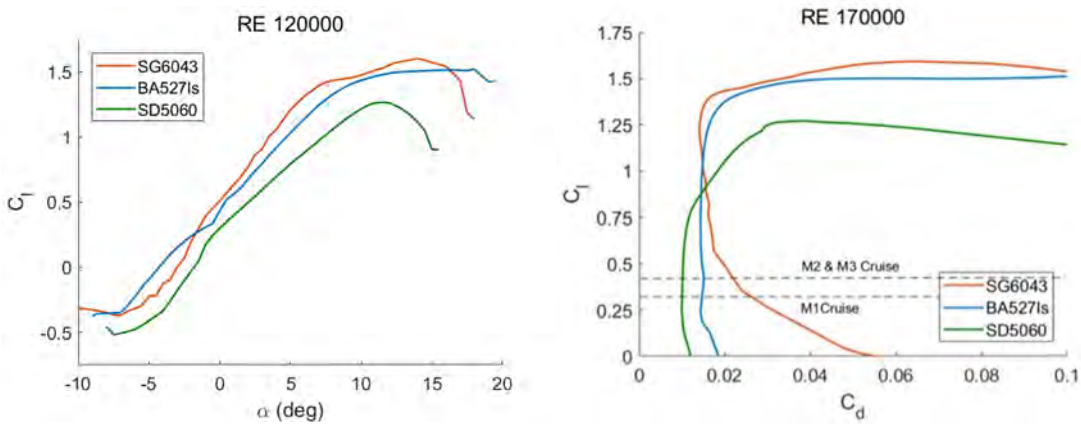

Figure 12: Aerodynamic properties of SG6043, BA527ls, and SD5060 airfoils at takeoff and cruise conditions

The BA527ls airfoil was selected due to its high $C_{l,max}$ of 1.5 at takeoff with favorable stall behavior and relatively low drag during cruise. Although the SD5060 airfoil has the lowest C_d value (0.01) at cruising conditions, its $C_{l,max}$ of 1.2 at takeoff was much lower than that of the BA527ls and SG6043 airfoils and would require a larger wing. While the SG6043 airfoil has a slightly higher $C_{l,max}$ than the BA527ls, it has a lower stall angle. With the risk of stall at these low Reynolds numbers, the plateau stall behavior of the BA527ls more favorable. Lastly, the BA527ls airfoil also has lower drag at cruise than the SG6043.

4.4.2 Aerodynamic Component Analysis

The wing geometry was initially sized at the November 5th test flight (Section 7.3) to have an AR of 4.5 with a 15.1 in. wingspan. This span was larger than the achievable span predicted by PlaneTools. It was suspected that because the fuselage covered approximately 1/3 of the span of the wing, a CFD study was required to quantify any decrease in lift from fuselage interaction. Figure 13 shows two contour plots from the CFD runs performed on semi-span models using STAR-CCM+; note the direction of V_∞ is labeled in the figure. One was performed with only the wing, and the other the wing and fuselage. Both models were set at the trim angle of attack of 5° and analyzed at an air velocity of 62 ft/s with atmosphere conditions set for Wichita, Kansas. These models neglect the effects of the propeller, the tail, and the landing gear. The center span is the right side of each picture and the wing tip is the left.

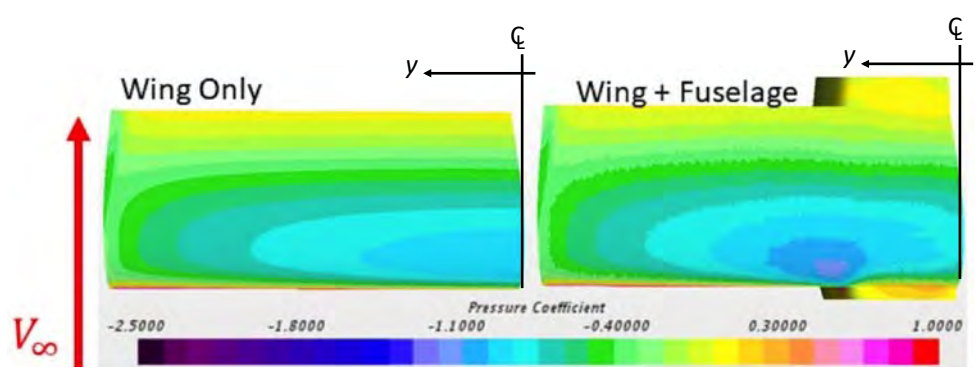

Figure 13: Pressure coefficient contours from CFD study. Wing only (left), wing with fuselage (right)

The contour plots show that the wing-only model has its peak C_p directly at the center span while the peak pressure contour for the wing-fuselage model is just outboard of the fuselage. The effect of this fuselage interaction is seen in the overall C_L value, with the wing and fuselage model having a 15% reduction in lift compared to the wing-only model. As the aircraft design evolved, this 15% lift reduction was applied to determine the expected lift as the fuselage shape remained constant throughout the design.

CFD was also used to check for signs of separation near the tail. Figure 14 shows a contour plot of the pressure coefficient over the fuselage. The aft end of the fuselage is the left side of the figure while the right is the direction of the aircraft nose. There is no sharp transition in C_p from negative to positive, which suggests the flow remains attached over the aft end of the fuselage implying a desirable taper angle.

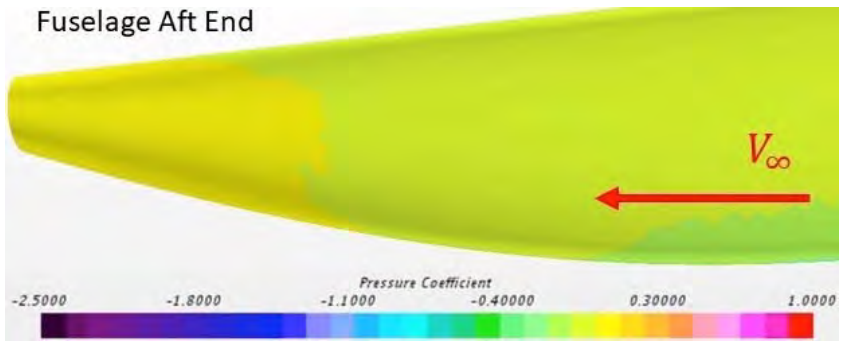

Figure 14: Pressure coefficient contour plot of aft end of fuselage

In an effort to reduce the wingspan, a study was performed to analyze the aerodynamic effect of endplates on wings. Due to aspect ratio effects, a wing with reduced span and AR is expected to have decreased lift and increased drag properties when compared to the original wing. By adding endplates, this loss in lift of the lower AR wing was minimized as endplates block some of the induced vorticity effects [8]. The endplates were sized using Eq. 12, which provides a relation for the effective aspect ratio (AR_{eff}) achieved when endplates of a specific height to wingspan (h/b) ratio are used [8]. This relation holds for endplates with $h/b \leq 0.4$.

$$\frac{AR_{eff}}{AR} = 1 + 1.9 * \frac{h}{b} \qquad \text{Eq. 12}$$

As described in Section 7.2, a wind tunnel test was performed to validate this endplate effect. A 7.55 in. semi-span wing with a chord of 3.36" was tested with and without endplates. The endplates had an overall positive lifting effect, and the change in lift coefficient (ΔC_L) values correlated closely to the expected ΔC_L between a wing with an AR of 4.5 and an AR_{eff} of 5.63 with the endplates.

Based on this endplate effect, a number of wing/endplate configurations were designed and tested at the December 10th test flight in Section 7.3. The final wing/endplate configuration selected was a wing with an AR of 2.34 and a span of 11 in. with 5.1 in. tall endplates. After factoring in the wing thickness, the effective endplate height is 4.4 in., satisfying that maximum h/b value of 0.4, giving the aircraft wing an

AR_{eff} of 4.11; therefore, minimally decreasing the lift characteristics to the original wing design, with a 25% reduction in span after accounting for endplate thickness.

4.4.3 Drag Analysis

The drag for the aircraft was estimated for the main components of the aircraft. The drag parameters for the wing were obtained from XFLR5 while the other components were estimated based on the frontal areas and drag coefficient estimates by Hoerner [9] and Page [10]. The drag breakdown for the aircraft during the M_3 cruise conditions is shown in Figure 15.

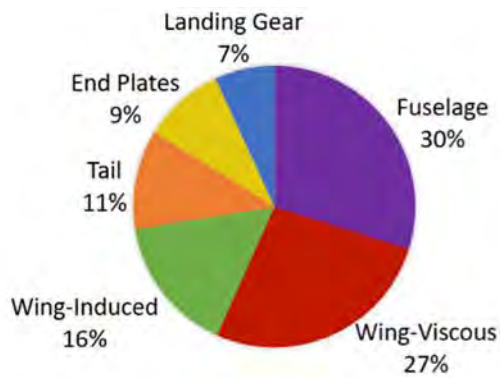

Figure 15: Drag breakdown for the M_3 cruise condition

The fuselage and wing-viscous drag are the largest contributors accounting for the majority of the overall drag for the aircraft, followed by the wing-induced drag, tail, endplates, and landing gear. The drag breakdown is similar for all flight conditions with the only difference being the induced drag, which is slightly less for the Mission 1 cruise condition due to the lower lift requirement for flying no payload.

To visualize the performance of the aircraft, the drag buildup was used to create an *L/D* curve plotted against a range of C_L values [10]. For comparison, the expected C_L values were obtained from AVL for the turn and cruise conditions of Missions 1, 2, and 3 and plotted across the L/D curve, shown in Figure 16.

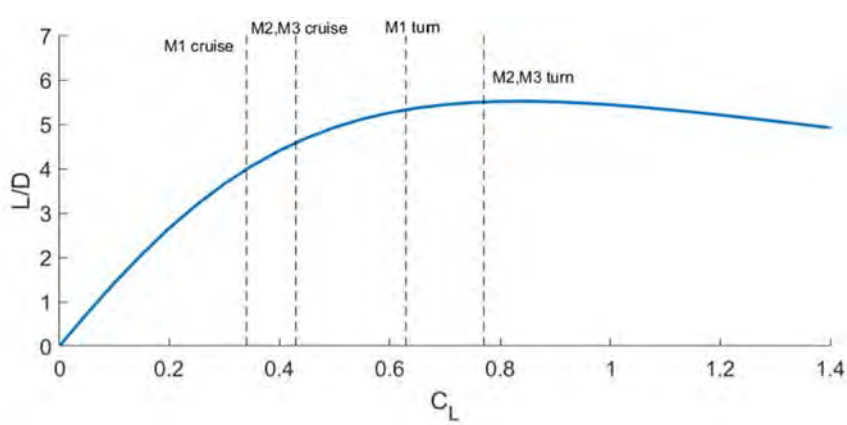

Figure 16: Expected *L/D* and C_L values for mission cruise and turn conditions

As shown in Figure 16, $(L/D)_{max}$ is positioned near the cruise and turn conditions. This allows for the aircraft to operate near peak efficiency throughout each flight.

After quantifying the effects on C_L due to the fuselage and endplates with CFD and wind tunnel testing, these characteristics were incorporated into the AVL model. Figure 17 shows a Trefftz plot for the Mission 1 cruise condition, which demonstrates the lift behavior over the wing. Over the center of the aircraft, an expected decrease in lift occurs due to fuselage interference. Towards the wingtips, the lift decreases less than expected due to the endplates, which decrease the vortices near the tips.

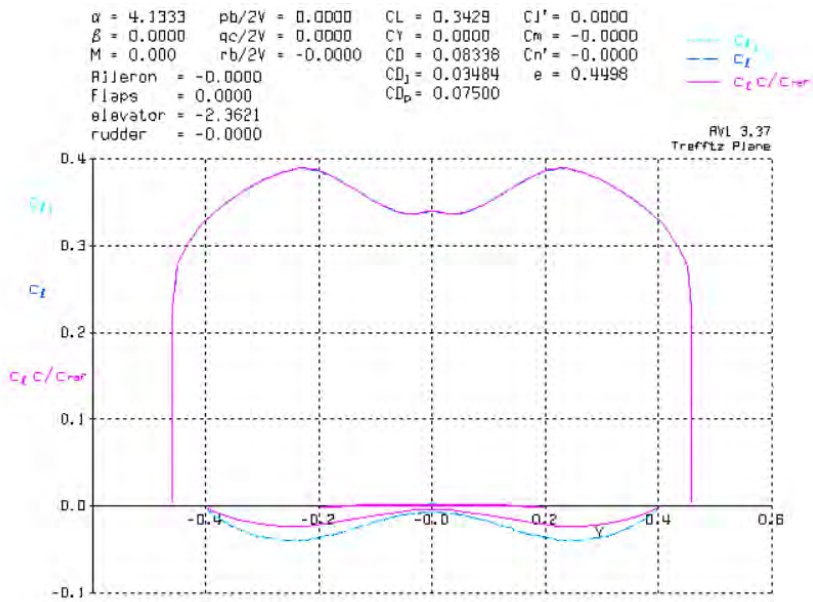

Figure 17: Trefftz plot for Mission 1 cruise conditions

Trim settings were obtained from these Trefftz plots and a trim condition study was performed using AVL to analyze the control surfaces within the designated bounds. In order to minimize the trim drag, limits were set for the elevator deflection (δ) to be no more than ± 3°. Based on anticipated flight velocities, a maximum angle of attack of 6° was set to ensure minimal induced drag from the required lift. The trim conditions for Missions 1, 2, and 3 are shown in Table 11 where it can be shown that the angle of attack and the elevator requirements were met. The low span efficiency value predicted by AVL is a result of the low AR and fuselage interaction.

Table 11: Trim conditions and lift and drag coefficients for Mission 1, 2, and 3 cruise conditions

	M_1 Cruise	M_2 & M_3 Cruise
e	0.45	0.43
α [°]	4.1	5.4
δ [°]	-2.4	-3.0
C_L	0.34	0.43
C_D	0.084	0.088
C_{D_i}	0.035	0.047
C_{D_0}	0.075	0.075

4.5 Stability and Control

4.5.1 Static Stability Analysis

During the preliminary design phase, it was determined that due to the small and lightweight design, the aircraft could be susceptible to external disturbances. Therefore, large control surfaces were required for the tail in order to ensure the aircraft had sufficient static stability to resist these disturbances. The vertical and horizontal tails were initially sized and located by establishing horizontal and vertical tail volume ratios of 1.6 and 0.2 respectively, as computed by equations, Eq. 13 and Eq. 14 [11].

$$V_h = \frac{S_h * l_h}{S * c} \qquad \text{Eq. 13}$$

$$V_v = \frac{S_v * v}{S * b} \qquad \text{Eq. 14}$$

Through a process involving a combination of test-flights and AVL analysis, the CG location, tail size, tail arm, and control surface sizes were iterated such that the aircraft was sufficiently stable while having enough control power to allow the pilot to have ample control authority over the aircraft. The aircraft has a static margin of 36%, and the main static stability derivatives, C_{l_β}, C_{m_α}, and C_{n_β} are negative, negative, and positive signs, respectively, ensuring a statically stable aircraft. Due to similar cruise conditions, the aircraft has similar static stability characteristics for all three missions; therefore, only the static stability derivatives for Mission 1 are shown Table 12.

Table 12: Static stability derivatives for Mission 1 calculated with AVL

C_{L_α}	4.40	C_{m_α}	-1.55	C_{Y_β}	-1.64	$C_{Y_{\delta_r}}$	0.009	C_{Y_p}	-0.51	C_{Y_r}	2.22
$C_{L_{\delta_e}}$	0.023	$C_{m_{\delta_e}}$	-0.06	C_{l_β}	-0.49	$C_{l_{\delta_r}}$	0.002	C_{l_p}	-0.60	C_{l_r}	0.57
C_{L_q}	13.10	C_{m_q}	-22.75	C_{n_β}	0.42	$C_{n_{\delta_r}}$	-0.01	C_{n_p}	0.06	C_{n_r}	-1.70

4.5.2 Dynamic Stability Analysis

The dynamic stability of the aircraft was analyzed for all three missions using AVL. These modes are visualized as roots of characteristic equations plotted on the complex plane. Negative poles describe a stable mode, while positive poles are unstable. The dynamic modes for each mission are shown in Figure

18. Phugoid (1), short period (2), Dutch Roll (3), roll (4), and spiral (5) modes are shown in the negative region of the $\zeta\omega_n$ axis; therefore, the aircraft is dynamically stable for each mission.

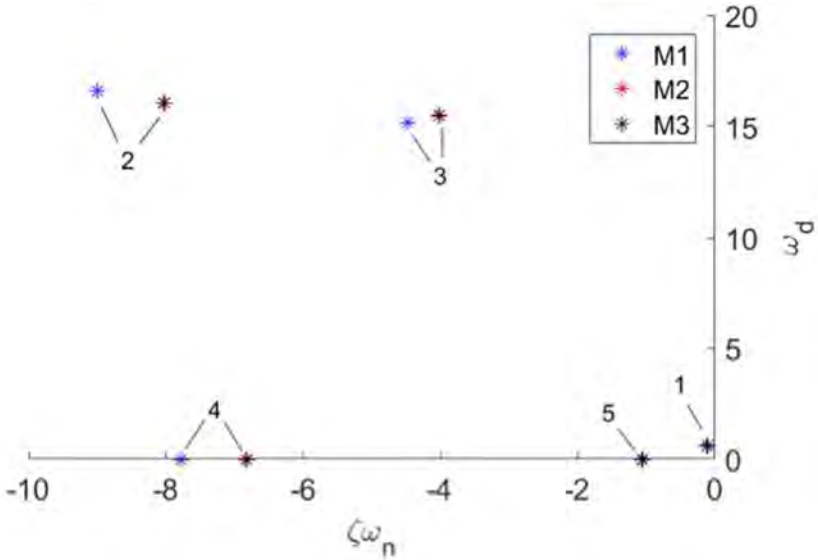

Figure 18: Dynamic stability modes: phugoid (1) short period (2) Dutch roll (3) roll (4) and spiral (5)

This aircraft was designed to satisfy the Level 1 flying quality of a Class I – small, light airplane. These requirements were derived from the military specification MIL-F-8785C and are presented in parentheses beneath each relevant dynamic stability parameter in Table 13 [12]. Due to the similarities in the flight conditions for each mission, the dynamic stability parameters are similar; therefore, only M_1 parameters are shown. Spiral mode requirement is not shown because the requirement is a maximum time to double; therefore, a stable mode is enough to satisfy a Level 1 flying quality for the spiral mode.

Table 13: Aircraft M_1 dynamic stability parameters and requirements in parentheses

	Mode	ζ	ω_n (rad/s)	$\zeta\omega_n$ (rad/s)	τ (s)
1	Phugoid	0.20 ($\zeta > 0.04$)	0.59	0.12	8.29
2	Short Period	0.48 ($0.35 < \zeta < 2.00$)	18.87	9.00	0.11
3	Dutch Roll	0.28 ($\zeta > 0.08$)	15.79 ($\omega_n > 0.4$)	4.48 ($\zeta\omega_n > 0.15$)	0.22
4	Roll	-	-	7.78	0.13 ($\tau < 1.4$)
5	Spiral	-	-	1.06	0.94

4.6 Predicted Aircraft Performance

The performance of the preliminary designed aircraft, as predicted by PlaneTools, is listed in Table 14.

Table 14: Preliminary design performance characteristics where mission scores are calculated using competitor assumptions from Table 3.

Performance Parameter	M_1	M_2	M_3
$C_{L_{max}}$	0.72	0.72	0.72
$C_{L_{cruise}}$	0.33	0.42	0.42
e	0.8	0.8	0.8
C_{D_0}	0.11	0.11	0.11
$(L/D)_{max}$	3.8	3.8	3.8
$(L/D)_{cruise}$	2.6	3.1	3.1
Rate of Climb	9.8 ft/s (3.0 m/s)	5.9 ft/s (1.8 m/s)	5.8 ft/s (1.8 m/s)
W/S	1.9 lb/ft^2 (91 N/m^2)	2.3 lb/ft^2 (110 N/m^2)	2.3 lb/ft^2 (110 N/m^2)
v_{cruise}	71 ft/s (22 m/s)	70 ft/s (21 m/s)	70 ft/s (21 m/s)
v_{stall}	48 ft/s (15 m/s)	53 ft/s (16 m/s)	53 ft/s (16 m/s)
Gross Weight	0.71 lbf (3.15 N)	0.86 lbf (3.83 N)	0.86 lbf (3.83 N)
Mission Score	1.00	0.03	2.00

5.0 Detail Design

Detail design combines the theoretical sizing from conceptual and preliminary design with detailed testing and analysis of individual components. Each sub-team considered the structural capabilities, subsystem design, weight, and mission performance in order to refine the dimensions of the competition aircraft.

5.1 Dimensional Parameters Table

Table 15 lists the characteristic parameters for *SCkywalker,* USC's entrant into the 2017-2018 DBF Competition. Each subsystem will be highlighted in the subsequent sections.

Table 15: Characteristic components properties for *SCkywalker*

Wing		Tail	
Airfoil	BA527ls	**Airfoil**	NACA 0010
Span	0.92 ft (0.28 m)	**Horizontal Span**	0.8 ft (0.24 m)
MAC	0.39 ft (0.12 m)	**Horizontal Chord**	0.23 ft (0.07 m)
Planform Area	0.36 ft^2 (0.03 m^2)	**Vertical Span**	0.42 ft (0.13 m)
AR	2.3	**Vertical Chord**	0.23 ft (0.07 m)
Incidence Angle	0°	**Planform Area**	0.28 ft^2 (0.03 m^2)
Static Margin	0.36	**Incidence Angle**	0°
Endplate Area	0.17 ft^2 (0.02 m^2)	**Tail Arm**	1.00 ft (0.31 m)
Fuselage		**Controls**	
Total Length	1.56 ft (0.48 m)	**Receiver**	Futaba 617FS
Nose Length	0.40 ft (0.12 m)	**Servo**	HK 5330
Tail Length	1.01 ft (0.31 m)	**Battery Model**	Elite 1500
Width	0.39 ft (0.12 m)	**Internal Resistance**	0.011 Ω
Height	0.22 ft (0.07 m)	**Cell Count**	5
		Pack Voltage	6 V
		Pack Weight	0.25 lbf (1.13 N)
Motor		**Propeller**	
Model	Hacker A10-7L	**Manufacturer**	APC
Gearbox	Direct Drive	**Mission 1**	7” x 5”
Kv	2200	**Mission 2**	7” x 5”
Power Rating	90 W	**Mission 3**	7” x 5”
No-Load Current (I_0)	1.1 A		
Internal Resistance	110 mΩ		
Weight	0.06 lbf (0.26 N)		

5.2 Structural Characteristics and Capabilities

The aircraft structure was designed to minimize the RAC by reducing weight of the fuselage, wing, and tail, while withstanding flight loads and 5g landing loads. The wing was designed to withstand a 5g load case with a gross weight of 0.86 lb (0.39 kg), allowing for a 75° bank angle with a safety factor of 1.5. To meet the team’s objective, materials were chosen to optimize the strength to weight ratio. The wings and tail are a balsa built-up design with carbon spar caps. The fuselage is a balsa built-up design with a plywood landing gear mount. In addition, fuselage considerations were made to accommodate interior accessibility and hardware mounting.

5.3 Sub-system Design

5.3.1 Wing

The wing's structural design was driven by the wing geometry and maximum aerodynamic loads. An Excel-based analytical tool, SparSizer, developed by former team adviser Mark Page, was used to perform trade studies on different materials for the wing skin, shear web, and spar caps. The spar cap and shear web thickness were sized to achieve safety factor of 1.5. Preliminary analysis was done using the wing dimensions in Table 15.

The primary wing structure was a full-span spar designed to transfer loads into the fuselage. The spar is an I-beam with carbon fiber caps and balsa wood shear web. Figure 19 shows the performance of the chosen spar design to maximum expected flight loads. The largest in-flight stresses in the shear web were calculated as 20% of the ultimate stress of the balsa. While this is low, most of the wing structure could not be reduced further without compromising material handling. Additionally, a balsa D-box was designed to carry torsional loads and a balsa rib structure was designed to transfer axial and transverse loads into the main spar.

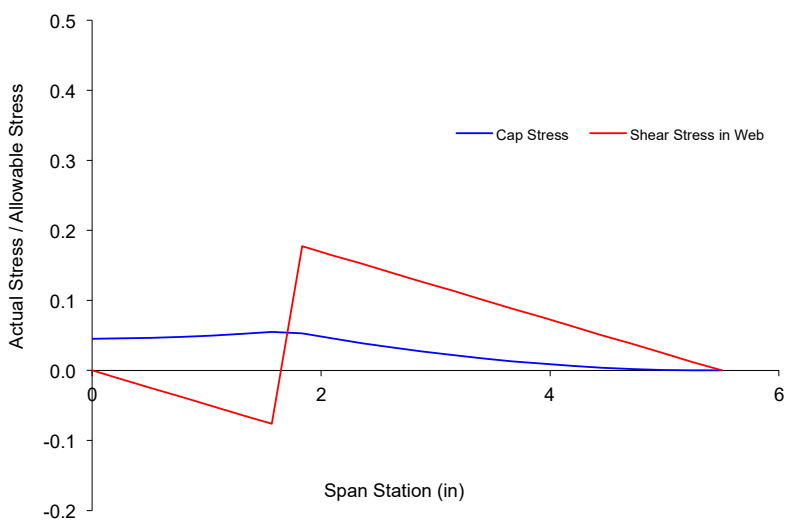

Figure 19: Percentage of allowable stress along the wing span

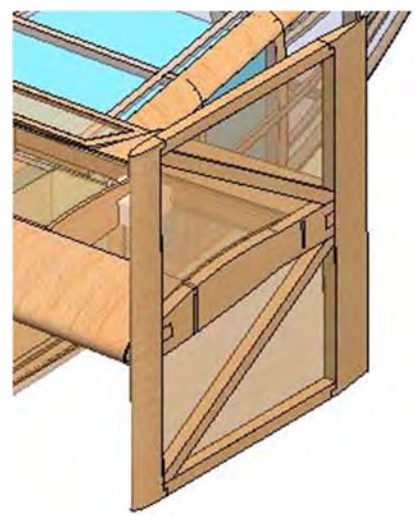

Figure 20: End plates attached to wingtips with interior structure visible

Balsa end plates were designed to have a truss structure to decrease weight while maintaining structural integrity during flight. The truss structure consisted of 0.19 in. (0.48 cm) balsa beams. For integration with the tips of the balsa wing, a rib-shaped mounting surface on the end plate was used to help with alignment to the last rib on the wing. This design allowed endplates to shear off in the event of a crash, causing minimal damage to the wing's main spar structure. The end plate design is shown in Figure 20.

5.3.2 Tail

The built-up tail was designed similar to the wing with balsa spars carrying the tail loads into the fuselage.

The balsa built-up design was chosen to minimize weight with five 0.06 in. (0.2 cm) balsa ribs evenly spaced span wise to maintain the airfoil shape and transfer flight loads to the main spar. Servos mounted to a plywood rib allow for the proper control deflections from the rudder and elevator.

5.3.3 Landing Gear

A conventional tail dragger design with a tail wheel was selected for the landing gear configuration. The main gear was chosen to be a steel wire gear to minimize weight. The main gear was bow-shaped, with outwardly mounted 1.45” diameter lightweight plastic wheels. The wheels were fitted with aluminum bushings and restrained with tight fitting plastic collars. The main gear is slightly forward swept to absorb slight bumps in the pavement just before takeoff. This main gear was mounted to a 1” by 3.75” section of plywood integrated into the fuselage using two nylon collars and 4 M2 nylon bolts, which were designed to be the first component to shear during a crash for ease of repair and disassembly for the ground mission. The rear of the aircraft was fitted with a 1” diameter lightweight wheel and 3/100” axle that was integrated into the rear bulkhead for structural support.

Finite Element Analysis resulted in 0.13” and 0.79” deflections for the 1g and 5g loads as displayed in Figure 21. Experimental stress tests resulted in deflections of 0.15” and 0.85” for a 1g and 5g loading, respectively. In the 5g loading case, the deflections were less than the 1” for propeller clearance.

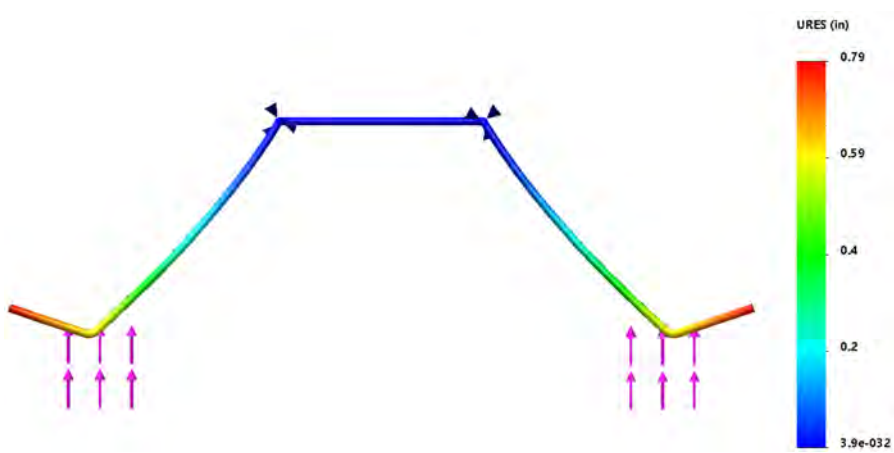

Figure 21: Landing gear under 5g load case with a deflection of 0.79 in.

5.3.4 Payload Restraints

In order to satisfy the competition requirements, the passengers must each have a seat and individual restraint. The seat was designed as a polystyrene foam ring to reduce weight. The seat attached to the bottom of the fuselage to laterally constrain any size of passenger. Passenger restraints were designed as wires threaded through the fuselage floor and wrapping around the top of the passenger. The wires twist together to secure the passenger as pictured in Figure 22. This method is difficult for quick passenger loading; however, it is sufficient for loading a single passenger aircraft.

Figure 22: Top view (left), bottom view (center), and front view (right) of the passenger restraint

5.3.5 Fuselage

Figure 23 shows the load paths from the wing, tail, and landing gear into the fuselage. Fuselage fixtures were utilized to distribute flight loads from the wing and tail into the fuselage. To distribute landing loads throughout the fuselage, landing gear mounts were utilized.

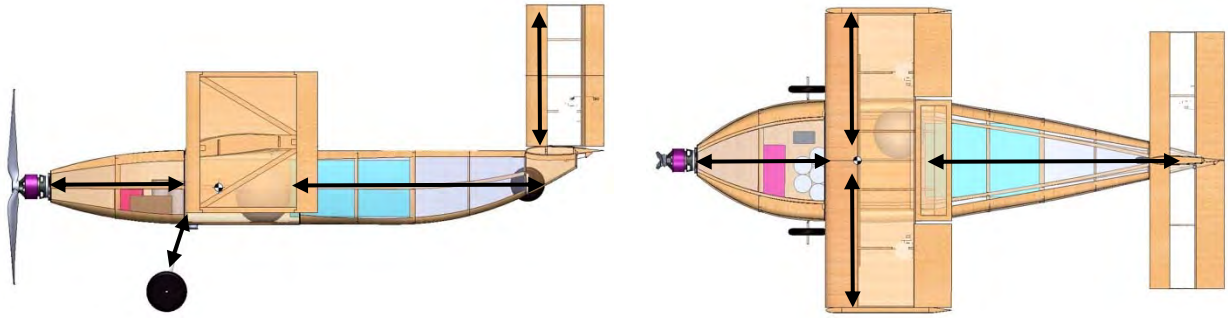

Figure 23: Side (left) and top (right) views of load paths

The fuselage was designed to withstand flight and landing loads at maximum gross weight while minimizing structural weight and spatially accommodating required payload. Structural design choices responded to FEA analysis (Figure 24, Figure 25) and in lab testing (Section 7.2). Areas with high loading conditions were reinforced with additional structure, such as plywood bulkheads or balsa sheeting.

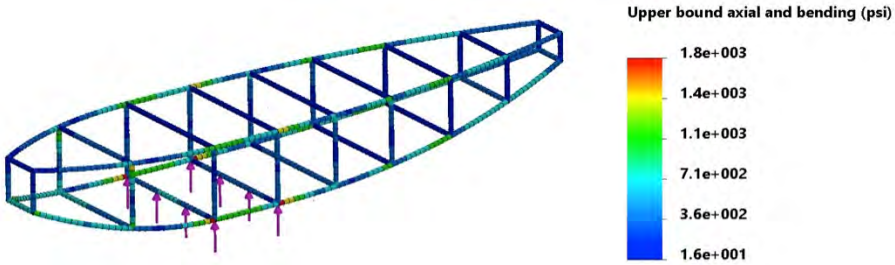

Figure 24: FEA analysis for main gear and tail wheel landing loads on the fuselage

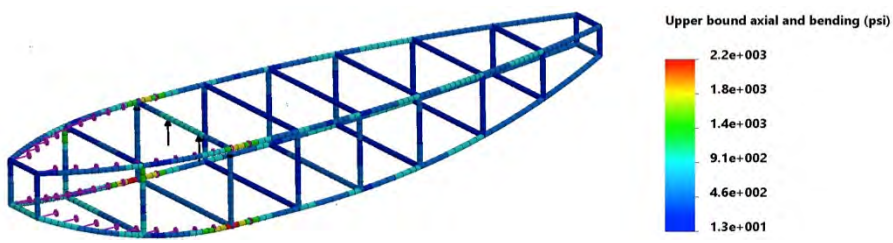

Figure 25: FEA analysis for in-flight motor torque, drag, and thrust loads on the fuselage

The nose of the fuselage was covered in 0.03 in. (0.08 cm) balsa sheeting to reduce deformation in flight and to support internal propulsion components. The sheeting integrated with a plywood motor mount to support thrust and torque loads from the motor. The wing and tail integration fixtures were designed to transfer in-flight loads from the wing and tail into the fuselage structure. A 0.03 in. (0.08 cm) plywood landing gear mount was designed to distribute landing loads throughout the rest of the fuselage.

5.3.6 Propulsion System

After preliminary sizing, the propulsion sub-team sought to reduce weight by exploring the motor Kv and battery pack voltage while maintaining the required power output. Applying this required power to Eq. 8, motors within a Kv range of 1700 to 2500 were tested to investigate the balance between voltage and current. Both static and dynamic testing was performed with the same assortment of battery packs and propellers.

The static tests confirmed that, while raising Kv increases the current draw as expected, the incremental increases in performance became marginal at Kvs greater than 2500 due to stall effects on the tested propeller. Dynamic tests confirmed that the Hacker A10-7L (2200 Kv) motor provided the required thrust at cruise while minimizing static current draw and weight.

Having selected a motor, NiMH batteries of various capacities were tested to determine the maximum current the batteries could achieve before performance suffered, as shown in Table 16. Batteries were tested to measure the capacity of low cell battery packs before the voltages fell below the ESC 5 V cutoff.

Table 16: Discharge rates and weight of commercially available NiMH batteries

	Capacity	Weight [g]	Discharge Rate [A]
Elite 1500s	1500 mAh	21.4	13
2/3 AA 650s	650 mAh	12.3	6.5
KAN 400s	400 mAh	7.7	5
2/3 AAA 300s	300 mAh	7.1	1
1/3 AA 300s	300 mAh	7.9	3

Initial capacity tests determined that the 2/3 AA will have difficulty completing missions; thus, the Elite 1500s were chosen for their higher energy density and higher discharge rate, allowing for the number of

cells to be lowered while maintaining the same power output.

Propellers were selected through static and wind tunnel testing (Section 7.2) to determine whether the propulsion package would produce enough thrust to satisfy the TOFL requirement while also completing all missions. The APC 7x5 propeller was selected due to its high dynamic performance in the wind tunnel compared to other propellers of similar diameter at the cruise speed predicted by PlaneTools.

A condensed summary of the propulsion subcomponents is shown in Table 17. The components are the same for all missions.

Table 17: Propulsion package breakdown for all missions

Propulsion Component	Description	Weight [g]
Motor	Hacker A10-9L 1700 KV	24.3
Rx Pack	Tenergy 1/3 AAA 170mAh (4s)	15.1
ESC	Castle Creations Thunderbird 09	9.8
Rx	Futaba 617FS	9.1
Servos	Hobby King 5330 (4x)	12.0
Connections	Servo wire, electrical connections, solder	12.0
Propeller	APC 7x5	8.7
Battery	Elite 1500s (5s)	113.0
Total (% EW)		**204.0 (63%)**

5.3.7 LRU Design

For the Ground Mission, eleven components of the aircraft must be removable and replaceable. Many components of the plane were already designed to be easily replaceable; however, components were redesigned to reduce weight. For instance, Velcro was a method replaced by masking tape since masking tape is lighter. The servo LRU was the only component that needed a new replaceable design; previously, servos were glued into the plane. The evolution of methods can be observed in Table 18.

Table 18: Initial and finalized methods for LRU components

Stage 1 (3 minutes)			Stage 2 (5 minutes)		
Component	**Initial Method**	**Finalized Method**	**Component**	**Initial Method**	**Finalized Method**
Servo	Box	Screws	ESC	Velcro	Masking Tape
Rx Battery	Velcro	Masking Tape	Control Surface	Tape	Tape
Main Propulsion Battery	Velcro	Velcro	Rx	Velcro	Masking Tape
Control Rod	Metal Rod	Metal Rod	Main Landing Gear	Nylon Bolts	Nylon Bolts
Landing Gear Wheel	Collar	Plastic Pressure Fit	Motor	Screws	Screws
Propeller	Aluminum Pressure Fit	O-ring	-	-	-

Various concepts were considered when looking at the servo LRU (Line Replaceable Unit). The three main configurations were screwing the servo into a rib, making a casing/box for the servo to sit in or using Velcro. In Table 19, a configuration downselect compared the three methods described; for each parameter, a configuration was given a score of -1 (bad), 0 (neutral), or 1 (good). The method selected was the screws because it was the lightest and simplest option that met the time constraints.

Table 19: Servo LRU configuration down select

Parameters	Screws	Box	Velcro
Weight	1	0	1
Integration	0	0	-1
Ease of Manufacturing	1	-1	1
Servo Security	0	1	-1
Removability	0	1	0
Total	**2**	**1**	**0**

5.4 Weight and Mass Balance

The EW for *SCkywalker* was 0.71 lb (0.43 kg). The flight batteries, ESC, and receiver were used as a ballast to ensure that the CG was within the static margin for all possible payload configurations. The coordinate system used to estimate the CG is shown in Figure 26.

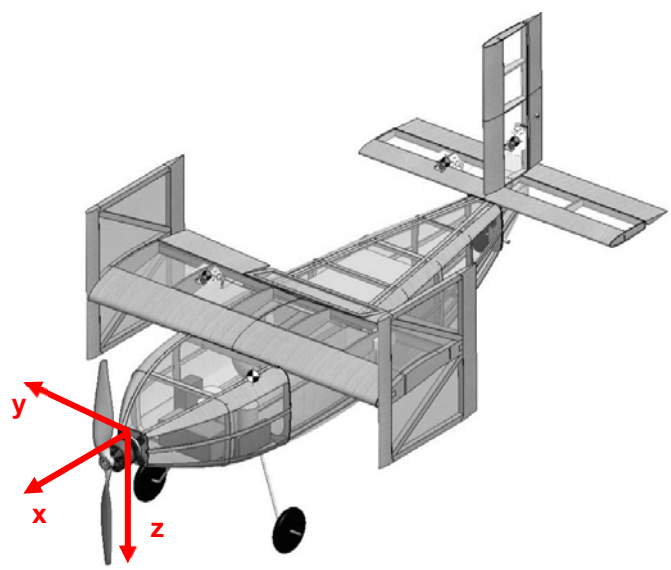

Figure 26: *SCkywalker* origin and coordinate directions

Table 20 shows each component's mass and CG location with respect to this coordinate system. The heaviest and lightest passenger configurations are included to demonstrate that the aircraft can support any of the five passenger weights without becoming unbalanced.

Table 20: Weight and mass balance table for all missions

Aircraft Component	Mass		X		Y		Z	
	(lb)	(g)	(in)	(cm)	(in)	(cm)	(in)	(cm)
M_1								
Fuselage	0.06	30	-7.3	-18.5	0.0	0.0	1.5	3.8
Wing	0.07	32	-7.2	-18.3	0.3	0.8	-0.2	-0.51
Motor	0.05	24	0.5	1.3	0.0	0.0	1.3	3.3
Propeller	0.02	9	1.4	3.6	0.0	0.0	1.3	3.3
Flight Batteries	0.25	113	-6.0	-15.2	0.0	0.0	1.2	3.0
Tail	0.05	22	-18.3	-46.5	0.6	1.5	-0.7	-1.8
Landing Gear	0.04	14	-6.0	-15.2	0.0	0.0	1.2	3.0
Passenger Seat	0.00	1	-7.5	-19.1	1.0	2.54	2.6	6.6
M_2, heaviest PAX								
PAX	0.15	68	-7.5	-19.1	1.0	2.54	1.6	4.1
Flight Batteries	0.25	113	-4.3	-10.9	-0.5	-1.27	1.7	4.3
M_2, lightest PAX								
PAX	0.02	11	-7.5	-19.1	1.0	2.54	2.1	5.3
Flight Batteries	0.25	113	-5.0	-12.7	-0.1	-0.254	1.7	4.3
M_3, heaviest PAX								
PAX	0.15	68	-7.5	-19.1	1.0	2.54	1.6	4.1
Cargo Block	0.00	2	-10.6	-26.9	0.0	0.0	1.4	3.6
Flight Batteries	0.25	113	-4.3	-10.9	-0.6	-1.5	1.7	4.3
M_3, lightest PAX								
PAX	0.02	11	-7.5	-19.1	1.0	2.54	2.1	5.3
Cargo Block	0.13	59	-9.2	-23.4	0.0	0.0	1.4	3.6
Flight Batteries	0.25	113	-3.6	-9.1	-0.1	-0.254	1.7	4.3

5.5 Flight and Mission Performance

The expected flight performance of the final aircraft, as predicted by PlaneTools, is listed in Table 21.

Table 21: Predicted aircraft performance parameters for each mission

Performance Parameters	M_1	M_2	M_3
$C_{L_{max}}$	0.72	0.72	0.72
$C_{L_{cruise}}$	0.33	0.42	0.42
e	0.8	0.8	0.8
C_{D0}	0.11	0.11	0.11
$(L/D)_{max}$	3.8	3.8	3.8
$(L/D)_{cruise}$	2.6	3.1	3.1
Rate of Climb	9.8 ft/s (3.0 m/s)	5.9 ft/s (1.8 m/s)	5.8 ft/s (1.8 m/s)
W/S	1.9 lb/ft^2 (91 Pa)	2.3 lb/ft^2 (110 Pa)	2.3 lb/ft^2 (110 Pa)
V_{cruise}	71 ft/s (22 m/s)	70 ft (21 m/s)	70 ft (21 m/s)
V_{stall}	48 ft/s (15 m/s)	53 ft/s (16 m/s)	53 ft/s (16 m/s)
TOFL	77 ft (23 m)	98 ft (30 m)	99 ft (30 m)
Battery Weight	0.27 lb (0.12 kg)	0.27 lb (0.12 kg)	0.27 lb (0.12 kg)

Based upon these performance parameters, the corresponding mission results and score parameters are listed in Table 22.

Table 22: Predicted score results for each mission configuration

Score Parameters	M_1	M_2	M_3
N_{PAX}	-	1	1
W_{CARGO}	-	-	0.07 oz (2 g)
T_{USC}	-	190 s	-
N_{laps}	-	-	6
$Mission\ Score$	1	0.03	2.00
$Total\ Flight\ Score$	3.03		
EW	0.71 lb		
WS	11.375 in		
RAC	8.07		
$Total\ Score$	**37.5**		

5.6 Drawing Package

The following drawing package includes a dimensional 3-view, structural arrangement, and subassembly detail drawings. All drawings were made using Solidworks [13].

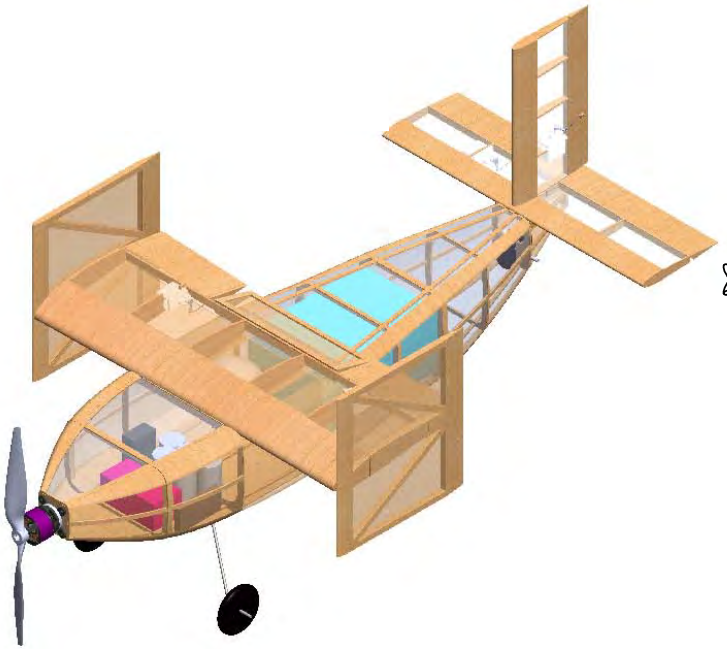

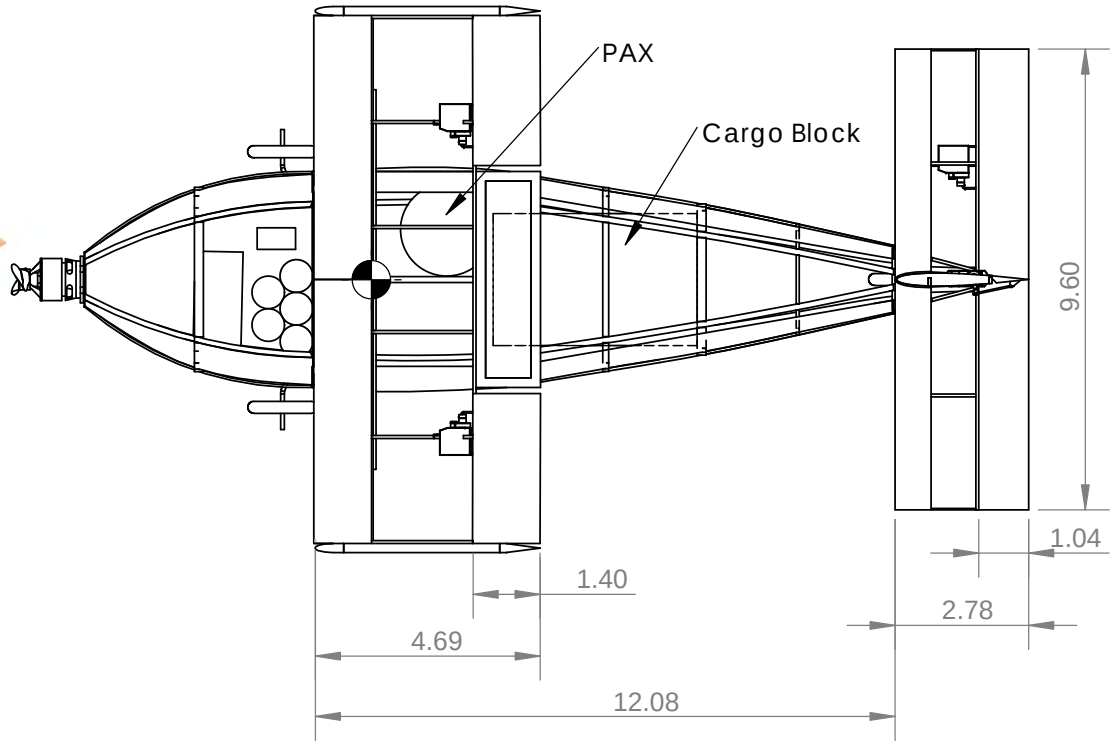

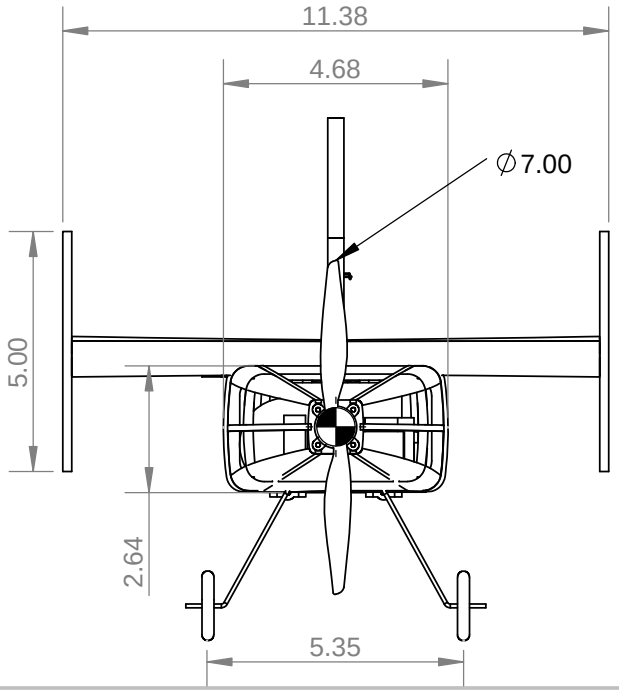

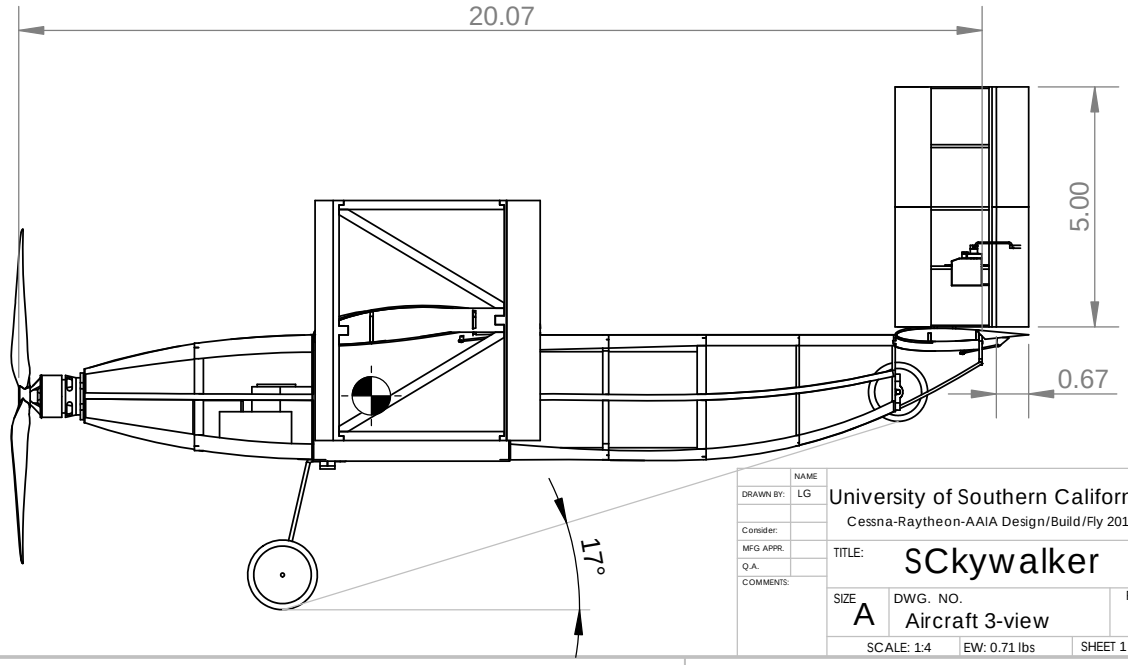

	NAME
DRAWN BY:	LG
Consider:	
MFG APPR.	
Q.A.	
COMMENTS:	

University of Southern California
Cessna-Raytheon-AAIA Design/Build/Fly 2018

TITLE: SCkywalker

SIZE A | DWG. NO. Aircraft 3-view | REV

SCALE: 1:4 | EW: 0.71 lbs | SHEET 1 OF 3

Structural Accomodations

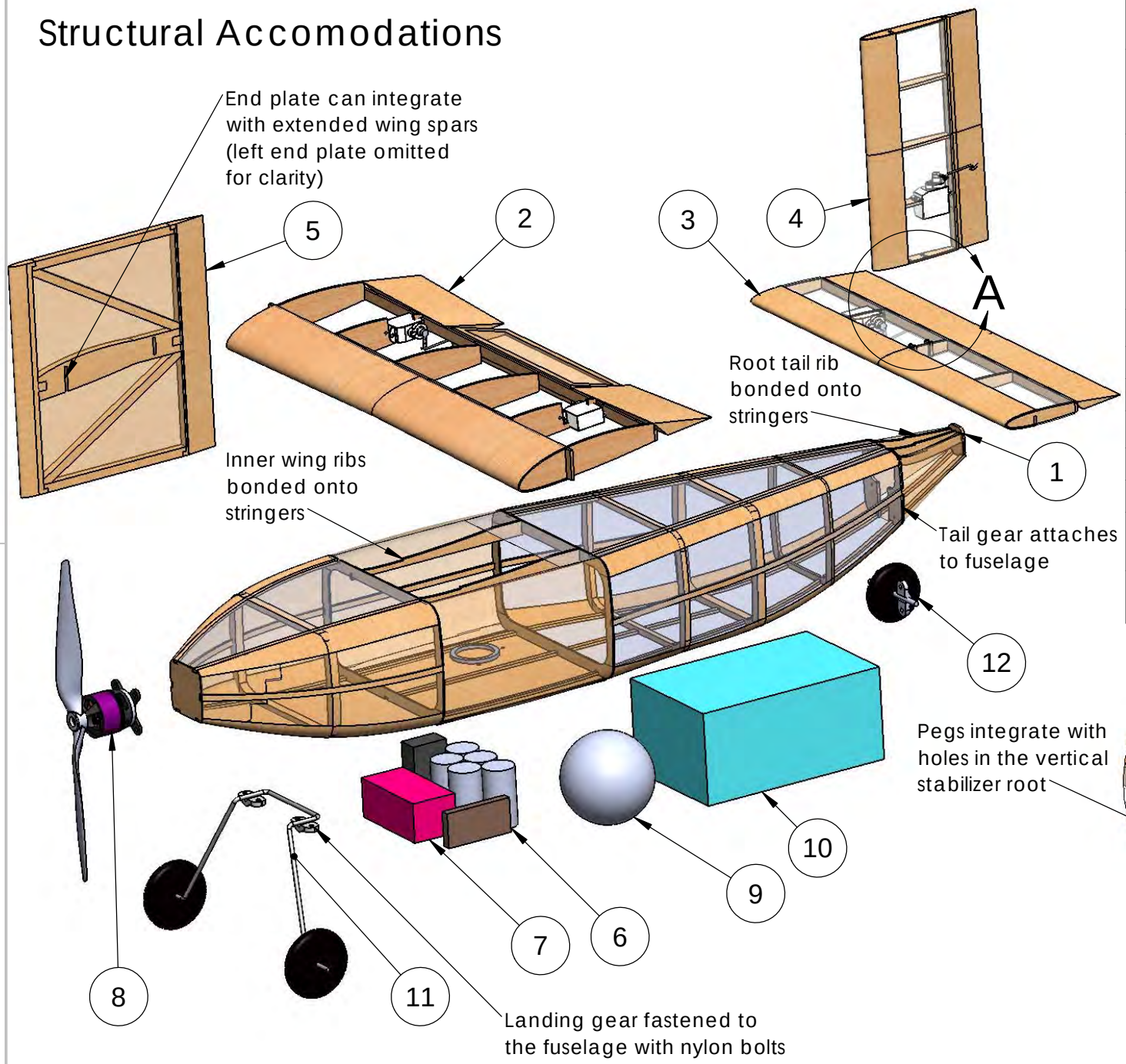

ITEM NO.	COMPONENT	DESCRIPTION	QTY.
1	Fuselage	Balsa/plywood built-up, solite covering	1
2	Wing	Balsa built-up, solite covering	1
3	Horizontal Stabilizer	Balsa built-up, solite covering	1
4	Vertical Stabilizer	Balsa built-up, solite covering	1
5	End Plates	Balsa truss, solite covering	2
6	Battery Pack	5 x Elite 1500s	1
7	Reciever	Futaba 617FS	1
8	Motor Assembly	Hacker A10 7L, 7x5 prop	1
9	Passenger	Super ball	1
10	Cargo Block	Fiberglass box	1
11	Main landing gear	Music wire, Plastic wheel	1
12	Tail gear	Music wire, Plastic wheel	1

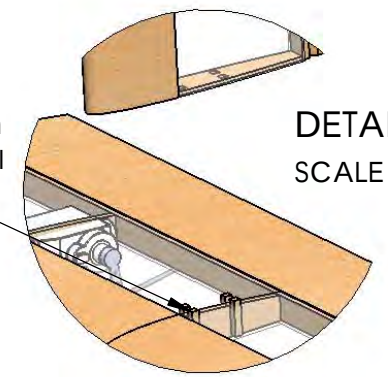

DETAIL A
SCALE 2 : 3

	NAME
DRAWN BY:	LS
Consider:	
MFG APPR.	
Q.A.	
COMMENTS:	

University of Southern California
Cessna-Raytheon-AAIA Design/Build/Fly 2018

TITLE: SCkywalker

SIZE A | DWG. NO. Structural Layout | REV

SCALE: 1:3 | EW: 0.71 lbs | SHEET 2 OF 3

Wing

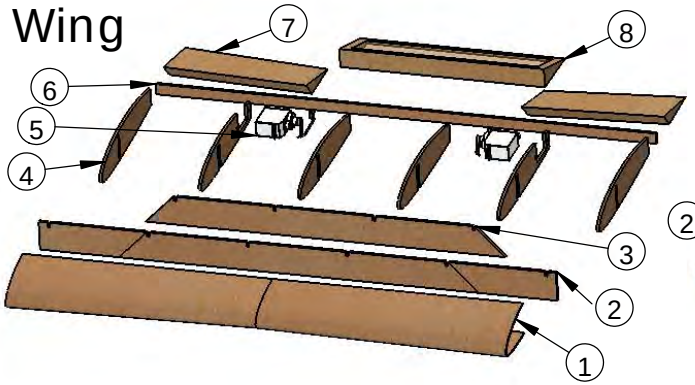

ITEM NO.	COMPONENT	MATERIAL	QTY.
1	C-box	1/32" balsa sheeting	1
2	Spar tips	1/16" balsa	1
3	Spar doubler	1/16" balsa	2
4	Rib	1/16" balsa	6
5	Servo	HK 5330	2
6	Aft spar	1/16" balsa	1
7	Aileron	Tapered balsa	2
8	Fairing	Tapered balsa, solite	1

Tail

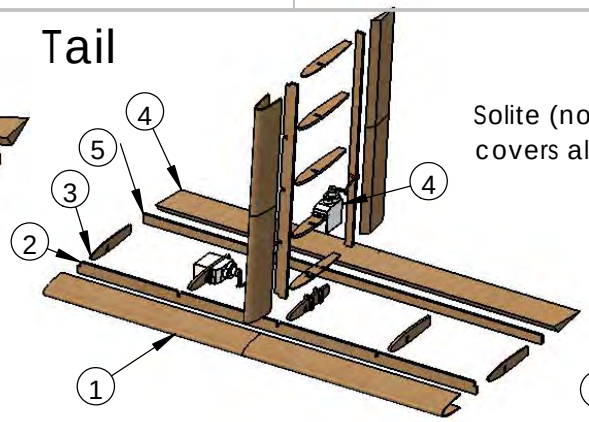

ITEM NO.	COMPONENT	MATERIAL	QTY.
1	C-box	1/32" balsa sheeting	2
2	Spar	1/16" balsa	2
3	Rib	Balsa built-up, solite covering	10
4	Servo	HK 5330	2
5	Aft Spar	1/16" balsa	2
6	Control surface	Tapered balsa	2

Fuselage

Solite (not shown) covers all openings

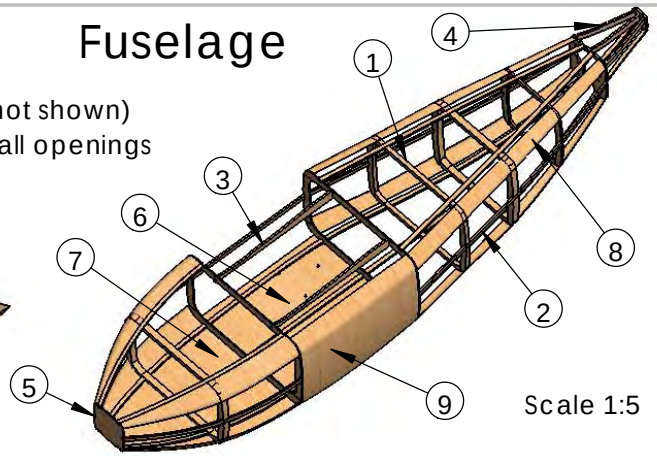

Scale 1:5

ITEM NO.	COMPONENT	MATERIAL	QTY.
1	Cross Sections	1/16-1/8" plywood/balsa	9
2	Stringers	1/16x1/8" balsa	6
3	Wing support stringers	1/16" plywood	2
4	Tail support stringers	1/16" plywood	3
5	Motor mount	1/16" plywood	1
6	Passenger floor	1/32" plywood	1
7	Battery floor	1/32" balsa	1
8	Corner sheeting	1/64" balsa	6
9	Side hatch	1/32" balsa	1

Payload Accomodations

Cargo block is loaded through a side hatch

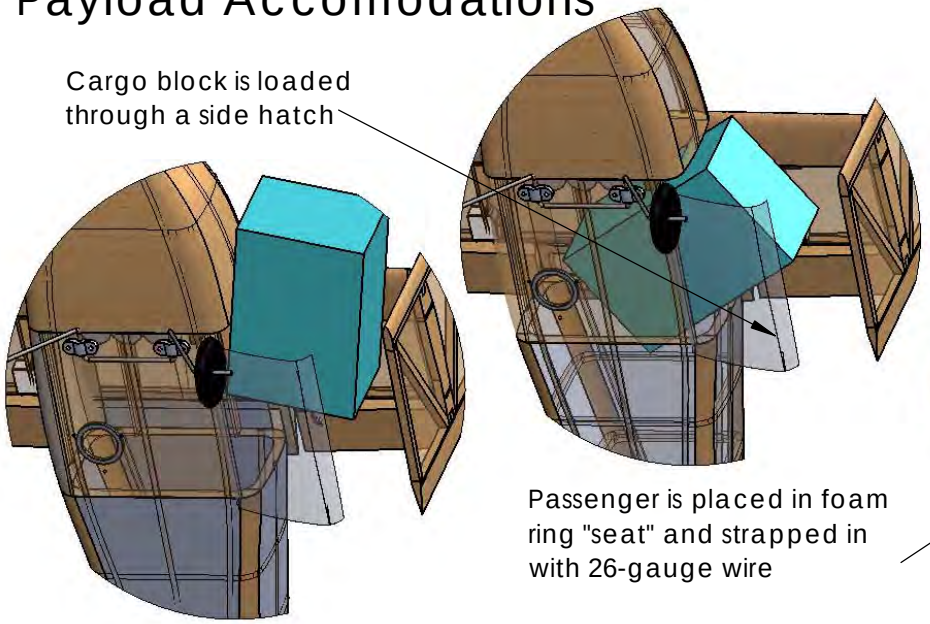

Passenger is placed in foam ring "seat" and strapped in with 26-gauge wire

Battery pack, speed controller, and reciever are loaded into the nose and fastened to floor using velcro

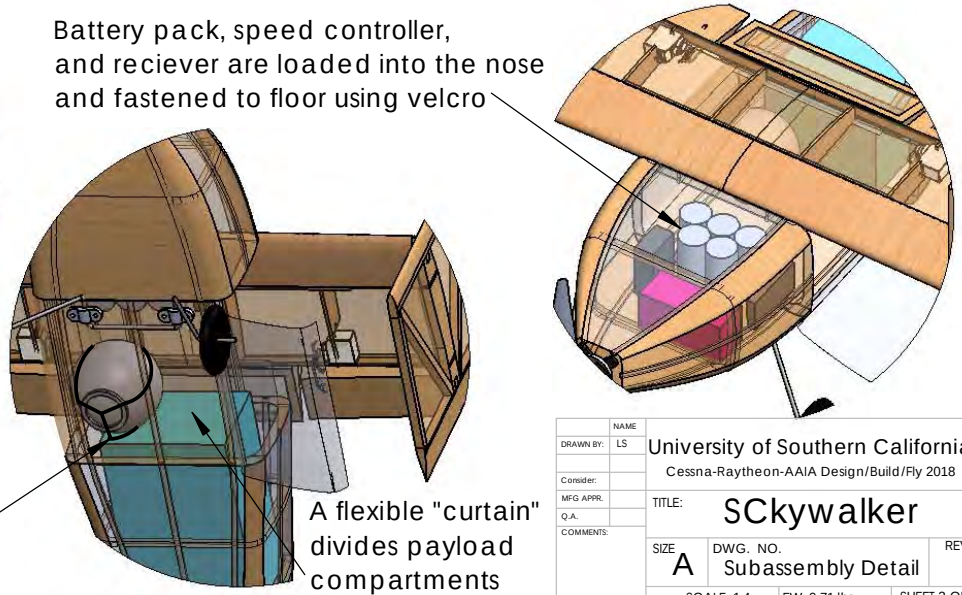

A flexible "curtain" divides payload compartments

	NAME
DRAWN BY:	LS
Consider:	
MFG APPR.	
Q.A.	
COMMENTS:	

University of Southern California
Cessna-Raytheon-AAIA Design/Build/Fly 2018

TITLE: SCkywalker

SIZE A | DWG. NO. Subassembly Detail | REV

SCALE: 1:4 | EW: 0.71 lbs | SHEET 3 OF 3

6.0 Manufacturing Plan

Numerous manufacturing processes were evaluated for each component of the 2018 competition, including the wing, fuselage, landing gear, passenger restraints, cargo blocks, and LRUs. The fabrication of each component was evaluated and selected as detailed in the following subsections.

6.1 Manufacturing Processes Investigated

In order to identify the best manufacturing process for each aircraft component, the team first considered the pros and cons of each technique.

6.1.1 Foam

Foam is relatively cheap and can be easily shaped using a hotwire foam cutter and sanding. Although nonstructural foam elements can be very lightweight, structural foam is often heavier than balsa and composite structures. The team has extensive experience building with foam to validate the sizing of a prototype aircraft, but often shifts toward balsa or composites later in the year to minimize plane weight.

6.1.2 Balsa Build Up

Balsa is the lowest density material used for construction of aircraft structures. Well-designed balsa structures can often be lighter than composite structures for smaller aircraft, as demonstrated by the historical success of balsa aircraft in previous AIAA DBF competitions. The accessibility of CAD software and laser cutters has made it simple to build lightweight balsa structures.

6.1.3 3D Printing

Additive manufacturing allows for the design of complex forms that would otherwise be impossible to build. The team has access to a Markforged Mark Two 3D printer that can create high-precision parts reinforced with fiberglass, carbon fiber or aramid fabric [14]. 3D Printing can be used for rapid prototyping of complex mechanisms and reducing lead times in making molds for composites.

6.1.4 Composites

Composites have high semi-isotropic strength to weight ratios. Additionally, composites are more durable and more easily repaired than other build methods. Building composites is expensive as a result of material costs and requires long lead times to prepare and cure parts.

6.2 Manufacturing Processes Selected

6.2.1 Wing and Tail Structure

The wing, tail, and end plates were constructed using a balsa built-up method to minimize weight. Figure 27 shows the overall wing design and fuselage fixtures for wing integration. The main spar is an I-Beam with 0.06 in. (0.2 cm) balsa shear web between 0.1 in. (0.3 cm) carbon fiber spar caps bonded with 15

minute epoxy. The balsa shear web was cut such that the grain ran at a positive and negative 45°. Six 0.06 in. (0.2 cm) balsa ribs were laser cut to the chosen airfoil shape and evenly spaced span-wise. The leading edge was covered with 0.03 in. (0.08 cm) balsa bent into a D-box. Once all the balsa parts were bonded with cyanoacrylate, the leading edge was covered with So-lite (not shown) to maintain an aerodynamic shape. The So-lite covered balsa ailerons at the trailing edge were then attached to the main wing structure using Flashbreaker tape as a simple hinge mechanism.

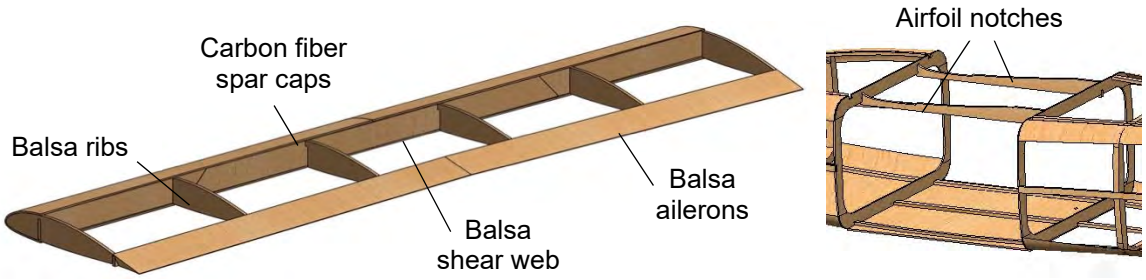

Figure 27: Balsa built-up wing with main components (left) and fuselage fixture for wing integration (right)

The wing-fuselage interface in Figure 27 utilized the tensile strength of balsa to distribute flight loads throughout the fuselage. The airfoil shape was laser cut into fuselage fixtures such that the airfoil's leading edge was coincident with the top of the fuselage. The inner two ribs were then attached to the fuselage fixtures using cyanoacrylate. The tail, shown in Figure 28, was manufactured and integrated in the same fashion as the wing.

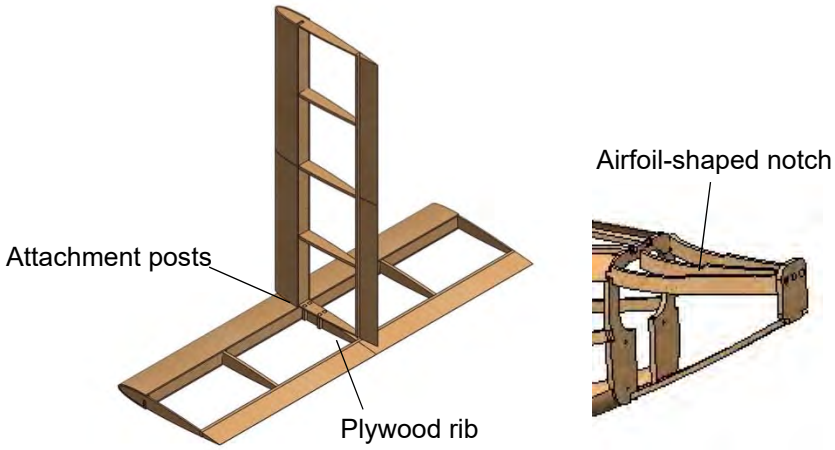

Figure 28: Balsa built-up tail with main components (left) and fuselage fixtures for tail integration (right)

6.2.2 Fuselage Structure

The balsa built-up method was chosen for the fuselage due to its high strength to weight ratio. The balsa fuselage was constructed from a combination of balsa and plywood cross-sections attached together with balsa stringers and sheeting as shown in Figure 29. Individual thicknesses were tailored and material was chosen for certain areas based on local loading conditions to balance the low weight and structural

integrity of the fuselage. The stringers and sheeting allowed for a more aerodynamic fuselage shape with the least amount of material. With laser cut balsa parts, more complex designs were implemented for balsa cross sections to take advantage of balsa's directional strength along the grain direction. The wing and tail fixtures also had the airfoil negative laser-cut to allow for those components to seat properly.

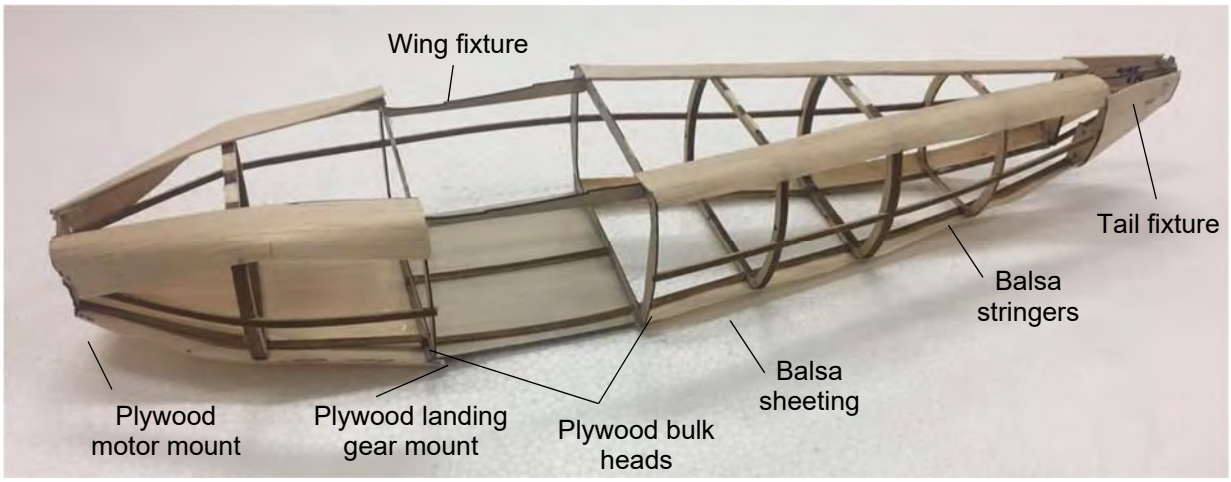

Figure 29: Balsa fuselage design

The assembly of the fuselage utilized the jig, shown in Figure 30. The jig aligned the bulkheads both laterally and longitudinally using protruding tabs, maintaining the desired spacing dimensions. The balsa stringers were then formed after soaking in water by bending them around the primary bulkheads. The fuselage was assembled with cyanoacrylate to keep the structural weight as low as possible. Once the 0.03 in. thick balsa sheeting was bonded onto the structure, it was then covered in So-lite which adhered to the sheeting around the fuselage corners to allow for a smooth corner with little So-lite deformity.

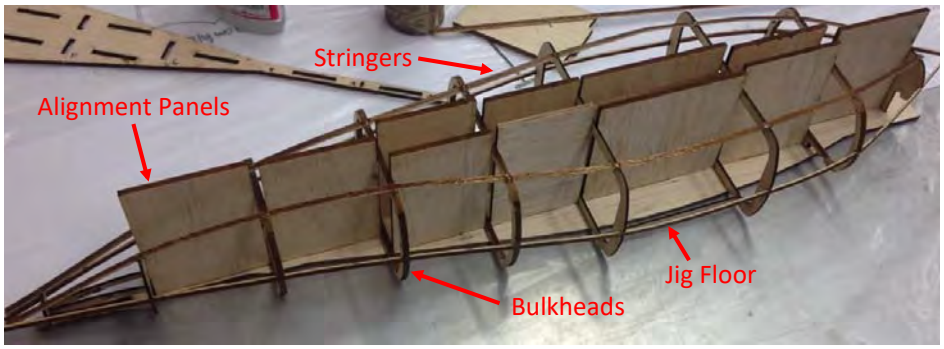

Figure 30: Jig used to align bulkheads and stringers for fuselage manufacturing

6.2.3 Landing Gear

The main bow gear was made out of 14 gauge bent wire due to its light weight compared to composites. A wire-bending jig was used to produce the main bow gear with precise angles. A 2.5" section of 20 gauge wire was cut for the tail gear and integrated into the fuselage with nylon bolts.

6.2.4 Passenger Restraints

Foam was chosen for the passenger seat due its nonstructural application, simplicity, and the low weight of foam. A 0.8 in. ring was fabricated and attached to the floor of the fuselage with Quik-Cure Epoxy for the passenger seat. To create a passenger restraint, three 26-guage wires were chosen for their high strength and low weight. The wires were threaded through the floor of the fuselage in a triangular shape and twisted together to secure the passenger.

6.2.5 Payload Blocks

In order to create lightweight cargo, the payload blocks were constructed using a two-part mold process. A skin of 0.10 kg/m^2 fiberglass and epoxy resin was laid up over a foam mold. Once the skin cured, the mold was removed, leaving a light, fiberglass box. In order to get the fiberglass box to the necessary weight, small washers are glued to the inside of the block.

6.2.6 Servo LRU

For a lightweight, reliable servo LRU, the servo for the wing is screwed into the second rib from the tip of each side of the wing. The servo sits in a notch in the rib as detailed in Figure 31 with the appropriate sized screws. For the tail surfaces, since the thickness of the airfoil is smaller than the wing's, the servo is slightly protruding above the rib. Since the servo protrudes on the lower surface close to the side of body, there is minimal lift and drag impacts. This design is shown in Figure 32 and is the same for both the horizontal and vertical stabilizers. Each servo is screwed into ribs that are made of 1/16" plywood.

Figure 31: Wing servo LRU

Figure 32: Tail Servo LRU

6.3 Manufacturing Milestones

A milestone chart was produced to stay on schedule and coordinate build between different subteams. Although the plan in Figure 33 only depicts the schedule for the aircraft prototype #5, the same scheduling was implemented for the construction of other prototype aircrafts and the competition aircraft. Lessons learned in the development of this aircraft were incorporated into the schedule for competition build. As shown, build and assembly requires upwards of four weeks to produce a high quality part. Simultaneous lab testing was conducted on the wing, tail, and fuselage, as detailed in Section 7.0 to ensure the aircraft would meet all load requirements once fully integrated.

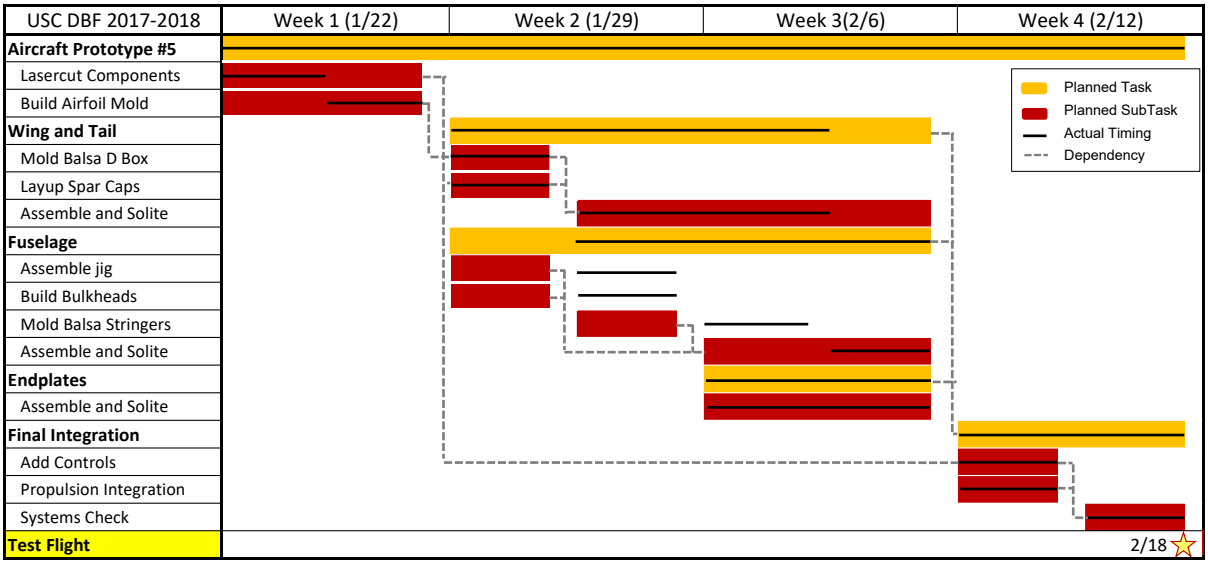

Figure 33: Aircraft manufacturing milestone chart showing planned and actual timing of objectives

7.0 Testing Plan

A test plan was implemented to verify propulsion, aerodynamic performance, stability and control and structural predictions. Experimental data was gathered both in the laboratory and at test flights. Testing occurred during the development of the aircraft to validate predictions and inform future design decisions. The test schedule is presented in Figure 34 and explored in further detail in Sections 7.1 through 7.4.

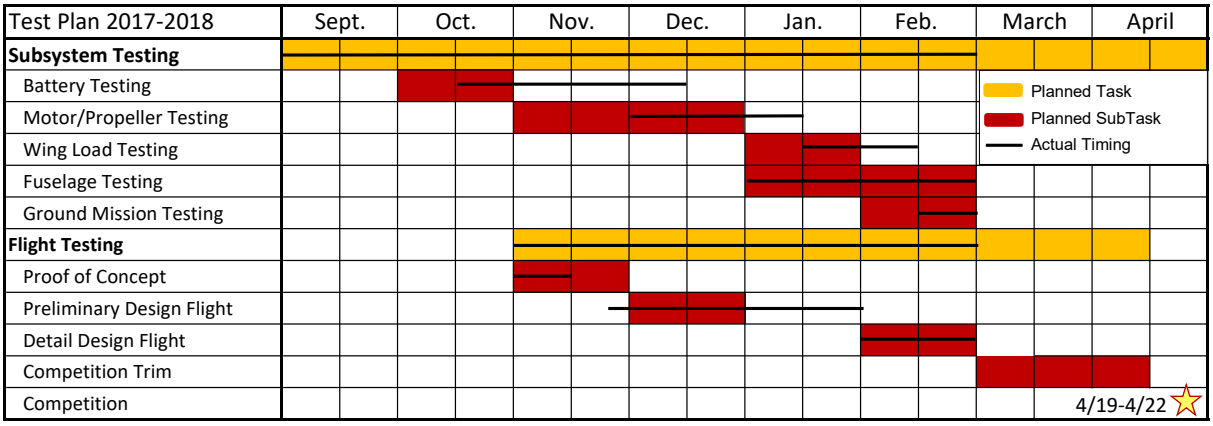

Figure 34: Testing plan for the 2017-2018 competition year

7.1 Test Objectives

Tests for each sub-team were conducted to ensure that the designed components perform adequately to meet all competition and design requirements.

Aerodynamics

- Flight tests were used to confirm AVL and XFOIL predictions
- Pilot feedback was used to verify that the aircraft's handling qualities were acceptable

Propulsion

- Static, wind tunnel, and flight tests were used to verify the expected performance of the system at both static and dynamic conditions
- Lab testing was conducted using a battery tester to characterize the discharge performance of assembled battery packs

Performance

- Flight tests were conducted to validate performance predictions provided by PlaneTools

Payloads

- Secure loading of the passenger and payload block were tested in flight
- The ground crew tested that the passenger could be loaded in the 5 minute window

Wing

- The aircraft was loaded to maximum takeoff weight and the wingtip test was performed to simulate technical inspection
- Failure points and deflections predicted in SparSizer were validated through wing loading tests

Fuselage

- Load testing was conducted to ensure the structure could withstand maximum design loads

Landing Gear

- Load testing was conducted to validate the expected deflection
- Ground handing tests ensured that the aircraft would track straight for takeoff

LRUs

- The team simulated the Ground Mission to verify the adequacy of the replaceable components

7.2 Subsystem Testing

7.2.1 Aerodynamics Testing

In order to validate the endplate and fuselage-interaction analysis performed with AVL and STAR-CCM+, the team performed wind tunnel testing on a 7.55 in. semi-span wing section with removable endplates and a fuselage fairing. The test model with these additions attached is pictured in Figure 35.

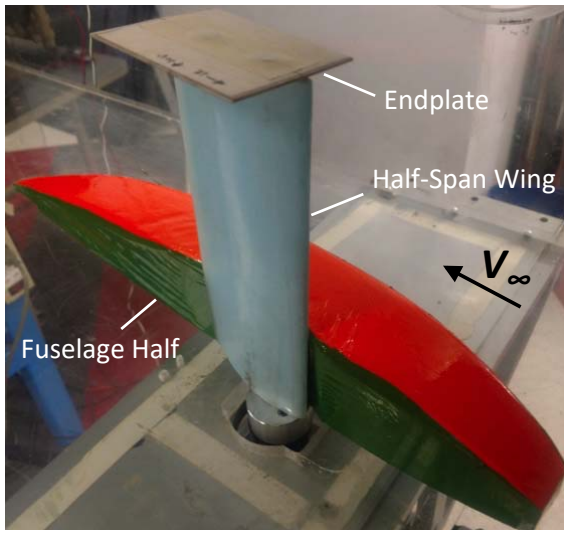

Figure 35: Semi-span wing model with fuselage fairing and endplate in $18'' \, x \, 18''$ cross-section wind tunnel

The tests were performed at the average predicted flight speed, $60 \, \mathrm{ft/s}$, for $-16° < \alpha < 24°$. The results are shown in Figure 42 (Section 8.1.1).

7.2.2 Propulsion Testing

Testing for propulsion consisted of two main objectives: characterize battery discharge rates and validate PlaneTools predictions via dynamic and static testing. Battery testing was conducted with the West Mountain Radio Battery Tester, which draws specified currents and logs the voltage of the battery packs over time [15]. The effective capacities of the battery packs were also measured at various current draws using the battery testing apparatus. The testing apparatus for the batteries can be found in Figure 36.

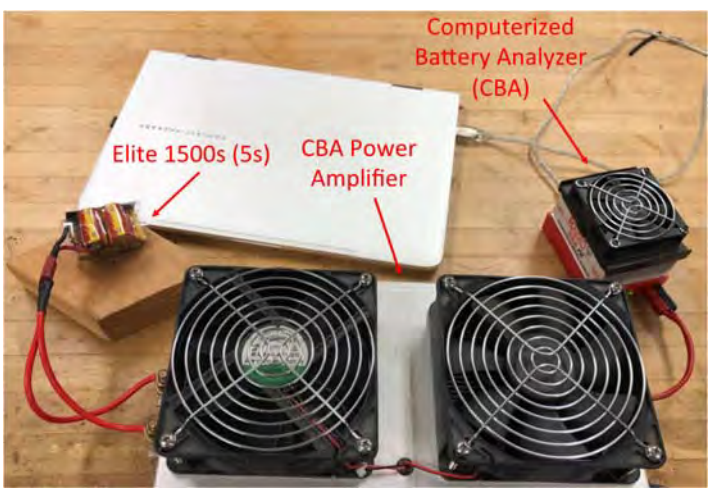

Figure 36: Battery discharge testing apparatus with a 5-cell Elite 1500 battery pack

Static motor testing was conducted using the RC Benchmark Dynamometer, which is capable of measuring values of thrust, current, RPM, and torque using an integrated Data Acquisition Board (DAQ) connected to various load cells [16]. An ESC is used to control the throttle setting of the attached motor

and propeller, as shown in Figure 37. The RC Benchmark Dynamometer was used to compare the static thrusts, currents, and torques generated by the propeller for various motors.

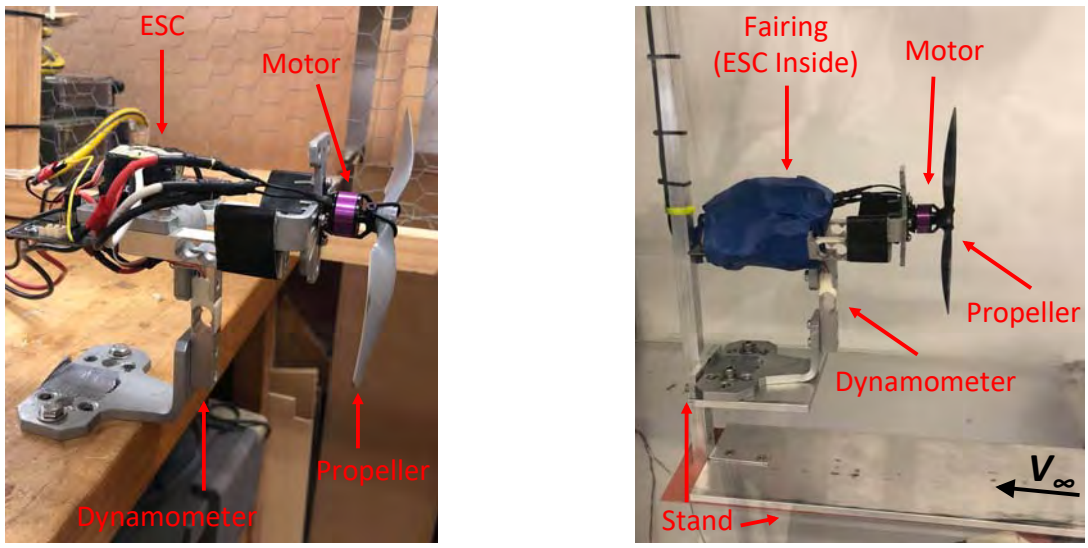

Figure 37: Side view of assembled dynamometer for static testing (left) and the wind tunnel testing (right)

To simulate dynamic conditions, the RC Benchmark Dynamometer was placed into a wind tunnel with a stand and fairing to determine the propulsion performance at a set air speed. The wind tunnel air speeds were defined by estimated cruise speeds predicted by PlaneTools. Data points collected from the dynamometer in the wind tunnel were validated with data collected from flight tests.

7.2.3 Structural Testing

Wing

Structural testing was performed on the balsa built-up wing to validate the ability to withstand maximum 5g lift loads without failure. The lift loading is simulated on the bottom of the half wing as shown on the left of Figure 38. To ensure that the wing design would pass the pre-flight tech inspection, the team loaded the aircraft to the maximum weight with payload (0.86 lbs.) and supported the aircraft at the wingtips. The wing tip testing is shown on the right of Figure 38.

Figure 38: Setup for load testing with ballast blocks (left) and wingtip testing (right)

Fuselage

The balsa fuselage underwent structural testing for 5g landing loads. A free-fall drop of 5 inches was assumed to be the worst-case landing situation. The testing setup before the drop is shown in Figure 39. The fuselage nose was also tested to validate ability to withstand in-flight motor torque. The pulley setup for mimicking counterclockwise motor torque is shown in Figure 40.

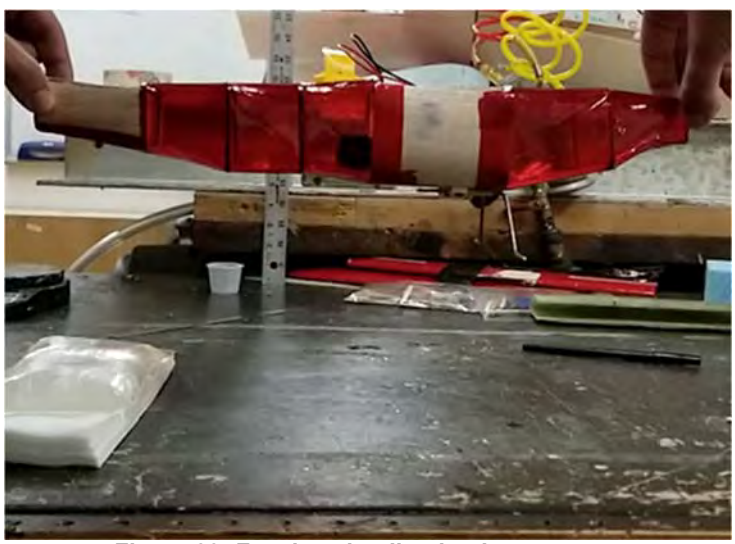

Figure 39: Fuselage landing loads test setup

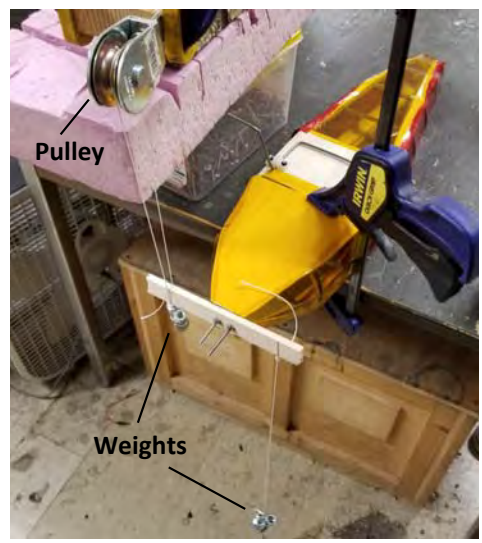

Figure 40: Fuselage torque test setup

7.2.4 Landing Gear Testing

The landing gear team ensured that the manufactured main and tail gear performed adequately by utilizing a test “mule” to simulate landing load cases and check ground handling before flight tests on a frame instead of the test plane. This setup is shown in Figure 41. The test mule allowed the team to alter fuselage length, wheel locations, incident angles, weight, etc. in order to simulate the aircraft design.

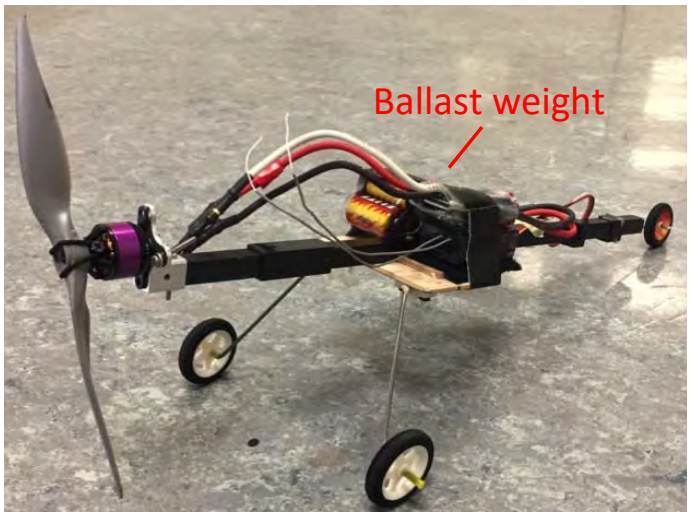

Figure 41: A landing gear test mule was designed for load testing and ground handling testing

7.3 Flight Test Schedule and Flight Plan

Flight tests were critical to the validation of the competition aircraft. Pilot feedback was used to determine aircraft stability, pilot workload, and the corresponding flight performance at different throttle settings and control inputs. Propulsion data was collected through a data-logging ESC that measures voltage, current, RPM and throttle position, which allowed the team to compare flight data to predictions.

The flight test schedule and objectives are displayed in Table 23. Each flight test had explicit design objectives that were used to incrementally validate the effectiveness of all aircraft subsystems. Flight test objectives that were not met were reattempted in subsequent tests. Note that there are upcoming test flights planned for February 25 and March 18.

Table 23: Flight Test Schedule

Date	Location	Objectives
Nov. 05, 2017	Sepulveda Basin, Van Nuys, CA	Determine minimum wing area required at takeoff
Dec. 10, 2017	Sepulveda Basin, Van Nuys, CA	Validate propulsion system sizing; Test lifting body and monoplane configuration
Jan. 14, 2018	Sepulveda Basin, Van Nuys, CA	Validate propulsion system sizing
Feb. 3, 2018	Sepulveda Basin, Van Nuys, CA	Determine minimum stable wingspan possible with endplates; Test LRU integration
Feb. 25, 2018	Sepulveda Basin, Van Nuys, CA	Test integrated competition aircraft; Record performance data
Mar. 18, 2018	Sepulveda Basin, Van Nuys, CA	Trim competition aircraft

Each flight test was separated into specific objectives, which included the acceptance criteria to ensure all objectives were met. A sample plan from the Nov. 5, 2017 test flight is shown in Table 24.

Table 24: November 05, 2017 test flight plan

Flight #	Flight Name	Payloads	Objectives	Acceptance Criteria
1	Trim Flight	50% PF	- Trim aircraft - Acquire power data	- Aircraft trimmed for level flight - Data acquired
2	Test with Flaps	50% PF	-Test flaps - Acquire power data	- Identify flap effects - Data acquired
3	Takeoff Test	50% PF	- Take off within 150 ft	- 150 ft TOFL requirement met
4	Cut Span	50% PF	- Determine minimum span to meet 150 ft TOFL requirement	- Minimum span to meet 150 ft TOFL requirement determined

7.4 Flight Checklists

The team adhered to a preflight checklist (Table 25) before each flight to ensure efficiency, proper data acquisition and team safety. It also serves as a final flight go or no-go evaluation criterion from the pilot. The on-site inspections checklist (Table 26) was used before and after each flight in order to ensure aircraft and crew safety. The inspection of each category of components allows for the systematic division of duties for aircraft inspection and maintenance.

Table 25: Pre-flight checklist

Component	Task
Fuselage (internal)	Secure and connect the fully charged battery Receiver has all connections plugged in and secured Load payloads (if applicable) CG aircraft
Fuselage (external)	Close and` secure all external hatches
Pilot's Checks	Check all` control system with receiver Motor run-up/Go No-Go decision

Table 26: Aircraft inspection checklist

Component	Items to Inspect	Discrepancies
Motor	☐ Motor mount and all fasteners ☐ Fuselage around motor mount free of cracks or fractures ☐ Motor is free of debris and damage to casing ☐ Propeller shaft is straight ☐ Propeller is fastened to shaft properly ☐ Propeller is free of damage	
Fuselage	☐ Battery is secure to fuselage and connected ☐ Receiver is connected and secure ☐ Speed-controller is secure and connected ☐ Servo wires are secure ☐ Fuselage is secure and free of debris Fuse` connectors secured (internal and external) ☐ Payload restraints secured and ready for loading (if applicable)	
Wing	☐ Wing is free of tears, cracks, and fractures ☐ Servo arms are secure with minimal play Control` surfaces are secure and free of obstructions ☐ Fuselage around wing mount is free of cracks and fractures ☐ Wing is securely mounted to fuselage	
Landing Gear	☐ Wheels spin freely and are secure ☐ Torsional stiffness of gear ☐ Landing gear mount is secure ☐ Fuselage is free of cracks and fractures around mount	
Tail	☐ Tail gear is functioning properly ☐ Free of tears, cracks, and fractures ☐ Servo arms are secure Control` surfaces are secure and free of obstructions ☐ Fuselage around tail mount is free of cracks ☐ Tail is securely mounted to fuselage	
Control Surfaces	☐ Check all control surface motion using transmitter Control` surfaces move freely without obstructions	

8.0 Performance Results

Predictions made during the Detail Design phase were compared to aircraft subsystem performance. Key subsystems were tested in lab and during flight tests to ensure each component performed as predicted.

8.1 Demonstrated Performance of Key Subsystems

8.1.1 Aerodynamics

In order to validate the endplate and fuselage-interaction analysis, the team performed wind tunnel testing. The lift-curves for the model configurations with and without endplates (detailed in Section 7.2.1) are shown in Figure 42.

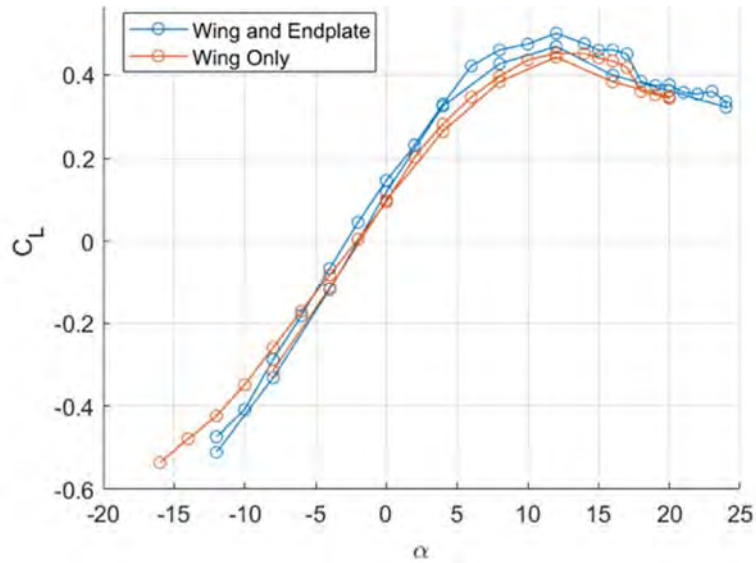

Figure 42: Wind tunnel results, C_L vs α curves of a 7.55 in. semi-span wing with and without endplate

The lift coefficients were lower than expected, as shown above; for instance, test flights with a known weight (W), dynamic pressure (q), and wing area (S) suggest $C_L = \frac{W}{qS} = 0.56$ was obtained for level cruise conditions. However, the trends remain consistent with predictions. Additionally, data gathered for the fuselage and wing configuration was corrupted from interference between the fuselage and force balance.

As predicted, the endplates have an overall positive effect on the lift of the wing. The increase in lift coefficient (ΔC_L) values correlate well with expected values from a lifting line analysis based on the AR and AReff of the wing with and without endplates. The expected ΔC_L at 4° was 0.03 and the wind tunnel ΔC_L was slightly higher at 0.04. As the aircraft design is further refined, additional wind tunnel testing will be performed to better understand the aerodynamic effects of the fuselage and endplates on the aircraft.

8.1.2 Propulsion

Battery tests were conducted to measure the time until battery pack voltages fell below the 5 V cutoff for the ESC. The capacity tests, shown in Figure 43, compared the maximum flight times for the 2/3 AA 650s and the Elite 1500s at the current drawn for the propulsion package.

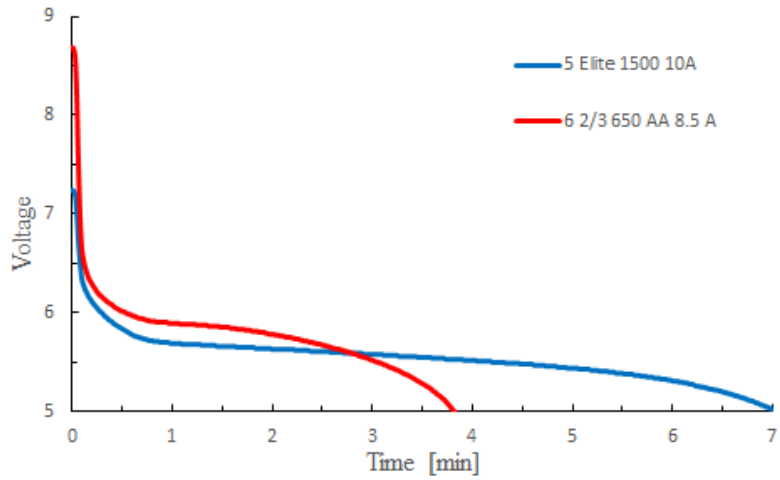

Figure 43: Voltage vs. time graph of 5 Elite 1500s at a 10 A current draw (blue) and 6 2/3 650s at an 8.5 A current draw (red)

The 2/3 AA 650s were drawn at 8.5 A, the dynamic current predicted by PlaneTools, while the Elite 1500s were tested conservatively at 10 A until the 5 V ESC cut-off occurred. Due to the higher internal resistance and the lower discharge rate of the 2/3 AA 650s, the 6-cell pack dropped to a voltage comparable to the 5-cell pack for the Elite 1500s. Based on the predicted cruise speeds from PlaneTools for these two battery packs, an estimated mission time of 2.6 minutes was calculated.

In addition to PlaneTools predictions, wind tunnel testing was conducted to simulate flight conditions to help determine the performance of the propulsion package in flight. The critical design propulsion package was placed onto the apparatus in Figure 37 and was tested at air speeds (55 ft/s-70 ft/s) similar to the predicted cruise speed. Wind tunnel testing results are shown in Table 27.

Table 27: Wind tunnel testing results for the critical design propulsion package

Hacker A10-7L (2200 KV)	60 ft/s Air Speed	70 ft/s Air Speed
Propeller	APC 7x5 E	APC 7x5 E
Battery Pack	Elite 1500s (5s)	Elite 1500s (5s)
Dynamic Thrust [lbf]	$0.25 \pm .01$	$0.18 \pm .03$
Dynamic Current, I_{crz} [A]	$8.9 \pm .1$	$8.1 \pm .1$
Dynamic RPM	9500 ± 100	10000 ± 100

During the flight tests on February 3rd, the number of 2/3 AA 650 cells was increased from 6 to 7 in an effort to increase performance; however, the increased current draw resulted in a harsher voltage drop, resulting in similar performance to the 5-cell Elite 1500s, as shown in Table 28.

Table 28: 2/3 AA 650s and Elite 1500s flight test comparisons

Hacker A10-7L (2200 KV)	Elite 1500s (5s)	2/3 AA 650s (7s)
Propeller	APC 7x5 E	APC 7x5 E
Static Current, I_{max} [A]	11.5 $\pm$ .1 A	11.2 $\pm$ .1 A
Static Thrust [lbf]	0.56	0.63
Cruise Current, I_{crz} [A]	9.1 $\pm$ .5	9.5 $\pm$ .5
Dynamic RPM	9300 $\pm$ 200	9100 $\pm$ 100
Cruise Speed [ft/s]	59 $\pm$ 3	62 $\pm$ 6
Battery Pack Weight [lbf]	0.25	0.21

The wind tunnel data for the 60 ft/s test (Table 27) was validated as it matched the corresponding Elite 1500 flight data (Table 28). While the 2/3 AA 650s were determined to have higher static and dynamic performance, their capacity rendered them unreliable for completing all missions in the predicted 19 ft/s winds at Wichita, resulting in the selection of the Elite 1500s for the competition propulsion package.

8.1.3 Structures

To validate the design of the wing and fuselage, the team conducted load testing that simulated in-flight and landing loads. Table 29 lists the structural testing performed as described in Section 7.2 as well as the results of each test. The wing lift test was conducted to failure. The fuselage landing and motor torque tests were not conducted to failure because the test loads far exceeded any in-flight or landing loads.

Table 29: Results of structural testing on the wing and fuselage

Test	Expected Load Limit	Actual Load Limit
Fuselage landing	4.4 lbf	8.8 lbf
Fuselage motor torque	0.06 lbf-in	2.1 lbf-in
Half Wing Lift	2.2 lbf	14.2 lbf

The wing failed at the point of integration between two shear web pieces, as shown in Figure 44; however, it failed far past its expected loading. Figure 45 shows an early iteration of the fuselage, which failed due to bending from a tail landing during testing. In subsequent fuselage iterations, balsa sheeting was added in the tail arm to avoid this failure mode. Though the fuselage was overbuilt, any decrease in structure could not be reduced further without compromising material handling.

Figure 44: Shear web failure at integration point

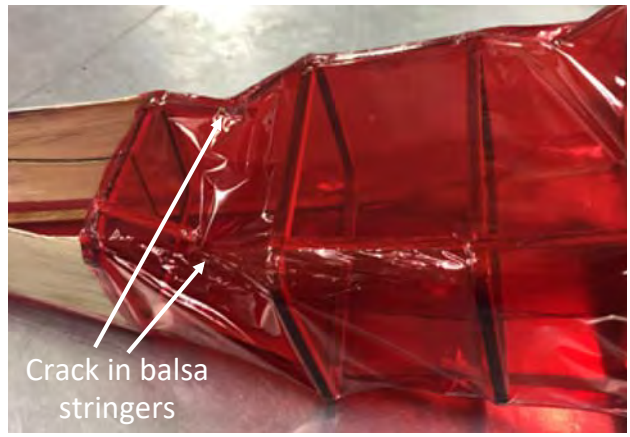

Figure 45: Fuselage failure in tail arm

8.2 Demonstrated Flight Performance of Completed Aircraft

Several test flights were carried out to validate predictions of aircraft performance. The goal of these flights was to evaluate the performance and capabilities of the detail design aircraft. Table 30 summarizes the flights to date as well as future flight test plans.

Table 30: Aircraft Performance evaluation from test flights

Date	Description	Problems	Solutions
Nov. 05, 2017	- Determine preliminary wing sizing	- Wingtip stall on landing	- Implement 2° of twist into wing
Dec. 10, 2017	- Propulsion sizing	- Pitch stability problems	- Smooth fuselage to prevent washing out tail - Increase tail area
Jan. 14, 2018	- Propulsion sizing	- Tip stall during turns/landing	- Increase wing twist to 5°
Feb. 3, 2018	- Wingspan sizing with endplates	- Landing gear preventing straight takeoff	- Increase wheel track - Reduce toe in
Feb. 25, 2018	- Simulate Missions	--	--
March 18, 2018	- Competition Trim	--	--

As shown, two test flights were repeated (Dec. 10, Jan. 14) as a result of pitch instability that caused the plane to stall and crash. Considerable effort was taken to reshape the fuselage to prevent the fuselage wake from washing out the tail. Additionally, multiple tail parameters were adjusted to ensure adequate elevator control for the pilot. The team successfully completed two out of three missions at its February 3rd test flight and the comparison of these flights to predictions is shown in Table 31.

Table 31: Comparison of predicted and flight-validated performance characteristics

	Parameter	Predicted	Flown	Δ %
M_1	**Flight Speed**	72 ft/s (22 m/s)	--	--
	Cruise Current	8.2 A	--	--
M_2	**Flight Speed**	70 ft/s (21 m/s)	59 ft/s (18 m/s)	-15 %
	Cruise Current	8.3 A	9.3 A	12 %
	T_{USC}	156 s	180 s	15 %
	$N_{PAX,M2}$	1	1	--
M_3	**Flight Speed**	70 ft/s (21 m/s)	59 ft/s (18 m/s)	-15 %
	Cruise Current	8.3 A	9.3 A	12 %
	N_{Laps}	6	--	--
	$N_{PAX,M3}$	1	1	--
	W_{Cargo}	2 g	3.08 g	0%

As shown above, predicted flight speeds are -15% lower on average and cruise currents are consistently higher than predicted. The difference between predicted and actual cruise velocity can be attributed to several factors, including the lack of headwinds at the California test location and simplifying assumptions made in the model for propeller efficiency. These results were used to improve the fidelity of the PlaneTools model and refine theoretical predictions. The team has currently completed the aircraft for the February 25 test flight and expects to complete all missions at this test flight.

Figure 46: A successful flight test on February 3 at Sepulveda Basin, Van Nuys, CA.

9.0 BIBLIOGRAPHY

[1] USC AeroDesign Team, "Aircraft Design Report, 2017 AIAA DBF Competition," 2017.

[2] USC AeroDesign Team, "Aircraft Design Report, 2011 AIAA DBF," 2011.

[3] USC AeroDesign Team, "Aircraft Design Report, 2013 AIAA DBF Competition," 2013.

[4] D. P. Raymer, in Aircraft Design: A Conceptual Approach, Reston, Virginia, AIAA, 1999, p. 78

[5] P. Carpenter, "R/C Airplane World," [Online]. Available: http://www.rc-airplane-world.com/watts-per-pound.html. [Accessed February 2018].

[6] A. P. P. Data. [Online]. Available: http://www.apcprops.com. [Accessed January 2018].

[7] Aerovironment, Inc., "Unmanned Aircraft Systems," 2016. [Online]. Available: https://www.avinc.com/uas/view/switchblade. [Accessed 17 September 2016].

[8] S. Hoerner and H. Borst, “Fluid Dynamic Lift,” Bricktown, NJ, 1975.

[9] S. Hoerner, "Fluid Dynamic Drag," Bricktown, NJ, 1965.

[10] M. Page, "Model Airplane Cook-book," 2008.

[11] L. Nicolai and G. Carichner, “Fundamentals of Aircraft and Airship Design: Vol. 1,” Reston, VA, AIAA, 2010.

[12] MIL-F-8785C, Flying Qualities of Piloted Planes, Military Specification, 1980.

[13] Dassault Systems, "Solidworks," [Online]. Available: http://www.solidworks.com/. [Accessed January 2018].

[14] Markforged, Inc., "THE MARK TWO," 2018. [Online]. Available: https://markforged.com/mark-two/. [Accessed January 2018].

[15] West Mountain Radio, "CBA IV - Computerized Battery Analyzer," 2018. [Online]. Available: http://www.westmountainradio.com/product_info.php?products_id=cba4. [Accessed January 2018].

[16] Tyto Robotics, "Dynamometer Series 1580," 2018. [Online]. Available: https://www.rcbenchmark.com/product/rcbenchmark_dynamometer/. [Accessed January 2018].

Clarkson University KnightHawks

Design-Build-Fly Team

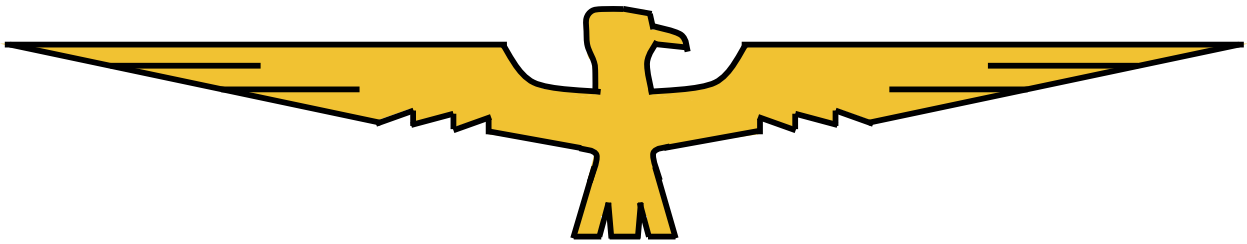

AIAA Design-Build-Fly Competition

Design Report

February 22, 2018

Table of Contents

Acronyms, Abbreviations, and Symbols 4

1.0 Executive Summary 5

2.0 Management Summary 6

2.1 Team Organization 6

2.2 Milestone Chart 8

3.0 Conceptual Design 8

3.1 Mission Requirements 8

3.2 Design Requirements 11

3.3 Configuration Selection 15

3.4 Configuration Refinement 18

3.5 Final Conceptual Design 20

4.0 Preliminary Design 20

4.1 Design Methodology 20

4.2 Mission Model 21

4.3 Preliminary Sizing 21

4.4 Aerodynamics 23

4.5 Stability and Control 24

4.6 Performance Estimates 26

5.0 Detail Design 27

5.1 Dimensional Parameters Table 27

5.2 Material Characteristics and Capabilities 28

5.3 Structural Design Selected 29

5.4 Sub-System Design and Integration 30

5.5 Weight and Mass Balance 37

5.6 Flight and Mission Performance 38

5.7 Drawing Package 39

42

6.0 Manufacturing Plan 44

6.1 Manufacturing Methods Considered 44

6.2 Manufacturing Methods Selected 44

6.3 Manufacturing Milestone 45

7.0 Testing Plan 45

7.1 Test Objectives 46
7.2 Subsystem Testing 47
7.3 Flight Test Schedule and Flight Plan 48
7.4 Flight Checklists 49
8.0 Performance Results 50
8.1 Demonstrated Performance of Key Subsystems 50
8.2 Demonstrated Flight Performance of Completed Aircraft 53
Bibliography 55

Acronyms, Abbreviations, and Symbols

Description	Acronym
Design Build Fly	DBF
American Institute of Aeronautics and Astronautics	AIAA
Unmanned Aerial Vehicle	UAV
Computer Aided Design	CAD
Figures of Merit	FoM
Max Empty Weight	EWmax
Stability Augmentation System	SAS
Length	L
Wingspan	b
Coefficient of Lift	$C_{"}$
Coefficient of Drag	$C_{\#}$
Rated Aircraft Cost	RAC
Zero Angle Coefficient of Lift	C_{Lo}
Coefficient of Moment	C_m
Electronic Speed Controller	ESC
Vertical Tail Volume Ratio	$V_{\%}$
Line Replaceable Unit	LRU
Nickel-Metal Hydride	NiMH
Acrylonitrile Butadiene Styrene	ABS
Remote Control	RC
Center of Gravity	CG
Mission 1	M1
Mission 2	M2
Mission 3	M3
RPM per Volt	KV

1.0 Executive Summary

The objective of the 2017-2018 American Institute of Aeronautics and Astronautics (AIAA) Design/Build/Fly (DBF) competition this year was to design and manufacture a dual purpose regional “jet” aircraft[1]. The aircraft must be capable of carrying both passengers (bouncy balls) and payload (weighted blocks) on three different flight missions that test the range, speed, and capacity of the aircraft in various configurations. The aircraft will also be evaluated on its performance in one ground mission where line replaceable units (LRUs) must be removed and replaced in a timely manner. The flights of the aircraft are to take place in Wichita, Kansas and will require the aircraft to demonstrate its payload carrying ability across three flights of differing duration.

For the first mission (M1), the aircraft must take off in 150 ft with no payload completing three laps in under five minutes. Mission 2 (M2), will consist of three laps under five minutes with the maximum number of passengers it is capable of carrying, which is declared during technical inspection. The passengers, represented by bouncy balls, will be sized by choosing randomly from a uniform distribution of five sizes. The passengers will vary in diameter from 27mm to 49mm and in weight from 0.4ozs to 2.39ozs. Each passenger must have its own seat with an individual restraint system. For the third mission (M3), the aircraft will fly as many laps as possible carrying at least half of the passengers carried in M2 with a team determined payload in under ten minutes. The ground mission consists of two stages where tools must be stored inside the aircraft (Stage 1) and outside the aircraft in a designated area (Stage 2). In each stage, certain aircraft components are eligible to be removed and the selected part is chosen based on the roll of a die.

After analyzing overall scoring, it was concluded that minimizing the rated aircraft cost (RAC) through weight and wingspan was the highest priority. This takes precedence over the flight mission performance, which will not significantly impact the final score. Because of its high priority, the goal during the design phase was to limit RAC while still maintaining an aircraft capable of flying all 3 missions.

The flying wing was considered the most appropriate aircraft for its small wingspan and large internal volume. It allowed for the use of foam construction, which is lighter, cheaper, and easier to manufacture than the balsa or composite alternatives. Leading and trailing edge foam spars allowed for greater than necessary strength in wing bending and torsion, while opening up the interior for a passenger cabin, payload tray, and electronics bay. The aircraft is controlled via solid foam elevons and flight tests have shown the control authority in both roll and pitch to be more than satisfactory. Additionally, the plane uses a receiver with a built in Stability Augmentation System (SAS), which allows for increased stability and higher flight speeds due to fewer large and inefficient pilot corrections. The plane has a single vertical tail with no controllable rudder to save weight by elimination of a servo. The passenger area is on the same level as the payload bay, but to the front left of it, adhering to the requirements in the rule set. The motor

is mounted ahead of the leading edge on a balsa boom to allow for a more stable center of gravity (CG) location.

Clarkson University's aircraft, the *Knighthawk* (Figure 1), maximizes score by being the lightest and smallest aircraft possible, as determined by the design team, that is capable of completing all three flight missions. *Knighthawk* will fly M2 with a single passenger for three laps in 190 seconds. It will fly Mission 3 carrying one passenger and one ounce of payload for a single lap in approximately 60 seconds. *Knighthawk* has a wingspan of nine inches and an empty weight of .5 pounds for an RAC of 4.5

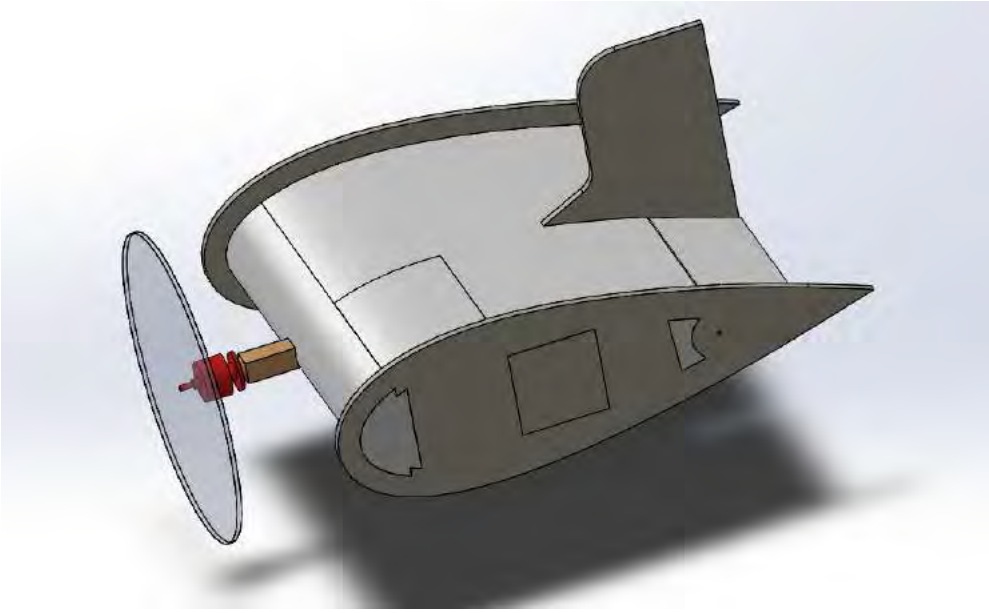

Figure 1 - *Knighthawk* in Flight Configuration.

2.0 Management Summary

2.1 Team Organization

The 2017-2018 Clarkson University Design Build Fly team consists of thirteen students participating on an extracurricular basis. Two members of the team are seniors, while the remaining eleven are juniors and underclassmen. The team is completely student-led but suggestions and guidance was given by faculty members and DBF alumni at design reviews. The leadership of Clarkson University DBF is divided into the executive board and the engineering design leads as shown in Figure 2.

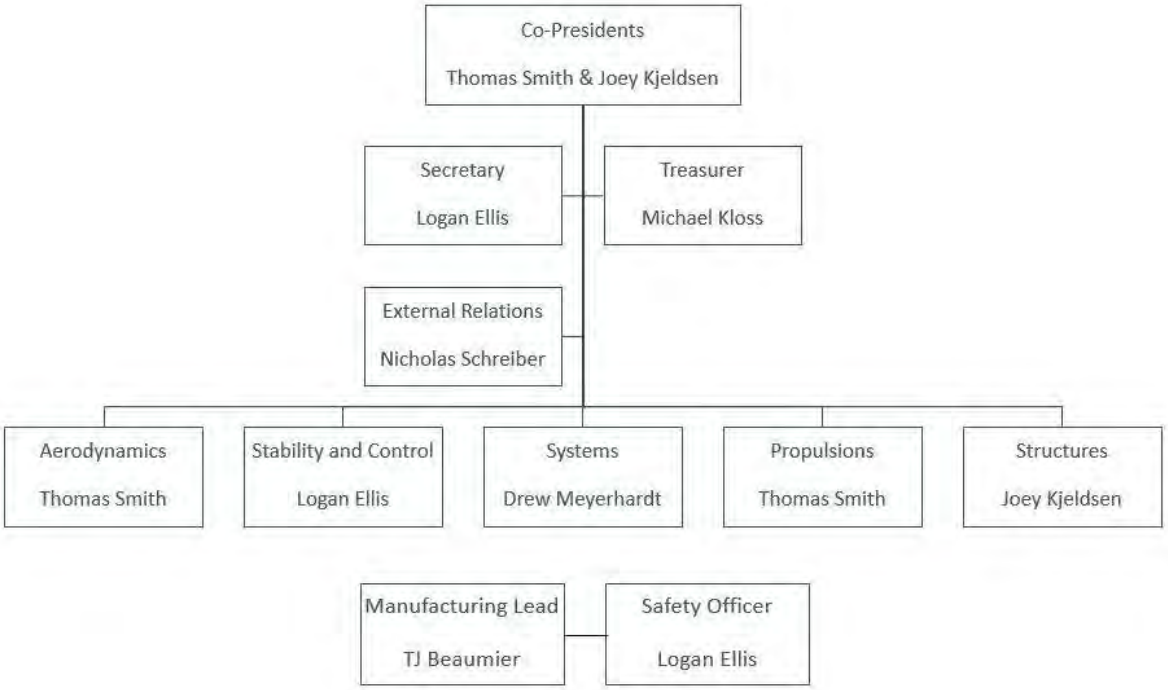

Figure 2 - Management Chart

The executive board consists of the two Co-Presidents, a Secretary, a Treasurer, and an External Relations & Event Planning Manager. The Co-Presidents serve as advisors and administrative leads by overseeing the design and build processes, advising team members on both technical and logistical matters, along with managing deadlines. The Secretary manages the DBF mailing list that notifies members of upcoming meetings, along with managing and organizing DBF shared files in our online storage. The Treasurer manages the DBF budget and orders components and materials required to manufacture the aircraft. The External Relations & Event Planning lead manages industry connections and sponsorships, as well as organizes the travel plans required to get to the competition in April.

The engineering design leads each manage a particular subsystem in the aircraft - Structures, Aerodynamics, Systems, Propulsions, and Stability & Control. The design team leads work with members to manufacture their subsystem, and work with each other to integrate the subsystems into a complete aircraft. Weekly meetings are held where the engineering design leads update the team on the status of their subsystems, and proposed changes are pitched by team members working on that system. Ideas that are met with no objections are worked into prototypes and any conflicting ideas are debated by the team. All final calls for the design are decided by the Co-Presidents.

2.2 Milestone Chart

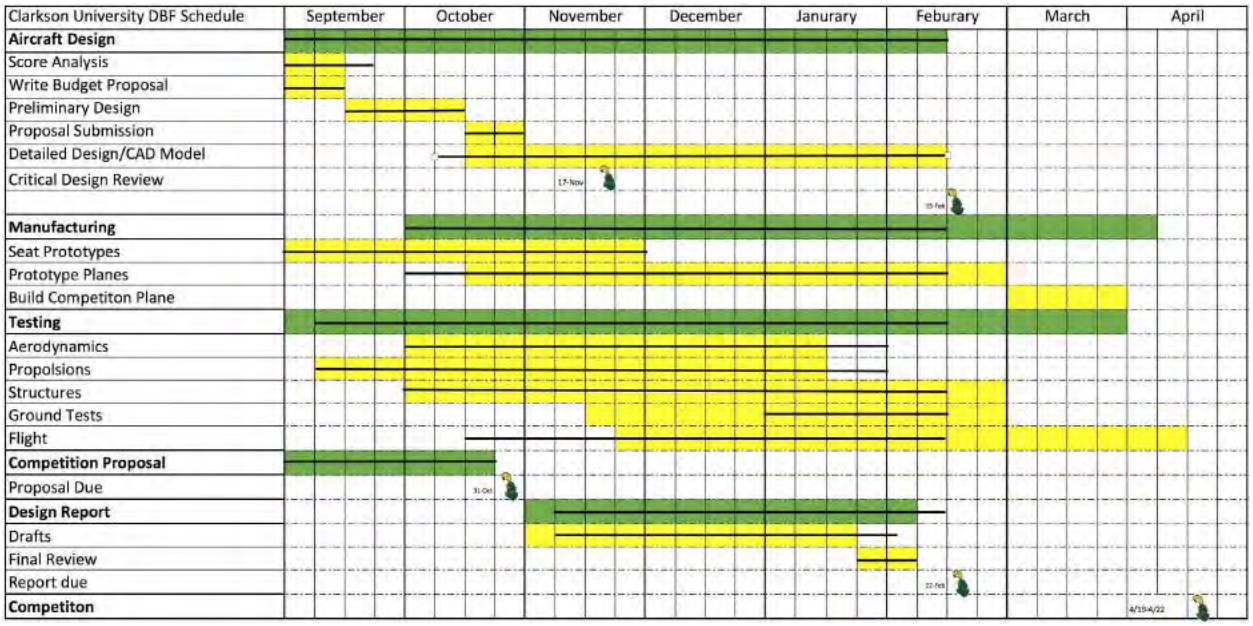

Figure 3 - Master Schedule showing current progress against planned timing

Shown above is the Gantt chart that was created and used to help the team meet its deadlines on time. The black lines through the highlighted boxes represents the team's progress and the green knight logos mark the dates of important milestones that need to be met.

3.0 Conceptual Design

The conceptual design phase consisted of analyzing the ruleset and scoring equations to decide on a set of design parameters for the competition plane. There were three main configurations considered based off of the need to minimize wingspan, an aspect that stood out in the scoring.

3.1 Mission Requirements

For the 2017-2018 DBF competition, the rules and requirements set by the AIAA simulate a dual purpose regional and business aircraft. The three flight missions and single ground mission are designed to test the vehicle's ability to transport payload as well as passengers, while having functional line replaceable units (LRUs) and maintaining a reasonable efficiency. The mission requirements were used in conjunction with the design requirements to optimize the aircraft for a high score.

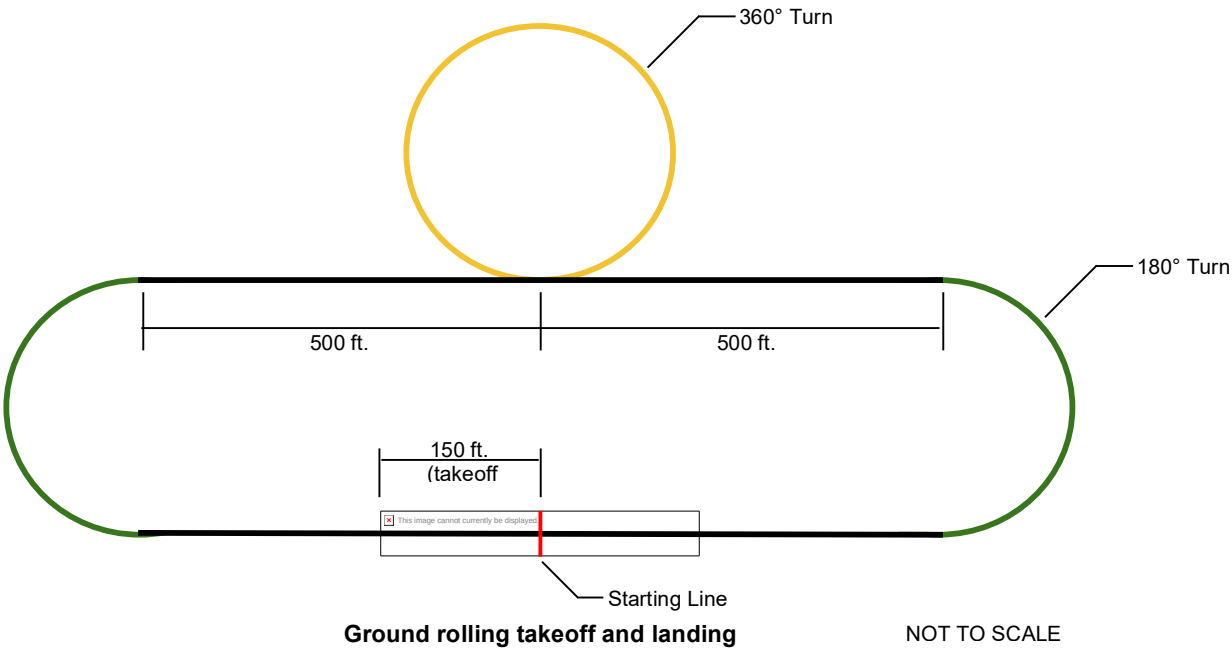

Figure 4 - AIAA Competition Course Layout

3.1.1 Scoring Summary

The total score for the 2018 Competition is given by Equation 1

$$Total\ Score = \frac{Written\ Score * Total\ Mission\ Score}{Rated\ Aircraft\ Cost} \qquad \text{(Eq. 1)}$$

The written score is determined as a grade on the design report. The mission score is the sum of the scores obtained on the three flight missions. The equation for total mission score is shown below in Equation 2.

$$Total\ Mission\ Score = M_{;} + M_{=} + M_{>} \qquad \text{(Eq. 2)}$$

The rated aircraft cost is a function of the plane's empty weight (EW) and the wingspan (b). The equation for RAC is given below by Equation 3.

$$RAC = EW * b \qquad \text{(Eq. 3)}$$

3.1.2 Mission 1: Demonstration Flight

For the first mission, the objective is to complete three laps within the five minute designated flight window with no payload; landing is not considered to be part of the five minute time window. Time starts when the aircraft throttle is advanced for the first take-off attempt and stops when the aircraft passes over the start/finish line in the air. Take-off must occur within the prescribed field length and the aircraft must

complete a successful landing in order to score points. The scoring is pass/fail and shown below in Equation 4.

$$M_1 = 1.0 \text{ for successful mission} \qquad \text{(Eq. 4)}$$

3.1.3 Mission 2: Short Haul of Max passengers

The objective of the second mission is for the aircraft to complete three laps within five minutes with the payload being passengers. The aircraft may carry any number of passengers, but the amount flown with cannot exceed the maximum number of passengers declared at tech inspection. The passengers must be carried internally and takeoff must occur within the prescribed field length of 150ft. Time starts when the aircraft throttle is advanced for the first take off attempt and will stop when the aircraft passes over the start/finish line in the air at the end of the third lap. The landing is not included in the five minute window; however, the aircraft must have a successful landing to get a score. Exact scoring is shown in Equation 5 below.

$$\mathbf{M_2} = 2 * \left(\frac{B_C\,(\#EFGGHIJHKG/MNH)}{QFR_C\,(\#EFGGHIJHKG/MNH)}\right) \qquad \text{(Eq. 5)}$$

Where Max_(#passengers/time) is the highest #passengers/time score of all teams

3.1.4 Mission 3: Long Haul of Passengers and Payload

Mission three simulates a long haul of both passengers and payload. The aircraft must carry passengers and payload internally. Half of the passengers from Mission 2 must be carried, as well as at least one payload block, but no more than the maximum number declared at tech inspection. The optimal score would result from the most laps completed in the ten minute window, while carrying as many passengers and payload as possible. Timing is the same as for the previous missions and a successful landing is required. The M3 score is given below by Equation 6.

$$\mathbf{M_3} = 4 * \left(\frac{B_C\,(\#EFGGHIJHKG*MSMFTEFUTSFV(SW)*\#TFEG)}{QFR_C\,(\#EFGGHIJHKG*MSMFTEFUTSFV(SW)*\#TFEG)}\right) + 2 \qquad \text{(Eq. 6)}$$

Where Max_(#passengers * total payload (oz) * #laps) is the highest (#passengers * total payload (oz) * #laps score for all teams

3.1.5 Ground Mission: Field and Depot LRU Replacement:

The ground mission must be successfully completed before attempting Flight Mission 2. This mission consists of a removal and replacement of two LRUs chosen at random with rolls of a single six sided die. There are 2 stages to this mission. Both stages must be completed within eight minutes, and after completing Stage 1, teams will immediately continue onto stage 2. Stage 1 consists of Field LRU Replacement, this must be completed in three minutes and the Replacement LRU and tools must start

within the payload bay prior to rolling the die. Stage 2 is the Depot LRU Replacement. All replacement LRUs and tools will start in the designated area. Tools are not required to start the aircraft and if a spare is not available, a team may remove the LRU, place it in a designated area and then reinstall it onto the aircraft. Two team members and a pilot may participate in the Ground Mission and only the team members can touch the aircraft. The aircraft must be flight ready at the start and finish of the Ground Mission. Successful completion of each Ground Mission stage will include the functional demonstration of replaced parts.

3.1.6 Additional Mission Requirements

In addition to the payload and range requirements for each mission, there are additional criteria that all aircraft must comply with to be eligible for competition. The aircraft must pass the wing tip load test with the largest payload intended to fly. The demonstrated maximum load will be recorded and cannot be altered after completing tech inspection. In addition, all flight missions must be flown in order. A new mission cannot be started until a team has obtained a successful score for the preceding mission. Flight Mission 1 and the Ground Mission can be completed in either order, but Flight Mission 2 cannot be attempted until Flight Mission 1 and the Ground mission are both successfully completed. For each mission, all passengers and payload blocks must be secured sufficiently as to assure a safe flight.

General mission specifications include that the aircraft propulsion system(s) must be “safed” (fuse or arming plug removed) during any time when crew members are preparing/handling the aircraft. Flight altitude must be sufficient for safe terrain clearance and low enough to maintain good visual contact with the aircraft. For a successful landing the aircraft must touch down on the paved portion of the runway without bouncing off. Any aircraft that obtains significant damage during landing will not receive a score for that flight, the definition of significant will be determined by the Flight Line Judge.

3.2 Design Requirements

The governing equations given by the ruleset were analyzed to determine the factors that would lead to the highest score at competition. The results from this study governed the decision making process for the aircraft configuration selection. Design parameters for each score component were generated and are tabulated below in Table 1.

Table 1 - Design Parameters

Missions and RAC	Objective	Design Parameter
M2. Short Haul of Max Passengers	Balance passenger number and flight speed to maximize the division of passengers by time	$(N_{Passengers}/T_{3\ Laps})$

M3. Long Haul of Passengers and Payload	Maximize product of passenger number, payload weight, and lap time for 10 minutes	$(N_{Passengers}N_{Laps}W_{Cargo}$
RAC	Minimize plane wingspan	S_{Plane}
RAC	Minimize empty plane weight	EW_{Plane}

3.2.1 Flight Score Sensitivity Analysis

In order to analyze the score equations, a baseline parameter was chosen for an aircraft whose score in Missions 2 and 3, when normalized with the top performer in those missions, is equal to 0.5. In order to do this however, a top performer prediction was necessary. The estimated top aircraft capability is shown below in table 2.

Table 2 - Estimated Top Performer

Missions and RAC	Aircraft Capability	Mission Score
2. Short Haul of Max Passengers	(3) 40 second laps carrying 10 passengers	2(1) = 2
3. Long Haul of Passengers and Payload	(8) laps carrying 10 passengers and 10 oz of payload	4(1)+2 = 6

To estimate a baseline aircraft, the predicted mission score from Table 2 was halved and a weight and wingspan for the baseline aircraft was predicted based upon team design sizing techniques and historical model aircraft data from previous competitions. Due to the emphasis on minimizing wingspan, it was assumed that this baseline aircraft used a biplane configuration, therefore the predicted wingspan was halved in the analysis. The baseline aircraft RAC for each mission is displayed below in Table 3.

Table 3 - Baseline Aircraft Parameters

Missions and RAC	Weight	Wingspan
2. Short Haul of Max Passengers	1 lb	20 inches
3. Long Haul of Passengers and Payload	3 lb	36 inches

Since the baseline aircraft for Mission 2 has a lower RAC, that RAC was used for the baseline aircraft. Since the baseline aircraft achieves one half the top performing aircraft's score, it is likely that the RAC used in the Mission 3 calculation is unfeasibly low, but remains a best case scenario nonetheless. With the baseline aircraft RAC and mission score determined, the baseline score was calculated using the score equations given in the rules. RAC, individual mission scores, and combined mission scores were then individually deviated from the baseline by a given percent while holding the other factors constant. The effect on total score was plotted and the results are given below in Figure 5.

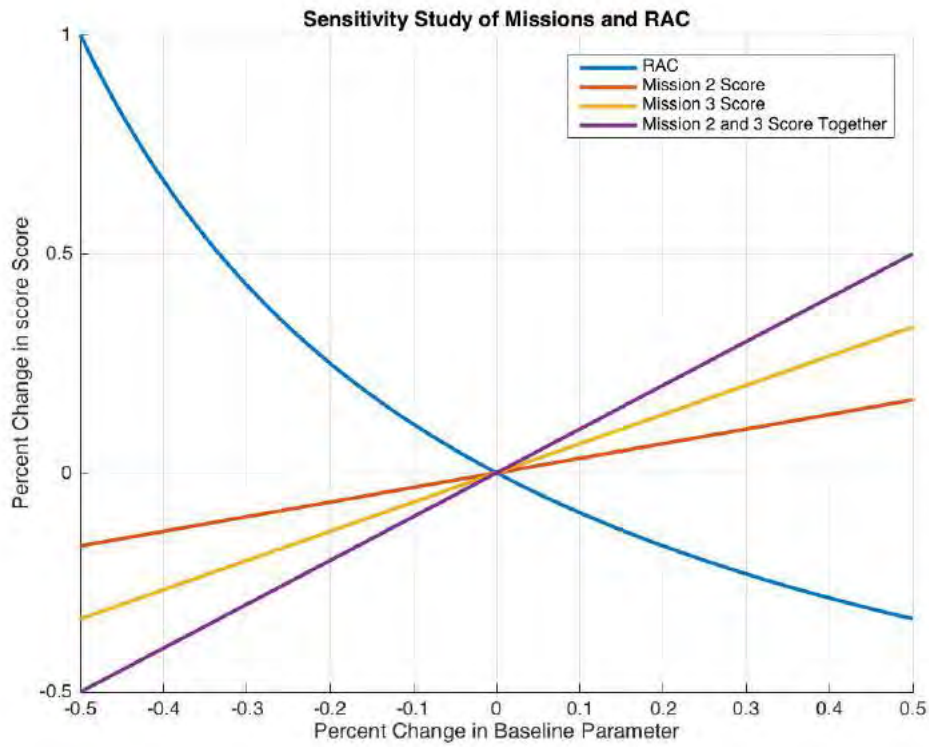

Figure 5 - Score Sensitivity Study

This score analysis indicates that minimizing RAC yields the greatest improvement of the baseline score. The only nonlinear relationship is when the RAC is changed with the other score factors held constant. Further analysis was necessary to determine which balance of RAC to mission score yields the highest score overall.

3.2.2 Aircraft performance prediction

In order to determine the highest scoring aircraft configuration, the team developed an RAC prediction tool which output theoretical minimum wingspan and weight for a given passenger number and payload weight input.

The inputs to the score prediction tool are the passenger number and payload block weight. When summed, this becomes the total payload weight. The total weight of the aircraft also includes the mass of the structure and systems, as shown in Equation 7.

$$W_{\text{XNKYKFZM}} = W_{\text{[F UTSFV}} + W_{\text{\UGMHG}} + W_{\text{\MKJYMJKH}} \qquad \text{(Eq. 7)}$$

The team used historical data both from previous competitions and other team experience to determine a multiplication factor for estimating structure weight. The equation for structure weight is given below in Equation 8.

$$W_{\text{\MKJYMJKH}} = Multiplication\ Factor * (W_{\text{\UGMHG}} + W_{\text{[F UTSFV}}) \qquad \text{(Eq. 8)}$$

The majority of systems weight comes from propulsion which is represented by the battery and motor weight in Equation 9.

$$W_{\text{\UGMHG}} = W_{\text{QS MSK}} + W_{\text{aF MMHKU}} \qquad \text{(Eq. 9)}$$

Assumptions were made about the relationship between power and mass of motors, allowing motor weight to be calculated as a function of payload weight, structure weight, and power to weight ratio.

$$W_{\text{QS MSK}} = Ratio_{\text{QS MSK bHN cM/ESb HK}} * Ratio_{\text{XNKYKFZMESb HK/bHN cM}} * (W_{\text{\MKJYMJKH}} + W_{\text{[F UTSFV}}) \qquad \text{(Eq. 10)}$$

The energy density of NiMH batteries is known, allowing battery weight to be calculated as a function of payload weight, structure weight, power to weight ratio, and flight time.

$$W_{\text{aF MMHKU}} = Ratio_{\text{aF MMHKU bHN cM/HIHKJU}} * Ratio_{\text{XNKYKFZMESb HK/bHN cM}} * FlightTime * (W_{\text{\MKJYMJKH}} + W_{\text{[F UTSFV}}) \qquad \text{(Eq. 11)}$$

Based on the need to fly in Wichita winds, a minimum flight speed was known, along with mission requirements that allowed flight time to be calculated. The team used a set power to weight ratio of 100W/oz based off of previous experience.

With this system of equations, there are equal equations and unknowns. Values for weights were iterated until all equations converged. The code was verified by plugging in payload weights from previous years and comparing it to the finished plane.

The final result of this code was a tool that could output an RAC for a given payload (i.e. passengers & payload). This allowed the team to generate a heatmap for total score based on payload. The results from such are shown below in Figure 6.

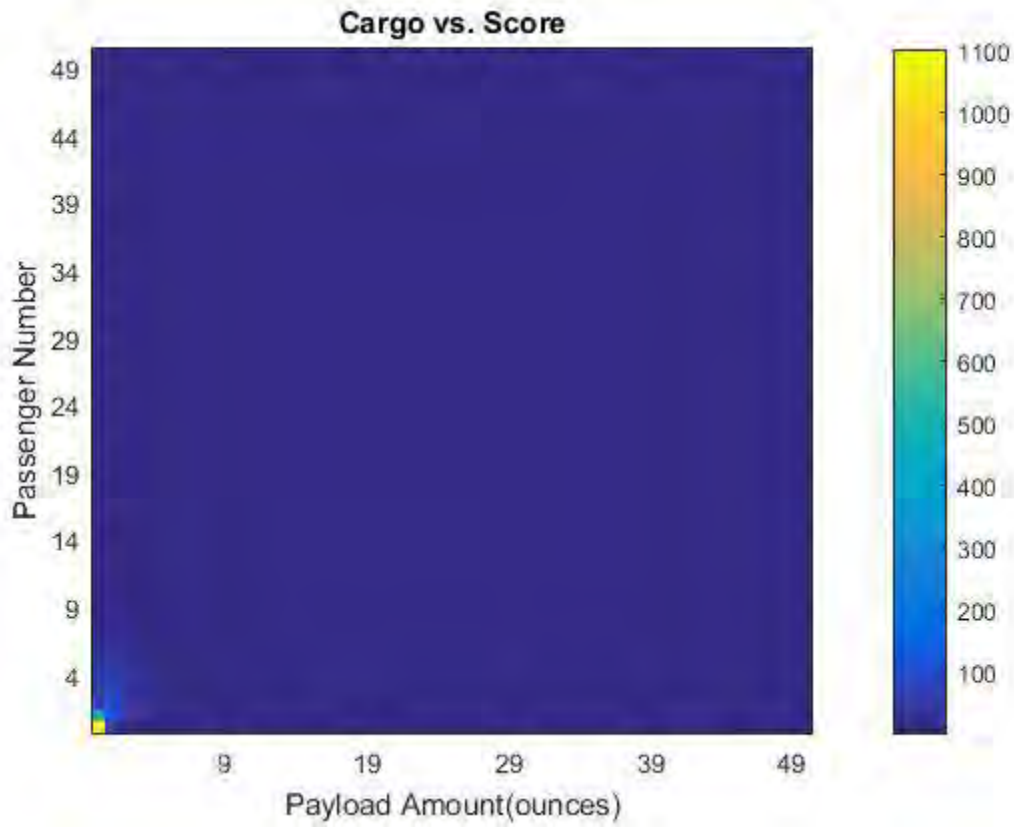

Figure 6 - Heatmap of Score Prediction

From the heatmap above, it was determined that minimizing RAC by carrying the minimum payload yields the highest competition score. This was the route the team chose to follow in the design of the aircraft.

3.2.3 Ground Mission Analysis

The score prediction tools outlined above do not account for the required ground mission, as this mission does not directly impact the score. Components related to the propulsion system are designed to be removable by nature, as the typical fastening system is Velcro, with the exclusion of the motor. Structural elements, such as ailerons, are typically attached via tape. The team agreed however, that this system could easily be swapped out for a rod on which they could rotate, therefore greatly expediting the removal process. For this reason, the conceptual design was focused mainly on minimizing RAC with confidence that LRU eligible components could be converted if they were not already easily removable.

3.3 Configuration Selection

The configurations considered were based off of the results of the score prediction tool. It was estimated that a plane could be constructed with a loaded weight between 8 and 14 oz, and a 3-5 ounce propulsion system. A preliminary propulsion system was specified and purchased for prototype flights and for code validation.

3.3.1 Configurations Considered for Testing

Multiple conceptual designs following competition requirements were initially considered in order to maximize aspects of the aircraft including manufacturability, weight, stability, and wingspan. After considering multiple designs, three were selected for further analysis. These three designs can be seen in below.

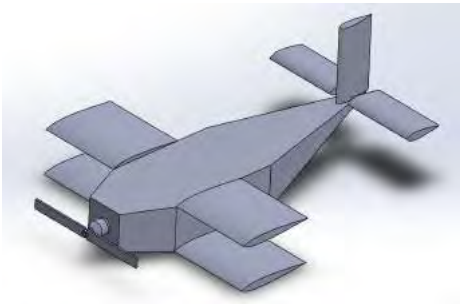

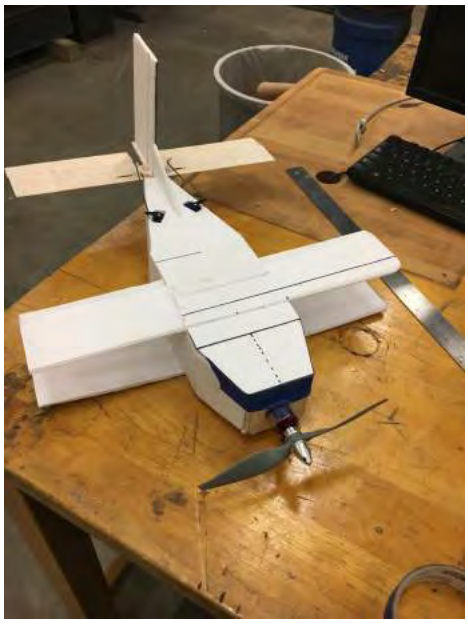

Figure 7 - Initial Biplane prototype model (Left) and Prototype (Right)

The biplane design was considered because of its relatively short wingspan and being a stable platform. Based on this year's rules, minimizing RAC was paramount so a short wingspan was a very important factor in this year's design. This design also had the benefit of being a comparatively traditional design that the team had experience analyzing. A problem with the biplane was that the fuselage had to be proportionally large to store all flight systems, as well as room for passengers and payload. Prototypes of this design were constructed and the aircraft flew rather well. Prototypes with this design were also promising as the balsa and foam structure held together by epoxy was very light and very stiff.

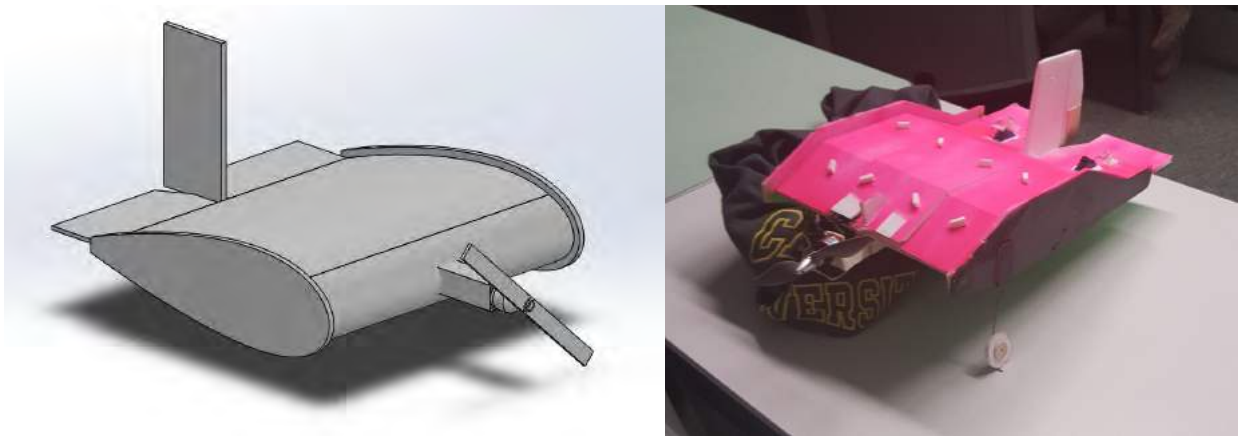

Figure 8 - Initial Pizza Box prototype model (Left) and Prototype (Right)

The lifting body configuration, also known as the “Pizza Box Flyer”, was evaluated because it allowed the capability for a much shorter wingspan than the biplane. Due to the size of the passenger, and the aisle next to it, the payload area required a minimum four inch wide fuselage. With the lifting body configuration however, this wide payload area could provide lift as part of the wings. Initially, there was concern over the stability of such an aircraft so a prototype was built. The results were promising, so long as the CG was far enough forward.

A tandem wing design was also considered, as the lift is shared between two wings. This configuration proved very popular during the 2017 competition in Tucson, Arizona where teams designed tube launched UAVs. The team noticed a trend with these planes in that they suffered from fuselage torsion issues. During flight, the wings would roll in opposite directions of each other causing the plane to fly unstably. Experienced RC pilots on the team expressed concern that such a design would need a heavy fuselage structure to counter this.

3.3.2 Configuration Selection Process

The overall configuration was then decided by quantifying each design aspect and comparing these scores. Figures of Merit (FoM) were derived from the score equation analysis and the score prediction studies. Since the primary goal of the design was to minimize the RAC as much as possible, the only design parameters considered in the selection process were those which influenced the RAC or the ability to complete all three missions. The score factors for the design parameters are displayed in Table 4 below.

Table 4 - Figures of Merit

Figures of Merit	Design Parameters	Score Factor	Biplane	Lifting Body	Tandem Wing
Wingspan	S_{Plane}	0.4	0	1	0
Weight	EW_{Plane}	0.4	-1	1	-1
Manufacturability	EW_{Plane}	0.1	1	0	0
Flyability	S_{Plane}	0.1	1	-1	0
		Ranking Sum:	-0.2	0.7	-0.4

The score factor for every FoM was assigned based upon how much direct impact it had on the competition score of the aircraft. The score factors are weighted such that they sum to one. Then each design was given a value from -1 to 1 based on whether the design positively, negatively, or did not affect the given design parameter. A score of 1 indicated that the design positively impacted that factor, such as the lifting body's positive impact on wingspan. A score of negative one meant that the it negatively affected the RAC in any possible way, such as how the tandem wing would require a heavy fuselage structure. Each score was multiplied by the score factor and summed for each configuration. The configuration with the highest score would imply that the RAC would be the lowest and that configuration would be chosen for the final design. Based on Table 4, the lifting body configuration was identified as the highest scoring configuration.

3.4 Configuration Refinement

After the pizza box style flying wing was identified as the highest scoring design, it was then refined. This configuration however, has few options. The main areas of investigation are the control surface and payload configurations.

3.4.1 Wing Configuration

It was determined that a lifting body design would minimize wingspan. Also, a narrower airfoil as a fuselage with smaller wings extending from it could save weight, as well as reduce drag by presenting a smaller planform area and by having a larger aspect ratio. During prototype test flights however, it became evident that visibility was a huge factor in the overall design that was not necessarily reflected by the FoM study. It was discovered that it was possible to design and fly an aircraft that met the requirements, but was too small for the pilot to see at the distances determined by the given flight course. There was distinct structural and visible advantage to using a single airfoil shaped fuselage with no additional protruding wings, and so a shape similar to that shown below in Figure 9 was chosen.

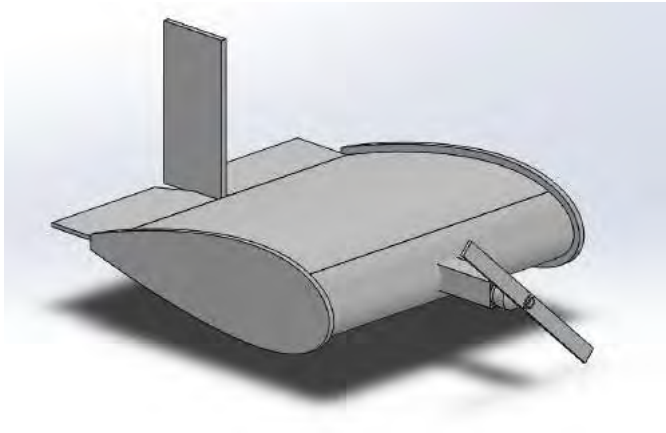

Figure 9 - Chosen Fuselage Shape

3.4.2 Tail Selection

The team considered multiple tail options for the conceptual layout. The two main options were a traditional tail, and a split vertical tail, that extends from the side plates of the aircraft. There would be strength and weight advantages to using a split tail. The manufacturing difficulty would also go down with this design. The team opted to go with a single tail however, because early testing indicated that the air going over each elevon interfered with the other when there was no vertical stabilizer separating the airflow, and a loss of control was experienced.

A flying wing like the one proposed in Figure 9 must use elevons for control, it was unknown however whether the aircraft would need a movable rudder as well. Given the light overall weight, having one less servo represents about an additional four percent weight savings. To decide this, a more refined prototype was built and the aircraft was flown with and without a controllable rudder. The prototype was flown in windy conditions , and the pilot determined he had sufficient control without a movable rudder. Based on this, the plane will have elevons as the only control surface.

3.4.3 Payload Configuration

The rules allow any payload shape and weight provided that it is a rectangular prism with each cardinal dimension summing to nine inches and no sides smaller than two inches. One design aspect noticed in testing is that there is a lower limit to the aircraft wingspan, due to the need for the pilot to see the plane and identify its orientation at all times without external assistance. This led to the logical conclusion that the longest side of the payload should extend in the same direction as the wingspan. For aerodynamic reasons, it is also desirable to make the maximum thickness of the wing as small as possible. For these reasons, the payload configuration was a 2x2x5 rectangular block, with the long side oriented perpendicular to the direction of travel. Using the minimum dimension of two inches allows for the airfoil to be as thin as possible for a given chord.

3.5 Final Conceptual Design

The final configuration uses the Pizza Box style with elevons and no controllable rudder shown below in Figure 10. The aircraft will carry the minimum payload configuration of 1 passenger and 1 ounce of payload.

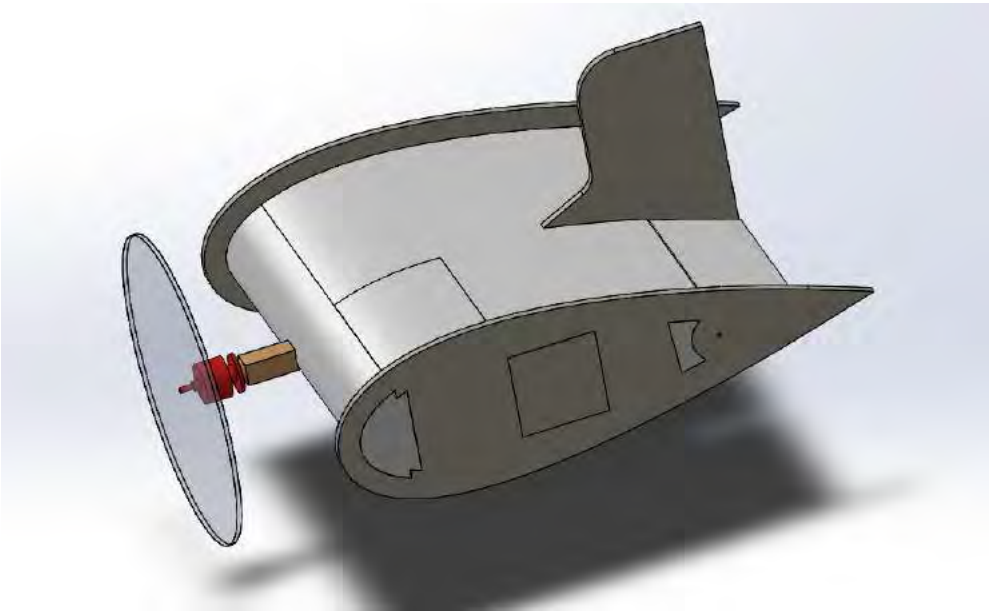

Figure 10 - Final Conceptual Design

4.0 Preliminary Design

The objective of the preliminary design phase was to determine and optimize the aircraft's parameters to maximize the final score. Taking into account the results of the score analysis, iterative prototyping, and successive flights, the optimal parameters for the design were decided upon by the team.

4.1 Design Methodology

The preliminary design was completed with two major design objectives to meet: minimize the RAC and complete all missions. Minimizing the wingspan was deemed to be the most important objective to meet in minimizing the RAC, as decreasing the wingspan itself would further reduce the weight of the aircraft. In order to complete all of the missions, the design would need to fully complete the ground missions. The nature of the ground missions required that many of the planes critical components be replaceable. This was the second major design consideration to take into account along with minimizing the wingspan. With many of the LRU eligible components already simple to remove and replace, this second consideration was not weighted as heavily when beginning the design of the aircraft.

4.2 Mission Model

In order to determine feasibility in the preliminary design process, a mathematical model was created that could roughly simulate aircraft performance. This model was made in four parts for each of the flight conditions listed below:

1. Takeoff - Takeoff was considered negligible due to the fact that the aircraft takes off in less than 10 feet during flight tests.

2. Climb - It was modeled that the aircraft climbed to a height of 50 feet from the ground altitude in Wichita, KS.

3. Cruise - In this flight condition, the lift was equal to the weight, and the thrust was equal to drag. The model induced a 20 mph gust for one direction of the flight. The returning path was modeled with no tailwind, which presents the worst case scenario for battery consumption.

4. Turn - The are two 180° turns and a single 360° turn. This is modeled as a coordinated turn with a 25 foot loss in altitude as such a piloting technique has been demonstrated to execute the maneuver faster.

4.3 Preliminary Sizing

The philosophy of the design was to minimize the wingspan and weight wherever possible, therefore size and weight of all aircraft components were minimized as much as possible.

4.3.1 Wing

The goal of the design team in sizing the wing was to determine the smallest wingspan possible. The lower limit on wing size is the minimum span that is still visible at the furthest extents of the flight course. A prototype plane was painted with bright colors and walked approximately 700 feet away. The wingspan was then incrementally shortened until the pilot could no longer accurately determine its orientation of the plane above the holder's head. It was determined that the smallest allowable wingspan was nine inches.

After the minimum visible size was determined, the aircraft internals, payload, and passenger were laid out on the aircraft planform to determine if such a wingspan would be able to hold all the necessary components. The team verified that the components would fit inside the aircraft.

4.3.2 Propulsion Sizing

The propulsion system was designed to be as light as possible while still allowing the aircraft to complete all three flight missions. The heaviest component of the propulsion system is the battery, and as a result range requirements are the primary factor increasing weight. Thus the most constrictive of the flight

missions is mission two where the aircraft is required to fly 3 laps of the course with a single passenger as payload.

Normally for propeller powered aircraft max range is achieved when flying at L/D_{Max}, which occurs approximately 60 ft/s for this aircraft. However due to the Wichita winds that the Knighthawk might have to fly through, effective range over the ground is increased with a higher airspeed. A script was made that solved for effective range assuming equal distance traveled in a 20 mph (30 ft/s) headwind and tailwind. Optimizing for this suggested that the aircraft should fly at 75 ft/s. Approximating the DBF course to be 3000 ft in length, this corresponds to completing three laps in about 2.5 minutes in the wind. The highest discharge rate NiMH batteries available can fully discharge in just over 3 minutes at minimum. This means that the lower bound on battery size does not come from range but from minimum flight-time. The minimum flight speed necessary to complete 3 laps in 3 minutes in 20 mph wind was found to be 66 ft/s. The propulsion system was designed to this fight speed.

Propeller selection was done using PropCalc software. Various commercially available propellers up to a maximum diameter of 7 inches were simulated. RPM was adjusted until thrust produced at 66 ft/s matched the expected drag force, the method used to estimate drag force is documented in 4.4.2. The propeller that required the least power under these conditions was 7x4 APC operating at 8300 RPM.

From drag force, flight speed, and flight duration the energy required can be calculated from equation 12.

$$Energy = Drag * Speed * Duration \qquad \text{(Eq. 12)}$$

An energy storage of 5 Watt Hours was found to be needed after accounting for propeller, motor, and battery inefficiencies. The highest energy density competition legal battery cells found at this scale were the PK NiMH 400mAh 2/3AAA (1.2V/cell). In order to get the required energy capacity 10 of these cells are needed. Accounting for voltage drop under high load this yields a battery pack which outputs 8 volts.

Finally with RPM, propeller, flight speed, and voltage determined, only Kv (RPM per volt in electric motors) needed to be determined. A motor from previous years was set up with the 7x4 APC propeller on a thrust test stand. Power was delivered to the motor with an adjustable voltage power supply. Voltage to the motor was adjusted until thrust and propeller RPM matched what was expected in static air. The voltage need to do this along with the test motor's Kv rating was used to estimate what Kv rating was needed.

$$Kv_{\mathrm{IHHVHV}} = Kv_{\mathrm{kHGM}} * \frac{\mathrm{l\ mnop}}{\mathrm{l\ qn\ ors\ t\ nu}} \qquad \text{(Eq. 13)}$$

A preliminary motor selection was made based on the required Kv, current draw, and motor weight. The preliminary motor selection was a ELE C20 PRO 1550Kv. This motor has performance benchmarks

indicating that it achieved ten ounces of thrust at seven volts with a 8x4 prop. The preliminary propulsion package is summarized below in Table 5.

Table 5 - Preliminary Propulsion System Components

Motor	Battery Pack	Propeller
ELE C20 PRO 1550Kv	8 x PK Cell 400mAh (9.6V)	7x4 APC

4.4 Aerodynamics

4.4.1 Airfoil Selection

The airfoil choice was especially important with the Pizza Box design, due to the aircraft's body and structure being the wing. As the payload for this year was predefined, the thickness of the wing could be directly determined from physical space requirements. The wingspan of the aircraft was also known from visibility constraints. Thus the thickness over chord (t/c) of the airfoil determined the minimum chord and wing area. From this a maximum cruise Cl could be determined and drag could be calculated. The team developed and ran a script to model various NACA 4 series airfoils in this way, searching for the airfoil that would give minimum cruise drag. The importance for this is detailed in Section 4.4.2. A NACA 1428 airfoil was determined to be optimal.

4.4.2 Drag Analysis

Due to the aircraft being a flying wing, the majority of the drag is from profile and induced drag from the lifting surface. A breakdown of the drag coefficients are presented below in Table 6.

Table 6 - Drag Breakdown

Component	$C_{\#}$
Wing	.021
Vertical Tail	.0025
Total	.0235

From the table above, it is evident that the majority of drag come from the wing/fuselage structure. The L/D ratio during the different missions was determined using XFLR5, shown in Figure 11. The main takeaway from this study is the Mission 1 cruise and Mission 2 cruise. It is necessary to operate as efficiently as possible so that the aircraft has enough power to complete the mission. For Mission 3, the

aircraft is only flying a single lap and so any inefficiencies are more than compensated for by the propulsion system.

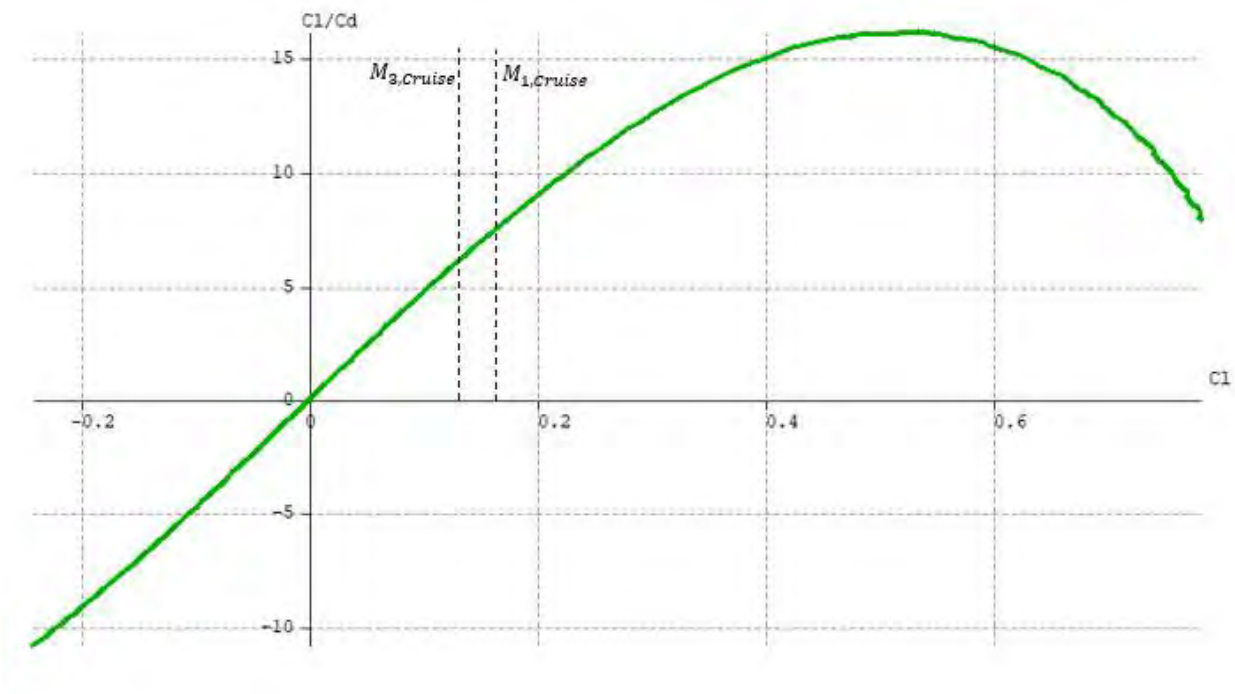

Figure 11 - L/D Ratio During Different Mission Phases

4.5 Stability and Control

4.5.1 Tail Sizing

The main tail sizing consideration for the chosen configuration is determining an appropriate size for the vertical tail. The following tail volume ratio relationship is used to determine vertical tail size[2].

$$V_v = \frac{S_v l_v}{Sb} \qquad \text{(Eq. 14)}$$

Using this relationship to solve for vertical tail area S_v with an ideal volume ratio V_v of 0.05 yields a vertical tail area of 6.67 square inches. Despite this, it was discovered through flight testing that this area would not be large enough to ensure the required yaw and roll stability. This is likely due to the small scale of the aircraft. Upon increasing this area and iterating tests, the area has been increased to 11.25 square inches. An added advantage of the larger tail is that it provides greater visibility for the pilot. The dimensions of the vertical tail are as follows.

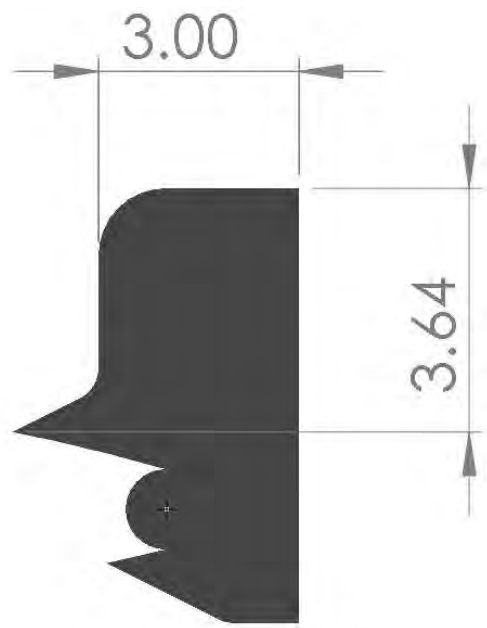

Figure 12 - Vertical Tail Dimensions

4.5.2 Longitudinal Stability

To verify the longitudinal stability, XFLR5 was used and compared to hand calculations. First, XFLR5 was used to plot C_M with respect to angle of attack. The results are shown in Figure 13 below.

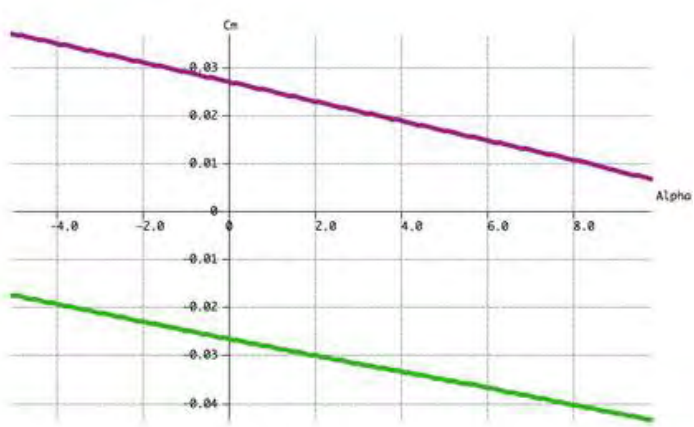

Figure 13 - C_M vs Angle of Attack

This plot shows results for both default configuration (green) and an elevon deflection of 5° (purple). The negative slope here indicated longitudinal stability. Additionally, the aircraft will trim at an elevon deflection of 2.5^o. These plots concur with the aircraft's behavior in the test flights. The equations describing these plots are as follows. Equation 15 is default configuration and Equation 16 is elevons deflected 5°.

$$C_Q = -0.0025\alpha - 0.026 \quad \text{(Eq. 15)}$$

$$C_Q = -0.0025\alpha + 0.026 \quad \text{(Eq. 16)}$$

With a $C_{M\alpha}$ of -0.0025, this aircraft will have positive longitudinal static stability, but only by a small margin. The static margin will therefore be SM=0.0025. Preferably, we would like a static margin closer to 0.1. To achieve this, the CG will be located approximately one inch forward from the aerodynamic center. Since the aerodynamic center is located near 0.3 of the total chord, the CG should be located at 0.2 of the chord. This will be two inches aft of the leading edge. Since internal volume is very limited on this aircraft, placing the CG is difficult. To achieve our desired CG location, the motor will be placed on a pylon extending from the leading edge of the aircraft. The batteries and other systems components will be placed as far forward as possible. Weights could also be added to the motor pylon to shift the CG further forward if needed.

4.6 Performance Estimates

Table 7 - Aircraft Performance Estimates

Performance Parameter	M1	M2	M3
Cl max	0.87	0.87	0.87
Cl cruise	0.117	0.132	0.147
e	0.8	0.8	0.8
Cd	0.021	0.022	0.024
L/D max	8.45	8.45	8.45
L/D cruise	5.57	6.01	6.12
Rate of Climb	7.3 ft/s	7.3 ft/s	7.3 ft/s
W/S	9.48 N/m^2	10.67 N/m^2	11.85 N/m^2
Vcruise	23.4 m/s	22.5 m/s	21.8 m/s
Vstall	8.26 m/s	8.76 m/s	9.24 m/s
Gross Weight	2.22 N	2.50 N	2.77 N

Mission Score	1.0	~0	~2

5.0 Detail Design

5.1 Dimensional Parameters Table

Table 8 - Aircraft Dimensional Parameters

Wing Geometry Data			
	Span	9 in.	
	Area	94.5 in.^{2}	
	Chord	10.5 in	
	Aspect Ratio	0.85	

Wing Aerodynamic Data: NACA-1428			
Cruise		Take-off	
Alpha:	2.00 deg	Alpha:	11.00
$C_{L\ airfoil}$	0.408	$C_{L\ airfoil}$	1.11
$C_{L\ alpha\ wing}$	0.095/deg	$C_{L\ alpha\ wing}$	0.095/deg
$C_{L\ wing}$	0.12	$C_{L\ wing}$	0.87
$C_{m\ alpha}$	-0.0025/deg	$C_{m\ alpha}$	-0.0025/deg
C_m	-0.03	C_m	0.02
$C_{d\ airfoil}$	0.0075	$C_{d\ airfoil}$	0.032
$C_{D\ wing}$	0.021	$C_{D\ wing}$	0.297
L/D	6	L/D	3

Aircraft Constraints/Geometry			
	Aircraft Empty Weight:	8 oz	
	Aircraft Payload Weight:	3 oz	
	Aircraft Max Weight:	11 oz	
	Cruise Velocity:	66 ft/sec	
	Avl. Static Thrust:	7 oz	
	Avl. Dynamic Thrust at Cruise Vel.	5 oz	
	Take-off Distance:	35 ft	
	Oswald's Efficiency:	90.0%	

5.2 Material Characteristics and Capabilities

Multiple construction techniques were investigated to identify the benefits and disadvantages of each. This involved making prototypes of key surfaces and structural members, refining these for each method until they met performance requirements, and extrapolating factors such as final weight and build time.

5.2.1 Balsa and Monokote

The teams greatest strength comes in its experience with balsa and monokote structures. Experiments done in past years have shown that balsa and monokote construction can be lighter than solid foam construction, however those experiments were done when making aircraft of a larger scale. One disadvantage of balsa and monokote this year is that the weight of the structure is largely related to the surface area, so as the aircraft is smaller and the ratio of internal volume to surface area is larger these structures are heavier. In addition, the nature of monokote construction requires that the balsa frame can support the tension in the monokote. This tension does not change with the scale and weight of the aircraft. Due to this, on an aircraft this small it was found that the monokote forces on the balsa structure are greater than the flight forces.

5.2.2 Composites

Similar to balsa and monokote, the size of the plane this year meant that carbon fiber or Kevlar resin structures did not have a weight advantage over foam and balsa alternatives. The reason for this is the sheets/stringers would need to be so small that there would not be enough surface area to glue efficiently. Such a structure would be offset by the weight in excess glue necessary to make the aircraft strong enough.

5.2.3 3D Printing

There is a tradeoff with 3D printing in that it makes otherwise impossible to manufacture structures possible at the cost of weight. The team has experimented with 3D printed ribs in the past and deemed it too heavy when compared to balsa for larger structures. An analysis this year showed the same result, that right now 3D printed parts cannot be made thin and light enough to compete with foam or balsa.

5.2.4 Foam

Due to the size of this year's plane, foam excels as a design choice. Entire sections of the aircraft were cut out from solid foam, and were found to be competitive in weight due to their low internal volume and lack of need for internal glue joints. Foam sections are additionally easy to manufacture and repair, making them ideal for rapid prototyping and repairs away from the shop.

5.3 Structural Design Selected

5.3.1 Aircraft Frame

A twin spar design was selected to support the wing of the aircraft. One of the spars form the leading edge of the wing, and the other is near the trailing edge, directly in front of the elevons. This design was necessary as it leaves room for the payload bay to be in the thickest part of the wing, allowing the wing to be as thin as possible.

The material selected for the aircraft frame is solid foam. Solid foam was chosen as the weight increase from using a solid spar is less that the weight of glue that would hold together a hollow structure at this scale. This also has the benefit of being about equally strong everywhere, allowing electronics and other internal components to be attached wherever is most convenient. Solid foam can also more easily be cut into a precise profile, allowing for a smoother leading edge of the wing.

5.3.2 Aircraft Skin

The aircraft's skin needs to be strong enough to not flex under aerodynamic forces, as well as support the box which forms the payload bay. A thin layer of uniform thickness was determined to be ideal for these requirements while minimizing weight. While building test prototypes, a method of construction where sheets of foam were bent across ribs was tried, however the number of ribs required for a uniform wing made this method heavy. Thus the skin material needs to be capable of supporting its own shape. Prototypes were made using heat molded foam sheets and precisely cut solid foam. Molding foam sheets with heat proved to be inconsistent, with the foam likely to warp when taken out the mold. Therefore solid foam will be used for these parts.

5.3.3 Internal Dividers

Sections of the hollow center of the wing need to be divided up into a distinct passenger area, payload bay, and electronics section. To do this a system of internal dividers was designed that would make vertical walls between the top and bottom surface of the wing. Materials considered for this included balsa and monokote, paper, and sheet foam. Monokote dividers were found to either be heavier than their counterparts or require support from the surrounding structure that they attached to in order to resist the tension in the monokote. Ultra-thin foam panels were found to be very light solution that required no reinforcement. In the case of the vertical dividers that ran across the wing, these panels even provided significant reinforcement due to their large area carrying shear flows. Paper weighed about the same as foam, but was not found to give as large of a structural benefit. While these internal dividers were not designed to carry any structural loads, the foam sheets were decided on as the optimal solution.

5.4 Sub-System Design and Integration

5.4.1 Internal Wing Frame

The wing and fuselage structure are the same thing in this flying wing design. The design consists of foamboard ribs on each side of the plane with foam stringers/spars on the inside. The structure is then covered with foam sheets on the top and bottom, which form the skin of the aircraft. The aircraft internal structure is shown below in Figure 14.

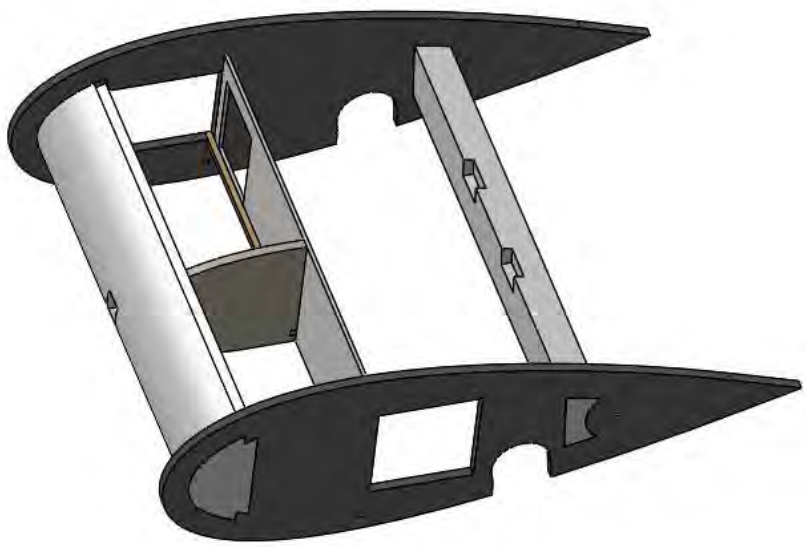

Figure 14 - Aircraft Internal Structure

5.4.2 Elevons and Vertical Tail

The elevons are made up of a solid piece of laser cut foam. They pivot on a thin piece of carbon fiber rod that extends the length of the aircraft. The elevons located in their pivot position is displayed in Figure 15.

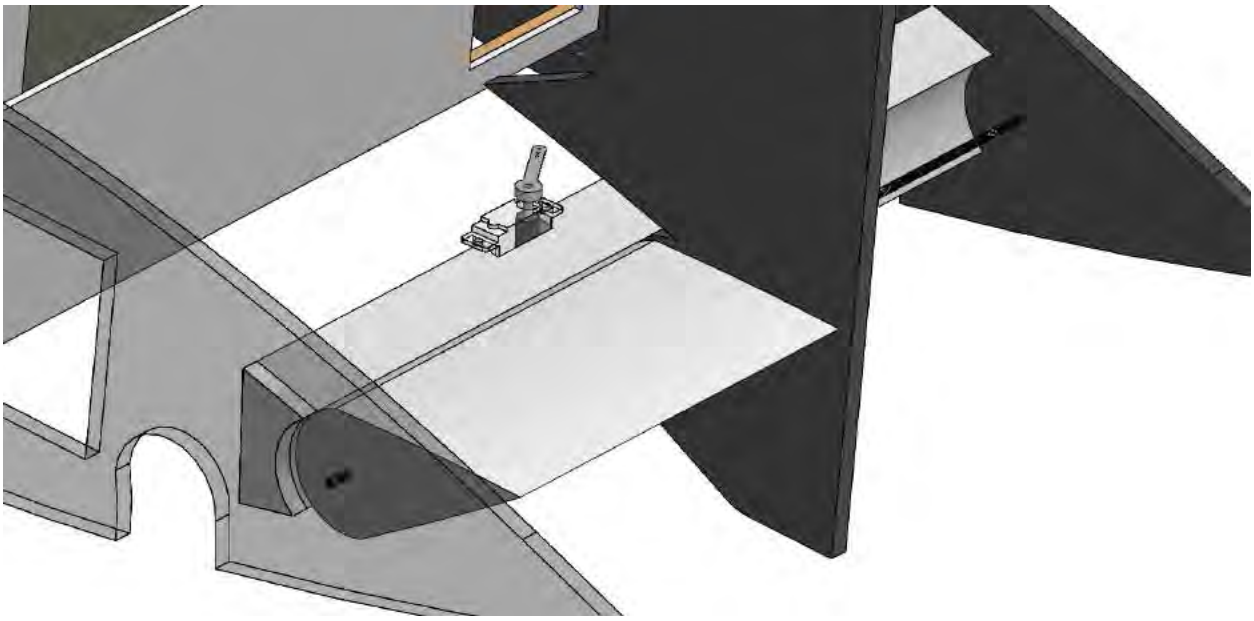

Figure 15 - Elevon Pivot System

The elevons are listed as potential LRUs and as such, they are removed by sliding the carbon fiber rod that they pivot on, out of the aircraft. The rod is friction fit into the side ribs of the aircraft and through a hole in the vertical stabilizer. The servos protrude through the upper surface of the wing and attach to the elevons via a control arm.

5.4.3 Passenger Bay

The design has the passengers being loaded via a door in the top surface of the aircraft. This top surface is held in place by a small piece of tape and a friction fit. The passenger restraint system consists of a balsa plate with a hole in which the passenger sits. Rubber bands attached to the seat are stretched over the passenger to secure it. As per the rules, there is a two inch aisle that extends from the furthest extent of the largest passenger and has ¼ inch of space in all other dimensions allowing for adequate headroom and legroom. The location and loading method of the passenger section are demonstrated below in Figure 16.

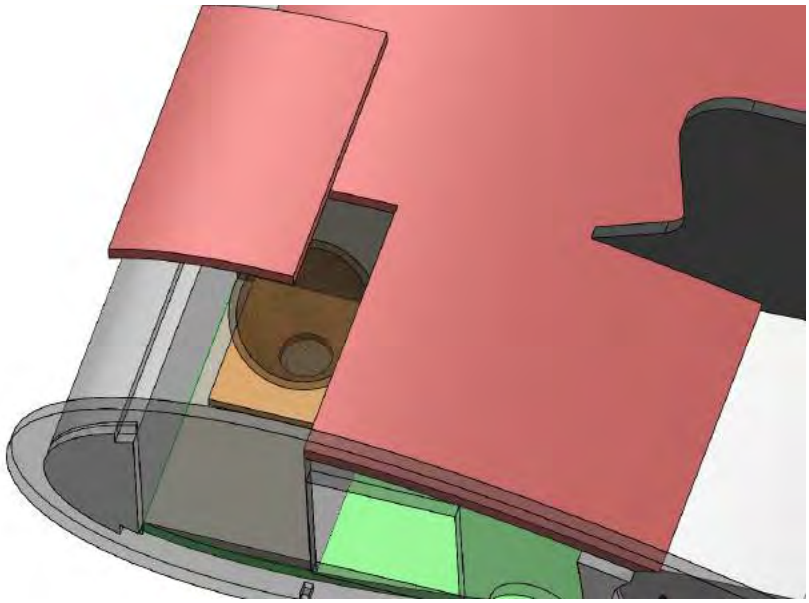

Figure 16 - Passenger Compartment with Largest Passenger Loaded

The rubber band restraint system is displayed below in Figure 17.

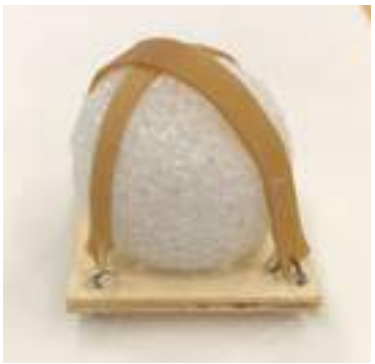

Figure 17 - Passenger Restraint System with Largest Passenger Installed

5.4.4 Payload Design

The payload is a hollow 2x2x5” foam block with sheet metal sheets on one side which bring the weight up to the minimum one oz. This is done so that the center of gravity can be positioned farther forward than if the block was homogenous. The payload has two of its sides be the minimum allowed two inches to allow for a thinner airfoil. There is excess space span wise within the plane to account for the long dimension.

5.4.5 Payload Bay

The payload is loaded into the aircraft via a door in the left side. This is shown below in Figure 18 with the payload being the transparent block. The door has a simple balsa structure that secures the payload in the middle of the aircraft so that the CG of the aircraft does not shift during flight.

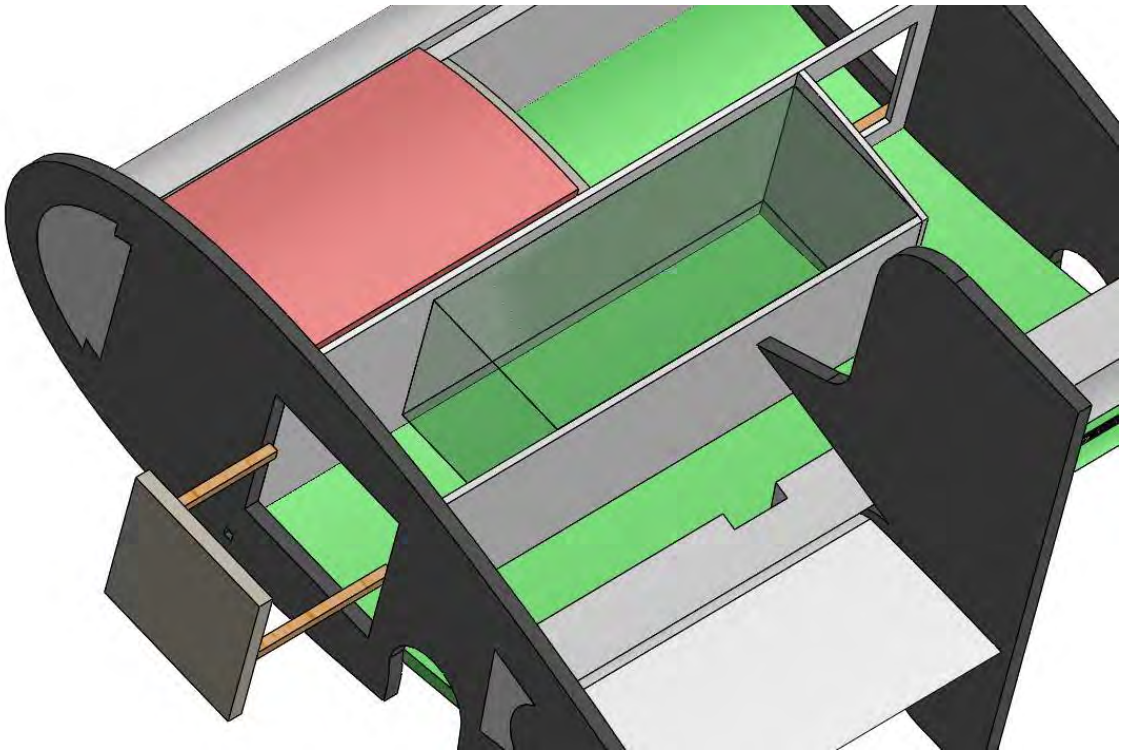

Figure 18 - Payload Location

5.4.6 Electronics Bay

The electronics on the aircraft are attached to a removable tray with Velcro. This allows for easy access and removal of the systems components during the ground mission as well as general serviceability. The electronics bay is next to the passenger section and is separated with a foam panel. Wires pass from the electronics bay to the rear servos through a hole in the aft portion of the bay. The tray remains in the aircraft by using magnets. The location of the servo wire passthrough hole near the edge of the aircraft means that excess slack is not required, which saves weight. The electronics tray is shown below in Figure 19.

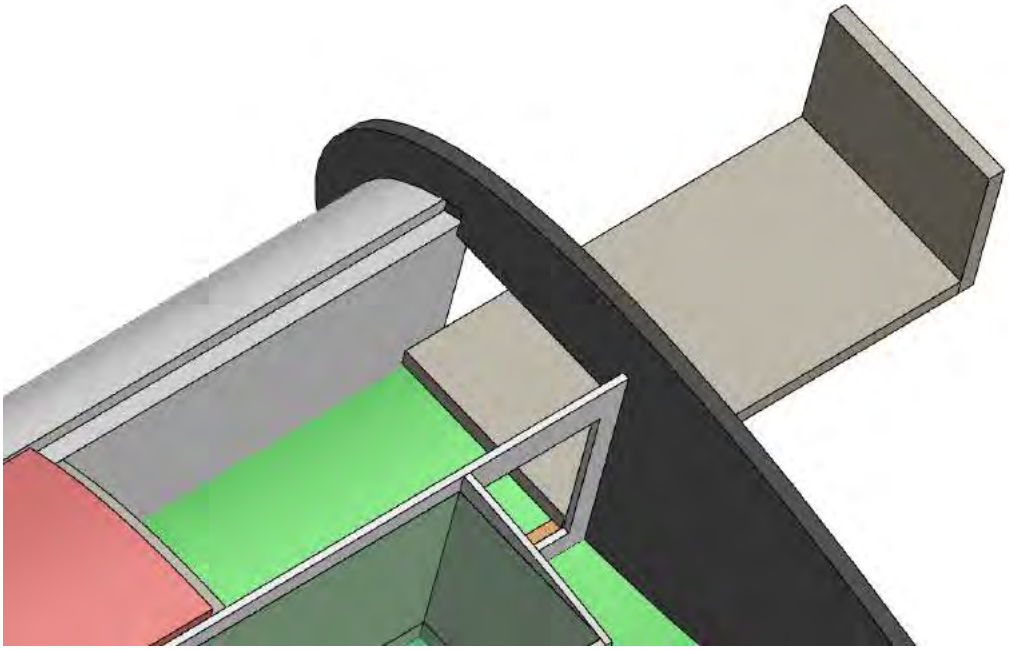

Figure 19 - Electronics Tray with Servo Wire Access Hole

5.4.7 Propulsion System

The motor is attached to a boom that extends beyond the leading edge of the plane. The boom is made of balsa wood and extends through the front foam spar. The motor boom is hollow to allow for the motor wires to pass through and into the electronics bay.

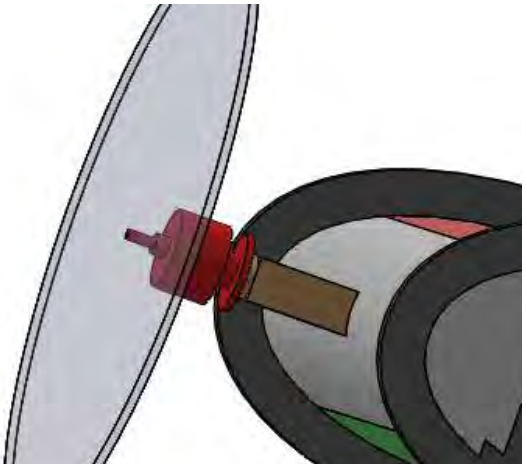

Figure 20 - Motor Mount

The motor consists of an ELE C20 PRO 1550Kv. This model is the same that was used during the preliminary design phase to test out prototype models. The goal in designing the propulsion system was to trade motor weight and KV. A lower KV means that it takes less current to produce the same amount of

thrust, thereby not requiring as heavy an ESC. The ELE C20 Pro was chosen based on competitive weight to other options, demonstrated reliability in flight tests, and an acceptable KV.

The chosen ESC is the Cheetah 10A Brushless ESC. The team has had a good experience with Cheetah brand products, and the model was also the lightest 10A ESC available.

The propulsion system is the same for each mission and is broken down below in Table 9.

Table 9 - Propulsion System Breakdown

Component	Model	Weight
Motor	ELE C20 Pro	26.2g (.9 oz)
Battery Pack	(10) PK Cell NiMH 400mAh 2/3AAA (1.2V/cell)	116g (4 oz)
Rx Pack	174F 4.8v 170mah NiMH 1/3 AAA Pack	29g (1 oz)
ESC	Cheetah 10A Brushless ESC	8.5g (.29 oz)
Receiver	Spektrum Ar6335 6 Channel AS3X NanoLite Receiver	2g (.07oz)
	Total	181.7g (6.26oz)

5.4.8 Landing Gear

The competition aircraft is designed to reduce weight and drag as much as possible. Drag is further reduced by using a motorless retracting landing gear design. On takeoff, the landing gear is set in the extended position, which is shown below in Figure 21.

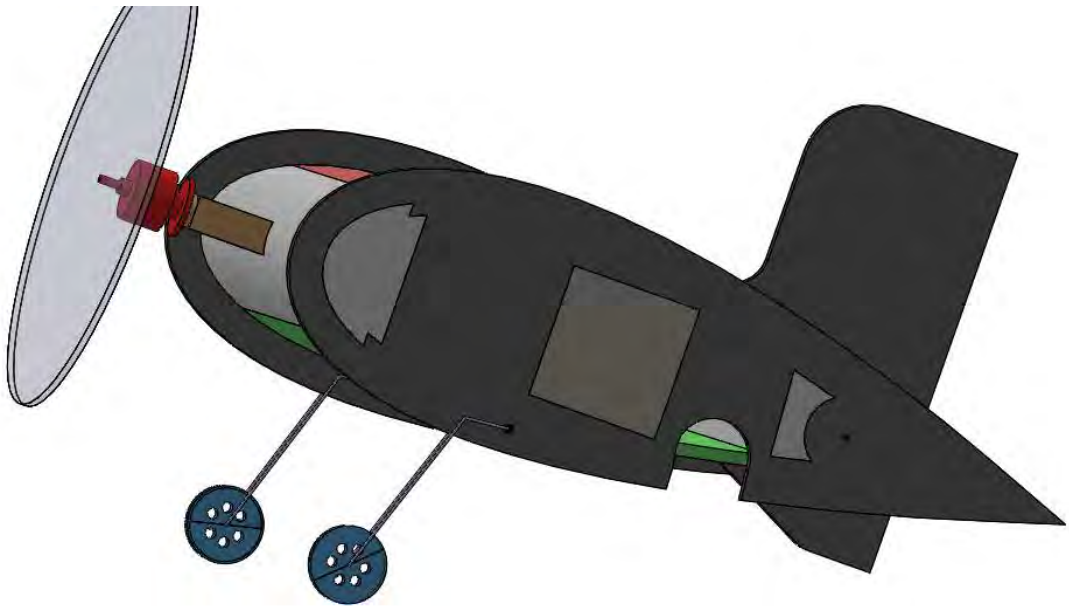

Figure 21 - Landing Gear in Extended Position

After takeoff, the gear is pushed back by wind resistance into its well. Once the wheel retracts fully, the wire come into contact with a magnet, thus keeping the landing gear locked in place. For landing, there is a bend in the landing gear wire that extends below the side pieces of the fuselage. These serve as landing skids. The retracted landing gear can be seen below in Figure 22.

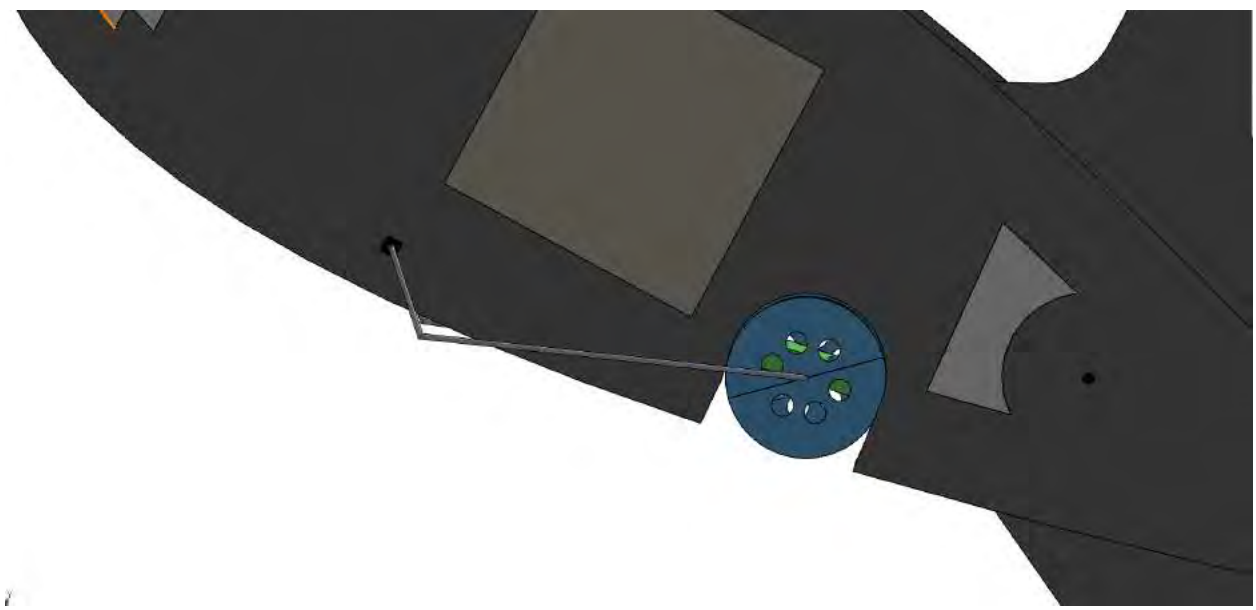

Figure 22 - Retracted Landing Gear with Wire Bends Serving as Skid

The landing gear and landing gear wheel are both listed as possible LRUs. The landing gear is made of a steel wire with a series of bends. The wire ends meet at the top where the gear meets the aircraft. The

gear is attached and removed by spreading the ends apart and sliding it into a piece of hollow carbon fiber square stock embedded in the fuselage. The landing gear wire is shown below in Figure 23

Figure 23 - Landing Gear Wire with Detached End

The wheel is made up of two 3D printed ABS halves and held together with rubber bands. To remove the wheel, the landing gear wire must be detached. The rubber band is then removed from the wheel. The wheel halves come apart off the wire, and the rubber band can be slid off the gear via the break at the top. The rubber band also serves as a tire, providing friction between the plane and the ground. The landing gear wheel assembly is shown below in Figure 24.

Figure 24 - Landing Gear Wheel Assembly

5.5 Weight and Mass Balance

The empty weight of the aircraft is 0.5 lb. This weight has been verified by constructed prototypes. Dimensions are taken from the nose of the aircraft, at the leading edge. The positive x-direction is in the

starboard direction spanwise. The positive y-direction is moving rearward from the leading edge. The positive z-direction is upwards from the upper wing surface.

Table 10 - Weight and Mass Balance Table

Component	Weight		X		Y		Z	
	(lb)	(kg)	(in)	(cm)	(in)	(cm)	(in)	(cm)
Mission 1	0.5	0.23	0	0	1.3	3.12	0	0
Fuselage	0.19	0.09	0	0	2.35	5.64	0	0
Motor	0.05	0.023	0	0	-2	-4.80	0	0
Propeller	0.01	0.0046	0	0	-2.62	-6.29	0	0
Batteries	0.25	0.12	0.5	1.2	.5	1.2	0	0
Mission 2	0.625	0.29	0	0	1.33	3.19	0	0
Passenger	0.125	0.058	-1.5	-3.6	-2	-4.8	0	0
Mission 3	0.685	0.32	0	0	1.44	3.46	0	0
Passenger	.125	0.058	-1.5	-3.6	-2	-4.8	0	0
Payload	0.06	0.028	0	0	5.54	13.3	0	0

5.6 Flight and Mission Performance

The final mission performance estimates are given below in Table 11.

Table 11 - Estimated Aircraft Performance

Performance Parameter	M1	M2	M3
Cl max	0.87	0.87	0.87
Cl cruise	0.117	0.132	0.147
e	0.8	0.8	0.8
Cd	0.021	0.022	0.024
L/D max	8.45	8.45	8.45
L/D cruise	5.57	6.01	6.12

Rate of Climb	7.3 ft/s	7.3 ft/s	7.3 ft/s
W/S	9.48 N/m^2	10.67 N/m^2	11.85 N/m^2
Vcruise	23.4 m/s	22.5 m/s	21.8 m/s
Vstall	8.26 m/s	8.76 m/s	9.24 m/s
Gross Weight	2.22 N	2.50 N	2.77 N
Mission Score	1.0	~0	~2

From these parameters, the mission scores can be predicted and are tabulated below in Table 12. Since Mission 1 is pass/fail, it is assumed the aircraft passed and received the 1 point associated with it.

Table 12 - Predicted Mission Scores

Parameter	M2	M3
M2 Passengers	1	-
M3 Passengers	-	1
M3 Payload (oz)	-	1
Total Mission Score	3	
Wingspan (in)	9	
Empty Weight (lb)	0.5	
RAC	4.5	
Total Score	$\frac{2}{3} * Report\ Score$	

5.7 Drawing Package

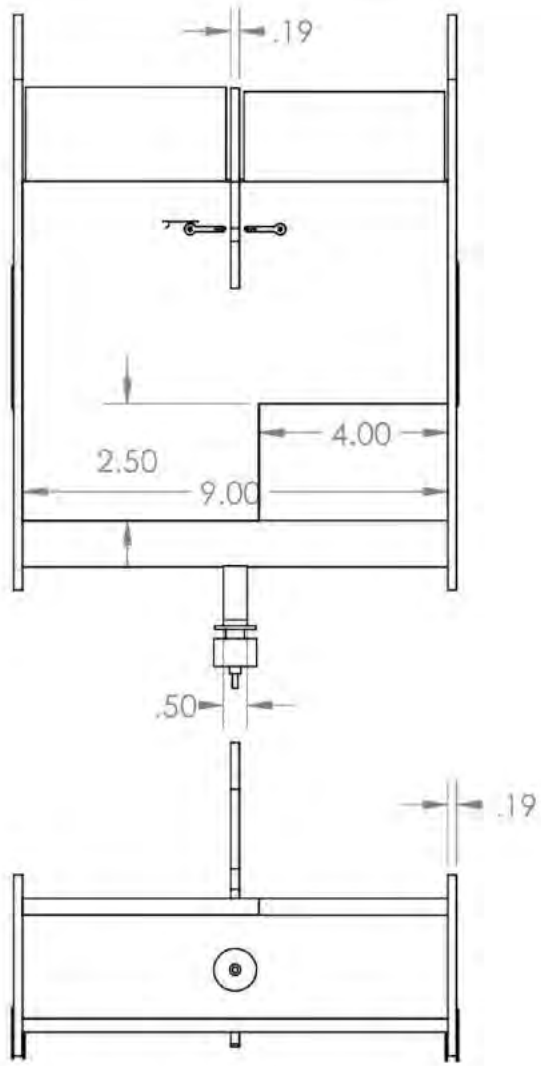

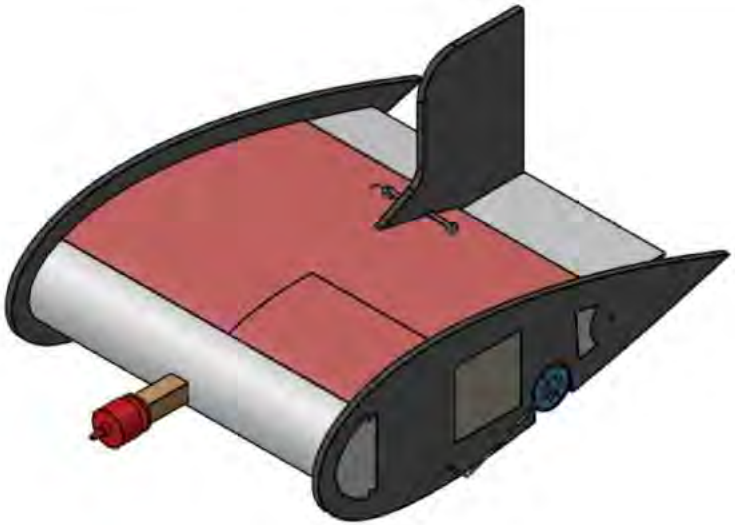

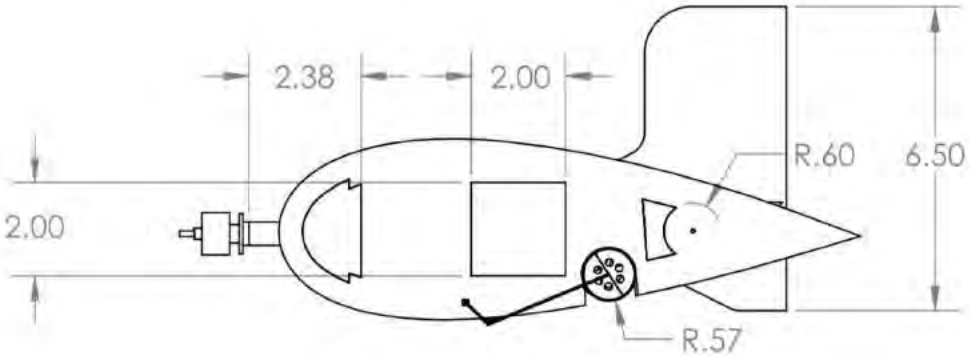

Comments	Clarkson University
Drawn By Thomas Smith Robert Shine	Knighthawk
REV C	3 View Drawing — SIZE B
Scale 1:4	Drawing Package — 2-20-2018 — 1 of 4

SOLIDWORKS Educational Product. For Instructional Use Only.

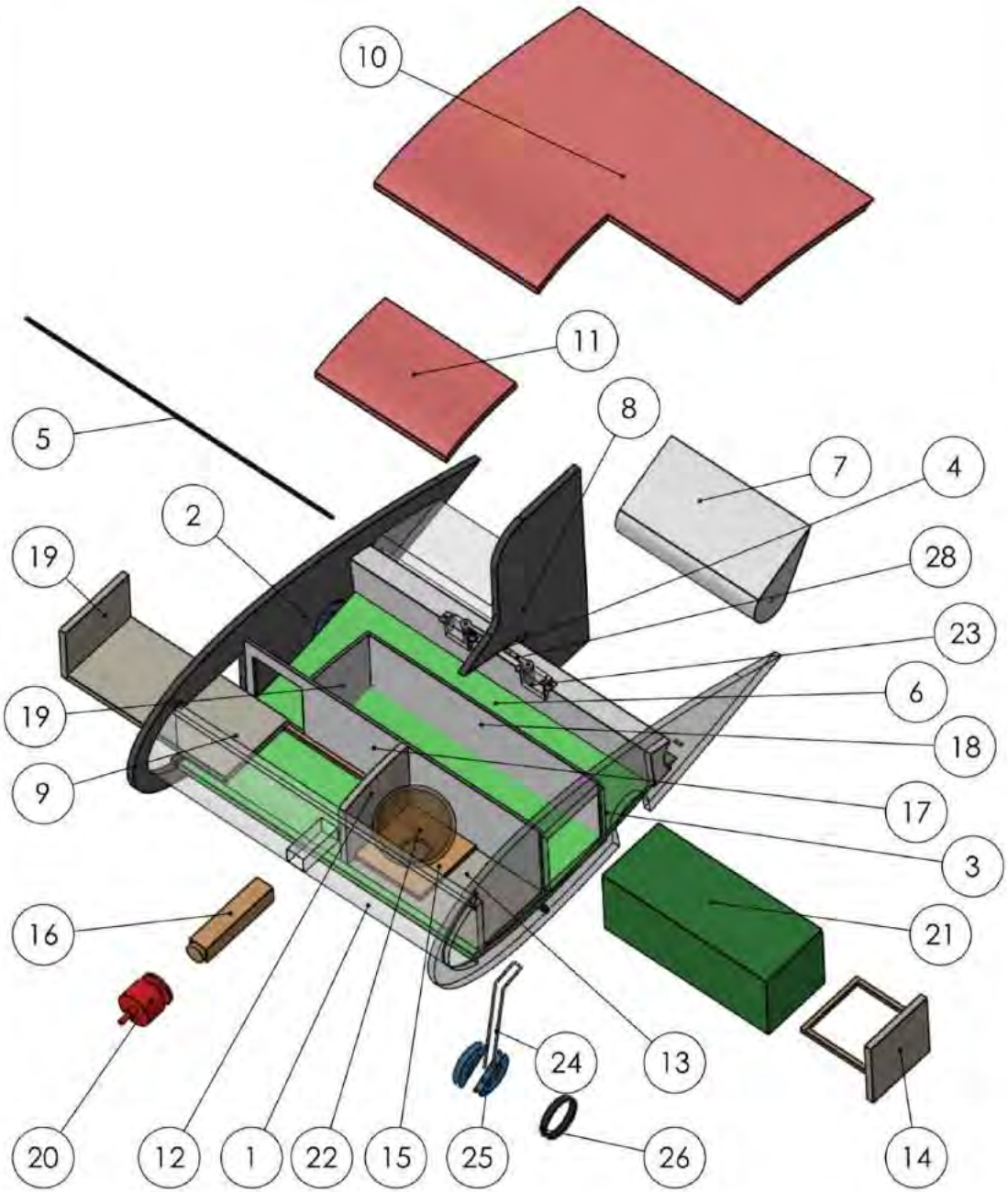

ITEM NO.	PART NAME	QTY.
1	Front	1
2	RightSide	1
3	LeftSide	1
4	Elevon Plug	1
5	Elevon Pivot	1
6	LowerSurface	1
7	Elevon	2
8	Vertical Tail	1
9	Battery Slider	1
10	UpperSurface	1
11	UpperSurface Plug	1
12	Passenger side	1
13	Lower Passenger Box	1
14	Left Side Plug	1
15	Seat	1
16	Motor Mount	1
17	Back plate	1
18	Payload Back	1
19	Payload Bay Side	1
20	Motor	1
21	Payload Block	1
22	Biggest Passenger	1
23	ServoAssembly	2
24	Landing Gear	2
25	Landing Gear Wheel	4
26	Wheel Rubber Band	2

Comments	Clarkson University		
Drawn By Thomas Smith Robert Shine	Knighthawk		
	REV C	Structural Arrangement	SIZE B
	Scale 1:4	Drawing Package 2-20-2018	2 of 4

SOLIDWORKS Educational Product. For Instructional Use Only.

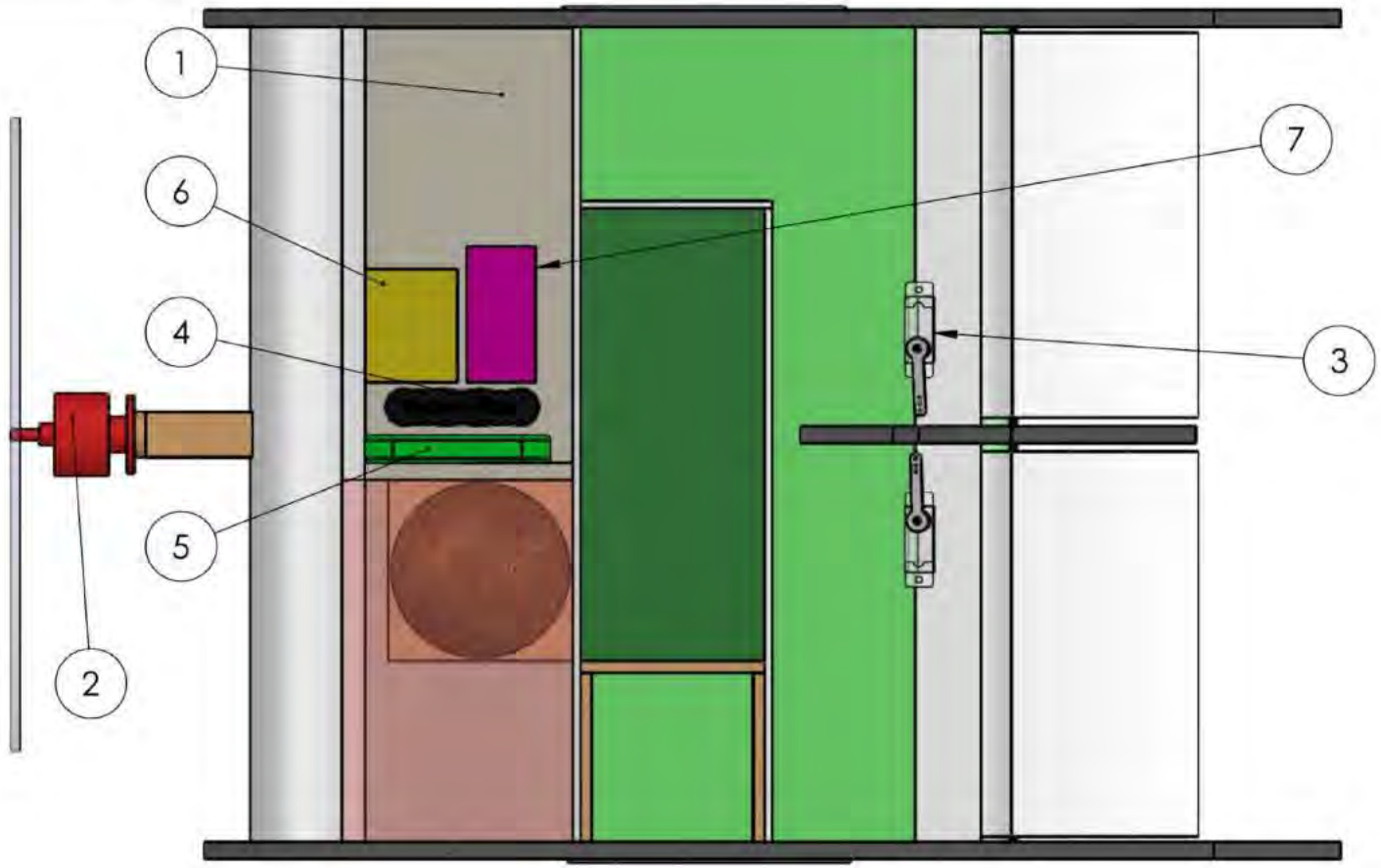

ITEM NO.	PART NUMBER	QTY.
1	Battery Slider	1
2	Motor	1
3	Servo Motor	2
4	RecieverPack	1
5	Propulsion Pack	1
6	Reciever	1
7	ESC	1

Comments	Clarkson University
Drawn By Thomas Smith Robert Shine	Knighthawk
REV C	Systems Layout — SIZE B
Scale 1:2	Drawing Package 2-20-2018 1 of 4

SOLIDWORKS Educational Product. For Instructional Use Only.

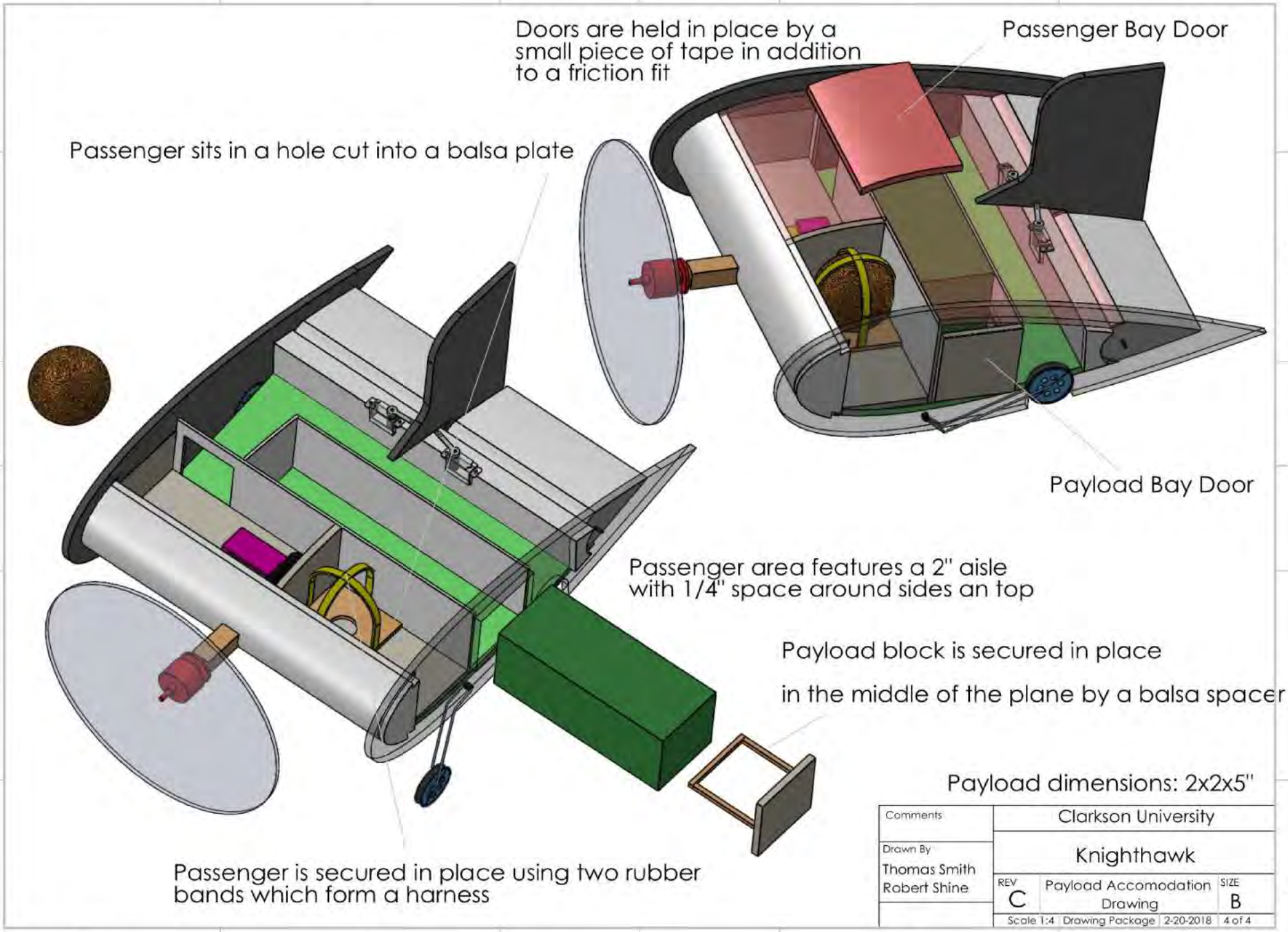

Comments	Clarkson University		
Drawn By Thomas Smith Robert Shine	Knighthawk		
	REV C	Payload Accomodation Drawing	SIZE B
	Scale 1:4	Drawing Package	2-20-2018	4 of 4

SOLIDWORKS Educational Product. For Instructional Use Only.

6.0 Manufacturing Plan

6.1 Manufacturing Methods Considered

6.1.1 Solid Foam Construction Techniques

Solid foam parts can be made using a variety of techniques include laser cutting, CNC, and hot wire cutting. The team recently acquired a laser cutter which is extremely useful in creating plywood templates for hot wire cutting. Attempts to cut the foam with the laser cutter left a lot of melting and a poor surface finish causing difficulty in making precision parts. Attempts at wire cutting wass slow and meticulous, but were improved by laser cutting plywood templates.

6.1.2 Balsa and Monokote Structures

The team has the most experience in balsa build up structures. Early prototypes showed that the weight of such structures were heavier than foam. The team investigated the possibility of using monokote as an aerodynamic covering to the aircraft skin, but the tension on the covered parts caused them to deform.

6.1.3 Composites

The use of composites in the past has typically be limited to premade spars and rods. The design this year indicates that a similar use case is probable for the elevon pivot and possible the motor boom. There is not a significant weight advantage to this technique over foam this year, as the scale would require impractically thin composite structures at a significantly higher expense.

6.1.4 3D Printing

Team experience has shown that 3D printed parts offer increased precision and manufacturability at the cost of weight. The best use cases for this technology is in small intricate parts.

6.2 Manufacturing Methods Selected

6.2.1 Aircraft shell

Hot wire cut solid foam sections were identified as the optimal construction technique for the aircraft shell. This consists of the two side ribs and the leading and trailing edge spars. The leading edge spar is part of the aerodynamic surface and precision hot wire cutting has proven to give excellent surface finish. The parts will be held together using micro-bubbled epoxy, which reduces the weight of the connections.

6.2.1 Aircraft Skin

The team was undecided on whether to use foam cut into the shape of the airfoil, or to bend a piece of straight foam into the correct shape. Earlier tests with hot wire cutting proved very successful and shaped

foam parts were identified to be stronger and lighter than the bent foam alternatives. It was for this reason then that the team opted to use this technique for the aircraft skin

6.2.1 Internal Dividers

The internal dividers are made of straight thin pieces of foam cut into shape using a knife. This is light and easy to manufacture. As a result of using shaped surfaces for the top and bottom of the aircraft, internal supports are not necessary and so the dividers are non-structural.

6.3 Manufacturing Milestone

A manufacturing schedule was developed to keep the team on track and to illustrate the production order, as well as to document various subcomponent dependencies. Figure 25 below represents the schedule for the competition aircraft leading up to the fly-off. A similar technique was used for the various prototype designs.

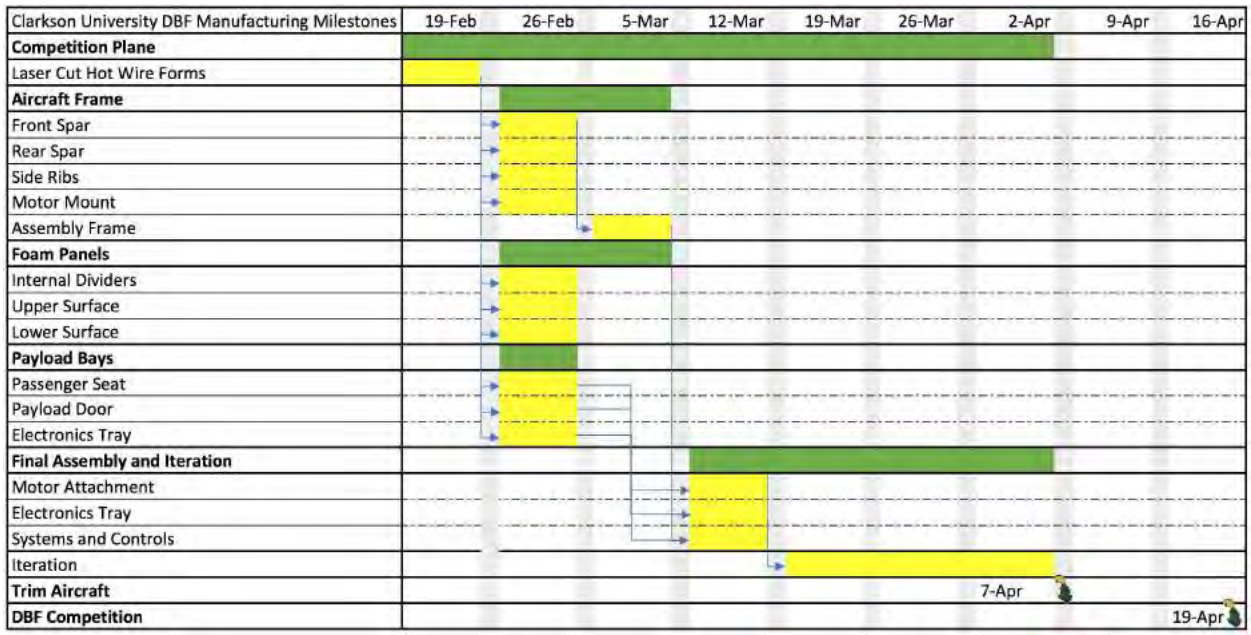

Figure 25 - Manufacturing Milestones Chart

7.0 Testing Plan

The testing plan involves both subsystem and flight tests. Below, a testing schedule can be seen and outlines the intended vs. actual testing schedule, first outlined at the start of the design process.

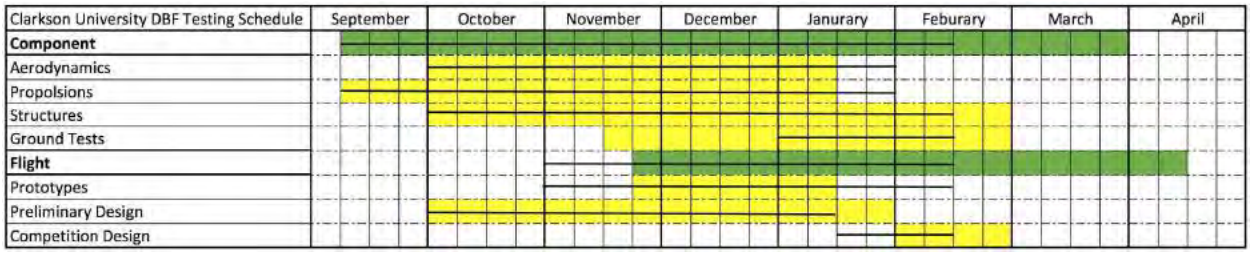

Figure 26 - Clarkson University Testing Plan

7.1 Test Objectives

Each design team described and submitted a series of tests to team leadership to allow for proper verification of their given objectives, subsystems, and performance estimates. The subteams, tests, and objectives are listed below and further expanded upon in section 7.2.

Aerodynamics

- *Utilize flight tests to confirm XFLR5 model*
- *Measure takeoff distance during flight tests to verify it is less than 150 feet*

Structures

- *Perform tip test on aircraft*
- *Demonstrate LRU serviceability time is within requirements*

Stability and Control

- *Verify optimal CG location*
- *Verify size and movement range of control surfaces to allow for optimal control*
- *Utilize pilot feedback to improve flight characteristics.*
- *Fine tune receiver SAS for improved flight characteristics during flight tests*

Systems

- *Verify all systems/servos work properly through stationary testing and test flights*

Propulsions

- *Verify flight speed and range of aircraft through thrust testing and test flights*

7.2 Subsystem Testing

7.2.1 Propulsion Testing

The propulsion testing consisted of verifying the propeller, motor, and battery selections independently and as a combined unit. The discharge performance of the battery was first tested to measure voltage decay and capacity. This was done in two ways. The battery was charged to capacity and then discharged using a multipurpose charger at a set current draw to determine the capacity. The battery was also connected to the tested motor and propeller combinations in static and dynamic conditions to measure actual performance. The chosen battery pack was identified to be a hard requirement as the cells used were the only choice for the capacity, current draw, and weight required by the design.

After the battery performance was determined, motor and propeller combinations could be tested using a switching power supply that allowed for matching the voltage and limiting the current to that of the battery. These tests were conducted using a thrust stand designed by the team and consisted of static measurements, as well as dynamic measurements measured in a wind tunnel. The thrust stand and its labeled components are shown below in Figure 27.

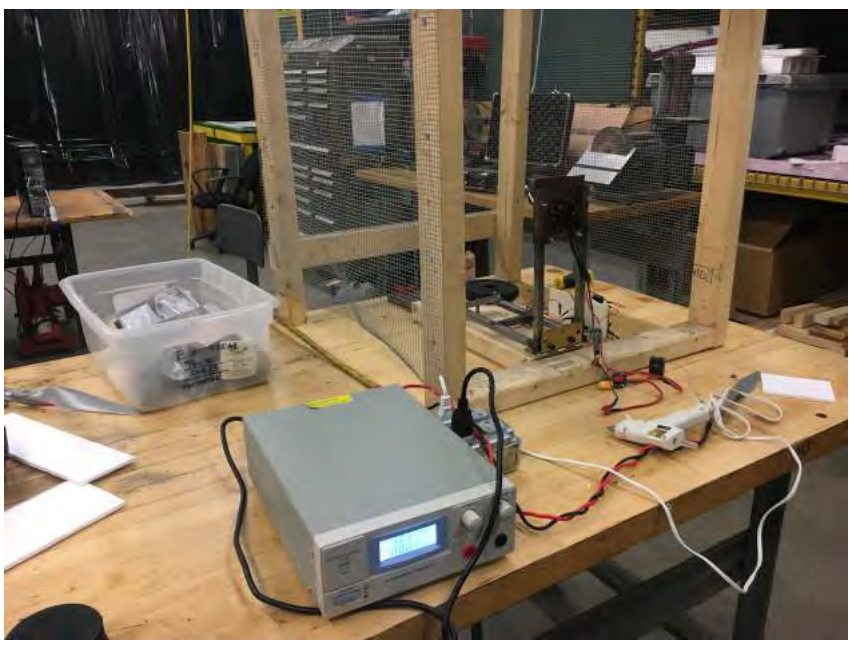

Figure 27 - Experimental Thrust Stand Setup

The main objective for the propulsion testing was to optimize the efficiency of the propulsion system at the target flight speed. This is because the plane is optimized to fly all three flight missions at the smallest weight and wingspan possible. Small gains in performance at the expense of efficiency runs the risk of running out of power before the mission ends. Since the mission scores for this plane will be so low once

normalized by the top performer for each mission, the only parameter worth designing for is efficiency and range.

7.2.2 Structural Testing

The overall weight and shape of the aircraft meant that the aircraft is sufficiently strong in a tip test. The outer skin of the aircraft was tested for deflection under aerodynamic pressure. The motor mount was also tested as previous prototypes have shown that the boom it is attached to tends to loosen itself from the foam on poor landings or when the propeller was not aligned with the ground properly. Impact tests were conducted so that the aircraft would stand a better chance a remaining flyable after such incidents.

7.2.3 LRU Testing

Parts that were identified as potential LRUs were designed from conception to be removable within a minimal amount of time. The trials were timed in a fashion identical to that which will be faced at competition. All LRUs applicable to the competition design were tested instead of being determined by a die roll. Each LRU must be removed and replaced within the given timeframe for its given stage.

7.2.4 Takeoff Performance Testing

The team conducted takeoff testing to verify that the aircraft was capable of taking off within the prescribed 150 feet. Possible conditions were accounted for as the aircraft took off in crosswind in both empty and loaded configurations. The takeoff was considered successful if the aircraft entered powered, controlled flight and left the ground in under 150 feet ground distance.

7.3 Flight Test Schedule and Flight Plan

Flight tests provide valuable pilot feedback that the design team can use to improve the design. Flight data is monitored using an eLogger Pro V3 to gather flight speed, power draw, and throttle position. Table 13 below lists the scheduled flight tests with intended goals. All flight tests are conducted at Bagdad Field, Potsdam, NY.

Table 13 - Flight Test Schedule

Date	# of Flights	Objective
Nov 25, 2017	1	Determine initial flight characteristics of Preliminary Design
Dec 2, 2017	4	Determine minimum controllable wingspan
Jan 23, 2018	3	Determine cruise speed and range of preliminary propulsion

		system.
Feb 3, 2018	8	Simulate competition missions, validate takeoff performance
Mar. 10, 2018	TBD	Experiment with SAS built into receiver to determine usefulness
Mar. 31, 2018	1	Trim Competition Aircraft

Each flight date consisted of multiple flights with different objectives. A flight plan from January 23, 2018 is shown below in Table 14.

Table 14 - Sample Flight Date Itinerary

Flight #	Objective	Acceptance Criteria
1	MTOW, Speed Flight	Record successful data from eLogger
2	MTOW, Range Flight	Identify range of aircraft (both flight time and distance)
3	1 Passenger, Range Flight	Determine if the aircraft can fly 3 laps with a single passenger (Mission 2 simulation)

7.4 Flight Checklists

Preflight checklists are kept for all tests and are conducted before each flight in order to ensure efficiency and to maintain team safety. These checklists also serve as a final decision by the pilot as to whether to fly or not. The checklists seen in Tables 15 and 16 are used before and after each flight to ensure that everything is working properly and that there is no visible damage to the aircraft that could jeopardize team safety, which is paramount.

Table 15: Pre-Flight Checklist

Component	Task
Fuselage (internal)	❏ Receiver is completely connected and secured to fuselage ❏ Load cargo (if applicable) ❏ Load and secure passengers (if applicable) ❏ Make sure CG is correct
Fuselage (external)	❏ Make sure all hatches are closed ❏ Landing Gear in takeoff position
Pilot Checklist	❏ Connect fuse/arm ESC

	❏ Complete a control check ❏ Run up motor ❏ Go No-Go decision is made

Table 16: Aircraft Inspection Checklist

Component	Items to Inspect
Motor	❏ Motor mount is securely fastened and there are no visible cracks ❏ Propellor is securely fastened ❏ Propellor is balanced and there are no visible cracks
Fuselage/Wing	❏ Receiver is securely fastened to the fuselage ❏ All wires are secured to the receiver ❏ ESC is secured to the fuselage ❏ Battery is secured to the fuselage and properly connected to the ESC ❏ There are no visible cracks ❏ Cargo is secured (if applicable) ❏ Passengers are secured and restrained (if applicable)
Control Surfaces	❏ All control surfaces move freely ❏ Elevon Pivot is secured ❏ All servos are working properly
Landing Gear	❏ Landing gear is locked in lowered position ❏ Wheels are free to spin

8.0 Performance Results

8.1 Demonstrated Performance of Key Subsystems

8.1.1 Propulsion System

The batteries were tested to characterize the performance of the cells. The battery was connected to the preliminary propulsion system and run at full power with battery voltage readings taken periodically via manual data point collection in the thrust stand user interface. The battery voltage vs. time data is displayed below in Figure 28.

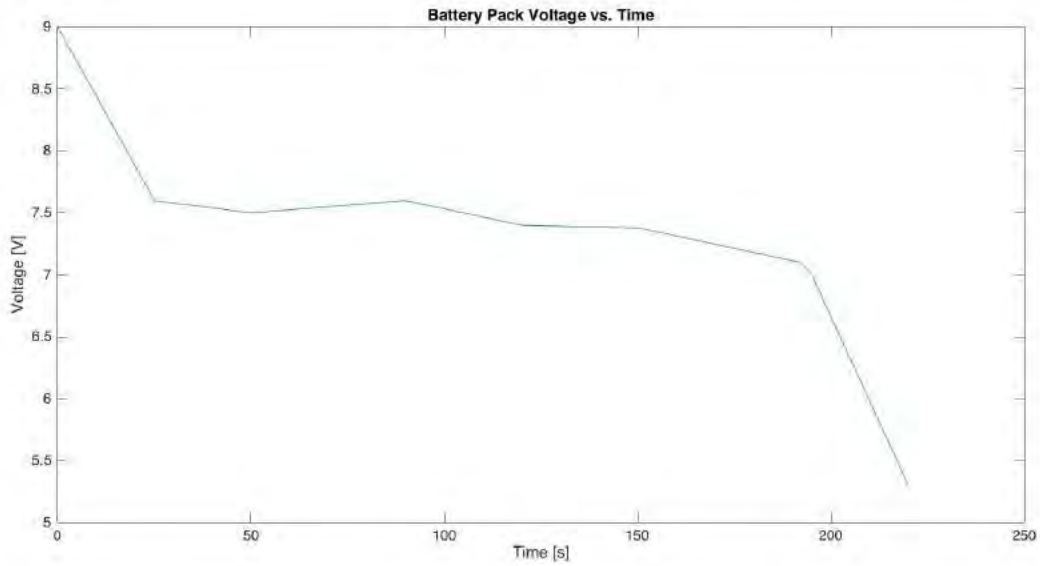

Figure 28 - Battery Voltage vs. Time

The test confirmed predictions that the battery will be able to last the 3 minutes allocated, but barely. This test showed that efficiency gains in the motor selection could prove significant. It was noted however, that the 3 minute flight time goal takes into account an unrealistically conservative headwind.

Three motors considered for the final design are specced below in Table 17.

Table 17 - Motor Comparison

	ELE C20 PRO 1550Kv	hexTronik 1500KV	Turnigy AX-2204C
KV	1550	1500	1450
Weight	26.2 grams	29 grams	20 grams
Max Current	9 Amps	9 Amps	8 Amps

Propulsion tests indicated that the motor current draw occasionally reached eight amps and so the ELE C20 Pro motor was chosen for the competition plane to give enough headroom. This motor selection was later used in flight tests and proved to be adequate.

8.1.2 Structural Tests

A wing tip test was performed and no observable deflection was noted. Since the 2nd moment of area of the plane in the longitudinal plane is so large, and the wingspan is so small, the structure was determined to be significantly stronger than necessary for structural integrity.

8.1.3 LRU replacement testing

LRUs were removed and timed to determine the worst case scenario that will be faced at competition. Timed trials for the two stages are tabulated below in Tables 18 and 19.

Table 18 - Ground Mission 1 LRUs

LRU Removed	Time(s)
Servo	90
Rx Battery	63
Propulsion Battery Pack	73
Control Pushrod	50
Landing Gear Wheel	20
Propeller	122

Table 19 - Ground Mission 2 LRUs

LRU Removed	Time(s)
ESC	68
Elevon	32
Rx Receiver	191
Landing Gear	22
Motor	244

From the tests, the worst case scenario timewise that could be faced is removing both the propeller and motor. In this case, the propeller removal is still much less than the 180 second limit and the motor is less than the 300 second limit. The testing did not indicate that any subcomponent redesign is necessary ahead of the competition fly off.

8.2 Demonstrated Flight Performance of Completed Aircraft

Flight tests were conducted in order to verify the aircraft's airworthiness and to verify that the aircraft was capable of completing all three flight missions at competition. Flight tests also served to provide valuable feedback to the design team. Some notable flight tests and conclusions drawn are tabulated below in Table 20.

Table 20 - Flight Test Findings

Date	Flight Objective	Conclusions Drawn
Nov 25, 2017	Determine initial flight characteristics of Preliminary Design	CG placement was too far back and was moved forward in future prototypes
Dec 2, 2017	Determine minimum controllable wingspan	A wingspan of 8 inches minimum is needed to achieve adequate roll authority
Jan 23, 2018	Determine cruise speed and range of preliminary propulsion system.	Flight cruise speed was 60 ft/s
Feb 3, 2018	Simulate competition missions, validate takeoff performance	No show stoppers noted

Flight test data was also compared to performance predictions. This data is tabulated below in Table 21.

Table 21 - Flight Test Findings

	Parameter	Prediction	Measured
M1	Air Speed	71 ft/s	67 ft/s
M2	Air Speed	70 ft/s	64 ft/s
	Time	192 seconds	155 seconds
M3	Air Speed	66 ft/s	60 ft/s
	Time	60 seconds	54 seconds

The predicted air speed was slightly higher than the measured values, but the difference between the two was considered acceptable. The measured lap times were much lower than the predicted values. This has to do with the fact that the wind speeds during the flight test were much lower than the 20 mph winds predicted for in the flight model. This inspires confidence moving forward as the aircraft has demonstrated the capability to fly all 3 missions significantly faster when facing significantly easier conditions. The team will try to conduct another flight test on a much windier day to get a closer approximation, but there are otherwise no concerns to note.

A photo of the flying aircraft is displayed below in Figure 29.

Figure 29 - Flying Competition Design

Bibliography

[1] "AIAA's Design•Build•Fly", *Aiaadbf.org*, 2018. [online], http://www.aiaadbf.org/. [retrieved 30 January, 2018].

[2] “MIT Open Courseware”, *Basic Aircraft Design Rules*, 2006. [online], https://ocw.mit.edu/courses/aeronautics-and-astronautics/16-01-unified-engineering-i-ii-iii-iv-fall-2005-spring-2006/systems-labs-06/

Virginia Tech
Design Build Fly
2017-2018
Atlas

Susan Bowen, Shreya Chandramouli, Zoe Guernsey, Erik Higgins, William Jennings, John Kiene, Austin Kleinfelter, Atul Kumar, Sapna Rao, Brady Reisch, JP Stewart, Avery Sebolt, Matthew Svoboda

TABLE OF CONTENTS

1 LIST OF TABLES 3

2 LIST OF FIGURES 4

3 LIST OF VARIABLES AND ACRONYMS 5

4 EXECUTIVE SUMMARY 6

1.1 DESIGN PROCESS 6
1.2 KEY MISSION REQUIREMENTS AND DESIGN DRIVERS 6
1.3 PERFORMANCE CAPABILITIES 7

5 MANAGEMENT SUMMARY 8

1.4 TEAM ORGANIZATION 8
1.5 PROGRAM SCHEDULE 9

6 CONCEPTUAL DESIGN 9

1.6 MISSION REQUIREMENTS 9
1.6.1 FLIGHT MISSION OVERVIEW 10
1.6.2 FLIGHT MISSION 1 11
1.6.3 FLIGHT MISSION 2 11
1.6.4 FLIGHT MISSION 3 11
1.6.5 GROUND MISSION 11
1.6.6 CUSTOMER REQUIREMENTS 11
1.6.7 SENSITIVITY ANALYSIS 12
1.7 DESIGN REQUIREMENTS 13
1.8 CANDIDATE CONFIGURATIONS 13
1.8.1 BLENDED WING BODY 13
1.8.2 BI-PLANE 14
1.8.3 OBLIQUE WING 14
1.8.4 FLYING WING 15
1.9 CONFIGURATION SELECTION PROCESS 16

7 PRELIMINARY DESIGN 18

1.10 DESIGN/ANALYSIS METHODOLOGY 18
1.11 AV1 PRELIMINARY DESIGN 19
1.11.1 AV1 DESIGN PROCESS 19
1.11.2 AV1 TEST RESULTS 19
1.12 AV2 AND AV3 PRELIMINARY DESIGN 20
1.12.1 COMPARATOR AIRCRAFT 21
1.12.2 SIZING BREAKDOWN 21
1.13 DESIGN/SIZING TRADES 23
1.13.1 AIRFOIL SIZING 23
1.13.2 STABILITY AND CONTROL SIZING 24
1.13.3 POWER SIZING 26
1.14 MISSION MODEL 28
1.15 AIRCRAFT CAPABILITIES ESTIMATES 29
1.16 AIRCRAFT MISSION PERFORMANCE ESTIMATES 31

8 DETAIL DESIGN 32

1.17 AV2 TO AV3 DESIGN CHANGES 32
1.18 DIMENSIONAL PARAMETERS 32
1.19 DETAILED DESIGN ELEMENTS 33
1.19.1 LANDING GEAR LOCATION 33
1.20 STRUCTURAL CHARACTERISTICS/CAPABILITIES 33
1.20.1 STRUCTURAL LOAD PATH 33
1.21 SYSTEMS SELECTION, INTEGRATION AND ARCHITECTURE 34
1.21.1 SEAT 34
1.21.2 PAYLOAD BLOCK 34
1.21.3 SERVO, RECEIVER, AND RECEIVER BATTERY SELECTION 34
1.22 WEIGHT AND BALANCE 34
1.23 FLIGHT PERFORMANCE PARAMETERS 35
1.24 MISSION PERFORMANCE AND RATED AIRCRAFT COST (RAC) 38
1.25 MISSION PERFORMANCE 38
1.26 DRAWING PACKAGE 39

9 MANUFACTURING PLAN 40

1.27 MANUFACTURING PROCESSES CONSIDERED 40
1.28 SUBSYSTEM MANUFACTURING 41
1.29 MANUFACTURING TIMELINE 44

10 TESTING PLAN 44

1.30 TEST OBJECTIVES 44
1.30.1 AERODYNAMICS TESTING 45
1.30.2 PROPULSION TESTING 45
1.30.3 SYSTEMS TESTING 46
1.30.4 MANUFACTURING TESTING 47
1.31 TEST SCHEDULE 48
1.32 TEST AND FLIGHT CHECK LIST 48

11 PERFORMANCE RESULTS 49

1.33 SUB-SYSTEM TESTING 49
1.33.1 PROPULSION PERFORMANCE 49
1.33.2 STRUCTURES PERFORMANCE 51
1.33.3 SYSTEM PERFORMANCE 51
1.34 AV1 PERFORMANCE 51
1.35 AV2 PERFORMANCE 52
1.36 AV2.5 PERFORMANCE 52
1.37 AV3 PERFORMANCE 53

12 BIBLIOGRAPHY 54

1 List of Tables

Table 1. Ground Mission LRUs 11
Table 2. Sensitivity Estimates with Realistic Values, with a 10 in. Wing Span and 0.7 Weight Fraction ... 13
Table 3. An Example of an Individual Subjective Selection Matrix 16
Table 4. Final Subjective Selection Matrix 16

Table 5. Objective Decision Matrix 17
Table 6. Predicted Scores for Atlas Concepts 17
Table 7. Lessons Learned from AV1 Testing 20
Table 8. Main Wing Airfoil Comparison 24
Table 9. Elevon Sizing Summary 25
Table 10. Comparison of Candidate Motors 27
Table 11. Comparison of Candidate ESCs 27
Table 12. Comparison of Candidate Propellers 28
Table 13. Predicted Preliminary AV2 Design Mission Performance 32
Table 14. Lessons Learned from AV2 Testing 32
Table 15. Final Design Dimensional Parameters 32
Table 16. AV3 Component Weight and CG Location 35
Table 17. Flight Performance Parameter by Mission 35
Table 18. Mission Performance Parameters and RAC 38
Table 19. Wing Manufacturing Trades 40
Table 20. Propulsion System Combinations 45
Table 21: Wind Tunnel Checklist 48
Table 22. Pre-Flight Checklist 49
Table 23. Propulsion System Final Configuration Options 49
Table 24. Demonstrated vs. Predicted Mission Performance for AV3 54

1 List of Figures

Figure 1. AV3 as Designed 6
Figure 2. Team Organization Chart 8
Figure 3. Gantt Chart 9
Figure 4. Competition Analogy to Real World Operations 10
Figure 5. DBF Flight Mission Course 10
Figure 6. Influence Coefficient Comparison for Unit and Realistic Values 12
Figure 7. Blended Wing Body Model 14
Figure 8. Bi-Plane Model 14
Figure 9. Oblique Wing Model 15
Figure 10. Flying Wing Model 15
Figure 11. The Design Spiral Process 18
Figure 12. Evolution of the Design 18
Figure 13. AV1 Prototype as Designed and Built 19
Figure 14. AV2 Prototype as Designed and Built 20
Figure 15. Comparison of Similar Historic Aircraft 21
Figure 16. Georgia Tech 2011 and Atlas V2 Weight Build Up 21
Figure 17. Carpet Plot Showing the Relationship Between Span, Takeoff Velocity, and Takeoff CL Based on AV2 Data 22
Figure 18. Thrust Required and Available vs. Aircraft Speed Compared with Three Takeoff Speeds 23
Figure 19. Power Required and Available vs. Aircraft Speed Compared with Three Takeoff Speeds 23
Figure 20. Top View of Basic Aircraft Configuration 25
Figure 21. NiMH Cell Capacity vs. Weight 26
Figure 22. Comparison of numerical methods and experimental data for Clark Y of AR = 0.5 29
Figure 23. Trimmed L/D, C_L, C_D, and K_n vs. Angle of Attack 30
Figure 24. AV3 Stick Fixed Static Margin at 15%c 30
Figure 25. AV3 Carpet Plot Comparing Cruise L/D, Battery Capacity, and Number of Laps 31
Figure 26. Landing Gear Location 33
Figure 27. Aircraft Primary Load Paths 34

Figure 28. Takeoff Distance Carpet Plot 36
Figure 29. Span Carpet Plot 36
Figure 30. Delta V from Propwash 37
Figure 31. AV3 Thrust and Drag 37
Figure 32. AV3 Power Required and Available 38
Figure 33. Simulated Toolpaths Using Both Ramp and Adaptive Clearing Carves 41
Figure 34. Completed Wing Section 41
Figure 35. Lightweight, Removable Control Surfaces 42
Figure 36. CNC Milled Carbon Endplates 42
Figure 37. Lashed Bushing and Tail Boom 43
Figure 38. Top Left: Passenger Seat with adjustable strap. Top Right: Basswood payload block. Bottom Left: Motor Mount with Nose gear. Bottom Right: All-flying tail. 43
Figure 39. Manufacturing Timeline 44
Figure 40. High Level Testing Plan 44
Figure 41. RCbenchmark Series 1580 Specification and Test Stand 46
Figure 42. NiMH Full Throttle Discharge Endurance 50
Figure 43. Thermal Evaluation of Propulsion System 50

2 List of Variables and Acronyms

AV[number]	Air Vehicle (i.e. AV1)
CA	Cyanoacrylate
C_D	Drag Coefficient
C_L	Lift Coefficient
CG	Center of Gravity
CNC	Computer Numeric Control
DBF	Design Build Fly
ESC	Electronic Speed Control
l_t	Tail lift moment arm
Kv	Motor Velocity Constant (RPM/V)
LiPo	Lithium polymer
L_{tail}	Lift due to the tail
$M_{fuselage}$	Fuselage aerodynamic moment
M_{tail}	Tail aerodynamic moment
NiCd	Nickel cadmium
NiMh	Nickel metal hydride
OML	Outer Mold Line
PWM	*Pulse Width Modulation*

3 Executive Summary

This report details the design, manufacturing, and testing process of the Virginia Polytechnic Institute and State University (Virginia Tech) entry, Atlas, in the 2017-2018 AIAA Design Build Fly (DBF) Competition. The AIAA DBF Organizing Committee has determined the need for a mixed-use regional/business aircraft which can act as a passenger short haul aircraft with the ability to provide long haul passenger and payload missions. The following mission requirements were provided:

- Staging flight without passengers or payload
- Rapid servicing with line replaceable units
- Short haul flights carrying passengers
- Long haul flights carrying passengers and payload

The RFP requirements and scoring methods led the Virginia Tech team to build a short-haul passenger with a minimum span blown wing configuration and an all flying conventional tail.

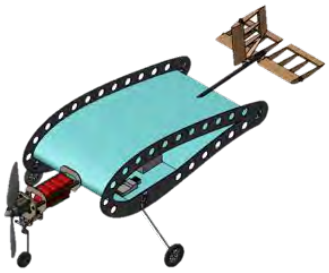

Figure 1. AV3 as Designed

3.1 Design Process

The customer's needs and requirements were studied through an in-depth scoring analysis and trade studies, then implemented in the preliminary and detailed design. Due to the complexity of the configuration, the program emphasized relevant testing over detailed analysis, comparing various configurations, it was determined that a blown flying wing design would result in the maximum overall score. The focus of this aircraft was to minimize the RAC (low weight and low span). The design process was iterative and emphasized testing at the component, subsystem, and air vehicle level. The end of the third design spiral marked the completion of the third air vehicle (AV3) which resulted in an aircraft that will carry 1 oz. of payload and complete at least three laps with a span of 8 in. as well as a maximum takeoff weight of 1.39 lbs. This configuration provides the customer with the highest scoring design.

3.2 Key Mission Requirements and Design Drivers

Scoring sensitivity analysis was done for each mission to determine which scoring parameters have the highest effect on the overall score. Due to the constants in the mission 1 and 3 scoring equations, the overall score is most directly controlled by empty weight and span. The team evaluated several conceptual

designs that assumed generous performance of competitors and consistently found that no reasonable number of passengers or payload weight could compensate for an extremely small and light aircraft.

Passenger and Payload Requirements: The aircraft is required to internally store passengers and payload in separate compartments within the aircraft. The passengers are bouncy balls of varying size and weights that will be provided based on a given distribution during competition. The payload block has a dimension requirement of the length, width, and height summing to at least 9 in. and must weigh less than 8 oz. Passengers must be restrained in individual seats while leaving space for an aisle, resulting in a passenger compartment with a minimum width of 4.0 in.

Takeoff Requirements: The aircraft must be able to takeoff within 150 ft. This places strong minimum power, span, and C_{Lmax} constraints on the system.

Line Replaceable Units Requirement: Replaceable components are vital to the completion of the ground mission. There are 2 stages to the ground mission, 1 with field LRUs and 1 with depot LRUs, adding up to 11 components which must be fully modular. The field stage allots 3 minutes to replace 1 of 6 components. All 6 of the components and tools used in the field round must fit within the payload bay of the aircraft prior to the start of the ground mission. The depot stage allows 5 minutes to replace 1 of the 5 potential components.

Mission Requirements: The 3 air missions as well as the ground mission must be completed successfully. This entails being able to complete a minimum of 3 laps with a successful takeoff and landing.

Span and Weight Requirements: Scoring analysis placed great importance upon the RAC and therefore the span and empty weight as seen in Equation 2. It was determined that, to maximize the overall score, the aircraft must have the lowest possible wingspan and weight.

3.3 Performance Capabilities

- Empty Weight: 1.24 lbs.
- Span: 8 in.
- Max Takeoff Weight: 1.39 lbs.
- Takeoff Speed: 31 mph
- Takeoff Distance: 128 ft.
- Cruise Speed: 45 mph
- Control surfaces: Conventional, all-flying tail
- 1 Passenger and 1 Payload Block weighing 1 oz.
- Range: >3 laps in 3.5 minutes

The design is heavily focused on decreasing weight and minimizing the wing span, requiring manufacturing to heavily consider the weight of components during construction. Virginia Tech's DBF team believes this innovative design will succeed at competition.

4 Management Summary

4.1 Team Organization

Virginia Tech's DBF team is a multi-disciplinary team consisting of students from all academic levels, disciplinary expertise, and experiences. There are nine project leaders shown in Figure 2. Team Organization Chart. Each manages a functional piece of the aircraft in addition to educating and leading underclassmen to ensure continuity of DBF at Virginia Tech.

- The **Chief Engineer** ensures technical excellence and collaboration across the team.
- The **Project Manager** controls the project plan, budget, travel arrangements, and team outreach.
- The **Aerodynamics and Flight Test** team is responsible for sizing the planform, generating the outer mold line (OML), and running performance analyses. Their flight test responsibilities include determining test objectives, instrumentation, test planning, test conduct, and data analysis.
- The **Stability** team works closely with Aerodynamics to assist with the OML, determine control surface sizing, and analyze static/dynamic stability and control.
- The **Propulsion** team determines the motor, battery and ESC sizing while conducting tests for performance and reliability.
- The **Structures** team oversees the CAD model, designs the internal structure, and conducts analysis and testing on design iterations.
- The **Manufacturing** team is responsible for determining the manufacturing methods and the construction of necessary tooling. The Manufacturing lead is responsible for production of all aircraft components.
- The **Systems and Report** lead maintains the system and sub-system requirements and ensures compliance across teams. They also create and format all written deliverables.
- The **Underclassman** lead works with the senior team and co-leads Propulsion and Manufacturing. The Underclassman lead is an integral part of continuity for the team as they are given the necessary experience to be a team lead in future years' competitions.

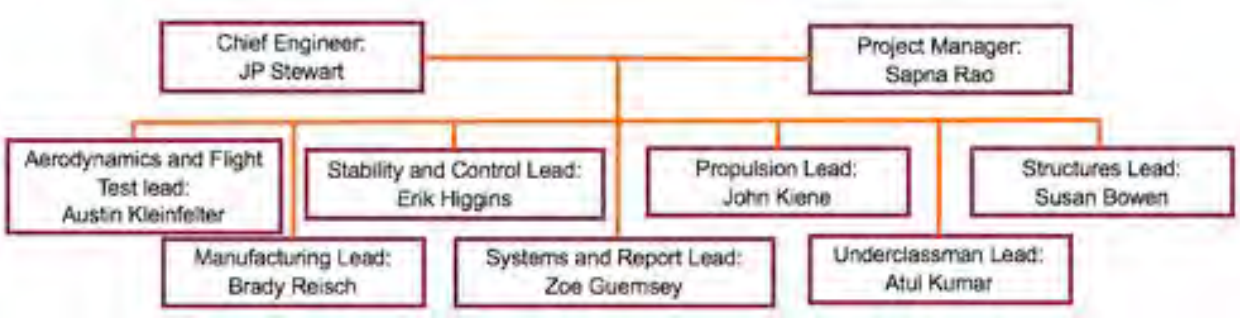

Figure 2. Team Organization Chart

4.2 Program Schedule

Figure 3 shows the high-level Gantt chart developed and maintained by the Project Manager to track project status. The orange bars represent the actual progress the team has made in comparison to the planned progress shown with maroon bars. The current date (report submission) is indicated with a red line, major milestones with diamonds, and the final competition fly-off is depicted with a star.

The design process started with an analysis of the request for proposal and conducting scoring analysis to identify key design drivers. Conceptual trades began by evaluating various configurations through decision matrices. With a design identified, preliminary design could determine the outer mold line and initial configuration sizing. The primary focus of the preliminary design phase was to test assumptions made in the configuration selection and rapidly prototype to de-risk the design. An initial sizing was conducted and Air Vehicle 1 (AV1) was built. Lessons learned were applied to the designs of future aircraft (AV2, 2.5 and 3) and iterated until the aircraft was fully compliant with the requirements. After submitting the DBF report, this design will be refined for competition to reduce weight and improve mission performance as additional production quality builds are being done.

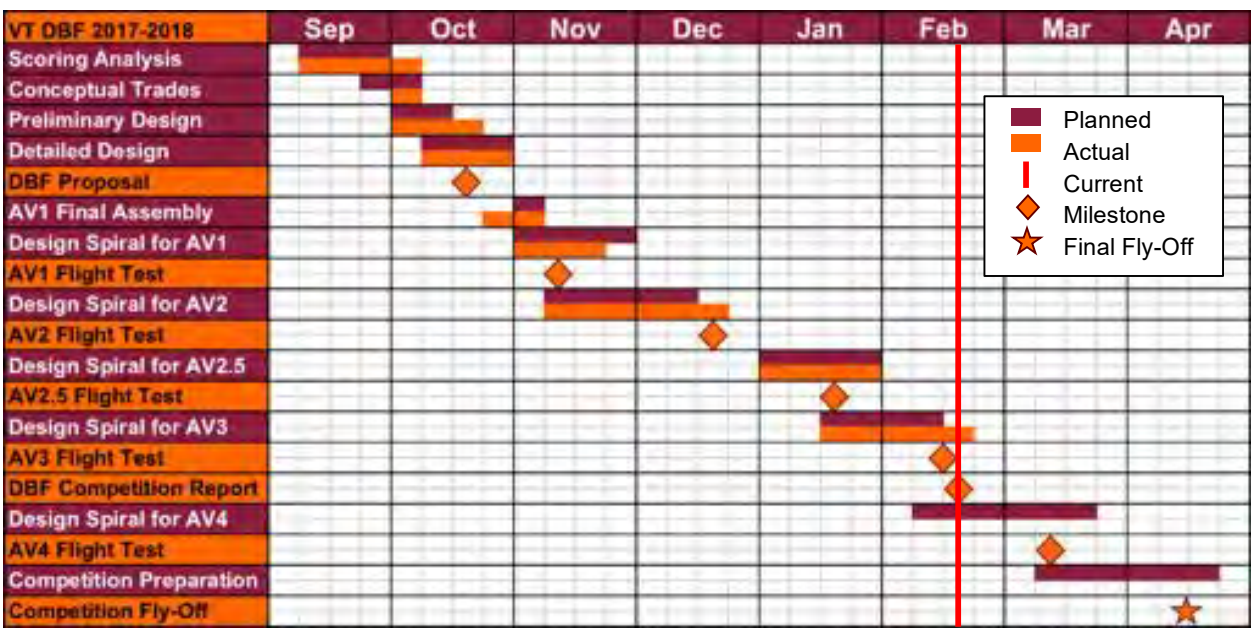

Figure 3. Gantt Chart

5 Conceptual Design

5.1 Mission Requirements

The 2017-2018 Design Build Fly RFP calls for the design and construction of a simulated regional and business class passenger aircraft. Elements in the RFP are intended to emulate the constraints of real world operations and are listed in Figure 4.

Figure 4. Competition Analogy to Real World Operations

To mimic full sized passenger aircraft, this design must not only transport bouncy ball "passengers" and payload blocks, but must also be capable of rapid servicing and therefore must be equipped with field and depot replaceable LRUs which will be tested during the ground mission. The aircraft must demonstrate its short and long range flying capabilities over the course of 3 missions. The competition will then assess the aircraft's abilities with the scoring equations given below.

$$!"\#\ \ \$\%\&'\&'"(*+",\ \%= \frac{./\ \ 01123\ 4256/1786/2*:6\ 1;\ <=0>>063\ 786/2}{4?@} \tag{1}$$

$$AB!\ \ =\ \ C\ '(DE\$F(\ \ *\ G\#\ \$\&HC\%'Dh\& \tag{2}$$

5.1.1 Flight Mission Overview

Figure 5 shows the competition flight course. Each flight begins with a takeoff and climb against the wind. The aircraft makes its first turn away from the spectator area when signaled by the flagman located 500 ft. upwind. On the downwind leg, the aircraft must complete a 360° turn in the opposite direction of its first turn. After passing the second flagman, the aircraft will turn toward the spectator area on the upwind leg and either land or continue to additional laps.

Figure 5. DBF Flight Mission Course

5.1.2 Flight Mission 1

Flight Mission 1 is a pass or fail mission which simulates an aircraft staging flight with no passengers or payload. This mission requires the completion of a short haul flight (3 laps within 5 minutes). Each lap can be seen in Figure 5 and is approximately 7500 ft. dictating the minimum range needed.

$$\text{J'EE'"(} \quad 1 * + \text{", \%=} \quad 0 \text{ ", } \quad 1 \tag{3}$$

5.1.3 Flight Mission 2

Flight Mission 2 is a second short haul flight; however, the aircraft must carry the maximum number of passengers for which it was designed. Here it is shown that the score is dependent upon the maximum score achieved during competition. The intent of this mission is to complete the course as quickly as possible with as many passengers as possible.

$$\text{J'EE'"(} \quad 2 * + \text{", \%=} \quad 2 * \frac{\text{N}\left(\frac{\text{\#QRSSTUVT WS}}{\text{XYZ T}}\right)}{\text{=; \textbackslash}\left(\frac{\text{\#QRSSTUVT WS}}{\text{XYZ T}}\right)} \tag{4}$$

5.1.4 Flight Mission 3

Flight Mission Three emulates a long-haul flight with the team's choice of passengers and payload. The team is given 10 minutes to complete as many laps as possible during this mission. Similar to Mission Two, the score here is dependent upon other teams' success, however the constant two added allows for the interpretation shown in 5.1.7 Sensitivity Analysis. This mission forces the aircraft to obtain a longer range while carrying a high amount of weight.

$$\text{J'EE'"(} \quad 3 * + \text{", \%=} \quad 4 * \frac{\text{N (\#5; >>23_2 />*5; `<6; a (6b)*\#<;5>)}}{\text{=; \textbackslash (\#5; >>23_2 />*5; `<6; a (6b)*\#<;5>)}} + 2 \tag{5}$$

5.1.5 Ground Mission

Before Flight Mission 2 or 3 can occur, the aircraft must pass the Ground Mission. During which, 2 LRU's must be removed and replaced within 8 minutes: 3 minutes for the first LRU and 8 minutes minus the time for the first stage mission for the second Table 1 shows the possible LRUs which can be chosen as the result of a dice roll.

Table 1. Ground Mission LRUs

Ground Mission LRUs		
Roll Result	Stage 1	Stage 2
1	Servo	ESC
2	Rx Battery	Control Surface
3	Main Propulsion battery	Rx Receiver
4	Control Pushrod	Main Landing Gear
5	Landing Gear Wheel	Motor
6	Propeller	Re-Roll

5.1.6 Customer Requirements

Customer Requirements were derived from the RFP. The team identified the following key requirements.

- Safely seat and restrain passengers internally
- Internally carry payload blocks with the length, width, and height summing to 9 in.

- The payload blocks must be placed in a separate compartment from the passenger
- Take off from ground roll within 150 ft.
- Have a minimum range of 7500 ft. to complete three laps
- Fast LRU replacement

5.1.7 Sensitivity Analysis

Scoring analysis was conducted to identify key design drivers. The first approach used was a sensitivity analysis, conducted by taking the partial derivative of the total scoring equation with respect to each variable, shown in **Error! Reference source not found.**. This shows that the influence of empty weight and wing span are independent of the performance of other teams. Estimates of realistic maximum scores for other teams were generated for the number of laps, number of passengers, and payload weights based on competitive aircraft in previous competitions. These estimated values were used to generate new influence coefficients corresponding to the "realistic" results in Figure 6. This shows the independent nature of span and weight leading to the conclusion that if other teams choose to maximize laps, passengers, and payload, the Virginia Tech team can exercise the most control over its score by minimizing span and weight.

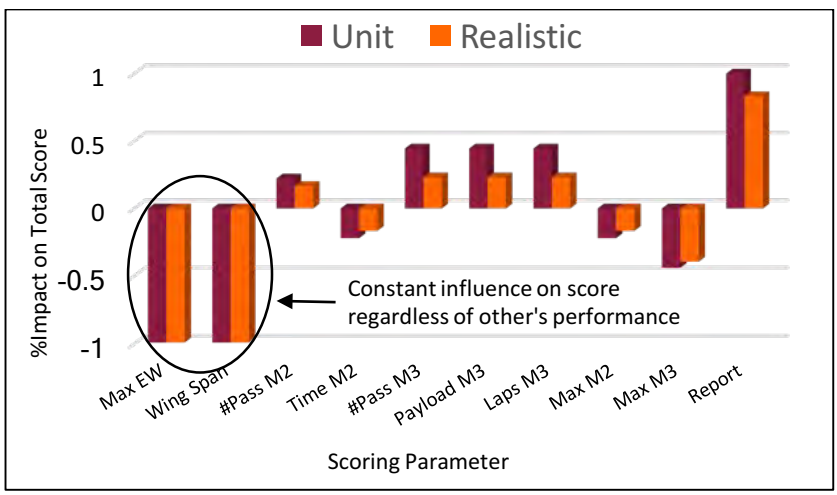

Figure 6. Influence Coefficient Comparison for Unit and Realistic Values

To validate the scoring analysis, a non-linear Excel optimization tool was used to parametrically "design" and score various configurations, allowing the interactions between each scoring variable to be considered. One of the trades conducted included a passenger and payload variation, shown in Table 2. This table was created by varying the number of passengers and payload to predict the empty weight and total competition score. For this example, a constant wingspan, weight fraction, and written score were used to measure only the effect of changing the passengers and payload. The weight fraction, wingspan and written score values were chosen from historical data found in previous Design Build Fly reports. From this table, it can clearly be seen that score increases as the number of passengers and payload weight decreases. It should be noted that the empty weight of 0.06 lb. for the 1 passenger, 1 oz. payload case is not realistic as it is based

on a weight fraction of 0.7. This analysis is not used to size the aircraft and is used only to bound the best possible competition score a competitor team could achieve. The total score using a realistic empty weight for sever cases would be significantly lower, however the trend towards higher total score remains the same.

Table 2. Sensitivity Estimates with Realistic Values, with a 10 in. Wing Span and 0.7 Weight Fraction

# Passengers M2/M3	Payload Weight (oz.)	Empty Weight (lbs.)	Total Score
50	50	0.7	0.2833
40	40	2.42	0.2846
30	30	1.81	0.3023
20	20	1.12	0.3613
10	10	0.6	0.5856
1	1	0.06	5.0275
10	20	0.87	0.4222
20	40	1.75	0.2832
30	50	2.35	0.2698

5.2 Design Requirements

Based on the team's scoring sensitivity analysis, Virginia Tech determined the key drivers to be to wing span and empty weight. All configurations demonstrate notional compliance to the customer requirements, however, during conceptual design additional focus was placed on these drivers.

5.3 Candidate Configurations

During the initial conceptual design phase, the team held several ideation sessions to explore hundreds of different configuration options. From the pool of conceptual designs, four not only met the customers' needs but also showed promise in meeting the design drivers. The four down-selected conceptual designs include a blended wing-body, bi-plane, oblique wing, and a flying wing.

5.3.1 Blended Wing Body

The first conceptual design was a blended wing-body (BWB) with a front mounted motor and propeller with tricycle landing gear. This design includes a vertical stabilizer with a rudder, as well as elevons on the trailing edge of the wing. The BWB allows for a large cargo volume relative to span and makes use of additional wing area on the sides. However, this additional area comes at the cost of additional span and the wing-fuselage junction is difficult to manufacture.

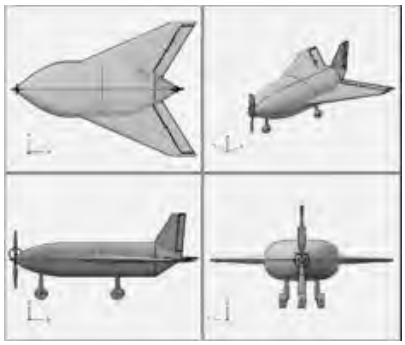

Figure 7. Blended Wing Body Model

5.3.2 Bi-Plane

The second conceptual design was a bi-plane with a front mounted motor and propeller in a tail dragger configuration. The main landing gear are placed underneath the main wings and in line with the struts for structural efficiency and to maximize wheel base width. The tailwheel is built into the empennage and directly steerable with the rudder, requiring one less servo. This design includes ailerons for additional roll control in addition to a conventional tail with a rudder and elevators. This concept was considered due to its relatively high lift given a limited span, allowing for a low takeoff speed. Another attribute of this aircraft is the ease in which LRUs could be accessed by removing the top wing along with a portion of the top of the fuselage. The primary detrimental factor of this concept is that the extra wing also causes extra weight and drag that increases more than the additional lift generated. Additionally, the span must be significantly larger than the fuselage to mitigate interference effects.

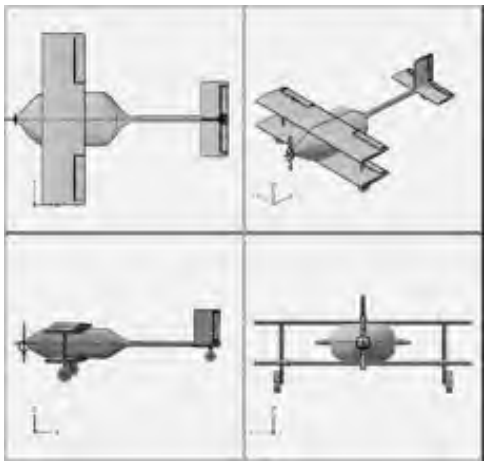

Figure 8. Bi-Plane Model

5.3.3 Oblique Wing

The third conceptual design was an oblique rotating wing with a traditional tricycle gear and conventional tail. The rotating wing concept was considered primarily due to its potentially small scored wingspan, large in-flight wingspan, and its potential for high passenger and payload capacity. With experience from previous competitions, the Virginia Tech Team weighed the possibility that this concept would be scored at the

largest wingspan during the decision process and tabled the configuration until the first Q&A confirmed that rotating wings would be scored by their maximum span. A non-rotating oblique wing was considered but further research suggested that the increase in lift from the additional area would be less than other designs with similar areas.

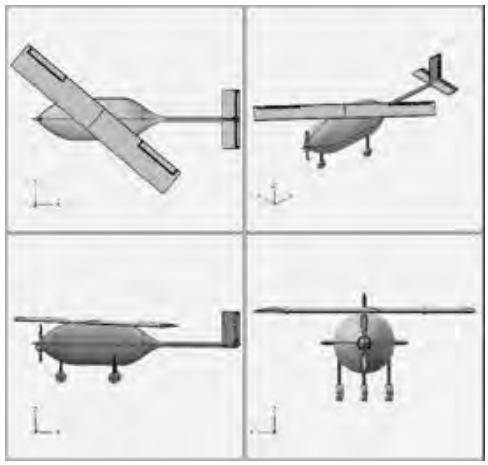

Figure 9. Oblique Wing Model

5.3.4 Flying Wing

The fourth conceptual design was a flying wing concept with a tractor mounted motor and propeller. Due to the expected high takeoff speeds, a tricycle gear was selected. The landing gear configuration for this concept consists of main gear mounted to the end plates at the rear for structural efficiency and as a vertical stabilizer and a single main steering wheel at the front. This concept has elevons at the trailing edge of the fuselage with vertical stabilizers at the trailing edge of the endplates. This design was considered due to its small wing span of 4.5” (based on the 4” minimum possible) and low weight which result in a low RAC and thus a higher overall score.

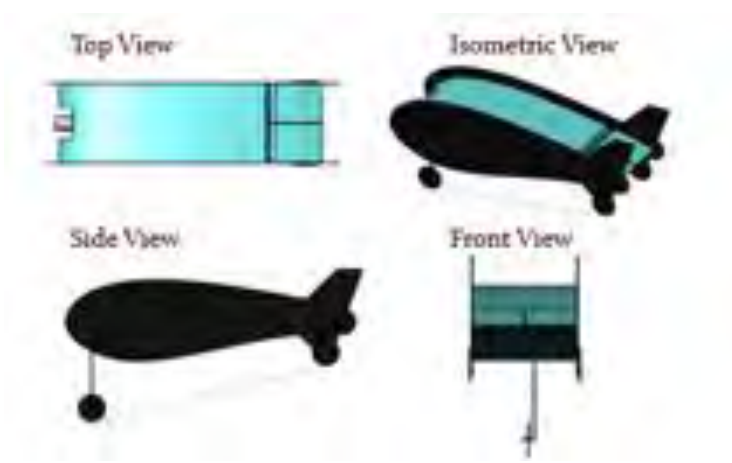

Figure 10. Flying Wing Model

5.4 Configuration Selection Process

Two conceptual selection processes were used – a subjective and objective method. Based on the results of the sensitivity and scoring analyses, the four conceptual designs above were subjectively scored by each team member using the selection matrix shown in Table 3. Here the weighting was assigned based on the results of the scoring analysis presented above. Each team member's scoring matrix was then compiled, shown in Table 4, to subjectively down-select the best design. The lowest total score determined the best design.

Table 3. An Example of an Individual Subjective Selection Matrix

Design Concept	Blended Wing-Body	Bi-Plane	Oblique Wing	Flying Wing	Weighting
Empty Weight	3	1	4	2	35%
Wingspan	4	3	1	1	35%
Passenger Capacity Score	2	3	1	3	10%
Payload Capacity Score	2	4	1	3	10%
Manufacturability	2	1	1	1	10%
Total Score	76.25	55	51.25	43.75	

Table 4. Final Subjective Selection Matrix

Design Name	Blended Wing-Body	Bi-Plane	Oblique Wing	Flying Wing
# 1st Preference	0	0	2	9
# 2nd	4	4	2	2
# 3rd	2	4	4	0
# 4th	5	3	3	0
# Samples	11	11	11	11
Avg. Rank	3.09	2.91	2.73	1.18
Median Score	3	3	3	1
Mode	4	2	3	1
Avg. Score	64.89	60.34	60.11	41.02

In addition to a subjective assessment, an objective sizing was conducted using realistic values for the number of passengers, payload, maximum takeoff weight, span, and aspect ratio to generate an overall Mission/RAC score correlating to the total competition score without factoring in the written report component. The result is shown below in Table 5. Note the oblique wing was initially scored based on a scored span of 4.5". The later released Q&A determined that the design would be scored with a 20" span and therefore, the actual score is over 4 times lower than shown.

Table 5. Objective Decision Matrix

Parameter	Flying Wing	Blended Wing	Oblique Wing	Biplane
# Passengers	1	1	4	1
Payload Wt. (lb.)	0.0625	0.0625	0.125	0.0625
Weight Frac	0.1	0.3	0.4	0.15
MTOW (lb.)	0.89	0.94	1.1	0.98
Span	4.5	12	4.5" scored (20" actual)	16
AR	0.3	1.86	5	4
Predicted Score: Mission/RAC	0.9	0.36	0.75 (0.17 actual)	0.24

From the results of both a subjective and objective selection process, it was clear that the flying wing, later dubbed Atlas was the best design concept and therefore was chosen to proceed to the preliminary design phase for risk mitigation. Because the 4.5" span Atlas concept was high-risk, a sensitivity study was conducted to evaluate predicted scores for the concept with wingspans of 4.5, 6.5 and 8" and the results are shown in Table 6.

Table 6. Predicted Scores for Atlas Concepts

Span (in.)	4.5	6.5	8
# Pax	1	1	1
Payload Wt. (lbs.)	0.0625	0.0625	0.0625
Total Cargo (lbs.)	0.14	0.14	0.14
Empty Weight (lbs.)	0.76	0.76	0.76
MTOW (lbs.)	0.9	0.9	0.9
Weight Fraction	0.16	0.16	0.16
AR	0.3	0.433	0.533
Predicted Score	0.89	0.62	0.5

The Atlas concept with increased spans of 6.5 and 8", scored 0.62 and 0.5, respectively, both score higher than the other concepts shown in Table 5. This is significant due to the flexibility to increase span (with negligible weight increase) if needed to meet design requirements, however the ultimate goal is to achieve the highest possible score which is obtained using a 4.5" span. This span and predicted score trade will be discussed in further detail in the next section.

6 Preliminary Design

6.1 Design/Analysis Methodology

The aircraft was designed using the “spiral” process shown in Figure 11. This process begins at the initial conceptual design and configuration selection. From this initial configuration, a historical empty weight was calculated using two methods:

1. A payload mass fraction vs. empty weight historical trend line
2. Using a comparator aircraft (Georgia Tech 2011)

From this initial configuration and weight estimate, the wing, stabilizer, and control surfaces are sized. This flows into a propulsion sizing before being run through the performance model. The design is iterated until it converges, and a prototype is built for ground and flight testing. The results of these tests are reviewed for compliance with the requirements and a new iteration (or spiral) begins with the previous aircraft as the point of departure. The process is repeated until the design meets all requirements and time constraints dictate that further cycles to increase score cannot be conducted.

Figure 11. The Design Spiral Process

The program has currently completed 3 design spirals which resulted in the AV1 design with a 4.5” span as shown in Figure 13. AV2 and AV2.5 design with an 8” span and an all flying tail as shown in Figure 14. Testing each of these aircraft revealed the lessons and changes for the succeeding design shown in Figure 11The comparison between AV2.5 and AV3 will be discussed further in Detail Design.

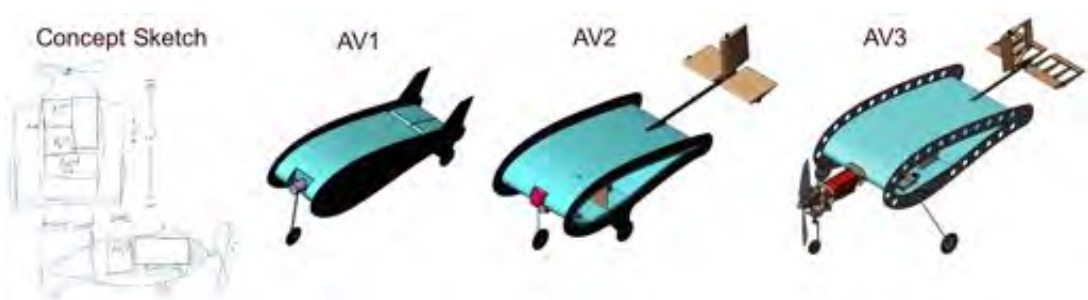

Figure 12. Evolution of the Design

6.2 AV1 Preliminary Design

6.2.1 AV1 Design Process

From the configuration selection, an extremely simple and quick design for AV1 was sized based on simple hand calculations to learn the challenges associated with building a flying a low aspect ratio aircraft and get experience with the materials and methods. Literature reviews resulted in little information on low speed and low aspect ratio (<0.5) aircraft and traditional analysis tools like AVL, XFLR5, and OpenVSP estimated $C_{LTO} < 0.3$ with questionable scatter due to dominant 3D effects discussed later. Additionally, initial models did not have good methods to estimate the impacts of prop-wash or the stability of the aircraft. The span of AV1 was set at 4.5” to reflect a 4” minimum span for the passenger and aisle with 0.25” of structural space on each side. Initial estimates from actuator disk models showed up to 10 mph of apparent airspeed increase (above the true aircraft airspeed) on the wing from prop wash at takeoff speed. A review of previous competition data showed an approximate maximum takeoff speed of 30 mph and the Georgia Tech 2011 aircraft [1] was used as the basis for the weight estimate. A chord of 15” was chosen from initial aspect ratio trades to keep stall speed at ~40 mph apparent speed over the wing with an estimated minimum velocity un-stick speed of 30 mph aircraft true airspeed. To improve ground handling, a tricycle landing gear was selected, however, main gear was placed on the bottom of the vertical surfaces for structural efficiency. As a result, tip-over was expected to be a significant concern. Additionally, this gear configuration fixed the takeoff angle of attack.

6.2.2 AV1 Test Results

AV1 was designed and built within a few days and weighed 1 lb. (0.3 lb. over estimate) when complete. Initial taxi testing showed that tip-over was a problem and the gear was moved forward for testing. While this helped, the aircraft’s ground handling was still very challenging, and the aircraft was never able to accelerate to takeoff speed. Even though it never flew, the aircraft provided many lessons summarized in Table 7.

Figure 13. AV1 Prototype as Designed and Built

Table 7. Lessons Learned from AV1 Testing

Lesson from AV1	Mitigations Implemented in AV2
The landing gear was at the trailing edge of the wing and structurally incorporated into the end plates. However, this resulted in roll-over tendencies at high and low speeds.	The tricycle main gear on V2 is further forward and tip-over margin is increased.
The fixed takeoff angle was set with the landing gear and there was no rotation. This resulted in the loss of weight on the nose wheel and ensuing loss of directional control.	V2 no longer has a fixed takeoff angle and instead rotates at takeoff speed.
Gross weight was initially estimated at 0.75 lbs. The addition of manufacturing weight creep and C.G. ballast weight, the takeoff weight as built was 1 lbs.	V2 will not require fixed ballast and the manufacturing methods have been changed to reduce weight.
The V1 aircraft's required takeoff speed was estimated to be nearly 50 mph (including blowing effects). The aircraft reached 30 mph before directional control was lost. Current test data shows the blowing effects to increase effective airspeed by 10 mph.	V2 has an increased span and area which has an estimated takeoff speed of 30 mph and does not require blowing to fly.
Initial tufted tunnel testing showed the upper surface of the wing to be extremely turbulent and separated behind the motor mount.	This is mitigated by reducing the size of the firewall and including a fairing.

6.3 AV2 and AV3 Preliminary Design

While AV1 was being designed, built, and tested, a portion of the team was working on developing the toolchain to design AV2. Trade studies and new aerodynamic and propulsion data relaxed the span to 8" for AV2 with the intent that it would be decreased again if possible for AV3 or beyond.

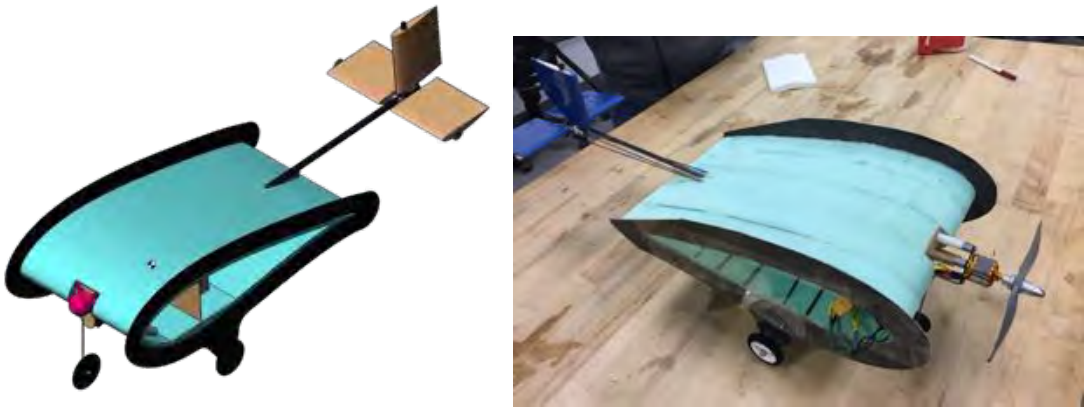

Figure 14. AV2 Prototype as Designed and Built

6.3.1 Comparator Aircraft

Two comparators were found with similar configurations to the Atlas and a comparison of key design parameters are shown in Figure 15. One comparator is the UCI 2013 DBF competition aircraft and the other is an R/C model built by hobbyists. Both aircraft are larger, heavier, and have a higher aspect ratio than the Atlas. However, the C_L, Power to Weight, and CG locations provide some historic basis for this configuration.

UCI 2013 [2]

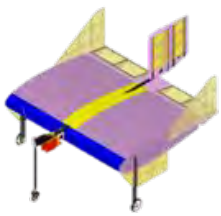

Span (in)	34
Aspect Ratio	1.13
Empty Weight (lbs)	3.98
T/W	1.81
P/W (W/lb)	125.6
$C_{L,TO}$	0.9
V_{TO} (mph)	15.68
Cg (x/c)	0.502

Vought V-173 [3] R/C Model

Span (in)	45
Aspect Ratio	2.16
Empty Weight (lbs)	5.94
T/W	N/A
P/W (W/lb)	101.053
$C_{L,TO}$	N/A
V_{TO} (mph)	N/A
Cg (x/c)	0.25

Figure 15. Comparison of Similar Historic Aircraft

The aircraft presented above are similar configurations but were designed for significantly more payload than the Atlas. The 2011 Georgia Tech aircraft [1] was a flying wing with a span of 24" designed to carry several golf balls. This competition winning aircraft was used as the basis for the weight estimates discussed in Design/Analysis Methodology. The Atlas V2 (empty) weight build up is compared with the Georgia Tech aircraft in Figure 16. Because of Atlas's low span, structural weight is lower than GT, however, the lower aspect ratio and associated low L/D results in a heavier propulsion system.

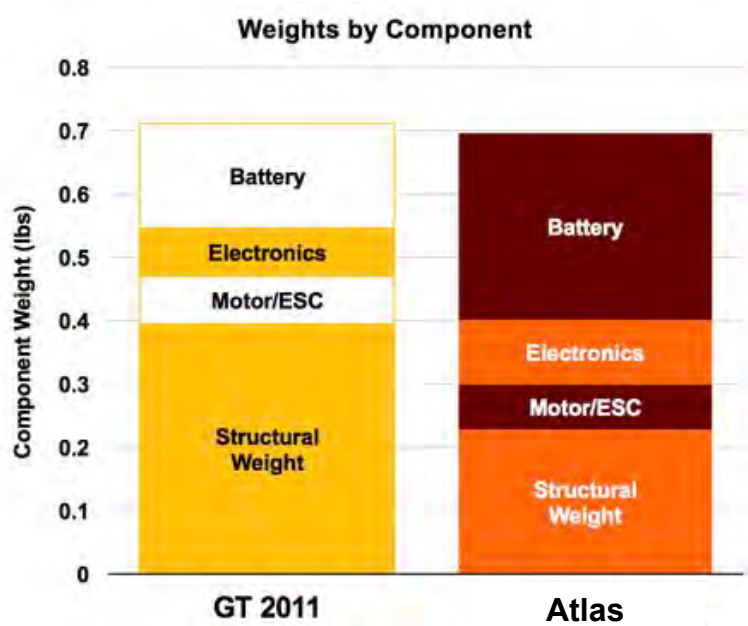

Figure 16. Georgia Tech 2011 and Atlas V2 Weight Build Up

6.3.2 Sizing Breakdown

Throughout the process of developing and testing the first design, a prominent parameter in successful flight capability was takeoff speed. With an initially conceived wingspan of 4.5 in., and a C_L of approximately 0.28 (based on a lifting line derivation of 3D C_L from 2D C_L as a function of aspect ratio), the first prototype

had a revised predicted takeoff speed of 51 mph apparent airspeed. As a result of challenges experienced with the 4.5” span, both 6.5” and 8” options were explored and are shown in Figure 17. This contour plot demonstrates the available range of span values given a C_L and a takeoff velocity. As it can be seen, a span of 6.5” corresponds to a C_L of approximately 0.38 with a takeoff velocity of roughly 34 mph. Comparing this takeoff speed to the 51 mph needed for a 4.5”. span, it becomes clear that a small increase in span greatly reduces takeoff speed. In a similar trend, a span of 8” corresponds to a C_L of approximately 0.45 and a takeoff speed of 28 mph.

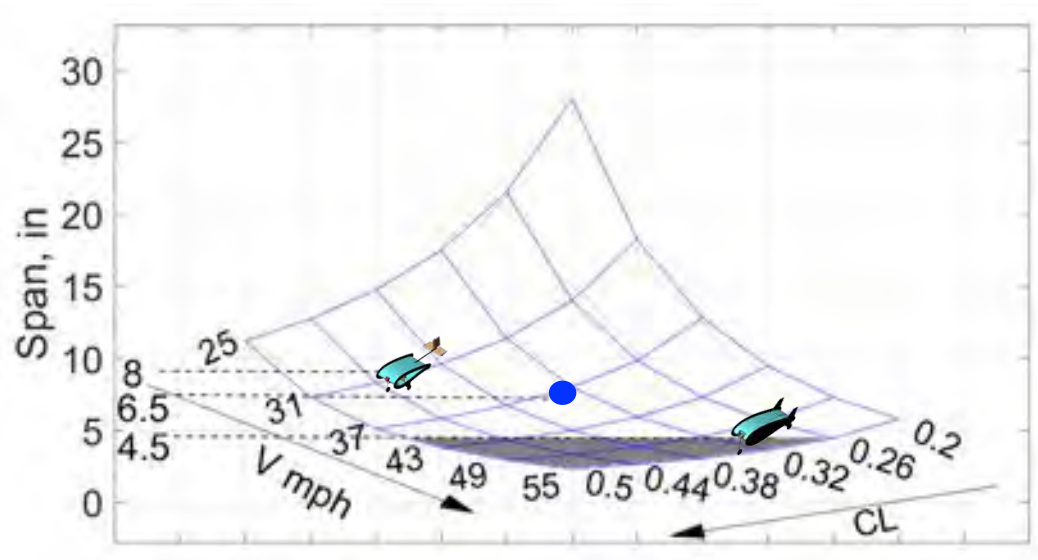

Figure 17. Carpet Plot Showing the Relationship Between Span, Takeoff Velocity, and Takeoff CL Based on AV2 Data

Initially, test data for the thrust and power available was collected for the Hacker A10-9L and is plotted with the thrust and power required, seen in Figure 18 and Figure 19. The takeoff speeds for the 4.5”, 6.5” and 8” span models are included as vertical lines on these plots. Note the significant decrease in takeoff speed of the 8” span model when compared to the initial 4.5” aircraft. From the flight test results of AV1, it was found that poor ground handling occurred at ground speeds in excess of 30 mph. Reducing the takeoff velocity required greatly increases the likelihood of successful takeoff as well as stability during ground roll.

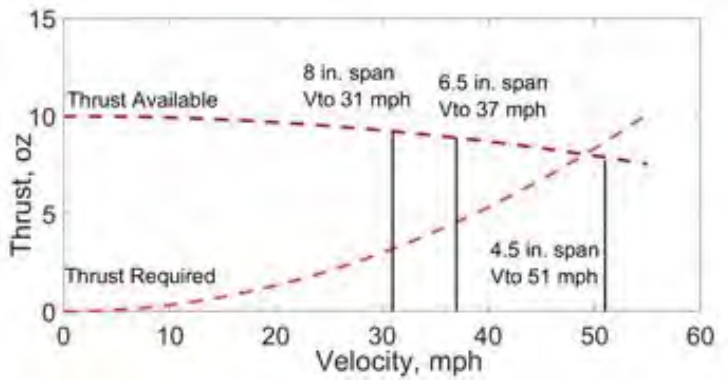

Figure 18. Thrust Required and Available vs. Aircraft Speed Compared with Three Takeoff Speeds

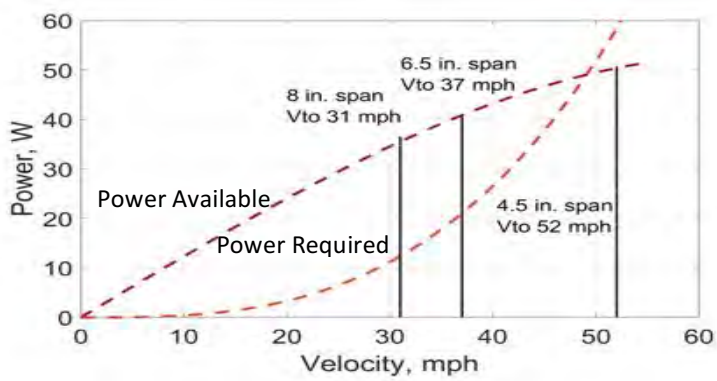

Figure 19. Power Required and Available vs. Aircraft Speed Compared with Three Takeoff Speeds

Later test data found the propulsion system to be underpowered and the revised propulsion sizing for AV2 and 3 will be shown in Section 10.1.1.

6.4 Design/Sizing Trades

6.4.1 Airfoil Sizing

As part of the airfoil selection process, several different airfoils were examined from the UIUC and airfoil tools databases. Due to the restrictions on the sizing of the passenger and the payload blocks, thickness becomes a very dominant factor in the selection of the airfoil. For a 15” chord, the maximum internal height for usable space is roughly 3”. Without greatly increasing the chord for a thinner airfoil, the 2” plus clearance needed to meet the internal layout requirements can only be met with an airfoil that has approximately 20% thickness. All airfoils in the team’s compiled database with thickness near or >20% were examined using XFOIL, as well as XFLR5, and down-selected based on the airfoil performance categories shown below in Table 8. The primary drivers in the airfoil consideration were thickness, maximum lift coefficient, and maximum L/D. Moment coefficient was also included as a measure of potential stability concerns. From these airfoils, The OneraHOR20, and Eppler 857, and NASA-LS-421 MOD were identified for further testing in prototype iterations as well as wind tunnel testing.

Table 8. Main Wing Airfoil Comparison

Airfoil Name	Thickness, %c	Cl max	L/D max	Angle for L/D max, deg	Cd min	CM Cruise	CM takeoff
REQUIREMENTS	>20	>1.5	>80	-	-	-	-
DefiantCanardBL20	20.9	1.58	105	8.00	0.01	-0.07	-0.04
Eppler1098	18.9	1.38	127	8.00	0.01	-0.13	-0.06
Eppler857	20.3	1.77	96	8.00	0.01	-0.11	-0.08
NASA421MOD.txt	21	1.64	86	5.00	0.01	-0.09	-0.06
NASALANGLEY-LS-0421	20.9	1.61	96	4.00	0.01	-0.09	-0.06
NRELS808.txt	21	1.65	87	8.00	0.01	-0.10	-0.07
OneraHOR20	20.4	1.71	98	9.00	0.01	-0.09	-0.06

The NASA-LS-421-MOD airfoil was used for the initial AV1 due to the favorable lift performance at higher angles of attack. For consistency, this airfoil was reused for AV2. Changing the airfoil was deemed to introduce significant uncertainty when comparing AV1 and AV2 with no compelling reason to change. After performing both flight and wind tunnel tests on AV2 and introducing stability improvements that lead to AV2.5, it was deemed that the NASA-LS-421-MOD airfoil provided satisfactory aerodynamic characteristics to continue testing with consistency across design spirals. At the beginning of the manufacturing process for AV3, it was decided to continue using the NASA-LS-421-MOD airfoil to assess performance estimates when shifting to NiMH batteries. As testing continued with AV3, it became clear that the thickness provided by the NASA-421-MOD airfoil and the flexibility that the airfoil shape allowed for internal layout outweighed the benefits of switching to a different airfoil. This decision was also compounded by the successful takeoff and cruise performance demonstrated by AV3 when flying in a worst-case weight scenario for 3 complete laps.

6.4.2 Stability and Control Sizing

On AV1, pitch and roll were controlled through surfaces on the main wing. This configuration led to issues with control power and excessive drag. To combat this, AV2 introduced a boom tail separate from the main wing which would improve flow around the fuselage and increased control power. To reduce the number of independent control surfaces, elevators and ailerons were combined into a single set of control surfaces called “elevons”. Elevons were initially sized to counteract the aerodynamic pitching moment of the aircraft. A Vortex Lattice Method through XFLR5 estimated that a nose-up pitch moment of about 0.3 ft-lbs would be needed to keep the plane in level flight at 8° angle of attack. Qualitative wind tunnel testing supported this claim, so this value was used for elevon sizing.

Since wing span is a primary design driver, it was decided that the elevons would have a total wingspan equal to that of the fuselage to provide the most roll authority possible. The current configuration can be seen in Figure 20. All-flying control surfaces were chosen to get the most control power from the control

surfaces. An inverted Clark Y airfoil was selected as an initial airfoil for the elevons due to the amount of low aspect ratio historic data available.

Tail sizing was explored by varying tail boom length and tail planform area. The effects that these variables had on pitch moment were determined by summing the moments due to lift forces and aerodynamic moments from the fuselage and tail about the center of gravity and setting this sum to zero, as seen below.

$$J_{;2/6,ef>2.} + J_{;2/6,1;0<} + h_{1;0<}i_1 = 0 \qquad (6)$$

This analysis assumed that the tail sees the same velocity magnitude as the fuselage and the surface can be trimmed for the flow angle. Initially, three different elevon aspect ratios were selected for analysis. Elevon planform areas could be determined from these aspect ratios assuming that elevon span was fixed so that the tail wingspan would be equal to the span of 8”. From these areas, the necessary tail boom length was determined. Table 9 shows the elevon planform area, required boom length, and required downforce for each aspect ratio. The team decided on elevons with an aspect ratio of 1 for the initial sizing placed on the end of a 4”. boom. In the end, a large chord of 3.5”. was selected as a larger size would improve manufacturability.

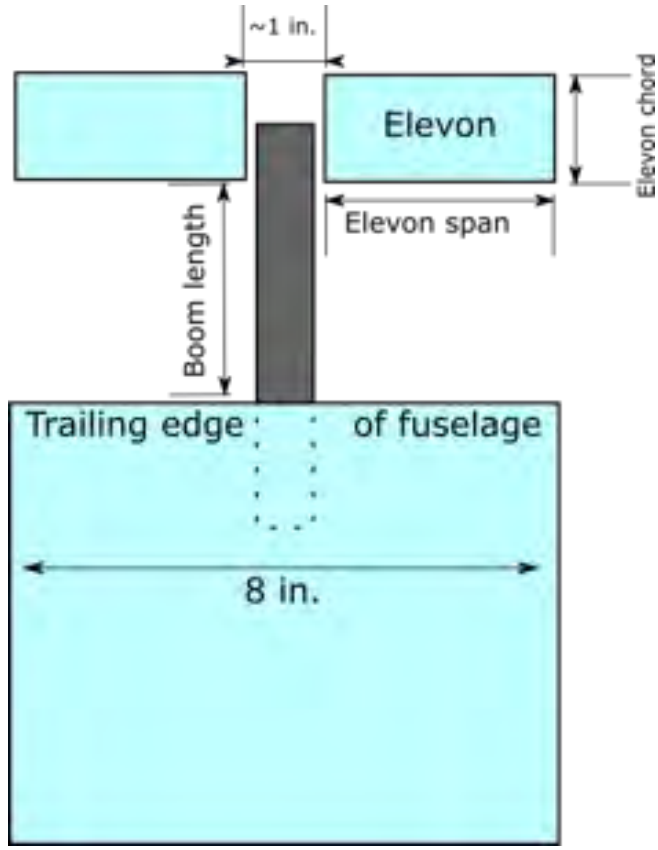

Figure 20. Top View of Basic Aircraft Configuration

Table 9. Elevon Sizing Summary

Aspect Ratio	Elevon Area, in^2	Elevon Chord, in	Required Tail Boom Length, ft.
1	12.25	3.500	0.166
1.5	8.167	2.333	0.475
2	6.125	1.750	0.713

The elevons will also provide a roll moment when differential elevon deflection is applied. An estimated motor torque of 20 oz-in. was used to test roll control power of the selected elevon configuration. It was determined that elevons would be able to counteract this torque for an approximate takeoff airspeed of 40 mph. The all-flying rudder was initially given the same size as an elevon and is placed roughly at the same location on the tail boom as the elevons. Flight tests showed that this size is sufficient for yaw control.

6.4.3 Power Sizing

For this aircraft, the propulsion package was down-selected based on a thrust, weight, and endurance that satisfied the mission requirements while keeping empty weight as low as possible. The team has separated the propulsion system into four major components: battery, electronic speed controller, electric motor, and propeller. Outside of these, attachments such as the prop nuts and motor mounts are for securing the package onto the aircraft and will add their respective weight to the overall empty weight.

The mission requirements state that the battery pack must have a nickel-metal hydride (NiMH) or nickel cadmium (NiCd) composition. Compared to conventional Lithium Polymer (LiPo) batteries, NiMH's are known for their lower maximum discharge current while being heavier in weight (if pack voltage and capacity were equivalent). Therefore, battery cell selection will be based on weight and maximum continuous discharge current. The energy density of NiMHs is higher than NiCd and because of the design sensitivity to weight, NiMHs were selected [10].

From a NiMH industry study using 45 cells from the MotoCalc database, the team found that capacity and weight of the cell correlate linearly, referenced in Figure 21.

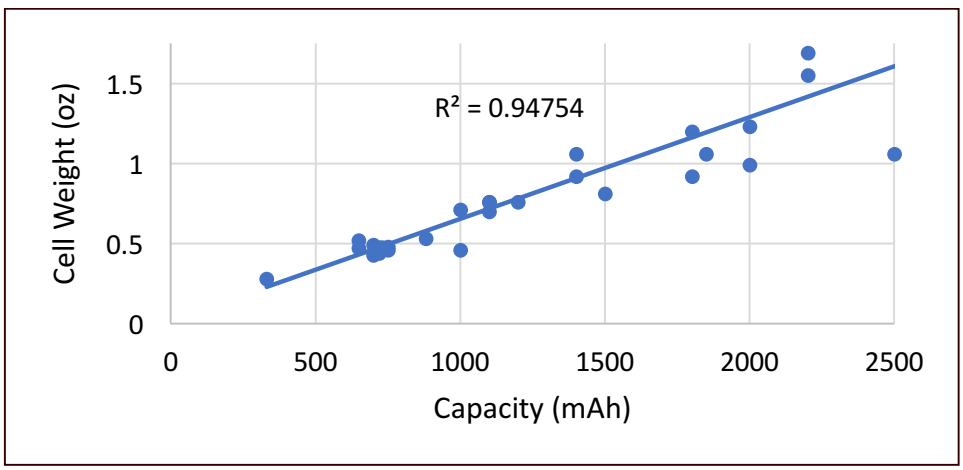

Figure 21. NiMH Cell Capacity vs. Weight

However, not all NiMH cells shown have a high enough continuous current limit to support the selected motor/propeller combo.

For discharge, the following formula is used:

$$Maximum\ Discharge\ Current = Capacity\ (mAh) * C\text{-}Rating \tag{7}$$

The team has selected batteries with a C-Rating above 9C such that the discharge current is high enough for any capacity chosen. After analysis of datasheets provided by battery manufacturers, the team has

chosen to test ELITE battery cells at 800 mAh and 1500 mAh that have a C-Rating of 10C, providing 8A and 15A of maximum continuous discharge current with the highest energy density, respectively. The 800 mAh cells were initially sized for AV2 but with later testing, were found to have inadequate current, requiring a change to 1500 mAh.

Electric motors have the following characteristics: Motor velocity constant (Kv, or RPM/V), maximum power (Watts), maximum continuous current (Amps), and weight. Motor performance is judged by the overall thrust, torque, and power produced based on the propeller chosen.

The team selected brushless motors because of the high power-to-weight ratio compared to brushed motors. Within brushless motors, the team has chosen to proceed with a direct-drive out-runner motor to avoid the weight penalty associated with a gearbox and in-runner. For the motor trade study, the team tested the following four out-runner motors referenced in Table 10. The results of this testing are presented in Section 9.1.2.The Turnigy D2826 was selected for AV2 and AV3 for its high Kv and high maximum continuous current.

Table 10. Comparison of Candidate Motors

Motor	Kv (rpm/V)	Max Power (Watts)	Max Continuous Current (A)	No-load Current (A)	Impedance (ohm)	Weight (oz)
Turnigy D2826 - 6	2200	342	36	0.8A at 8V	0.16	1.94
Scorpion SII - 2208	1280	150	14	0.47A at 10V	0.15	1.587
EMAX MT2213	935	200	12	0.5A at 10	0.18	1.869
Cobra C2208/20	2000	200	18	0.8A at 8V	0.064	1.446

The electronic speed controller (ESC) is the power converter between the DC battery and the brushless 3 phase DC motor that controls power via a pulse width modulation (PWM) signal from the receiver. The ESC was down selected based on the measured continuous and burst current of the propulsion system. After this, final ESC selection will be dependent on the lowest weight and volume occupied within the vehicle structure. For testing, the team has compared the Hobbywing Skywalker 40A, Arris Simonk 30A, and KISS 24A Racing ESC before selecting the Arris 30A for its low weight and maximum continuous current of 30A.

Table 11. Comparison of Candidate ESCs

ESC Brand	Max Burst Current (A)	Time of Max Burst (sec)	Max Cruise Current (A)	Weight (oz)
Hobbywing Skywalker 40A	55	10	40	1.52
Arris Simonk 30A	45	15	30	0.67
KISS Racing Spec 24A	30	10	24	0.29

Propellers for the propulsion package will be selected via the following criteria at 2000 Å* PWM (100% throttle): current draw, static and dynamic thrust, and torque. Motor and propeller configuration performance was estimated prior to testing utilizing the UIUC Propeller Database [11], and results were verified with both static and dynamic testing. Final selection of the propeller model was based on the maximum achievable thrust for the given current limits of the battery and motor. Secondary criteria for propeller selection will be based on the overall propeller weight, as well as the weight of any propeller nuts and adapters. The team has chosen to look at the following propellers mentioned in Table 12. Tunnel test data showed that the APC 9x6E would provide the most thrust in the takeoff and cruise speed ranges.

Table 12. Comparison of Candidate Propellers

Propeller Model	Diameter (in)	Pitch	Propeller Weight (oz)
APC Electric	7	4	0.42
APC Sport	7	8	0.46
APC Slow Fly	8	3.8	0.25
APC Electric	8	8	0.53
APC Electric	9	6	0.63
APC Electric	9	9	0.63
APC Electric Slow Fly	9	4.7	0.63

6.5 Mission Model

For this competition, the mission model consists of completing 3 laps within 5 minutes for both missions 1 and 2, as well as the maximum number of laps possible within a 10-minute time period for mission 3. This leads to a required range of 7500 ft. based on a lap distance (including turns) of 2500 ft. each. Therefore, the required minimum flight speed to complete 3 laps within 5 minutes assuming constant speed is 17 mph while the aircraft cruises at 43 mph, exceeding the requirement. Historical data for the competition period was studied and the winds were estimated to be less than 20 mph. The effects of wind were considered as a knockdown of the range and at 20 mph wind speeds, the aircraft requires a 20% increase in no-wind range estimates for mission completion.

Through the analyses conducted in preliminary design, assumptions have been made based on knowledge and references relevant to each subject. These assumptions play a large factor in predicting the mission performance of the aircraft, especially with respect to flight parameters that are difficult to measure reliably during flight tests. In particular, takeoff speed, takeoff distance, rate of climb, cruise speed, turn radius, and lap distance are all compared to determined values from flight test results with the understanding that there is a certain degree of uncertainty in each of the values. This uncertainty is taken into consideration when using predicted values for performance estimates, as well as when determining actual metrics from flight data.

6.6 Aircraft Capabilities Estimates

Due to the low aspect ratio and large thickness of the flying wing, many typical analysis tools could not be used. It was decided, instead, to begin with existing experimental data for low aspect ratio wings and numerical methods to determine aerodynamic characteristics. The primary source of experimental data was NACA TR-431 on low aspect ratio Clark Y airfoils [4]. This data was used for rough C_L and C_D estimates as well as validation for numerical methods such as Vortex Lattice Method, 3D Panel Method, and Computational Fluid Dynamics. VSPAero was used for Vortex Lattice Method approximations with the model being created in OpenVSP. XFLR5 was used for its 3D Panel Method routine to provide additional results for comparison. The CFD program selected was OpenFOAM as the team had experience with this software suite. An angle of attack sweep was conducted with the Clark Y airfoil in each of these programs as a validation case and the results compared with the experimental data, which can be seen in Figure 22 below. Based on this data, CFD proved to be the most robust method for simulating a wing of this aspect ratio, so it was decided to use OpenFoam for determining more detailed aerodynamic characteristics. Force and moment coefficients can be calculated using a function within OpenFOAM.

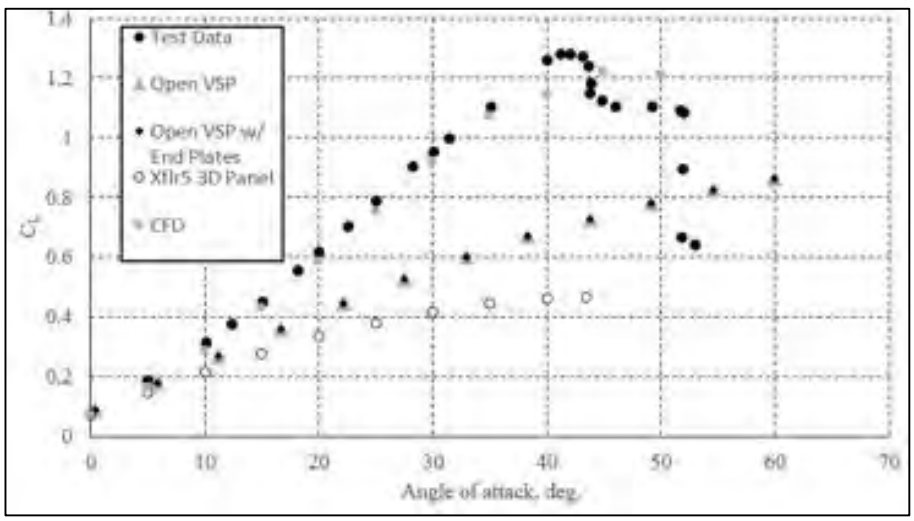

Figure 22. Comparison of numerical methods and experimental data for Clark Y of AR = 0.5

Figure 23 below shows the trimmed lift-to-drag ratio, trimmed C_L, trimmed C_D, and static margin for both AV2 and AV3. The takeoff angle of attack of the design has remained fairly constant at 11 degrees resulting in a takeoff C_L of approximately 0.36, C_D of approximately 0.12, L/D of 2.9, and Kn of about 7% with C.G at 25%c.

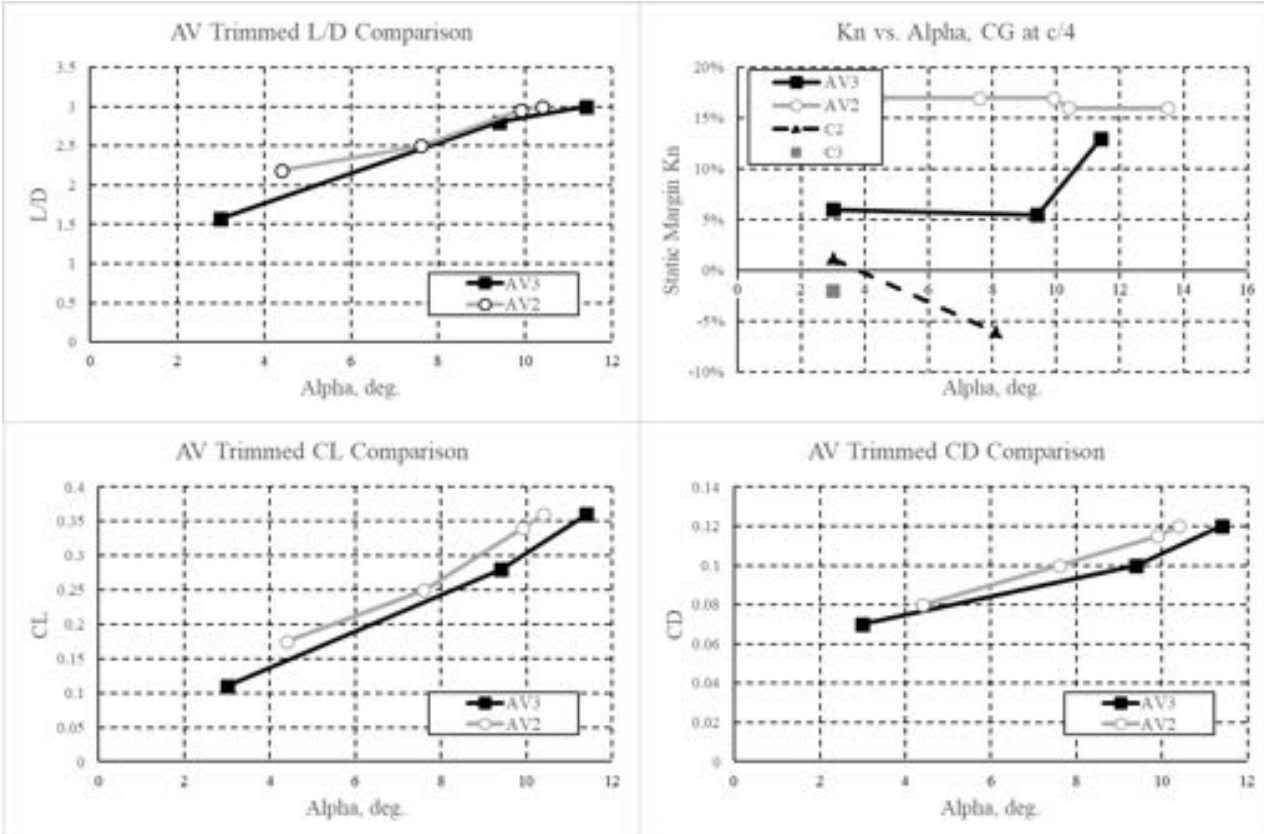

Figure 23. Trimmed L/D, C_L, C_D, and K_n vs. Angle of Attack

The stick fixed static margin Kn was deemed to be close to unstable and the C.G. location was moved forward to approximately 15% chord as shown in Figure 24.

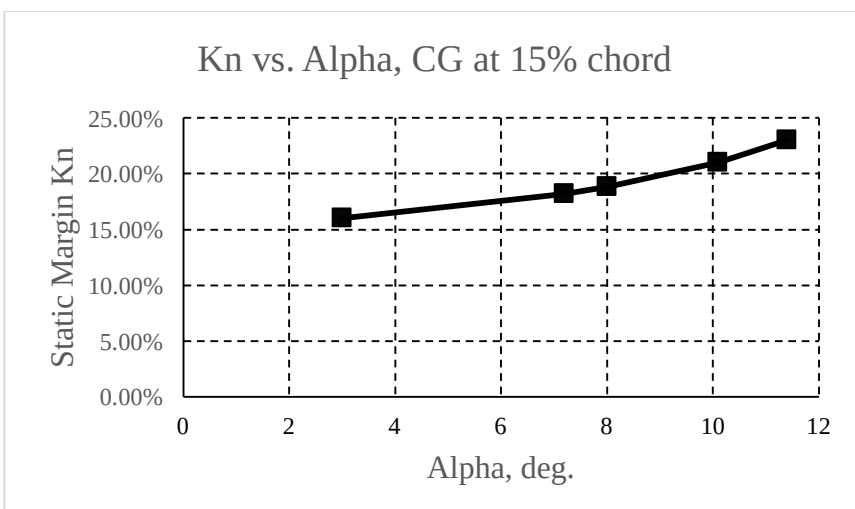

Figure 24. AV3 Stick Fixed Static Margin at 15%c

Initial flights with AV2 were conducted with only an R/C receiver. While the aircraft was controllable, the small span had little roll damping and is difficult to see during portions of the course. In order to reduce pilot workload and increase reliability, an OpenPilot Atom stabilization system is used by the team for levelling. The typical flight configuration is an attitude hold mode where bank and pitch angles are proportional to stick position. PID gains were set experimentally and the stabilizer has made a remarkable improvement in the flying qualities.

6.7 Aircraft Mission Performance Estimates

As discussed in section 3.1, Flight Missions 1 and 2 require that the aircraft must have the ability to fly a minimum of 3 laps. Flight Mission 3 however, does not have a lap restriction, rather the mission is scored based on the maximum number of laps that the aircraft completes successfully. To demonstrate the range of laps that the aircraft can fly, a contour plot based on the aircraft L/D and battery capacity are shown in Figure 25 below. The preliminary design for AV3 is shown on the contour plot with an estimated L/D of 2.9 and a battery capacity of 1500 mAh giving a predicted 4.1 lap capability for the aircraft. This capability comfortably meets the 3-lap requirement for Missions 1 and 2 and allows for flexibility to fly additional laps for mission 3. It is important that the predicted lap capability is a significant amount greater than the requirement to allow for maneuver flexibility, as well as accounting for wind factors, and potential in-flight problems.

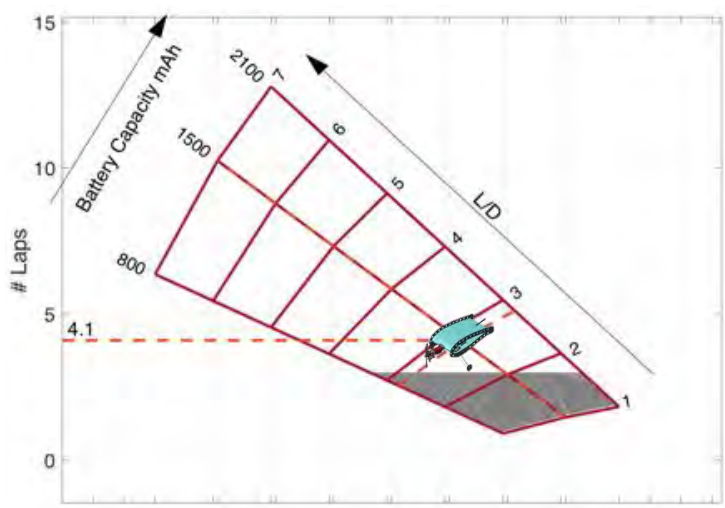

Figure 25. AV3 Carpet Plot Comparing Cruise L/D, Battery Capacity, and Number of Laps

The predicted mission performance for the preliminary aircraft design is shown in

Mission	TOGW (lbs.)	Wingspan (in.)	# of Passengers	Payload Weight (oz.)	# of Laps	Mission Time (s)
Mission 1	1.24	8.0	0	0	3	157
Mission 2	1.33	8.0	1	1	3	163

Mission 3	1.39	8.0	1	1	1	59
RAC	9.92					

Table 13, along with the RAC. Under the assumption that a given team will decide to maximize the number of passengers and payload for missions 2 and 3, the Virginia Tech believes that this RAC will provide a significant competitive edge due to the low wingspan and empty weight.

Table 13. Predicted Preliminary AV2 Design Mission Performance

Mission	TOGW (lbs.)	Wingspan (in.)	# of Passengers	Payload Weight (oz.)	# of Laps	Mission Time (s)
Mission 1	1.24	8.0	0	0	3	157
Mission 2	1.33	8.0	1	1	3	163
Mission 3	1.39	8.0	1	1	1	59
RAC	9.92					

7 Detail Design

7.1 AV2 to AV3 Design Changes

Using the lessons learned from the flights of AV2 shown in Table 14, the team moved into the third design spiral.

Table 14. Lessons Learned from AV2 Testing

Lesson from AV2	Mitigations Implemented in AV3
In crosswinds, the aircraft still had a tendency to tip over.	The tricycle gear base was widened and the nose and main wheel moved forward to compensate for the C.G. shift.
The first flights of AV2 with a C.G. at c/4, were marginally stable, the nose was extended to move it further forward.	The nose was designed further forward and using CFD data, the tail was moved forward as well.
At distance, the aircraft can be difficult to see and control. Stability augmentation results in a significant reduction in pilot workload.	Stability augmentation has “earned” it’s weight on AV3.

7.2 Dimensional Parameters

Dimensional parameters for critical design characteristics are given in Table 15.

Table 15. Final Design Dimensional Parameters

Dimensional Parameters					
Wingspan (in.)	8		**Mission 1**	**Mission 2**	**Mission 3**
Chord (in.)	15	***TOGW (lbs.)***	1.24	1.33	1.39
Wing Area (in.^{2})	120	***W/S (lbs./in.2)***	0.0103	0.0111	0.0116
Aspect Ratio (AR)	0.53	***T/W***	1.36	1.27	1.21
Elevon Chord (in.)	3.5	***P/W (W/lb.)***	64.5	60.1	57.6
Elevon Area (in.^{2})	12.25				

Rudder Chord (in.)	3.5
Rudder Area (in.^{2})	12.25
Horizontal Tail Vol. Ratio	0.120
Vertical Tail Vol. Ratio	0.225

7.3 Detailed design elements

7.3.1 Landing gear location

The gear position shown in Figure 26 was placed relative to the C.G. in accordance with the recommendations in Roskam [7] with the C.G. >15° (23° designed) forward of the gear contact point and a tip-over angle of <55° (53° designed). The nose gear height is set such that the chord line is 3° nose down for takeoff. This is to increase the control effectiveness of the nose wheel steering and prevent early liftoff.

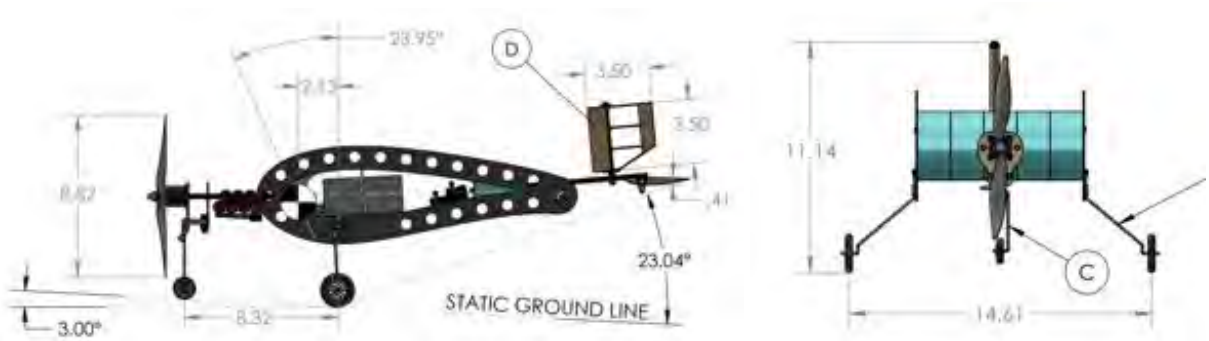

Figure 26. Landing Gear Location

7.4 Structural Characteristics/Capabilities

Given the small aspect ratio, the bending load of the wing was not a sizing case. The primary structural considerations are: the torsional stiffness of the fuselage, torsional stiffness of the tail-boom, the bending loads on the landing gear, the bending loads from the gear on the endplate, and the adhesion of the endplate and fuselage sections. Structural analysis was not considered to be a design driver and is verified experimentally for each component.

7.4.1 Structural load path

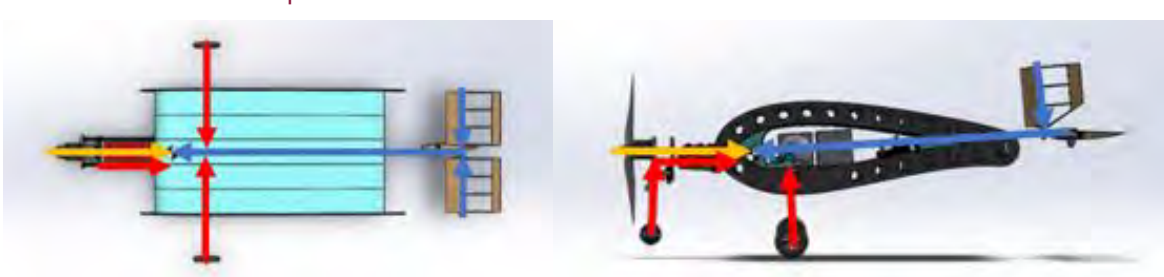

Figure 27. Aircraft Primary Load Paths

7.5 Systems Selection, Integration and Architecture

7.5.1 Seat

For this reason, the seats are designed for the largest passenger to be touching the floor of the aircraft while concentric to the seat. The passenger is restrained with a piece of elastic and Velcro portions which allow for different size passengers. See Figure 38 for an image of the seat.

7.5.2 Payload Block

The payload block is a 2” x 2” x 5” block built from laser cut balsa sides and ballasted with additional balsa to reach a weight of 1 oz. The payload block will be secured into the aircraft behind the passenger compartment between two bulkheads.

7.5.3 Servo, Receiver, and Receiver Battery Selection

- Power-HD DSP-33 servos were selected as they were the smallest (20 x 8.7 x 22 mm) and lightest (3g) servos available with at least 5 oz-in or torque.
- The Futaba R2106FG receiver is the smallest (38 x 21 x 10 mm) and lightest (4g) Futaba receiver available with at least 5 channels.
- The Tenergy 170 mAh NiMh cells (20g for a 4S) were initially selected from stock on hand. Since then the team found Gold Peak 1/3AAAA 100 mAh NiMh cells and will be switching to them as they are expected to be ~12g.

7.6 Weight and Balance

The weight and balance table is referenced to a point ~2.5” in front of the nose. The negative x -axis faces the trailing edge. The positive y-axis points out the right-wing tip and the positive z-axis points out of the bottom of the aircraft.

Table 16. AV3 Component Weight and CG Location

Empty Weight									
Components	Weight (oz)	C.G. Loc (in x-axis)	C.G. Loc (in y-axis)	C.G. Loc (in z-axis)	Components	Weight (oz)	C.G. Loc (in x-axis)	C.G. Loc (in y-axis)	C.G. Loc (in z-axis)
Fuselage	2.44	-14.87	0.00	-0.07	Mission Two – Lightest Passenger				
Endplates	1.38	-15.78	0.00	-0.08	Lightest Passenger	0.40	-12.21	0.00	0.49
Main Gear	0.68	-11.88	0.00	3.80	Aircraft Total	18.78	-9.51	0.17	0.35
Nose Gear	0.31	-3.55	-0.18	3.23	Mission Two – Heaviest Passenger				
Nose Assembly	0.91	-5.12	0.02	0.74	Heaviest Passenger	2.39	-12.18	0.00	0.06
Tail Assembly	0.51	-26.26	0.06	-1.24	Aircraft Total	20.77	-9.77	0.15	0.31
Elevons	0.19	-28.58	0.28	-0.84	Mission Three – Lightest Passenger and Payload				
Rudder	0.10	-26.88	0.25	-2.86	Lightest Passenger	0.40	-12.21	0.00	0.49
Servo Tray	0.40	-18.07	-0.16	-0.03	Payload Block	1.00	-14.43	0.00	-0.09
Battery	6.90	-6.68	0.00	0.29	Aircraft Total	19.78	-9.76	0.16	0.32
ESC	0.69	-6.67	0.00	1.08	Mission Three – Heaviest Passenger and Payload				
Propeller	0.67	-2.37	0.00	0.00	Heaviest Passenger	2.39	-12.18	0.00	0.06
Receiver Battery	0.68	-13.02	3.12	0.70	Payload Block	1.00	-14.43	0.00	-0.09
Receiver	0.15	-11.51	3.04	0.88	Aircraft Total	21.77	-9.98	0.14	0.29
Stability Augmentation	0.31	-11.45	1.68	0.63					
Seat	0.01	-12.23	0.00	0.95					
Bulkhead	0.03	-13.29	0.01	-0.27					
Empty Weight / Mission One									
Aircraft Total	18.38	-9.45	0.17	0.34					

7.7 Flight Performance Parameters

Table 17. Flight Performance Parameter by Mission

Parameters	Mission 1	Mission 2	Mission 3
TOGW (lbs.)	1.24	1.33	1.39
W/S (lb./in.^{2})	0.0103	0.0111	0.0116
V_{stall} (mph)	38	40	41
V_{cruise} (mph)	45	45	45
Takeoff Distance (ft.)	81	105	128
Time for 360° Turn (s)	12	12	12
Mission Time (min)	2.6	2.7	0.93

The aircraft's takeoff distance can be related to thrust available and takeoff C_L. To assist with exploring the design space, the carpet plot shown in Figure 28 was created. The initial AV1 design (4.5" span) was estimated to have a takeoff distance of 138 ft., nearly at the 150 ft. design limit. In the first flight tests of this aircraft, the takeoff speed was found to be unacceptably high. By relaxing the span to 8" (AV2), the possible takeoff C_L and wing area increases. For AV2.5, the center of gravity was moved forward by extending the motor forward, and a variety of motor and propeller combinations were tested to assess takeoff performance. Many of these tests resulted in takeoff distances of approximately 75 ft. using a LiPo battery. Transitioning to AV3, Figure 28 below shows a predicted takeoff distance of 129 ft. at a C_L of 0.36.

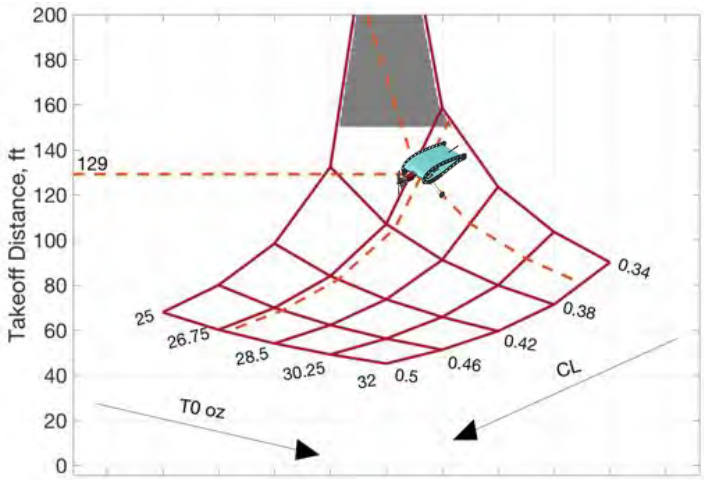

Figure 28. Takeoff Distance Carpet Plot

The predicted takeoff speed for AV3 is 43 mph, shown in Figure 29 based on a wingspan of 8”. Figure 29 shown as a calibrated air speed (CAS), accounting for induced flow velocity from the propeller using actuator disk theory. The accuracy of these predictions will be discussed in further detail in section 10.

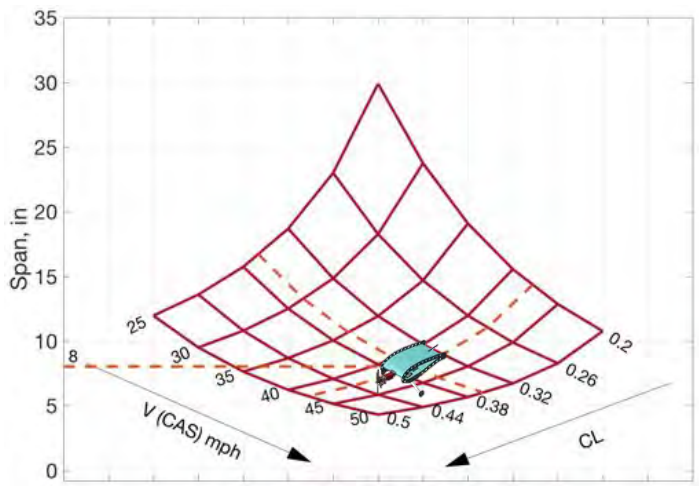

Figure 29. Span Carpet Plot

The induced flow velocity used to adjust for calibrated air speed is shown in Figure 30 below. This induced flow velocity was determined using actuator disk theory.

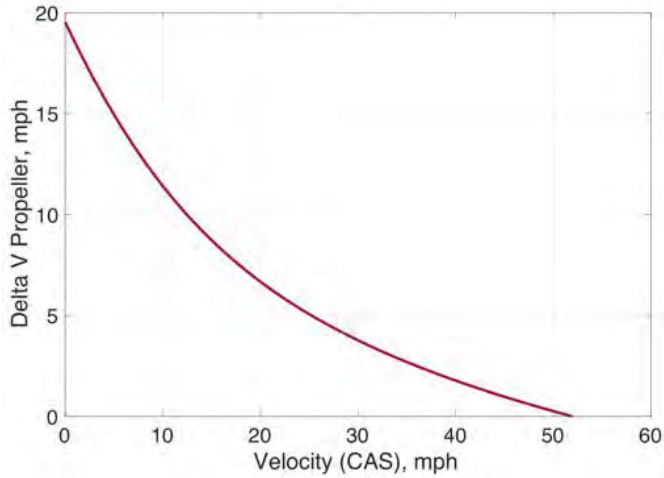

Figure 30. Delta V from Propwash

Test data for the thrust and power available has been collected for the AV3 propulsion system. These are plotted against the thrust and power required, shown in Figure 31 and Figure 32. In these figures, the thrust available and power available are calculated using an apparent velocity that includes the induced flow velocity due to the propeller, shown above.

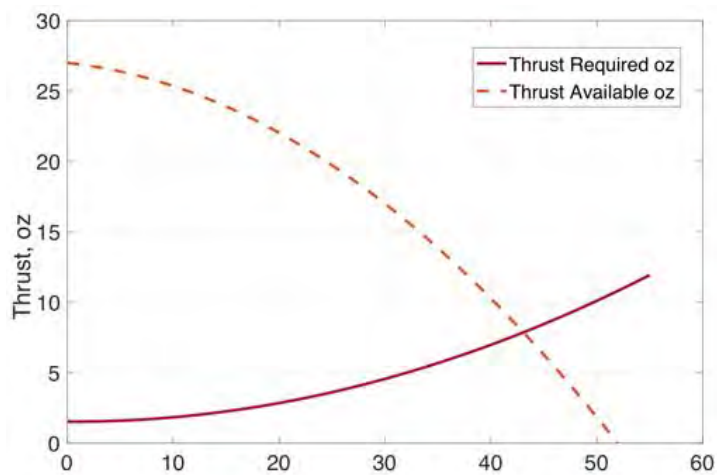

Figure 31. AV3 Thrust and Drag

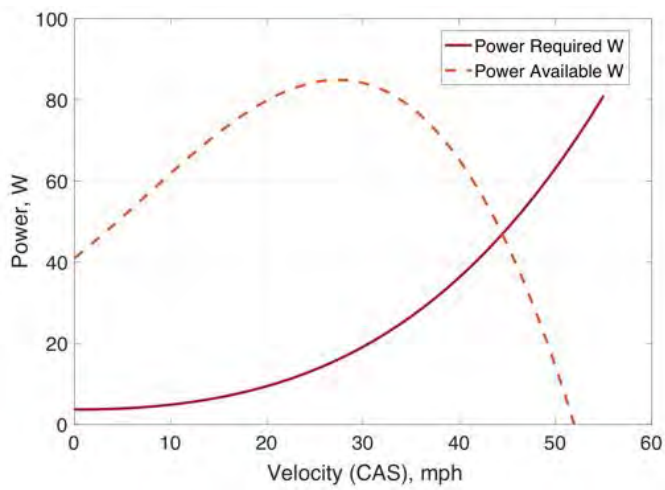

Figure 32. AV3 Power Required and Available

7.8 Mission Performance and Rated Aircraft Cost (RAC)

Table 18. Mission Performance Parameters and RAC

Mission	TOGW (lbs.)	Wingspan (in.)	# of Passengers	Payload Weight (oz.)	# of Laps	Mission Tiime (s)
Mission 1	1.24	8.0	0	0	3	156
Mission 2	1.33	8.0	1	1	3	162
Mission 3	1.39	8.0	1	1	1	56
RAC	9.92					

7.9 Mission Performance

As defined above, mission 1 requires the aircraft to complete 3 laps within a 5-minute time period with a minimum flight speed needed of 25 ft/s. The current AV3 is designed to support 65-75 ft/s cruise speed which leads to mission completion in roughly 2.6 to 3.2 minutes of the allotted 5 minutes, assuming constant flight speed. This capability is well within the requirements, allowing for significant flexibility should in flight problems occur. Mission 2 requires the aircraft to again fly 3 laps within a 5-minute time period, however carrying a number of passengers. As discussed in the scoring analysis, one passenger has been selected for AV3 which results in a low score assuming that another team will choose to maximize the number of passengers. Mission 3 requires the aircraft to fly with at least half of the number of passengers flown in mission 2, as well as some amount of payload. As discussed above, 1 oz. of payload has been selected for AV3. Under the assumption that another team will maximize the number of passengers and payload carried for this mission, the projected mission 3 score is 2 of the possible 6 points.

While the current design does not maximize the score for mission 2 or mission 3, the RAC of AV3 is shown to be significantly lower than any other concept that would be needed to support the effort of

maximizing the number of passengers and payload weight that the aircraft could carry. Through the scoring analysis conducted, it was identified that minimizing the empty weight and wingspan results in a greater overall increase to competition score than choosing to maximize passengers and payload weight. The induced structural weight, as well as wingspan needed to achieve the highest mission score results in a significant penalty to the RAC, and further the overall competition score. Combining these factors holistically, the Virginia Tech team believes that the low wingspan, light weight concept of AV3 will achieve the highest overall competition score.

7.10 Drawing Package

The following drawing package includes a dimensioned 3-view, structural arrangement, aircraft systems layout, and payload and passenger drawing. All drawings were made using SolidWorks.

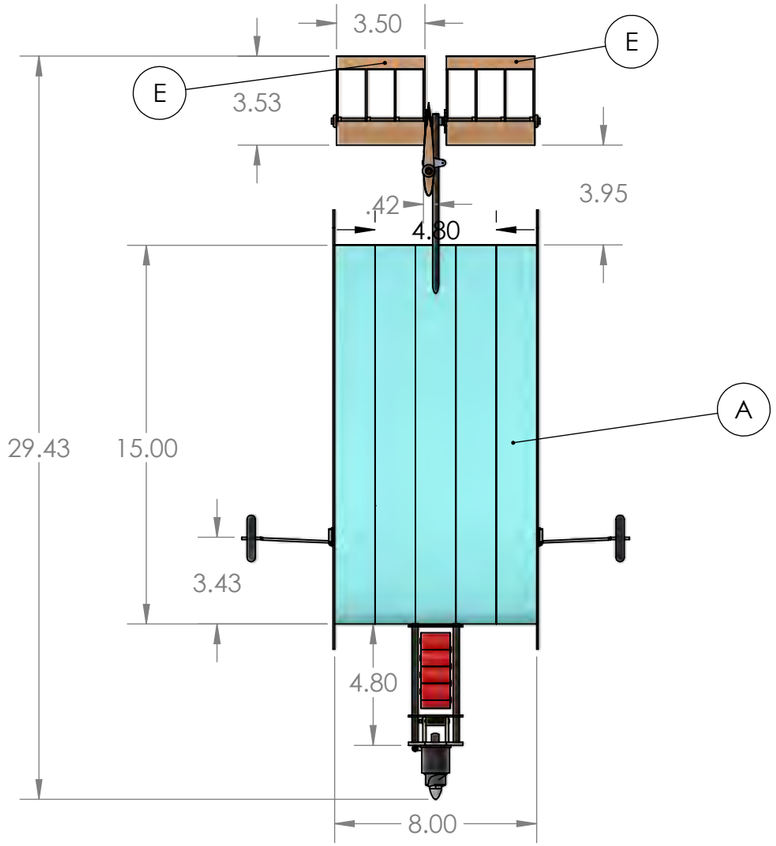

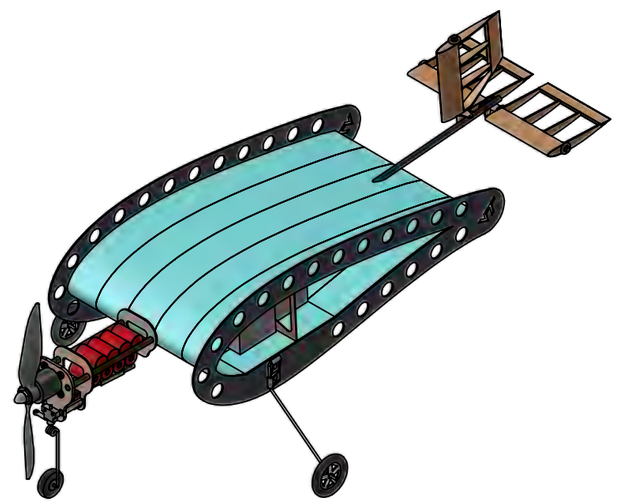

FUSE-001 Fuselage Subassembly	NOSE-001 Nose Subassembly
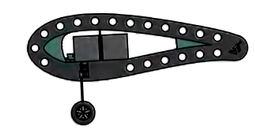 SCALE: 1:12	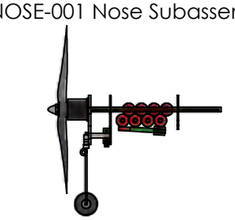 SCALE: 1:8
TAIL-001 Tail Subassembly	TRAY-001 Servo Tray Subassembly
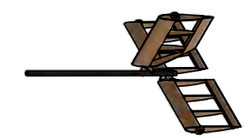 SCALE: 1:8	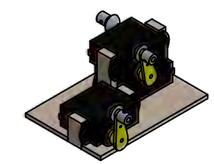 SCALE: 1:2

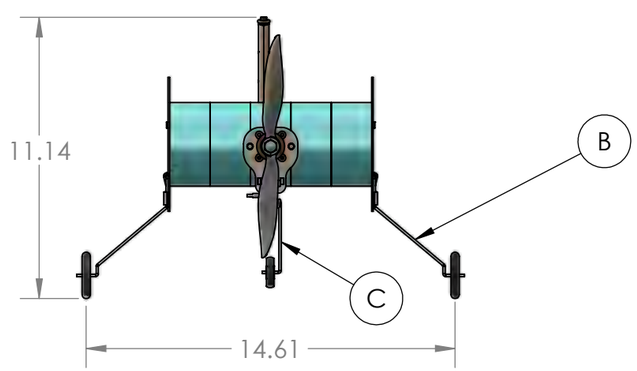

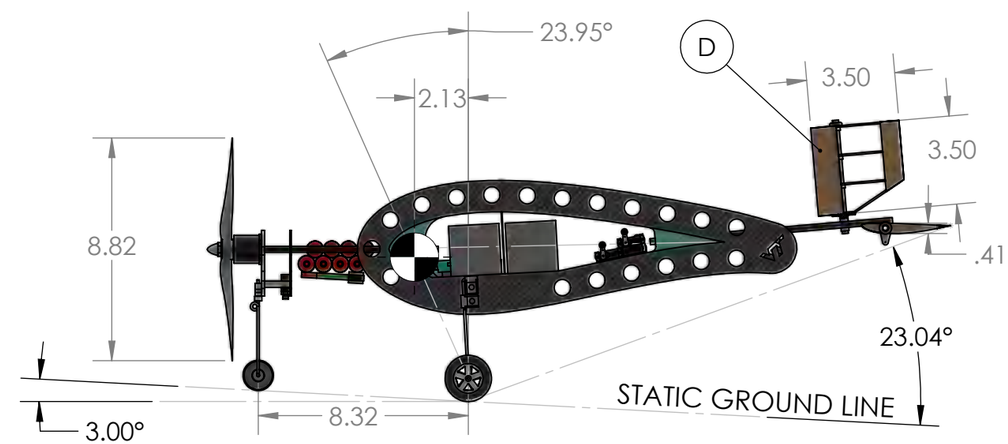

MAJOR COMPONENTS	
A	FUSE-101 Foam Fuselage
B	FUSE-113 Main Gear
C	NOSE-113/119 Nose Gear
D	TAIL-201 Rudder
E	TAIL-101/102 Elevons

NOTE:
DIMENSIONS ARE IN INCHES
TOLERANCES:
ANGULAR: ± 0.05
ONE PLACE DECIMAL ± 0.1
TWO PLACE DECIMAL ± 0.07
THREE PLACE DECIMAL ± 0.05

	NAME
DRAWN BY:	S. Bowen
CHECKED BY:	M. Svoboda
CHIEF ENGINEER:	JP Stewart

VIRGINIA TECH

AIAA - DESIGN BUILD FLY 2017-2018

DOCUMENT TITLE: **AIRCRAFT 3-VIEW**

SIZE	APPROVAL DATE:	REPORT TITLE:
B	2/22/2018	**DRAWING PACKAGE**
	SCALE: 1:6	SHEET 1 OF 4

SOLIDWORKS Educational Product. For Instructional Use Only.

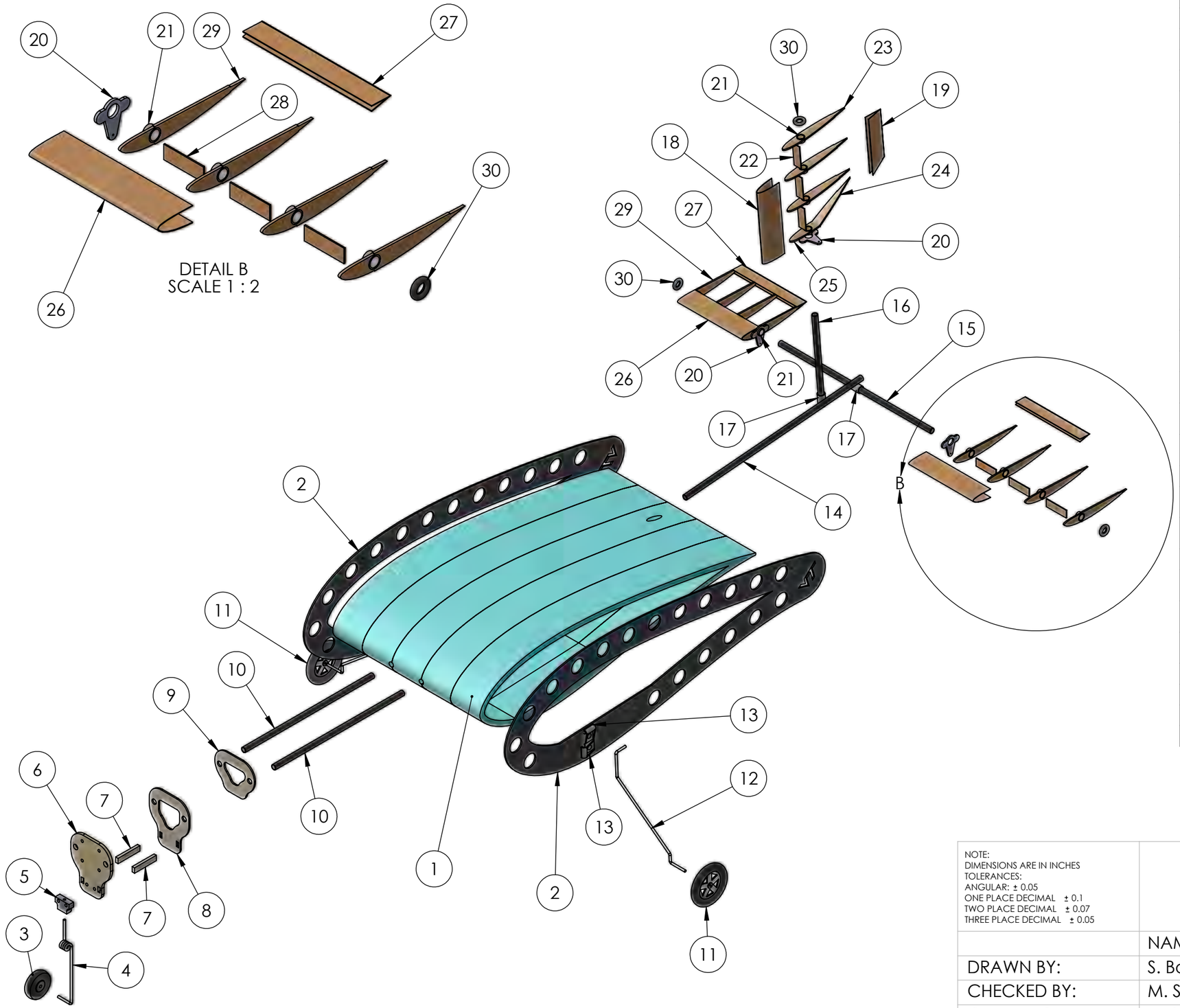

ITEM	PART NAME	MATERIAL	QTY.
1	FUSE-101 Fuselage	Foam	5
2	FUSE-111 Endplate	Carbon Fiber - Balsa	2
3	NOSE-119 Nose Wheel	Rubber - Plastic	1
4	NOSE-113 Nose Gear	Steel	1
5	NOSE-117 Nose Gear Mount	Aluminum	1
6	NOSE-103 Forward Firewall	Plywood	1
7	NOSE-109 Nose Servo Mount Stick	Balsa	2
8	NOSE-105 Mid Firewall	Balsa	1
9	NOSE-111 Aft Firewall	Balsa	1
10	NOSE-101 Nose Boom	Carbon Nanotube	2
11	FUSE-115 Main Wheel	Rubber - Plastic	2
12	FUSE-113 Main Gear	Steel	2
13	McMaster-3192T410 Main Gear Mount Bracket	Plastic	4
14	TAIL-301 Tail Boom	Carbon Nanotube	1
15	TAIL-305 Elevon Boom	Carbon Nanotube	1
16	TAIL-307 Rudder Boom	Carbon Nanotube	1
17	TAILI-705 Large Hinge Bushing	Plastic	2
18	TAIL-203 Rudder LE Sheeting	Balsa	1
19	TAIL-207 Rudder TE Sheeting	Balsa	1
20	TAIL-701 Control Horn	Carbon Fiber - Balsa	3
21	TAIL-703 Small Hinge Bushing	Plastic	12
22	TAIL-213 Rudder Shear Web	Balsa	3
23	TAIL-205 Rudder Main Rib	Balsa	3
24	TAIL-211 Rudder Slanted Rib	Balsa	1
25	TAIL-209 Rudder Bottom Rib	Balsa	1
26	TAIL-103 Elevon LE Sheeting	Balsa	2
27	TAIL-109 Elevon TE Sheeting	Balsa	2
28	TAIL-105 Elevon Shear Web	Balsa	6
29	TAIL-107 Elevon Rib	Balsa	8
30	TAIL-707 ORing	Rubber	3

NOTE:
DIMENSIONS ARE IN INCHES
TOLERANCES:
ANGULAR: ± 0.05
ONE PLACE DECIMAL ± 0.1
TWO PLACE DECIMAL ± 0.07
THREE PLACE DECIMAL ± 0.05

	NAME
DRAWN BY:	S. Bowen
CHECKED BY:	M. Svoboda
CHIEF ENGINEER:	JP Stewart

VIRGINIA TECH

AIAA - DESIGN BUILD FLY 2017-2018

DOCUMENT TITLE: **STRUCTURAL LAYOUT**

SIZE	APPROVAL DATE:	REPORT TITLE:
B	2/22/2018	**DRAWING PACKAGE**
	SCALE: 1:4	SHEET 2 OF 4

SOLIDWORKS Educational Product. For Instructional Use Only.

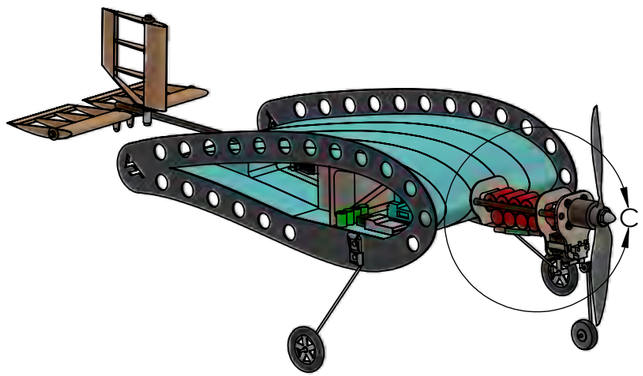

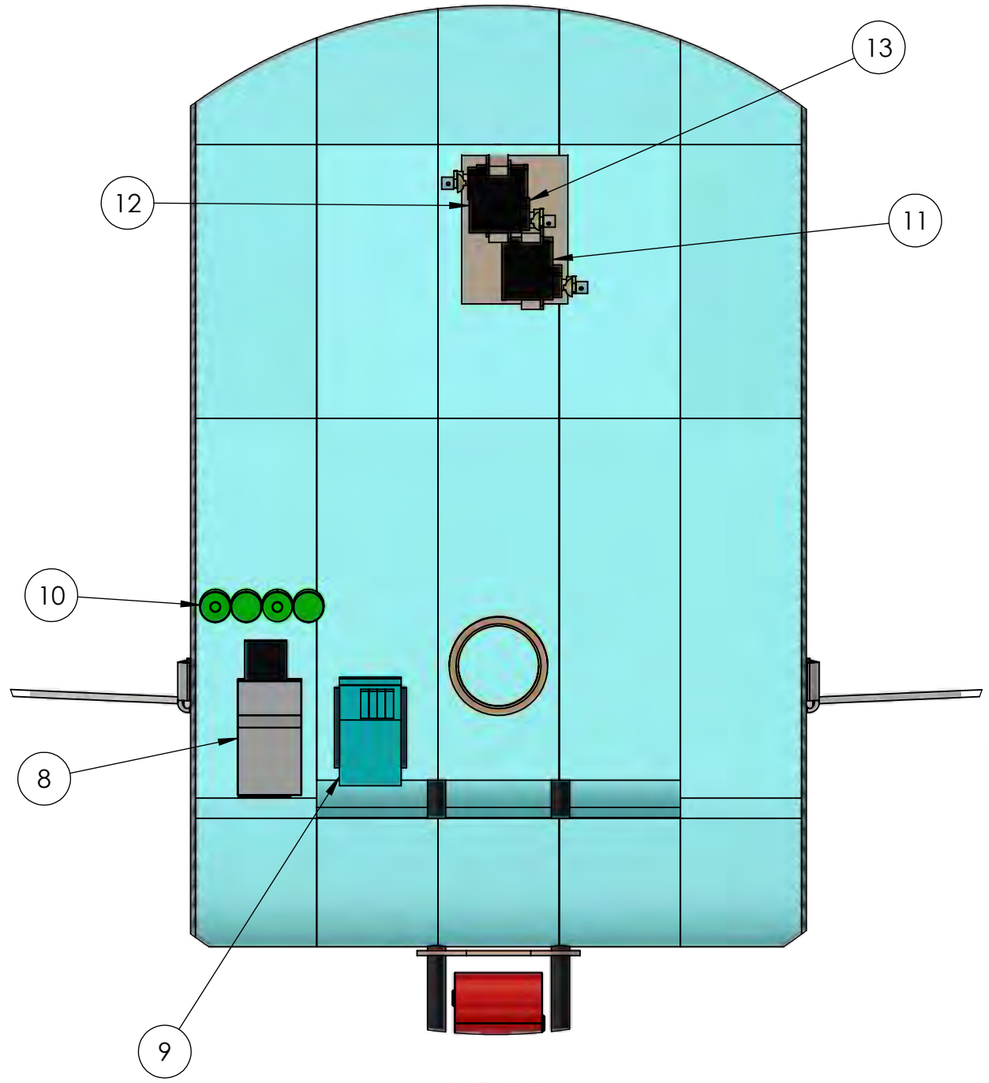

DETAIL D
SCALE 1 : 2

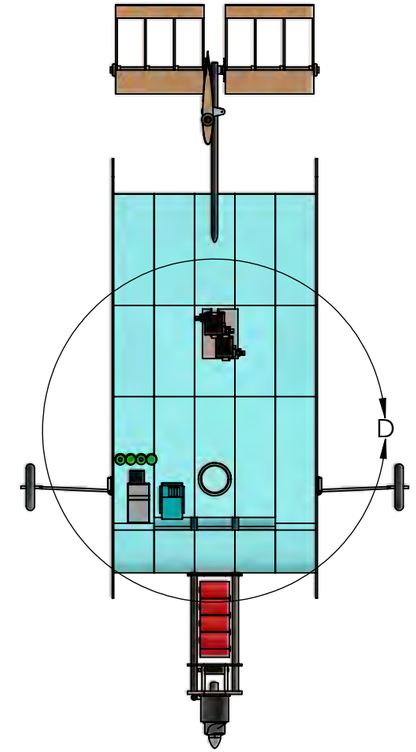

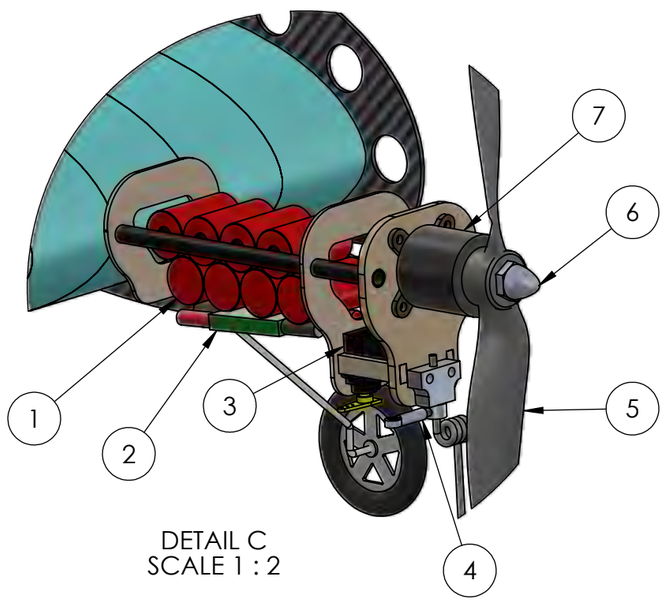

DETAIL C
SCALE 1 : 2

ITEM	PART NAME	MANUFACTURER
1	8s 1500 mAh Battery Pack	Elite
2	30A Electronic Speed Controller	Arris
3	Nose Wheel Servo	DSP-33
4	NOSE-115 Nose Wheel Steering Arm	Dupro
5	9x6 Thin Electric Prop	APC
6	Prop Nut	APC
7	D2826-6 2200 kv motor	Turnigy
8	2106GF Receiver	Futaba
9	Stability Augmentation	CC3D
10	4s 170 mAh Receiver Pack	Tenergy
11	Left Elevon Servo	DSP-33
12	Right Elevon Servo	DSP-33
13	Rudder Servo	DSP-33

NOTE:
DIMENSIONS ARE IN INCHES
TOLERANCES:
ANGULAR: ± 0.05
ONE PLACE DECIMAL ± 0.1
TWO PLACE DECIMAL ± 0.07
THREE PLACE DECIMAL ± 0.05

	NAME
DRAWN BY:	S. Bowen
CHECKED BY:	M. Svoboda
CHIEF ENGINEER:	JP Stewart

VIRGINIA TECH

AIAA - DESIGN BUILD FLY 2017-2018

DOCUMENT TITLE: **SYSTEMS LAYOUT**

SIZE	APPROVAL DATE:	REPORT TITLE:
B	2/22/2018	**DRAWING PACKAGE**
	SCALE: 1:6	SHEET 3 OF 4

SOLIDWORKS Educational Product. For Instructional Use Only.

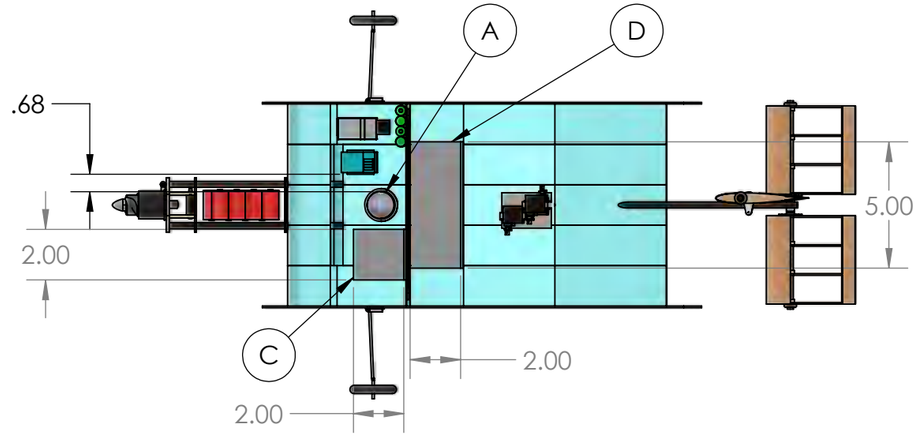

Mission 3 Configuration - Smallest Passenger

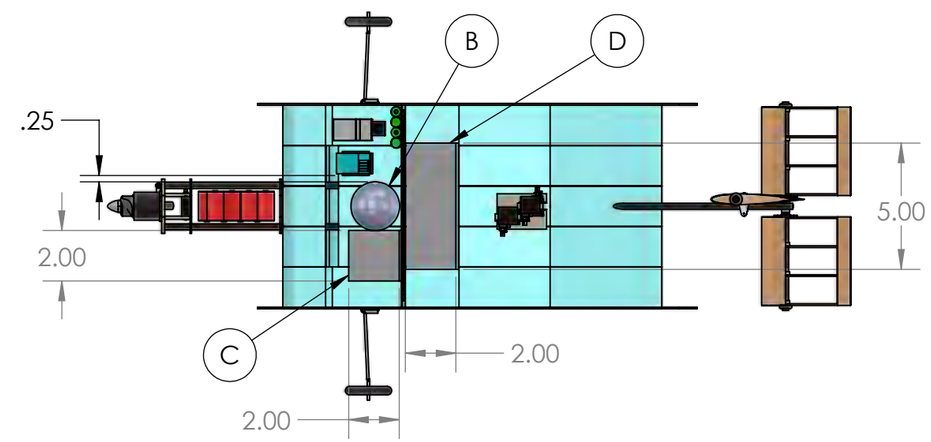

Mission 3 Configuration - Largest Passenger

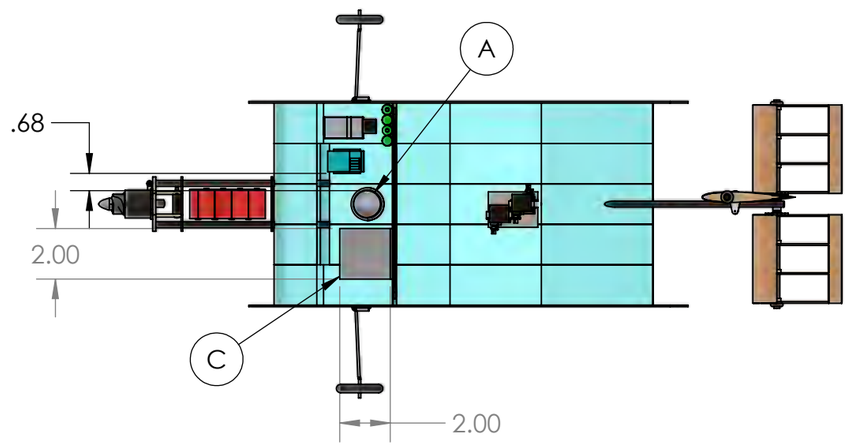

Mission 2 Configuration - Smallest Passenger

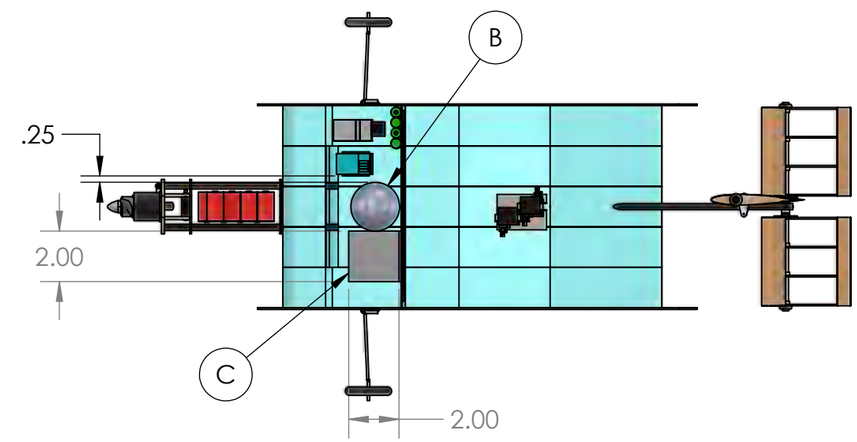

Mission 2 Configuration - Largest Passenger

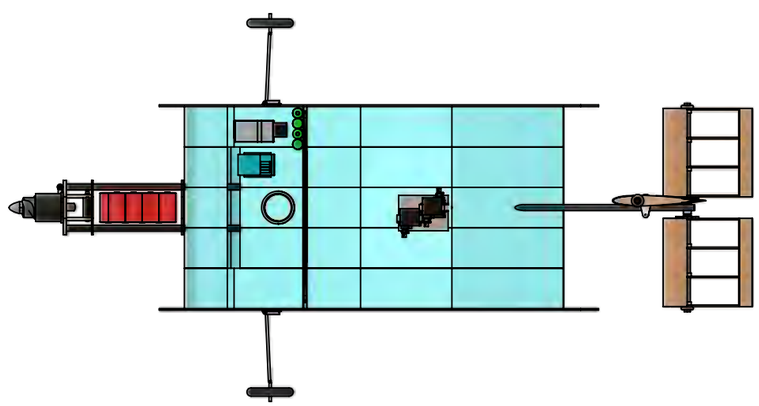

Mission 1 Configuration

ITEM	ITEM NAME	DIMENSIONS
A	Smallest Passenger	27 mm Diameter
B	Largest Passenger	49 mm Diameter
C	Passenger Aisle	2" x 2" x 2"
D	Payload Block	5" x 2" x 2"

NOTE:
DIMENSIONS ARE IN INCHES
TOLERANCES:
ANGULAR: ± 0.05
ONE PLACE DECIMAL ± 0.1
TWO PLACE DECIMAL ± 0.07
THREE PLACE DECIMAL ± 0.05

VIRGINIA TECH

AIAA - DESIGN BUILD FLY 2017-2018

DOCUMENT TITLE: **PAYLOAD CONFIGURATIONS**

	NAME	SIZE	APPROVAL DATE:	REPORT TITLE:
DRAWN BY:	S. Bowen	**B**	2/22/2018	**DRAWING PACKAGE**
CHECKED BY:	M. Svoboda			
CHIEF ENGINEER:	JP Stewart		SCALE: 1:6	SHEET 4 OF 4

SOLIDWORKS Educational Product. For Instructional Use Only.

8 Manufacturing Plan

This section describes the materials and processes used in the manufacture of each subsystem, as well as the aircraft construction timeline. A combination of foam, balsa/basswood, and composites were used in the construction of this aircraft. For each component, a manufacturing method was selected that could produce each in a lightweight and time-efficient manner, while complying with structural requirements.

In order to effectively ensure that parts met specifications, configuration management best practices were applied to the CAD model and drawings. The drawings were organized in a hierarchal drawing tree, organized by four major build stations: the fuselage, motor mount, tail, and servo tray. These drawings allowed the team to "red-line" revisions directly on the drawing, speeding up the feedback cycle.

8.1 Manufacturing Processes Considered

The team had experience with several manufacturing techniques acquired over the past few competition years. As such, several techniques were qualitatively evaluated on the measures of merit (MOM) described below.

Weight – Since the concept behind our aircraft is aggressively minimizing RAC, weight was the highest MOM with a value of 5.

Manufacturability – The ability to produce the aircraft, both quickly and within tolerance, was critical for the team to refine the design as much as possible before competition.

Reparability – In addition to the usual concerns with crashworthiness, there is added emphasis on reparability with the mission profile including LRUs.

Experience – The team has broad experience with balsa and composite aircraft, as well as foam prototyping.

Cost – While important to keep in mind, cost was not a significant constraint on this year's design.

With these measures in mind, the team investigated several viable processes for manufacturing the fuselage. These processes are described in detail below:

Table 19. Wing Manufacturing Trades

		Manufacturing Process		
MOM	**Value**	**Balsa/ Basswood**	**Milled Foam**	**Composites**
Weight	5	3	5	3
Manufacturability	4	3	4	2
Reparability	4	2	4	2
Experience	2	3	2	4
Cost	1	4	5	2
Total	16	45	66	**41**

The processes in Table 19 were evaluated, with each MOM having a weight on a scale from one to five, with five being the best. Based on the measures of merit, a foam design was found to be the best option, due largely to its ease of manufacturing and reparability (tested through flight tests). To confirm these results, prototypes for all models were built. Of the three methods, the foam sections produced the highest quality prototype in the shortest amount of man hours, with minimal surface defects, no twist, and a smooth finish.

8.2 Subsystem Manufacturing

- Fuselage/Lifting Surface – On early prototypes, 2" blocks of foam were epoxied together and cut into the shape of the airfoil. The cutting was initially done with a band saw, then moved to a hot-wire for a smoother finish, albeit with some linear pitting across the piece. To improve the surface finish, this process was changed to the CNC router so that the airfoil interior could also be milled, further reducing weight. The CNC adaptive carve used to cut out the fuselage had a high spindle speed with a low feed rate to achieve the desired smoothness, as well as high step down to reduce time to complete the carve. Pieces for the aircraft were faced to 1.6 in. and cut into precise shapes. These pieces were bonded with a mixture of 30-minute epoxy and Cell-o-Fill. Since only one side of the foam was faced, there would occasionally be small gaps, which would be filled with wood filler and sanded smooth.

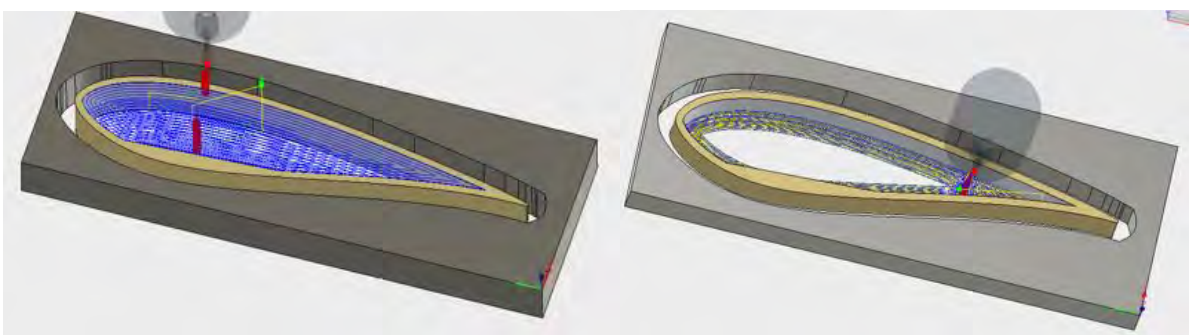

Figure 33. Simulated Toolpaths Using Both Ramp and Adaptive Clearing Carves

Figure 34. Completed Wing Section

- Control Surfaces – The elevons and rudder were built from ribs, shear webs, and thin sheeting along the leading and trailing edges. The ribs and webs were laser-cut using shapes from the CAD

model. The ribs would be cut with circular holes at the quarter chord, and low-friction bushings inserted, bonded together with CA. The ribs were placed in a jig and bonded with the webs. For the leading and trailing edges, 1/32nd in. thick balsa was sanded to half thickness and cut. The leading-edge piece was treated with ammonia and then bonded to the leading edge of the ribs. The trailing edge pieces were attached to the upper and lower surfaces, then sanded to make the trailing edge sharp. The assembled were then covered with SoLite.

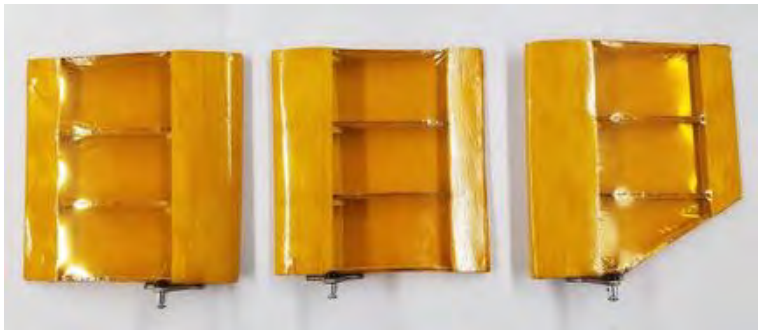

Figure 35. Lightweight, Removable Control Surfaces

- End Plates – These were made of a sheet of 1/32nd in. balsa sandwiched between two sheets of 0/90 carbon fiber laid up in the same orientation on a glass surface and wetted with the resin matrix before removing the excess resin. Peel-ply and breather cloth was laid across the layup, and two-sided pressure tape was applied to the edges of the glass to create an airtight seal. Vacuum bag was pressed onto the tape and a one-way air hose was connected. Once sealed, the glass sheet was placed in the oven to cure. The finished pieces were then secured and cut into the end plate shape with the CNC. A ramp pass was used with a high spindle speed, to cut through the material, and low feed rate to reduce the load on the bit, to achieve the desired carve. A low step down was used to cut through each layer of the composite endplate individually. As a weight reduction measure, evenly spaced circular holes were cut in the endplate to reduce weight. The endplate was then covered in SoLite.

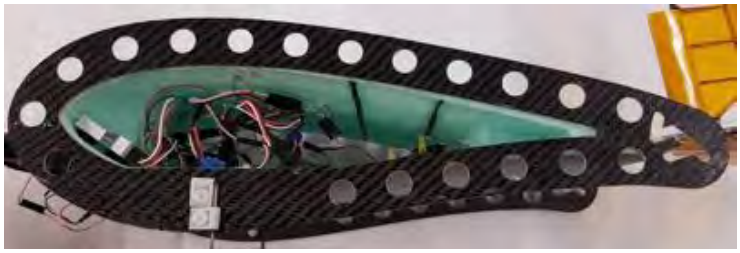

Figure 36. CNC Milled Carbon Endplates

- Seat – The seat was made from two pieces of balsa laser cut into rings. An elastic strap is attached to the seat in order to restrain passengers in flight. This strap also includes several Velcro patches, accounting for the varying passenger sizes.
- Payload – Sides of the payload block were cut and bonded with CA. Ballast was added to make the block weigh 1 oz.

- Landing Gear – The nose gear was made using an off-the-shelf steel wire mounted to the firewall, and a stock wheel held on by two collets. The main gear consists of a steel wire attached with nylon clamps and bolts and stock wheels, held on by collets. This configuration allows the landing gear to remain rigid during taxi, takeoff, and landing, but also allows for some spring and controlled failure in the case of a hard landing to minimize impact on the fuselage.
- Motor Mount – The motor mount was constructed with two carbon rods that were attached to the front of the fuselage. Three wood plates were laser cut, two of them 1/32nd in. thick plates to contain the battery and one of them a 1/16th in. thick basswood piece to support the motor. The motor is mounted to the basswood plate via an aluminum cross-plate.
- Tail – The tail boom was made from purchased carbon tube with an outer diameter of 0.236" and inner diameter of 0.196". Two IGUS bushings were lashed onto the tube as shown in Figure 37. The two elevon and rudder hinges are then bonded to the bushings and the control surfaces rotate on the hinge.

Figure 37. Lashed Bushing and Tail Boom

Figure 38. Top Left: Passenger Seat with adjustable strap. Top Right: Basswood payload block. Bottom Left: Motor Mount with Nose gear. Bottom Right: All-flying tail.

8.3 Manufacturing Timeline

Figure 39. Manufacturing Timeline

9 Testing Plan

9.1 Test Objectives

A high-level testing map is shown below in Figure *40*. This figure shows the high-level testing sequence of each group including each milestone as discussed below.

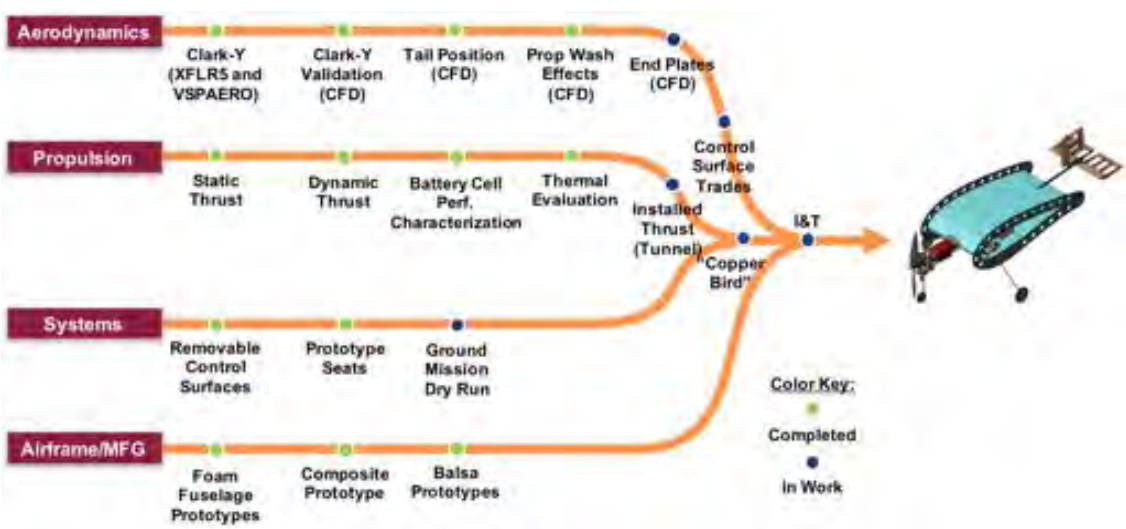

Figure 40. High Level Testing Plan

9.1.1 Aerodynamics Testing

For the Aerodynamics branch, the testing begins with XFLR5, VSPAero, and Xfoil approximations to validate experimental lift and drag coefficients for low aspect ratio Clark Y airfoils presented in NACA TR431. These approximations are intended to replicate the data presented in the NACA report and were then repeated using CFD and wind tunnel tests. Replicating the report data for the Clark Y airfoil at low aspect ratios allowed validation of calculation methods, especially for CFD simulations and wind tunnel testing which are prone to uncertainty. Once the processes have been validated, they can be readily applied to the airfoils and aspect ratios selected for various trades during the preliminary design stage. Two aspects of the preliminary design that are particularly difficult to measure the effects of analytically are the end plates and the wash effects of the propeller over the surface of the body. CFD and wind tunnel tests are to be used to characterize these effects through flow visualization as well as numerical data acquisition for the forces and moments acting upon the aircraft in various configurations.

After developing the capability to run full CFD simulations with reasonable certainty in the results, a number of more detailed trade studies could be conducted for different airfoils, wingspans, endplate sizes, and control surface sizes. CFD simulations have been an integral part of the detailed design process and have been used to predict the performance effects of design changes between each design spiral. This will continue after the time of this report as the AV4 design spiral begins to determine optimal endplate size to reduce tip vortex interference, as well as the best placement and sizing for the tail to counteract torque and improve flight stability.

9.1.2 Propulsion Testing

The objective of propulsion testing is to determine whether the combinations mentioned in Table 20 below meet the requirements for thrust while maintaining the lowest possible empty weight. Candidates for testing were selected based on design criteria from 6.4.3 Power Sizing.

Table 20. Propulsion System Combinations

Motor	Battery	Propeller
Turnigy D2826 - 6	ELITE 1500 8s	APC 9x6E
Scorpion SII-2208	ELITE 1500 8S	APC 9x4.7SF
EMAX MT2213	ELITE 800 10S	APC 9x9E
Cobra C2208/20	ELITE 1500 8S	APC 9x6E

Static and dynamic tests of configurations were conducted using an RCbenchmark Series 1580 dynamometer, with the data collection parameters shown in Figure 41, along with pulse width modulation signal, and downstream flow speed utilizing an anemometer shown in also shown in Figure 41.

Specification	Min.	Max.	Tolerance	Unit
Thrust	-5	5	0.5%	kgf
Torque	-1.5	1.5	0.5%	Nm
Voltage	0	35	0.5%	V
Current	0	40	1%	A
Angular speed*	0	190k	-	eRPM
Coil resistance	0.003	240	0.5%	Ohm
Digital scale	0	3	0.5%	kgf

*Electrical RPM, divide by the number of motor poles to obtain true mechanical RPM

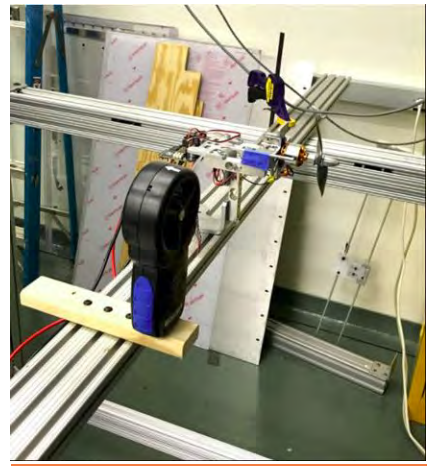

Figure 41. RCbenchmark Series 1580 Specification and Test Stand

Tests conducted include battery endurance, output voltage over time, static thrust, torque effects, and thrust effects in varying free stream speeds. A rig including the dynamometer, pitot probe, and a digital anemometer was constructed for static tests, as well as higher level wind tunnel tests. All data collection parameters listed above are monitored using the RCbenchmark GUI, and are synchronized over time. For analysis, the synchronized time series data is outputted to Visual Basic macros within Excel to develop charts and organize data collection.

For high-level dynamic tests, the team has utilized the Virginia Tech Open Jet Wind Tunnel to conduct wind tunnel tests. The wind tunnel is powered by a 30-horsepower motor connected to a centrifugal fan capable of propelling up to 15 # 3E of air, and discharges into a 6-degree, 4 m diffuser. The flow is then directed into a settling chamber, then through a honeycomb mesh with fiberglass screen to reduce circulation and turbulence and insure a uniform flow. Flow speed can be manipulated through a variable frequency drive, allowing for a maximum fan speed of 1180 rpm. At maximum fan speed, the flow rate through the test section is 30 m/s (67.1 mph). Analysis of data collected from wind tunnel tests is detailed in section 10.1.1.

Additional Analysis conducted includes a complete thermal evaluation of the propulsion system, including the temperature monitoring of the motor, battery, and ESC under operating conditions to insure the service life of components and to verify that system cooling is sufficient for each mission.

9.1.3 Systems Testing

The third branch of the map represents the Systems group which is responsible for testing the components critical to the ground mission, as well as the integration of the final aircraft. The first step for the Systems group centers around removable control surfaces. This is heavily governed by the requirements set in the RFP for the ground mission. Each control surface must be integrated in such a way as to meet the requirements of the RFP as well as to allow for the greatest success for the ground mission. Therefore, this phase focuses primarily on evaluating the timely removal and replacement of each component via

prototyping and aircraft testing. Another aspect of the Systems group testing includes the seats for the passengers and the restraint of the payload blocks. The Systems group evaluated a variety of different passenger restraint options and determined the most effective arrangement of the passengers and payload. This was carefully monitored with the center of gravity in mind, thus the Systems group worked closely with the structures team to assess appropriate arrangement of all systems that must be incorporated in the final design. Finally, the systems group will perform a series of ground mission dry runs to simulate each phase of the ground mission, building up to a complete execution of the evaluation that must be completed at competition. At the time of this report, individual LRUs have been tested for compliance with the RFP and the ground mission requirements. The next step consists of a series of ground mission dry runs to identify areas where problems may occur and to prepare for successful competition performance.

9.1.4 Manufacturing Testing

The final branch of the testing map represents the Manufacturing group which is responsible for the construction of all prototypes as well as the final aircraft. The Manufacturing group begins with creating foam fuselage prototypes that are used to support aerodynamic testing, as well as the development of a repeatable manufacturing plan. While the Manufacturing group is ultimately responsible for the construction of the aircraft, it is critical to the success of the team and the schedule for the Manufacturing group to develop reliable and repeatable processes. The foam fuselage prototypes serve as a light weight, easily constructible option for the preliminary design which allowed for quick results, as well as significant opportunity for underclassmen training. Once the foam manufacturing process became reliable, the Manufacturing group moves to balsa and composite methods which will be used for the final aircraft. In these stages, the Manufacturing team works closely with the Aerodynamics, Propulsion, and Systems groups to meet evolving design requirements. This includes developing and refining new processes to construct end plates, control surfaces, landing gear, servo mounts, and other features as necessary. Throughout the entirety of the testing process the manufacturing group will continually evaluate methods to reduce weight and improve consistency between prototypes.

9.2 Test Schedule

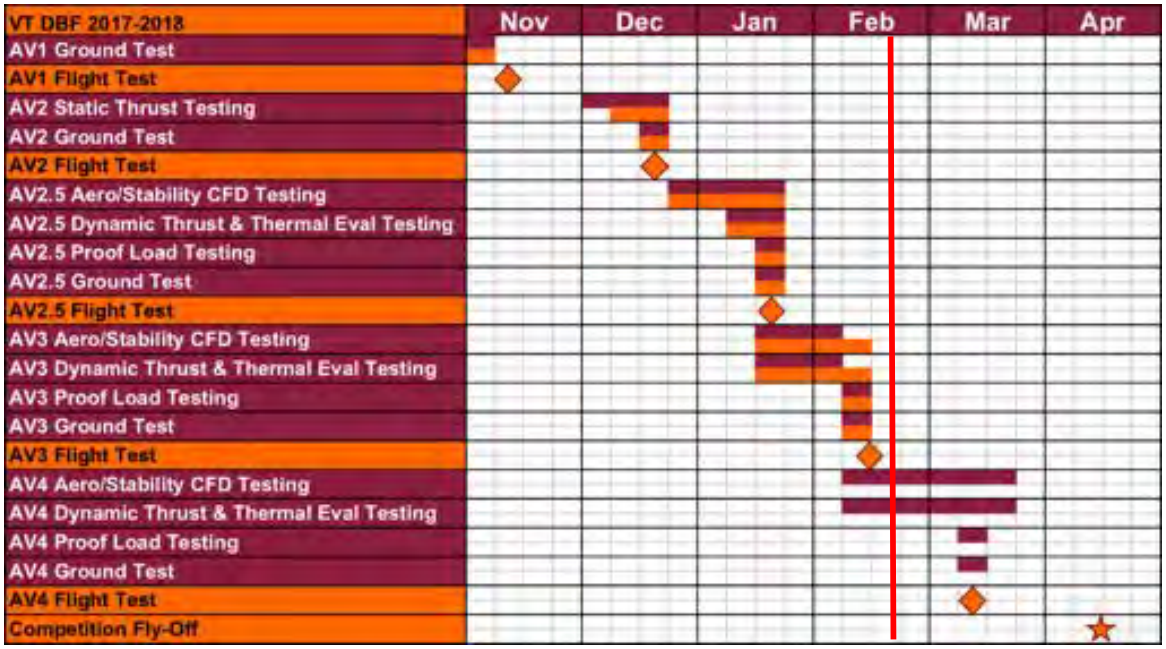

Figure 28. Testing Gantt Chart

9.3 Test and Flight Check List

For all wind tunnel testing, the check-list in Table 21 was used.

Table 21: Wind Tunnel Checklist

Component/System	Action
Open-Jet Computer	Turn on computer, check equipment connections
Open-Jet GUI	Load wind tunnel status program, check and record pressure and temperature in lab
Open-Jet Test Section	Set up proper mount for aircraft or propulsion test stand, ensure any previously mounted equipment is removed and stored safely
Open-Jet Fan	Turn on fan system, set rpm corresponding to desired flow speed
Conclude Testing	Shut down all systems, return to previous setup and check all equipment connections. Verify tunnel environment is clear

For each flight test, the check-list given in Table 22 was used.

Table 22. Pre-Flight Checklist

Component/System	Action
Motor	Screws tight, thread locked and firewall secure
Propeller	Nut tight, blades in good condition, blade oriented correctly
Landing Gear	Gear legs secure, collets tight and thread locked, wire not bent
End Plates	Secure, no damage
Payload Mounts	Installed and secure
Tail boom	Secure, no cracks
Control Surfaces	Minimal slop, pushrods and guides secure, o-rings in place
Servos	Secure, arms attached and screwed in
Propulsion Battery	Charged and secure
Received Battery	Charged, connected, and secure
CG Location	Verify location for given mission loading
Stability Augmentation	Armed, leveled on flat surface with chord parallel to ground
Control Surface Directions	Sense correct, rates set to takeoff, attitude hold mode engaged
Propulsion System	Check full throttle power, no vibration or communication loss

10 Performance Results

At the time of this report, a total of 22 flights have been attempted across the various design iterations. Each test was conducted with clear expectations and the lessons learned from each will be presented below.

10.1 Sub-system Testing

10.1.1 Propulsion Performance

The following configurations shown in Table 23 were tested statically at 2000 PWM to obtain maximum static thrust:

Table 23. Propulsion System Final Configuration Options

Motor	Battery	Propeller	ESC	Static Thrust* (ozf)	Total Weight (oz)
Turnigy D2826 - 6	ELITE 1500 8s	APC 9x6E	Arris 30A	27.2	9.93
Scorpion SII-2208	ELITE 1500 8S	APC 9x4.7SF	Arria 30A	25.4	9.787
EMAX MT2213	ELITE 800 10S	APC 9x9E	Arris 30A	17.4	8.369
Cobra C2208/20	ELITE 1500 8S	APC 9x6E	Arris 30A	27.1	9.646

The first propulsion system was tested with a variety of battery sizes, shown in Figure 42 to determine whether an 8S could produce the endurance and initial thrust required for takeoff.

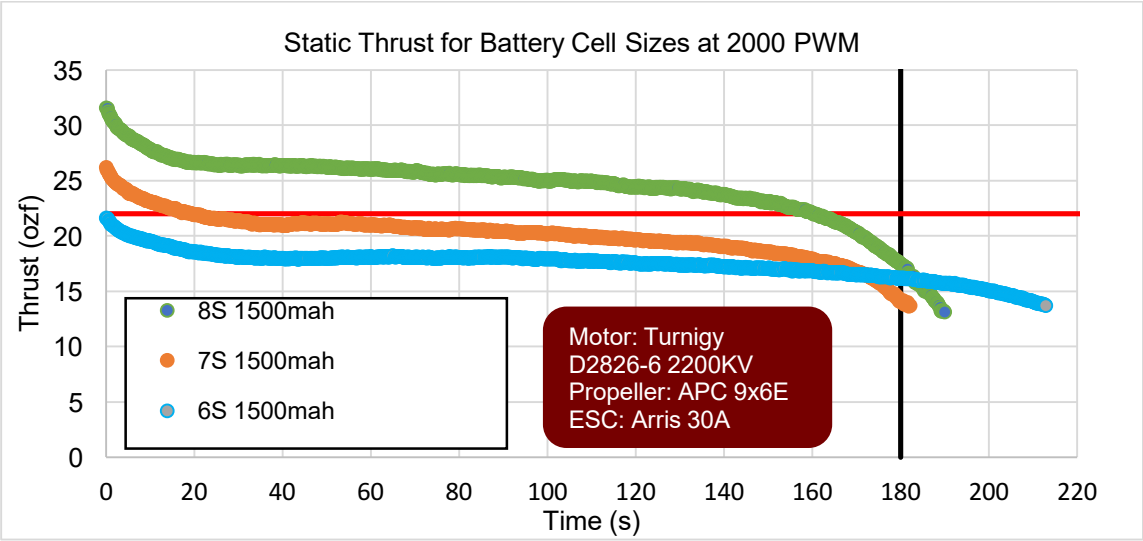

Figure 42. NiMH Full Throttle Discharge Endurance

The 8S 1500 mAh battery was selected because it produced 31 ozf at burst current and maintains thrust above 22 oz for a longer period of time compared to the 7S battery. The 22 oz line represents the minimum thrust needed to maintain cruise performance. It should be noted that this plot shows the endurance at full throttle (2000 PWM). Under normal flight conditions, the pilot will reduce the throttle setting to roughly 75-80% for a majority of cruise flight, resulting in an extension of endurance capability.

A thermal evaluation, shown in Figure 43, was conducted on the system that shows the temperature of the motor at each cell size.

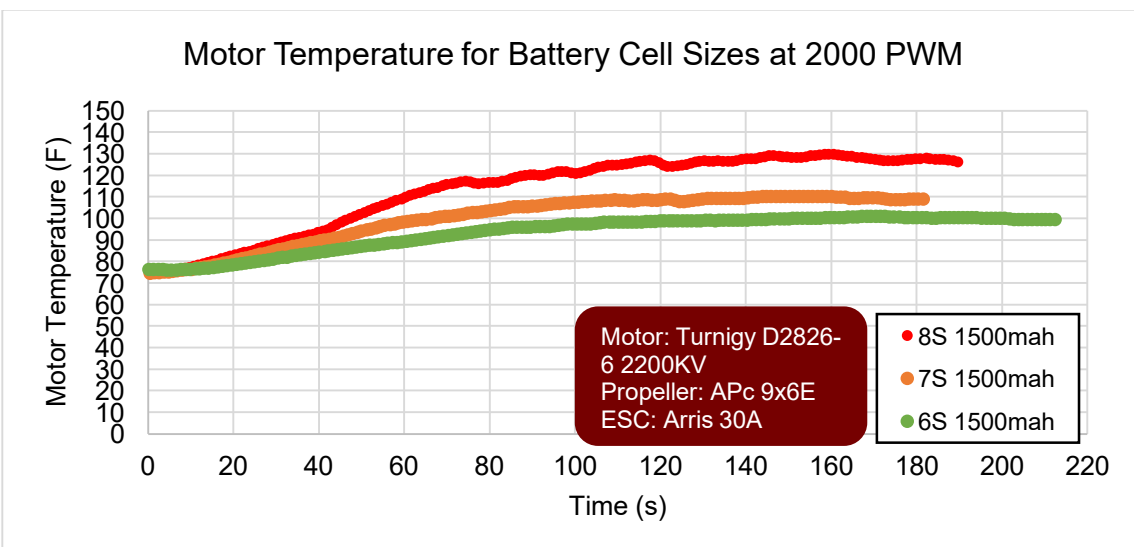

Figure 43. Thermal Evaluation of Propulsion System

Although the chart above shows the motor reaching 130°F on an 8S battery, this does not include the fact that the motor is being cooled while moving in the air. Furthermore, after completing several flight tests with the same configuration, the motor temperature measured immediately after landing was 84°F.

10.1.2 Structures **Performance**

The structural loading of each air vehicle was determined not to be a critical design factor through repeated drop testing. The carbon fiber endplates were demonstrated to be extremely robust in every instance that the airplane, protecting the foam fuselage. The control surfaces on the tail, as well as the firewall on the motor mount were designed to be extremely easy to replace in the event of significant damage due to the airplane crashing. The primary mitigation to protecting the structural integrity lies in the impact absorption from the wire landing gear supports.

10.1.3 System Performance

At the time of this report, all LRU components identified in the ground mission have been independently tested for compliance and integrated into the aircraft. Beginning with the design spiral for AV3, the passenger and payload were integrated into the internal layout of the built airplane for flight tests. In addition to routine checks of each LRU before every flight test, each LRU integrated into the airplane has been evaluated for ease of removal. AV4 will be designed and manufactured for complete compliance with the RFP, as well as repeatable success during the ground mission.

10.2 AV1 Performance

Starting with the first design iteration, AV1, a total of 3 ground tests and 3 flight tests were conducted. Leafing up to the initial testing of AV1, it was expected that the aircraft would have a takeoff ground speed of approximately 50 mph. After conducting these tests, it became apparent that ground control was a very serious concern. The aircraft demonstrated very limited ground stability and was extremely susceptible to tip over at ground speeds in excess of 10 mph. From the 3 flight attempts, it became clear that a wingspan of 4.5” corresponding to a ground speed of approximately 50 mph posed a significant challenge. To gain a better understanding of the flow characteristics after these tests, AV1 was covered in tufts and subjected to a flow visualization test in the Virginia Tech Subsonic Open Jet Wind Tunnel. Flow visualization testing showed that significant flow separation occurred behind the motor mount which was not faired. The tests also showed reversed control surface effectiveness in some attitudes due to vortices shed from the motor mount at high angles of attack.

Learning from these tests, it was determined that span would be increased to reduce takeoff speed and improve lifting performance. The is landing gear were moved forward to reduce the possibility of tip over during ground roll, and a tail would be added to improve stability and provide greater control authority to the pilot.

10.3 AV2 Performance

For the second design iteration, AV2, a total of 5 flight tests were conducted. The first four of these tests were conducted using a Turnigy D2826-6 2200 Kv motor and a 3S Turnigy 1Ah 35 C discharge LiPo battery with an APC 7x4E propeller, demonstrating a takeoff distance of approximately 40 feet with a static thrust of 26.84 ozf. at a weight of approximately 1.1 lbs. During each of these four flights, the aircraft demonstrated significant roll instability after taking off. In an attempt to reduce the severity of the roll instability, a contra rotating motor was tested, but resulted in 10 ozf. of static thrust which was insufficient for the aircraft to takeoff. From these tests, it was decided that a stability augmentation system would be added, accompanied by a forward shift in CG by extending the motor forward to provide a better static margin.

10.4 AV2.5 Performance

AV2.5 was a continuation of the second design iteration in which the motor was extended forward and a stability augmentation system was integrated. It was decided to give this aircraft a different designation to separate test results and show a clear distinction due to the significant CG shift. A total of 6 flight tests were conducted with AV2.5. During the first 4 of these tests, the aircraft was flown with a Turnigy D2826-6 2200 Kv motor and a 3S Turnigy 1Ah 35 C discharge LiPo battery with an APC 7x4E propeller that demonstrated takeoff within approximately 50 feet at a weight of approximately 1.2 lbs. AV2.5 experienced improved ground control due to the forward CG shift compared to AV2, but still experienced tip over during high speed taxi, especially in the presence of crosswinds.

The most notable change during these flights was the integration of a stability augmentation system which allowed the adjustment of PID gains, as well as the limitation of control surface deflections. The stability augmentation system was programmed to allow for 3 modes: manual pass through, rate control, and attitude hold. Manual pass through gives the pilot full control over the aircraft with no stability augmentation. Rate control provides stabilized damping where the roll, pitch, and yaw rates are proportional to stick position. In attitude hold, bank and pitch angles are proportional to stick positions where a bank limit of 60 degrees was set. While in attitude hold mode, the stability augmentation system will provide a restorative response proportional to the aircrafts current attitude. In turn, if the pilot were to command a bank angle in excess of the limit, the augmentation system would provide the response necessary to not exceed the set angle. The most significant factor of the stability augmentation system is that in attitude hold mode, the system will autonomously provide restorative control for the aircraft to maintain level flight while still allowing pilot input. This alleviated many stability problems encountered in previous flight attempts, especially in roll.

A further flight was conducted using the same propulsion system resulting in approximately a 75 ft. takeoff distance to assess stability augmentation response after adjusting the PID gains. During this flight, the stability augmentation system was also turned off to allow manual flight until an unstable, involuntary

roll was seen. The stability augmentation system was then engaged in attitude hold mode and the aircraft recovered nearly instantaneously with limited pilot input or altitude loss.

One final flight was conducted with AV2.5 in winds on the order of 15-20mph to determine the effectiveness of the stability augmentation system in high winds. The weight for this flight was increased to 1.4 lbs. due to the addition of a Pixhawk to obtain in-flight data. The aircraft demonstrated approximately a 60 ft. takeoff distance with a direct headwind of 15 mph using the same propulsion system. Despite flying with high winds, the aircraft was stable in all phases of flight with the stability augmentation system engaged.

Following these flight tests, a series of tests were conducted in the Virginia Tech subsonic open jet wind tunnel to assess the tip over problems that all design iterations encountered. During this test, a sweep was conducted from a direct headwind (0 degrees) to a quartering tailwind (180 degrees) over a range of 0-20 mph airspeed where each control surface was commanded through a full spectrum of deflection independently before combining controls. The rudder was then removed, and this test was repeated. Entertaining the idea of a tail dragger configuration, a modification was tested in the same fashion, but experienced the same prevalence of tip over manifesting in different ways. As a result of the testing, it was determined that the landing gear needed to be moved outward from the fuselage, as well as farther forward from the AV2.5 position.

10.5 AV3 Performance

Combining all the lessons learned from previous design spirals, AV3 testing converged to minimal configuration changes other than motor, propeller, and battery combinations as needed to achieve successful takeoff within the 150 ft requirement using NiMH batteries, as well as the endurance to safely complete 3 full laps. The first two flights with AV3 were flown with the same propulsion system used for AV2.5 with a weight of approximately 1.45 lbs. resulting in approximately a 60 ft. takeoff distance, however the motor did not provide enough thrust to sufficiently maintain cruise performance. The next two flights tested different motor and propeller combinations intended to reduce the overall weight of the aircraft. These tests had takeoff distances of approximately 60 feet with the same battery. Converging on a motor and propeller combination, AV3 was flown a final time with a Turnigy D2826-6 2200 Kv motor, APC 9x46E propeller, and a 3S Turnigy 1Ah 35 C discharge LiPo battery as a check flight before switching to an 8s Elite 1500 mAh NiMH battery pack. This was flown at a weight of approximately 1.33 lbs with an approximate takeoff distance of 75 ft.

On the first flight with NiMH batteries, the aircraft achieved an approximately 80 ft. takeoff and demonstrated a shallow climb before experiencing an esc failure. Replacing the esc, AV3 was then flown an additional 2 times using 8S Elite 1500 mAh NiMH batteries and a Turnigy D2826-6 2200 Kv motor with an APC 9x46E propeller. The first of these flights demonstrated approximately a 105 ft. takeoff distance, satisfactory climb, and 3 minutes of endurance before landing safely at a weight of approximately 1.3 lbs. The last test conducted on AV3 simulated a worst-case weight scenario with the a Turnigy D2826-6 2200

Kv motor, 8s Elite 1500 mAh NiMH batteries, and heavier receiver batteries than previously flown. The gross weight of the aircraft for the last flight was 1.4 pounds and demonstrated approximately a 160 ft. takeoff due to a late rotation by the pilot. The flight was conducted as a simulation of mission 1 and mission 2 profiles where 3 complete laps were completed in 3 minutes and 6 seconds from initial throttle to successful landing. Worst case weight scenario means that the airplane was flown at a gross weight loaded with the heaviest passenger, as well as a 1 oz payload. This weight would only be required for mission 3 where a minimum of 1 lap must be completed, however the aircraft demonstrated successful capability to fly 3 laps at this weight. A summary of the predicted vs. flown performance for AV3 is presented in Table 24 below.

Table 24. Demonstrated vs. Predicted Mission Performance for AV3

AV3	Mission 1		Mission 2		Mission 3	
Parameters	Predicted	As Flown	Predicted	As Flown	Predicted	As Flown
TOGW (lbs.)	1.24	-	1.33	1.34	1.39	1.39
W/S (lb./in.^{2})	0.0103	-	0.0111	0.0112	0.0116	0.0116
V_{stall} (mph)	38	-	40	31	41	36
V_{cruise} (mph)	45	-	45	44	45	44
Takeoff Distance (ft.)	81	-	105	105	129	160
Time for 360° Turn (s)	12	-	12	15	12	15
Mission Time (min)	2.6	-	2.7	3.1	0.93	1.03

For AV4, weight reductions have been identified to further improve mission performance. AV4 flight tests will focus on repeatability of mission performance while maintaining competition compliance.

11 Bibliography

[1] University of California Irvine, 2012-2013 DBF Report

[2] “Chance Vought V-173 Flying Pancake building log, ” RC Groups Forum, May 2009. https://www.rcgroups.com/forums/showthread.php?1043305-Chance-Vought-V-173-Flying-Pancake-building-log/page5

[3] “There Will Be Buzz,” Georgia Tech 2010-2011 DBF Report

[4] Zimmerman, C. H., "Characteristics of Clark Y Airfoils of Small Aspect Ratios," NACA TR-431, Jan. 1933.

[5] “Motocalc Cell Table,” *Motocalc Cell Table*. Capable Computing, Inc.

http://www.motocalc.com/data/cell.html

[6] A. Borgoltz, “0.7m Subsonic Open Jet Wind Tunnel,” Kevin T. Crofton Department of Aerospace and Ocean Engineering | Virginia Tech.

http://www.aoe.vt.edu/research/facilities/openjet.html.

[7] J. Roskam, *Airplane Design IV Layout of Landing Gear and Systems*. Lawrence, KS: DARcorporation, 1986.

[8] L. M. Nicolai and G. E. Carichner, *Fundamentals of Aircraft and Airship Design, vol. 1*. Reston, VA: American Institute of Aeronautics and Astronautics, 2010.

[9] D. P. Raymer, *Aircraft Design: A Conceptual Approach, 5th ed*. Reston, VA: American Institute of Aeronautics and Astronautics, 2012.

[10] J. Gundlach, *Designing Unmanned Aircraft Systems A Comprehensive Approach*, 2nd ed. Reston, VA: American Institute of Aeronautics and Astronautics, 2014.

[11] G. Ananda, UIUC PDB - Vol 1, 03-Feb-2015. [Online]. Available: http://m-selig.ae.illinois.edu/props/volume-1/propDB-volume-1.html.

[12] Brandt, J. B., *"Small-Scale Propeller Performance at Low Speeds,"* M.S. Thesis, Department of Aerospace Engineering, University of Illinois at Urbana-Champaign, Illinois, 2005.

TRILOBUZZ

AIAA DESIGN/BUILD/FLY
2017-2018
DESIGN REPORT

Georgia Institute of Technology®

TABLE OF CONTENTS

Table of Figures 5
List of Tables 6
Acronyms and Nomenclature 7
1 Executive Summary 8
1.1 Design Process 8
1.2 Key Mission Requirements and Design Features 8
1.3 System Performance Capabilities 9
2 Management 10
2.1 Team Organization 10
2.2 Milestones 10
3 Conceptual Design 11
3.1 Mission Requirements 11
3.1.1 Mission and Score Summary 11
3.1.2 Estimated Maximum Mission 2 and Mission 3 Scores 14
3.1.3 Aircraft Constraints 15
3.1.4 Flight Score Sensitivity Analysis 16
3.2 Translation into Design Requirements 19
3.3 Configurations Considered 20
3.4 Component Weighting and Selecting Process 21
3.5 Final Conceptual Design Configuration 22
4 Preliminary Design 23
4.1 Design Methodology 23
4.2 Design Trades 23
4.2.1 Constraint Sizing 23
4.2.2 Propulsion System Selection 24
4.3 Mission Model 25
4.3.1 Description and Capabilities 25
4.3.2 Uncertainties 26
4.4 Aerodynamic Characteristics 26
4.4.1 Analysis Methods 27
4.4.2 Lifting Surface Analysis 29
4.4.3 Drag Analysis 29

4.5 Stability and Control 31
4.5.1 Static Stability Analysis 31
4.5.2 Dynamic Stability Analysis 33
4.6 Mission Performance 33
5 Detail Design 34
5.1 Final Design – Aircraft 34
5.2 Structural Characteristics 35
5.2.1 Layout and Design 35
5.2.2 Operating Envelope 35
5.3 System and Subsystem Design and Implementation 36
5.3.1 Wing Body and Payload Bays 36
5.3.2 Vertical Stabilizer 37
5.3.3 Elevons 37
5.3.4 Receiver and Transmitter Selection 38
5.3.5 Propulsion System 38
5.3.6 Servo Selection 39
5.3.7 Landing Gear 40
5.3.8 Passenger Seat and Payload Blocks 40
5.4 Weight and Balances 41
5.5 Performance 42
5.5.1 Flight Performance 42
5.5.2 Mission Performance 43
5.6 Drawing Package 44
6 Manufacturing 49
6.1 Processes Investigated 49
6.2 Processes Selected 50
6.2.1 Airframe Structure 51
6.2.2 Control Surfaces and Vertical Tail 51
6.2.3 Rapid Prototyping 51
6.3 Manufacturing Milestones 52
7 Testing Plan 53
7.1 Objectives and Schedule 53
7.2 Structural Testing 54

7.3 Flight Testing 54
7.4 Checklists 55
7.4.1 Propulsion Test Checklist 55
7.4.2 Flight Test Checklist 55
8 Performance Results 56
8.1 Component and Subsystem Performance 56
8.1.1 Propulsion 56
8.1.2 Structural Tests 57
8.2 System Performance 58
9 Bibliography 60

TABLE OF FIGURES

Figure 1.1: Aircraft in flight 9
Figure 2.1: Team organization chart 10
Figure 2.2: Aircraft design milestone chart showing planned and actual progress 11
Figure 3.1: Competition flight course 12
Figure 3.2: Wind speed versus maximum speed required 17
Figure 3.3: Physics-based scoring analysis of the design space 18
Figure 3.4: Scoring sensitivity analysis 18
Figure 3.5: Considered configurations: monoplane (left), full delta (center), clipped delta (right) 20
Figure 3.6: Final clipped delta configuration 22
Figure 4.1: The team's preliminary design methodology highlighting the multidisciplinary iterations 23
Figure 4.2: Constraint sizing design point selection 24
Figure 4.3: Vortex lift conceptualization by Anderson [1] 27
Figure 4.4: Maximum lift coefficient of various planforms [2] 27
Figure 4.5: Lift estimation for clipped delta planform; wind tunnel data from Lamar [7] 28
Figure 4.6: Pitching moment estimation for clipped delta planform; wind tunnel data from Lamar [7] 28
Figure 4.7: Final design VORSTAB lift curve 29
Figure 4.8: Breakdown of various sources of drag 30
Figure 4.9: Drag coefficient prediction using vortex lift calculation 31
Figure 4.10: Moment coefficient derivative versus angle of attack at the CG 32
Figure 4.11: Simulation of lap trajectories for M1 (left) and M2/M3 (right) 34
Figure 5.1: Load paths of major forces 35
Figure 5.2: V-n diagram showing loading as a function of velocity for all flight missions 36
Figure 5.3: Trilobuzz body CAD 37
Figure 5.4: Elevon attachment mechanism 37
Figure 5.5: Motor mount 39
Figure 5.6: Removable servo prototype 39
Figure 5.7: Landing gear 40
Figure 5.8: Prototype passenger seat with and without a passenger 41
Figure 5.9: CAD Predicted CG Location 41
Figure 5.10: Thrust available and thrust required versus velocity 43
Figure 5.11: Simulation of lap trajectories for M1 (left) and M2/M3 (right) 44
Figure 6.1: Airframe during construction 51
Figure 6.2: Multiple prototype aircraft before a flight test 52
Figure 6.3: Aircraft manufacturing milestone chart showing planned and actual timing of objectives 52
Figure 7.1: Aircraft and subsystem testing milestone chart with planned and actual timing of objectives 53
Figure 7.2: Thrust test rig 54

Figure 8.1: Battery discharge rates 57
Figure 8.2: Predicted thrust versus actual thrust for different propellers 57
Figure 8.3: Wingtip test 58
Figure 8.4: Trajectory of aircraft during competition laps from GPS data 59

LIST OF TABLES

Table 3.1: Ground Mission stage 1 die roll outcomes 13
Table 3.2: Ground Mission stage 2 die roll outcomes 13
Table 3.3: Estimated highest M2 and M3 performance 14
Table 3.4: Passenger specifications and distribution 15
Table 3.5: Rules and requirements translated into design requirements 20
Table 3.6: Figures of Merit 21
Table 3.7: Configuration scoring values 21
Table 3.8: Aircraft configurations' Figures of Merit 22
Table 4.1: Preliminary power and wing area 24
Table 4.2: Motor specifications 25
Table 4.3: Breakdown of various sources of drag 30
Table 4.4: Relevant stability coefficients and derivatives for static stability 32
Table 4.5: Dynamic stability characteristics 33
Table 5.1: Final aircraft dimensions 34
Table 5.2: Selected propulsion and electronics components 38
Table 5.3: Weights and balances 42
Table 5.4: System flight performance parameters for each mission 42
Table 5.5: Aircraft mission performance parameters 44
Table 6.1: Manufacturing FOM Weighting 49
Table 6.2: Example airframe manufacturing process selection 50
Table 7.1: Propulsion testing checklist 55
Table 7.2: Pre-flight checklist 56
Table 8.1: LRU replacement times 58
Table 8.2: Comparison of predicted and actual performance averages 59

ACRONYMS AND NOMENCLATURE

	Number of Laps flown	Θ_{wind}	Wind Direction
	Number of Passengers Carried	n	Load Factor
	Wetted Area of the Wing	R_T	Taper Ratio
0	Gravitational Acceleration	AR	Aspect Ratio
	Takeoff Safety Factor	R_e	Reynolds Number
	Takeoff Distance	$\dot{}$	Velocity Derivative with respect to time
/	Thickness to Chord Ratio	T	Thrust
AVL	Athena Vortex-Lattice	m	Mass
C.G.	Center of Gravity		Flight Time
C_D	Aircraft Drag Coefficient	MTOW	Maximum Takeoff Weight
$C_{D,0}$	Aircraft Zero-Lift Drag Coefficient		Density
C_{fw}	Turbulent Plate Friction Coefficient of the Wing		Wing Fuselage Interference Factor
C_L	Aircraft Lift Coefficient	$\dot{}$	Time Derivative of Heading
C_l	Aircraft Rolling Moment Coefficient	K_1	Drag Constant
C_m	Aircraft Pitching Moment Coefficient		Lifting Surface Correction
C_n	Aircraft Yawing Moment Coefficient	β	Sideslip Angle (degrees)
C_Y	Aircraft Side Force Coefficient	α	Angle of Attack (degrees)
ESC	Electronic Speed Control	W	Weight (lbs)
EW	Empty Weight	e	Oswald Efficiency
FOM	Figures of Merit	S	Reference Area (ft^2)
L'	Airfoil Thickness Location Factor	V	Velocity(ft/s)
LRU	Line Replacement Units	MTOW	Maximum Takeoff Weight
M1	Mission One	P	Power
M2	Mission Two		Takeoff Speed
M3	Mission Three	K_A/K_B	Weight Regression Coefficient
NiCad	Nickel-Cadmium	$\dot{}$	Position Derivative with respect to time
NiMH	Nickel-Metal Hydride	D	Drag
RAC	Rated Aircraft Cost		Propeller Efficiency
TMS	Total Mission Score		Thrust Required

1 EXECUTIVE SUMMARY

This report details the design, testing, and manufacturing of Georgia Institute of Technology's Trilobuzz entry in the 2017-2018 AIAA Design/Build/Fly (DBF) competition. The objective of the 2017-2018 American Institute of Aeronautics and Astronautics (AIAA) Design/Build/Fly (DBF) contest is to simulate the design of a dual purpose regional and business aircraft and is designed to include:

- Passenger compartment: to carry super balls with sizes ranging from 27mm to 49mm
- Longitudinal Aisle: minimum width and height of 2 inches running the length of the passenger compartment
- Payload bay: that carries a payload block with L(in)+ W(in)+ H(in) greater than or equal to 9 inches
- Line Replacement Units (LRUs): certain components must be modular for quick maintenance

The aircraft is designed to complete the following 4 tasks:

1. The Ground Mission: removal and replacement of two Line Replaceable Units (LRUs) chosen at random
2. Empty Flight of the *Trilobuzz*
3. Flight of the *Trilobuzz* with passengers carried in the passenger compartment
4. Flight of the *Trilobuzz* with passengers carried in the passenger compartment and payload block carried in the payload bay

1.1 Design Process

Georgia Institute of Technology approaches every competition with the desire to maximize score and achieve victory. Conceptual designs that translate key mission requirements and scoring equations into design concepts were developed to achieve this goal. The team then chose a configuration from a range of possible concepts that maximized score. In the preliminary design phase, the design was further refined by evaluating different wing and control surface configurations, lightening methods, motors, and propellers. Throughout the process, weight estimates, drag estimates and aerodynamic coefficients were calculated and introduced into a flight simulation environment that simulates mission performance. A detailed design with dimensions was then created, prototyped, and subsequently flight tested to validate the assumptions made during the design phase. Through the analysis of flight scoring and aircraft contribution to RAC, it was determined that minimizing empty weight and wingspan was critical for this year's design.

1.2 Key Mission Requirements and Design Features

Balancing key mission requirements was the basis for a successful system design. Design metrics were developed for each mission requirement and scoring factor to maximize system performance and overall competition score.

Empty Weight: The aircraft's empty weight is a significant driver of total score as a function of Rated Aircraft Cost (RAC). Use of the lightest materials possible was combined with a highly efficient truss structure to design an aircraft that was as light as possible without compromising the ability to complete all three flight missions.

Wing Span: The wingspan is another component of RAC that was considered vital for maximizing score. Therefore, a delta wing configuration was identified as the highest scoring configuration.

Replaceable Components: For the completion of the ground mission, the aircraft had to contain Line Replacement Units (LRUs). To this end, components not deemed necessary were not included in the aircraft design. This design choice also helped in lowering the empty weight. It was determined that elevons were the only control surfaces required for completion of all missions.

1.3 System Performance Capabilities

All features designed to maximize the performance of the system can be summarized by the following performance capabilities:

- Empty Weight of 1.19 lbs and MTOW of 1.34 lbs
- Reliable takeoff and landing
- Top speed of 90.72 ft/s
- Secure storage of a single passenger
- Proven capability through 5 iterations and 20 test flights, as shown in Figure 1.1.
- Estimated RAC of 14.01 and final score of 0.219.

Figure 1.1: Aircraft in flight

The final design is a clipped delta wing aircraft with one motor and one set of control surfaces. The aircraft is designed to minimize weight and wingspan while still satisfying the requirements of carrying a passenger, having an aisle, and carrying a payload block in a separate payload bay. The team chose an unconventional and ambitious design to maximize the total score.

2 MANAGEMENT

2.1 Team Organization

A hierarchical structure was used in the completion of the *Trilobuzz,* with leadership established amongst senior members and flowing down to the newer members of the team as shown in Figure 2.1. The work was divided into Manufacturing, Computer Aided Design (CAD) and Structure, Aerodynamics, Electrical and Propulsion, and Payload. During the design, construction, and testing phase, each member contributed extensively to the rapid prototyping process to construct the planes, meet deadlines, share new ideas, and write the report.

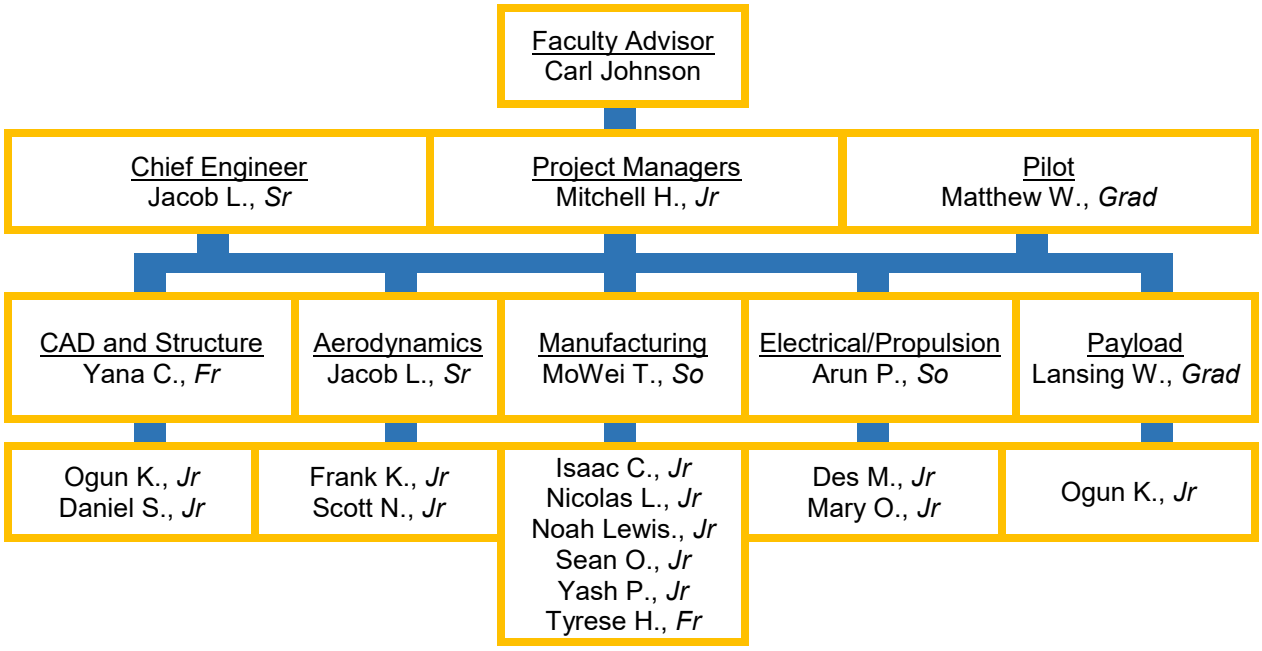

Figure 2.1: Team organization chart

2.2 Milestones

A milestone chart was established at the beginning of the design process to capture major deadlines of design and manufacturing goals. Progress was monitored by the project manager to ensure all major milestones were met. The team worked throughout the entire academic year and established stringent deadlines early to ensure testing and flight experience before the competition in April. The team met frequently with the faculty advisor to discuss progress. The milestone chart is shown in Figure 2.2, capturing planned and actual timing of major events.

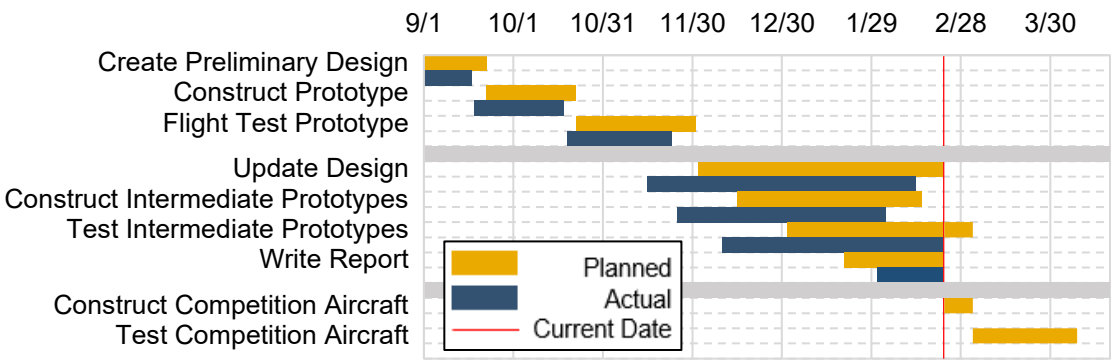

Figure 2.2: Aircraft design milestone chart showing planned and actual progress

3 CONCEPTUAL DESIGN

In this early phase of design, the team analyzed the competition rules to produce a feasible design that maximized score. The rules were distilled into design requirements and scoring factors. Quantitative analysis was performed to pinpoint key scoring drivers and constrain the design space. These scoring factors were then translated into Figures of Merit (FOM) and used to evaluate aircraft configurations and design decisions. This process in its entirety is presented in the following sections.

3.1 Mission Requirements

3.1.1 Mission and Score Summary

The AIAA Design/Build/Fly 2017/2018 competition consists of three flight missions, a ground mission, and a design report. The total score for each team is calculated using Equation 3.1.

$$= \quad * \quad / \tag{3.1}$$

Equation 3.2 breaks down the Total Mission Score (TMS). The TMS is the sum of the three mission flight scores. Equation 3.3 breaks down the Rated Aircraft Cost (RAC). The RAC consists of the maximum empty weight of the aircraft recorded at competition (EW_{max}) in pounds, and longest distance between wingtips in inches, measured perpendicular to the fuselage axis (WS).

$$= \quad 1 + \quad 2 + \quad 3 \tag{3.2}$$

$$= \quad * \tag{3.3}$$

It was determined during sensitivity analysis that the scoring equation is more sensitive to changes in RAC than TMS. TMS can range from approximately three to nine (assuming all missions are completed), whereas RAC can vary greatly depending on aircraft configuration. Equation 3.3 shows that minimizing aircraft weight and wingspan minimizes RAC. Increasing aircraft performance for faster mission times necessarily requires an increase in weight and size, which results in a greater RAC.

All flight missions are flown along the same distance and pattern per lap. For flight missions, the individual portions of the flight pattern seen in Figure 3.1 are as follows:

1. Successful takeoff of aircraft
2. Climb to safe altitude
3. 180º U-turn, 500 ft. upwind from the start/finish line
4. 1000 ft. downwind
5. 360º turn along the backstretch
6. 180º U-turn
7. 500 ft. final approach with a successful landing

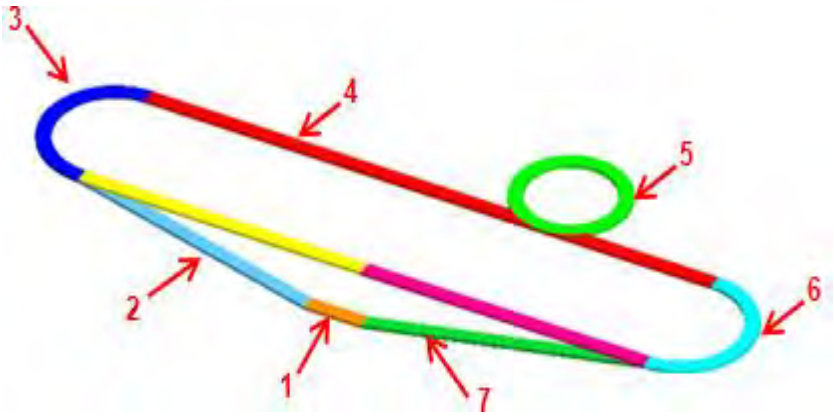

Figure 3.1: Competition flight course

Each lap is roughly 2500 ft when accounting for the three turns involved. A complete lap is defined as crossing the start/finish line, completing the defined pattern, then crossing the start/finish line while still in the air. The required number of laps is defined by each mission. The ground mission must be completed before the second flight mission.

Mission 1 Demonstration Flight: For this mission, the aircraft must takeoff within the prescribed field length. The team must complete three laps within a five-minute time window, and then complete a successful landing to receive a score. Time starts when the throttle is advanced for the first takeoff attempt and ends when the aircraft completes three laps. Landing is not part of the five-minute window. The scoring for Mission 1 (M1) is binary; a successful mission is scored 1.0 and a failed mission is scored 0.0.

Ground Mission: The ground mission is comprised of two stages and must be successfully completed before attempting Mission 2. Three team members may participate in this mission: two crew members and the pilot. One line-replaceable unit (LRU) must be replaced during each stage within eight minutes total. The Stage 1 LRU is selected at random by the roll of a die and must be replaced within the first three minutes of the eight-minute period. Once successfully replaced, the team may immediately begin replacing the second LRU, also selected randomly by the roll of a die. Stage 2 must be completed within the remainder of the eight-minute period. The results of the first and second die roll are listed in Table 3.1 and Table 3.2, respectively.

A functional demonstration of the replaced LRU must be performed to complete a stage and continue. The aircraft must be flight ready at the start and finish of the ground mission. The ground mission is considered successful if all the above conditions are met. Failure to meet any of the above criteria will result in a failure for the ground mission. There is no score for completion of the ground mission.

Table 3.1: Ground Mission stage 1 die roll outcomes

Roll	LRU
1	Servo
2	Receiver battery
3	Main propulsion battery
4	Control pushrod or pull-pull cable
5	Landing gear wheel
6	Propeller

Table 3.2: Ground Mission stage 2 die roll outcomes

Roll	LRU
1	Electronic speed control (ESC)
2	Control surface (chosen at random with additional roll) 1: left aileron/elevon 2: right aileron/elevon 3: (left) elevator 4: (right) elevator 5: rudder, upper rudder, left rudder, or left ruddervator 6: rudder, lower rudder, right rudder, or right ruddervator
3	Receiver
4	Main landing gear (if required chosen at random with additional roll) Odd: left Even: right
5	Motor
6	Roll again

<u>Mission 2 Short Haul of Max Passengers</u>: The payload for Mission 2 (M2) is passengers (super balls). The aircraft is to be loaded with a team-chosen number of passengers that does not exceed the maximum number of passengers declared at technical inspection. All passengers must be carried internally. The team must complete three laps within a five-minute time window, and then complete a successful

landing to receive a score. Time starts when the aircraft throttle is advanced for the first takeoff attempt and ends when the aircraft completes three laps. Landing is not part of the five-minute window. Points are awarded based on Equation 3.4.

$$2 = 2 * \frac{(\quad / \quad)}{(\quad / \quad)} \tag{3.4}$$

“ ” refers to the number of passengers carried, “Time” refers to the flight time, subscript “Buzz” refers to the parenthetical value for *Trilobuzz*, and subscript “Max” refers to the maximum value of the parenthetical quantity across all teams for M2.

<u>Mission 3 Long Haul of Passengers and Payload</u>: The payload for Mission 3 (M3) is passengers (super balls) and payload blocks. The number of passengers must be at least 50% of the number of passengers carried during M2. At least one payload block must be carried but may not exceed maximum number of payload blocks declared at technical inspection. Both passengers and payload must be carried internally. The team must complete the mission within a ten-minute time window, and then complete a successful landing to receive a score. Time starts when the aircraft throttle is advanced for the first takeoff attempt and ends when the aircraft crosses the start/finish line on the final lap. Landing is not part of the ten-minute window. The mission score for M3 is a function of the number of passengers, the total weight of payload blocks, and the number of laps completed. The awarded score is described by Equation 3.5.

$$3 = 4 * \frac{(\quad * \quad * \quad)}{(\quad * \quad * \quad)} + 2 \tag{3.5}$$

“ ” refers to the number of passengers carried, “ ” refers to the total weight of the payload blocks in ounces, “ ” refers to the number of laps completed, subscript “Buzz” refers to the parenthetical value for *Trilobuzz*, and subscript “Max” refers to the maximum value of the parenthetical quantity across all teams for M3.

3.1.2 Estimated Maximum Mission 2 and Mission 3 Scores

Mission 2 and Mission 3 scores are both dependent on the score of the highest performing team at the competition. Thus the sensitivity of the score to design variables is dependent on the estimate for the highest performing team. Table 3.3 contains the estimated performance values that were used to calculate preliminary mission scores for *Trilobuzz*. The maximum number of passengers and M3 laps were estimated based on trends from past competitions. Maximum payload was estimated based on the assumption that the highest scoring team would contain an equal weight of passengers and payload. The lap time was estimated from the team’s experience with the class of high capacity aircraft that are expected to lead the scoring in missions 2 and 3.

Table 3.3: Estimated highest M2 and M3 performance

M2 Max Passengers	M2 Min Time (s)	Max Payload (oz)	M3 Max Laps
35	90	39.2	20

3.1.3 Aircraft Constraints

The competition rules stipulate design constraints that all competing aircraft must adhere to, including requirements for ground rolling takeoff, propulsion system, passengers, payload, and serviceability:

Ground Rolling Takeoff: All aircraft must independently takeoff and land on a runway, with a takeoff field length of 150 feet. This is a requirement for all three missions.

Propulsion System: The aircraft must be propeller driven and electrically powered, with all components of the propulsion system commercially available. These include the motor, propeller, speed controllers, receiver, and batteries. The battery selection is limited to NiCad or NiMH, but may be of any cell count, voltage, or capacity. There is no limit to the weight of the battery packs. The entire propulsion system must be armed by an external safety plug or fuse. The arming device must be mounted on the exterior of the aircraft and be accessible from behind.

Passengers: Passengers, represented by various sized super balls, are payload for M2 and M3. Passengers must be secured sufficiently to assure safe flight without possible variation of center of gravity (CG) outside of the aircraft design limits. Passengers will be provided in technical inspection and on the flight line and will be randomly selected from a pool of passengers according to the distribution described in Table 3.4.

Table 3.4: Passenger specifications and distribution

Diameter (mm)	Weight (oz)	Distribution (%)
27	0.40	15
32	0.67	20
38	1.12	30
45	1.85	20
49	2.39	15

Each passenger must have its own seat with an individual restraint system that accommodates all passenger sizes. Additionally, all passenger seats must be on one level, planar surface, with a minimum spacing of 0.25 inches between the largest passenger size. There may not be more than four seats in any given row. There must be a longitudinal aisle with height and width no less than 2.00 inches running the length of the passenger compartment. The aisle may be on either side of the seats if only one or two adjacent seats are in a row.

Payload: The payload will be made up of cuboid blocks with length, width, and height dimensions summing to greater than or equal to nine inches, with no dimension measuring less than two inches. Teams are to supply their own payload blocks. All payload blocks for each team must be the same size, with no more than 0.25-inch variation per side. The weight of each payload block may be determined by the team and each block may have a different weight. Payload bay(s) must be a separate, enclosed compartment behind and/or below the passenger compartment.

Serviceability: All aircraft must be designed to be serviceable by allowing for the removal and replacement of several aircraft components. The components that must be replaceable are outlined in the Ground Mission description in Section 3.1.1.

3.1.4 Flight Score Sensitivity Analysis

A sensitivity analysis on the flight scoring drivers was performed to understand the design trades and mission objectives that maximize TMS as divided by the RAC. Mission scores are functions of payload capacity, flight speed, and endurance of the aircraft. The RAC is a function of the aircraft empty weight and the maximum wingspan. This analysis was conducted to examine the design space and determine the general scoring trends.

Empty Weight: Aircraft empty weight was divided into propulsion and structural components. The propulsion system weight is proportional to the number of battery cells used. Based on previous team experience, 1500 mAh NiMH cells were selected as representative batteries, weighing 0.05 lbs each. Based on testing of battery discharge rate, the average current draw is 15 amps. The electric motor weight was estimated at 0.5 lbs / kW from past experience, and speed controllers that met the pack voltage were cataloged. The propulsion weight assessment is summarized by Equations 3.6 and 3.7.

$$= \quad (1.2 \text{—} \times 15 \quad) \tag{3.6}$$

$$= \quad (0.05 \text{—}) + \quad (0.5 \text{—}) + \tag{3.7}$$

Structural weight was estimated using the team's experience, with a baseline minimum weight which increases with wing area. The coefficients K_A and K_B in Equation 3.8 were adjusted to match past years' Design/Build/Fly planes, and Equation 3.9 summarizes the empty weight assessment.

$$= \quad + \quad (\quad - \quad) \tag{3.8}$$

$$= \quad + \tag{3.9}$$

Maximum Speed: The maximum speed directly effects the scoring of M2 and must be high enough for the aircraft to complete three 2,500 ft lap lengths within five minutes with the assumed wind conditions. The maximum speed was calculated using simple power-required calculations that stem from the drag polar and the power available from the propulsion system, as seen in Equation 3.10.

$$- \quad = (\frac{1}{2} \quad {}^{3} \quad {}_{,0} + \frac{2}{\quad}) - \quad = 0 \tag{3.10}$$

Analysis was conducted of Wichita, Kansas weather trends for the month of April to determine what airspeeds should be expected during competition. Based on the analysis and team experience, 15 mph winds are expected, with an extreme weather condition of winds upwards of 45 mph, so a flight speed requirement of 61 mph was set.

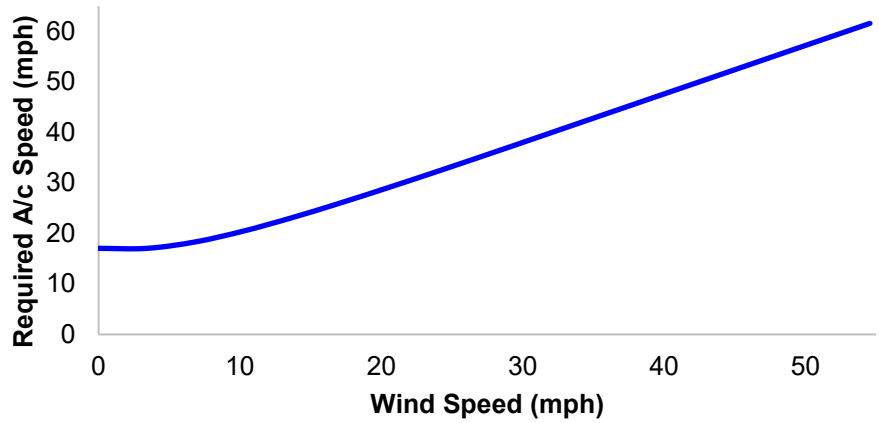

Figure 3.2: Wind speed versus maximum speed required

Takeoff: The power-to-weight ratio necessary for takeoff in the prescribed takeoff distance of 150 ft must be considered when selecting a propulsion system. Equation 3.11 describes power-to-weight for a rolling takeoff, and includes such terms as the takeoff distance, , gravitational acceleration, $_0$, and wing loading, / . The takeoff safety factor, , was set to 1 due to the clipped delta configuration that was selected. Clipped delta aircraft run into flight performance issues such as reduction of aerodynamic efficiency before they achieve stall angle of attack, so can be set to 1, representing confidence in takeoff safety. More detail as to why a clipped delta configuration was chosen is provided later in Section 3.4.

$$- = \frac{2}{0}(-) \tag{3.11}$$

Approach: Wing loading is the only concern when considering landing approach. A maximum value at this condition constrains the sizing of the aircraft. Using this value, wing loading can be calculated using Eq. 3.12.

$$- = \frac{1}{2} \quad 2 \tag{3.12}$$

The relationships discussed above can be used to determine the RAC as a fallout of the aircraft speed and payload capacity for a conventional configuration. To isolate the effect of speed and payload, these parameters are analyzed independently. The scoring sensitivity in Figure 3.3 shows the estimated flight score for a combination of wing area and battery cell counts. The plot represents a physics-based tradeoff between speed and aircraft weight, as governed battery count and wing area. The white area represents configurations that cannot meet the speed requirements. The M3 score is assumed to be fixed.

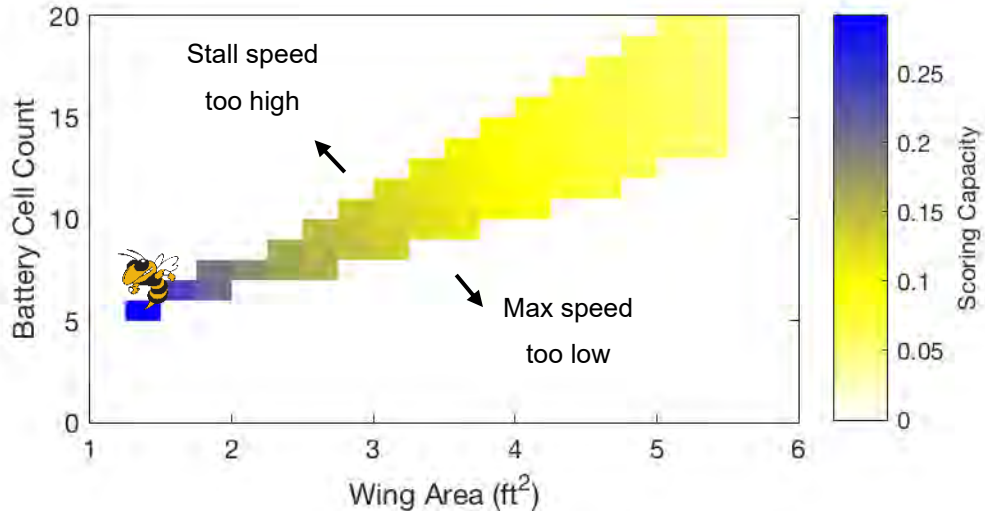

Figure 3.3: Physics-based scoring analysis of the design space

The maximum score occurs when wing area and the battery cell count is minimized. The chosen design point is marked with Buzz at a battery cell count of six and wing area of 1.35 ft^2. The chosen design point should result in a maximized competition score. The scoring sensitivity to changes in payload weight, aspect ratio, empty weight, and lap time was analyzed to determine the importance of each factor. The percent change in score as a response to the percent change of these variables is plotted in Figure 3.4. It is clear that empty weight and aspect ratio should be minimized at all costs, and that lap time and payload weight are insignificant in comparison. This analysis assumes that wing loading is constant, and that wing area is independent of aspect ratio. Based on this analysis, it was determined that a single passenger should be carried for M2 and M3, and a single payload block with minimal weight should be carried for M3 so that aircraft size factor could be minimized, and score maximized.

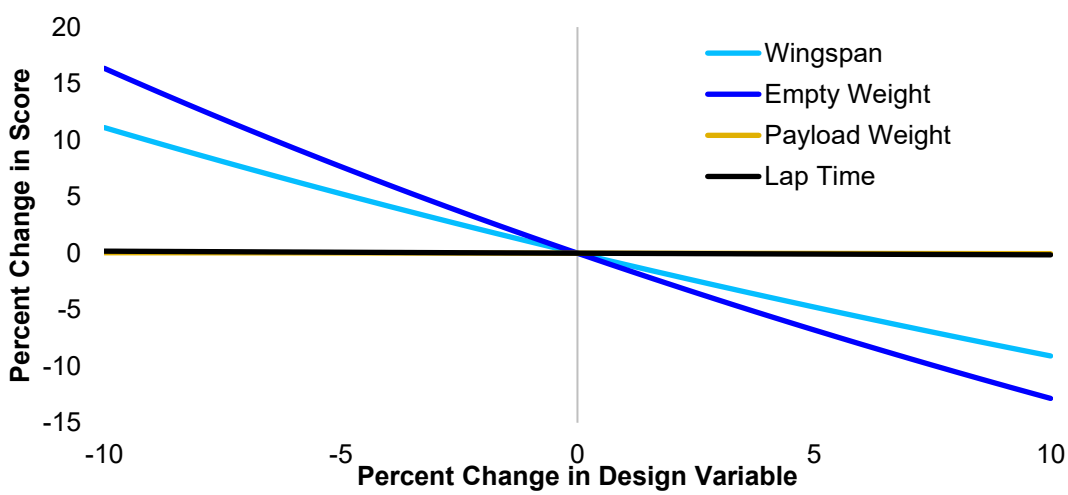

Figure 3.4: Scoring sensitivity analysis

3.2 Translation into Design Requirements

The scoring analysis revealed that the overall flight score is driven principally by the RAC. Several aspects were of particular importance:

Empty Weight: Any configuration that fails to be as light as possible will not be competitive. Effort must be made to reduce the aircraft empty weight. However, the structure must be able to withstand the expected loads. Such considerations must be carefully balanced to secure the passengers/payload and decrease empty weight.

Wing Span: Besides empty weight, wing span is the other component of RAC. The lowest wing span for the chosen design must be determined to reduce RAC and keep the aircraft competitive. Decreasing wing span has adverse effects on aircraft stability and aerodynamic efficiency, thus reducing possible M2 and M3 scores, but as scoring sensitivity has shown, RAC has a much stronger impact on score than the individual mission scores.

Speed: As per Missions 2 and 3, the aircraft top speed has a significant impact on the mission score. Mission 2 score is dependent on the time the aircraft takes to finish three laps. The faster the aircraft finishes three laps, the higher the Mission 2 score will be. However, increasing top speed increases propulsion system weight and must be balanced against the empty weight requirement.

Passengers: As per Missions 2 and 3, the aircraft must carry at least one passenger. The passenger cabin must contain an individual “seat” for each passenger and have an aisle that measures 2 inches in width and height running its length. The passenger cabin must therefore have a great enough volume to contain the selected number of passengers and a “seat” mechanism to totally secure passengers.

Payload: As per Mission 3, the weight of payload carried by the aircraft has a significant impact on the mission score. M3 score is dependent on the number of laps flown and the weight of the payload carried. Increasing payload weight implies increasing score. However, increasing weight requires more propulsion system weight, and therefore must be balanced with empty weight requirements.

The analysis conducted in Sections 3.1 and 3.2 were translated into qualitative design metrics that were used to evaluate and select an aircraft configuration, summarized in Table 3.5.

Table 3.5: Rules and requirements translated into design requirements

Mission/Scoring Requirement	Design Requirement
Low Empty Weight	The aircraft structure shall be robust but made from minimal material to reduce weight.
Low Wing Span	The aircraft shall have the smallest wing span possible while maintaining the ability to complete all mission requirements.
High Top Speed	The propulsion system shall be powerful enough so that the aircraft can fly at expected competition windspeeds and complete M2 and M3 in minimal time without sacrificing overall aircraft weight.
Passenger Cabin	The aircraft shall have passenger seats that totally restrain passengers in flight and a volume great enough to contain a seat for every passenger and a 2”x2” aisle in the passenger cabin.
Payload Bay	The aircraft shall have sufficient interior volume to contain the number of payload blocks determined by the team.

3.3 Configurations Considered

The analysis conducted in Sections 3.1 and 3.2 shows that minimizing the wingspan and reducing the empty weight are the most critical design considerations. Configurations taking advantage of vortex lift were considered. Vortex lift is a unique kind of lift generation detailed in section 4.4. Three low aspect ratio configurations, the monoplane, full delta, and clipped delta emerged as possible choices. An alternative biplane configuration was ruled out due to excessive weight, drag, and inferior maximum lift. All three configurations ensure minimal wingspan and enable the examination of the extremes of leading edge sweep on flight performance.

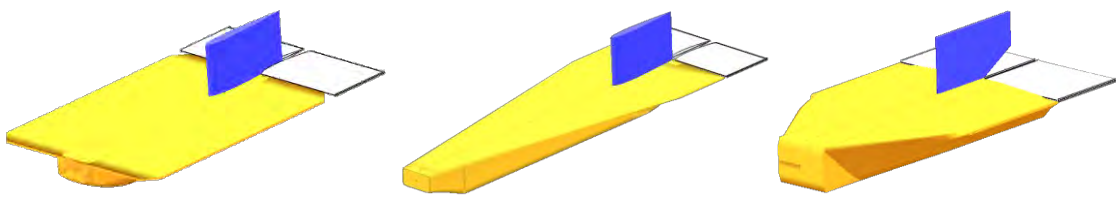

Figure 3.5: Considered configurations: monoplane (left), full delta (center), clipped delta (right)

The first configuration in Figure 3.5 shows a short-span monoplane examined by the team. This configuration has no leading-edge sweep but maximum wing area of the three configurations for the same wing span and chord length. The CG location needed to maintain static longitudinal stability was found to be very far forward, which complicates integration of the payload and propulsion battery.

The full delta configuration of Figure 3.5 has the maximum leading-edge sweep of the three configurations, which is understood to be aerodynamically beneficial. However, the team’s experience with heavily swept designs has shown that a full delta configuration can have difficulties with roll stability and control authority. The full delta configuration also has reduced static longitudinal stability at high angles of attack. The extreme leading edge sweep complicates the storage of passengers and payload blocks into the front of the aircraft.

The clipped delta configuration shown in Figure 3.5 has approximately 60° leading-edge sweep and a chord length intermediate between the box delta and full delta for the same wing area. The C.G was expected to be in a more feasible location and the internal volume more closely matched what was necessary to contain all required components.

3.4 Component Weighting and Selecting Process

To assess each configuration from a quantitative standpoint, Figures of Merit (FOM) were created based on the most important configuration factors. The FOM are shown in Table 3.6. Each FOM was assigned an importance of 0 through 5, with 5 being the most important factor and 0 being a non-factor in design.

Table 3.6: Figures of Merit

Figure of Merit	**0**	**1**	**2**	**3**	**4**	**5**
Weight						**5**
Stability				**3**		
Speed			**2**			
Payload Integration				3		

Due to the strong effect of RAC on scoring, weight and wingspan were determined to be the overwhelmingly critical design factors. The stability of the aircraft was a significant design factor due to the need to reliably complete flight missions. The speed of the aircraft was considered significant as well to complete flight missions within the time window. Passenger and payload carrying capacity was determined to be a non-factor due to the understanding that reducing RAC is always more important than increasing mission score. For final selection, each configuration was given a scoring value for each figure of merit, and that rating was then multiplied by the FOM value. The scoring values are shown in Table 3.7. The configuration with the highest total quality was then selected for further analysis in the design process.

Table 3.7: Configuration scoring values

Score	**Value**
1	Inferior
2	Below Average
3	Good
4	Very Good
5	Superior

The three configurations discussed previously are shown in Table 3.8 with their respective scores for each of the relevant FOM. These results, combined with those from the qualitative analysis, lead to the team's choice of configuration for the *Trilobuzz* aircraft system. Table 3.8 shows that the clipped delta has the highest FOM score.

Table 3.8: Aircraft configurations' Figures of Merit

		Aircraft Configurations		
		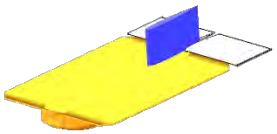	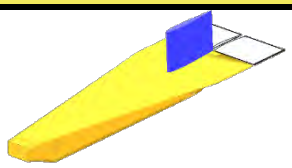	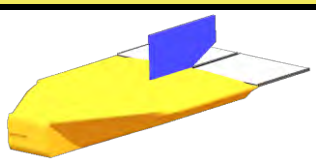
FOM	**Value**	**Monoplane**	**Full Delta**	**Clipped Delta**
Weight	**5**	5	3	5
Stability	**3**	1	3	5
Speed	**2**	2	4	3
Payload Integration	**3**	2	2	4
Value	**N/A**	**38**	**38**	**58**

3.5 Final Conceptual Design Configuration

The final configuration is a clipped delta wing aircraft with a vertical stabilizer, two elevons, and a single-engine tractor propulsion system, as shown in Figure 3.6. This configuration offers maximum efficiency with regards to wing span and intrinsically low weight when compared to any conventional aircraft. Issues with stability and reliability were mitigated over the course of a rapid prototyping process that is discussed later in this report.

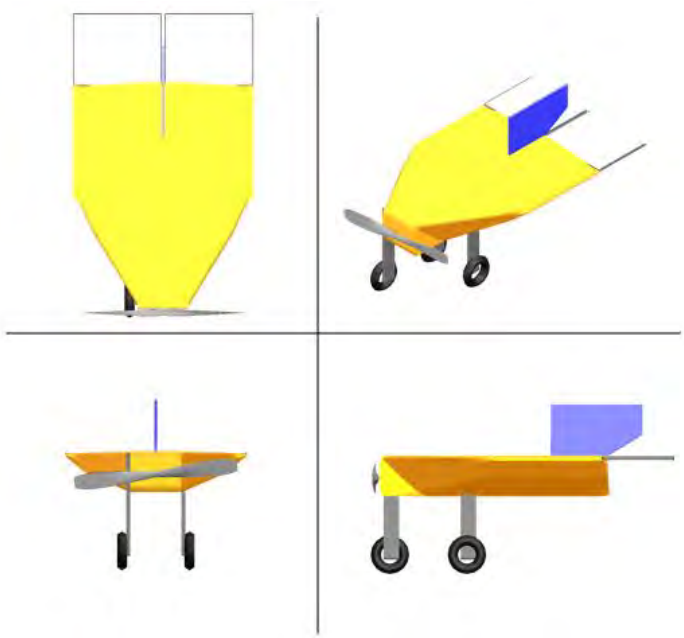

Figure 3.6: Final clipped delta configuration

4 PRELIMINARY DESIGN

The preliminary design phase was performed to identify limiting factors and constrict the design space. Trade studies of the wing area and propulsion system were performed to identify a combination capable of meeting important mission and environmental requirements. Weight, drag, power, propeller performance, battery data, and aerodynamic coefficients were calculated and combined to estimate mission performance for all three flight missions.

4.1 Design Methodology

The team approached the design process with an iterative, performance-focused, multidisciplinary analysis. Constraint sizing was performed to select a weight-normalized design point that satisfies objectives for all three missions. From these design points, the team analyzed possible propulsion systems, system aerodynamic characteristics, built mission models, and compared them to estimates generated as part of the sizing process. Stability and mission performance calculations were made using these more detailed models. Georgia Tech's iterative preliminary design methodology, shown in Figure 4.1, details the roughly sequential process through which information coalesces in advance of the detailed design process. An example of the iteration process is modifying the wing area at constant wing-loading if propulsion weight is lower than expected, re-evaluating stability and mission performance, or modifying the propulsion system to meet pilot requests. The design shown in this report is the final product of a more complex, iterative procedure that seeks to maximize the overall score at every stage.

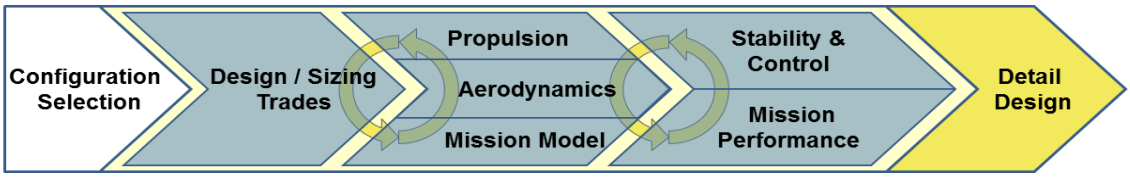

Figure 4.1: The team's preliminary design methodology highlighting the multidisciplinary iterations

4.2 Design Trades

4.2.1 Constraint Sizing

The performance requirements in terms of wing loading and power to weight ratio were essential to selecting an appropriate design point. Empty weight and wingspan, the two factors of RAC, were influenced by these two variables. Therefore, a constraint sizing analysis was conducted on these variables to reveal a design space capable of meeting all requirements, with results shown in Figure 4.2. Landing and takeoff constraints were found by restricting the aircraft to 20° angle of attack and 24 mph. The other mission-based constraint is the takeoff distance of 150 feet, which is rendered inactive by the environmental requirement to be capable of flight at 61 mph. A design point in this space was chosen based on a very conservative estimate for the wing loading due to the risks associated with extremely low aspect ratio designs.

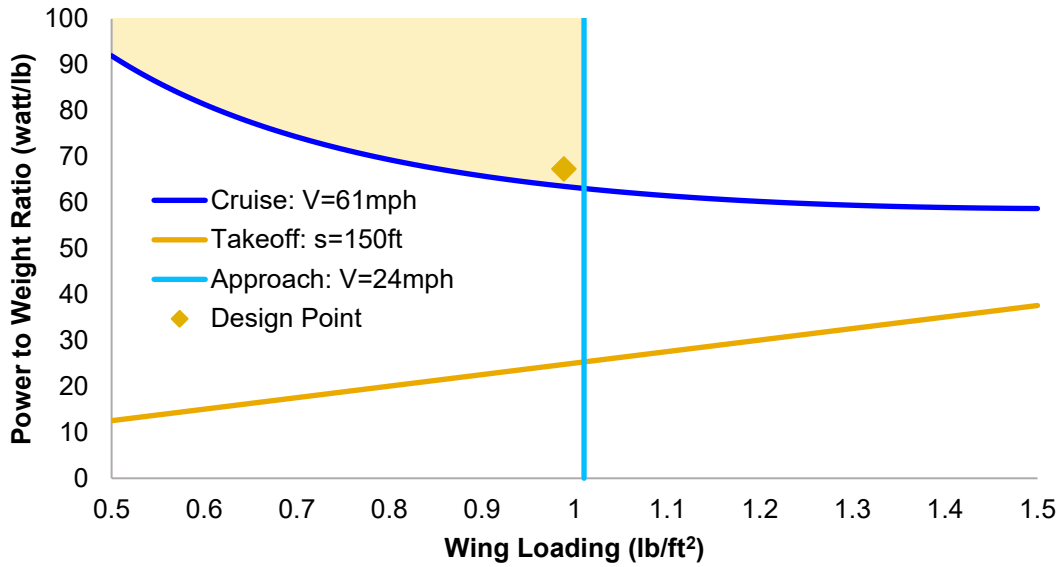

Figure 4.2: Constraint sizing design point selection

The results of this process allowed for a preliminary calculation of power, weight, and wing area, summarized in Table 4.1. The power requirement listed represents the power needed to satisfy all requirements at the chosen wing loading, while the power selected represents the power requirement of the design point, including desired margins and propulsion systems availabilities.

Table 4.1: Preliminary power and wing area

Parameter	Preliminary value
Wing loading (psf)	0.989
Power loading (watt/lb)	18.86
Estimated weight (lb)	1.34
Wing surface area (ft^2)	1.35
Power required (watts)	84.9
Power selected (watts)	90

4.2.2 Propulsion System Selection

A fixed pitch folding propeller was selected to reduce operational complexity and to fit inside the cargo bay. A propeller efficiency of ~60% and a motor efficiency of ~70% was assumed from past experience, leading to a power requirement of around 85 watts for the propulsion system. From the analysis performed in Section 3.1.4, it was determined that a 6-cell 1500 mAh battery minimizes RAC, while also providing margin for the cruise requirements. A direct-drive brushless out-runner motor with a high motor constant (Kv) was selected to draw more power out of a 6-Cell battery. Motors were researched that fit these criteria and a

database was created, containing over 50 motors from various companies, including Hacker, Tiger, Scorpion, Cobra, and AXI.

A propeller database was also generated based on airplane size and speed. The propellers tested were 9x6, 9x7, 9.5x6, 10x5, 10x6, 10x7, 10x9, 11x6, 11x7, and 11x8 Aeronaut folding propellers. MotoCalc, a commercially available motor analysis tool, was then used to estimate the motor efficiency, static thrust, and thrust at 30 mph for each motor and propeller combination. Feasible combinations were sorted by weight and selected for further analysis.

The top motor-battery-propeller combinations were analyzed and their variation with speed was graphed, allowing the team to evaluate the most effective propulsion system to meet takeoff and max speed requirements. Three motor combinations were selected and purchased for testing, as shown in Table 4.2. Section 8.1.1 will go into further detail regarding these tests.

Table 4.2: Motor specifications

Motor	Kv	Battery (Cells)	Current (Amps)	Best Propeller	Static Thrust (lb.)	Propulsion System Weight (lb.)
Cobra 2217-12	1550	6 (1,500 mAh)	26	10x7	1.50	0.20
Scorpion SII-2212-18	1850	6 (1,500 mAh)	24	9x6	1.32	0.15
Hacker A30-22S	1440	7 (1,500 mAh)	20	11x8	1.80	0.24

4.3 Mission Model

4.3.1 Description and Capabilities

The three missions were simulated via a set of first order differential equations (Equations 4.1-4.3) defining the position and orientation of the vehicle throughout the flight. By integrating these equations over time using a 4th Order Runge-Kutta approach in MATLAB and logic defining each of the required mission segments, it is possible to define the position, velocity, and orientation of the vehicle over time. The thrust (T) is defined as a function of velocity, with the relationship defined by MotoCalc, the analysis tool used in the propulsion system selection. The drag (D) is represented via a parabolic drag relationship. The load factor is explicitly defined for each turn segment, but if it exceeds the estimated maximum lift coefficient, it is limited to that value.

$$\dot{\ } = \tag{4.1}$$

$$\dot{\ } = \frac{-}{} \tag{4.2}$$

$$\dot{\ } = \frac{\sqrt{\ ^2-1}}{} \tag{4.3}$$

4.3.2 Uncertainties

There are limitations to the approach used above. The lack of a vertical dimension in the equation means that the approach cannot model the aerodynamic effect of changing altitude. The energy required, saved, and lost by climbing and diving is also not included. The lack of any wind model discounts any additional drag due to sideslip, or the acceleration of the aircraft as due to headwinds or tailwinds. The flight path used for each lap assumes an ideal course, with the pilot achieving perfect, uninterrupted turns between each 1000 ft. leg. Finally, there are additional uncertainties in the mission predictions due to any errors or inaccuracies in the thrust and drag predictions.

4.4 Aerodynamic Characteristics

The results of the conceptual design show that substantial improvements in mission score can be achieved by minimizing aspect ratio. Therefore, configurations with very low aspect ratios were exclusively researched, analyzed, and tested. For aircraft with aspect ratios less than 2, potential flow calculations began to deviate from actual lift measurements due to a nonlinear component of lift called vortex lift. At the tips of all aircraft wings, high-pressure air from the lower surface curls around the side edge of the wing to reach the low-pressure air above the wing surface, creating wingtip vortices. If the edge is thin and sharp, the flow will tend to separate. In delta wings, this separation induces the flow to curl around the edge and reattach itself to the upper wing surface along primary and secondary attachment lines, creating a vortex as shown in Figure 4.3 by Anderson [1]. The upward bevel on the leading and side edges of the wing helps to generate flow separation and direct flow into the vortices. The vortices are also more energized than ordinary flow, allowing the delta-wing to achieve dramatically higher angles of attack before stall. The vortices persist to a degree after stall, which results in very gentle stall behavior.

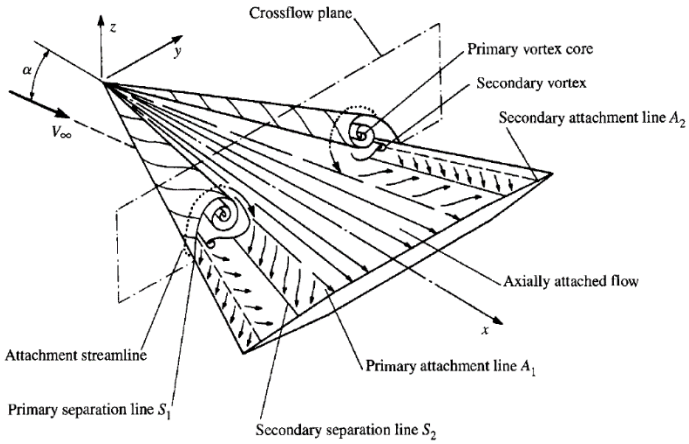

Figure 4.3: Vortex lift conceptualization by Anderson [1]

Within the class of planforms specialized for vortex lift there exist major differences in the leading and trailing edge sweep angles, as well as the overall taper ratio (R_T). Wind tunnel tests for a variety of possible such flat plate planforms were obtained by the National Advisory Committee for Aeronautics by Tosti [2]. Figure 4.4 shows a comparison of various wing planforms, along with corresponding maximum coefficient of lift, $C_{L,\,Max}$, and aspect ratio, AR, from the NACA Technical Note. The clipped delta configuration with the highest $C_{L,\,Max}$ was selected for further analysis.

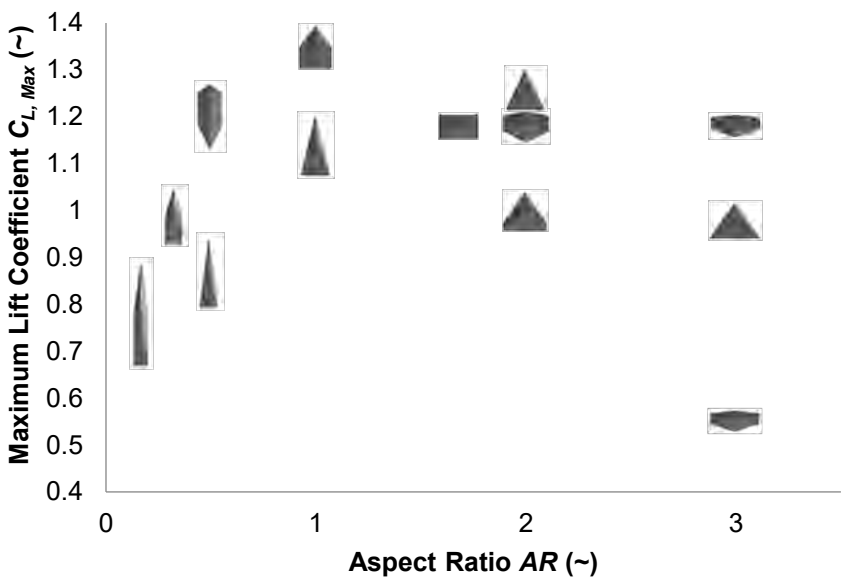

Figure 4.4: Maximum lift coefficient of various planforms [2]

4.4.1 Analysis Methods

Since traditional potential flow theory does not account for vortex lift, analysis tools and techniques dependent on potential flow theory are not valid for this kind of aircraft. The accuracy of three different vortex lattice applications were evaluated against experimental wind tunnel data to identify the tool best

able to predict the aerodynamic characteristics of low aspect ratio aircraft. The first tool is Athena Vortex Lattice by Drela & Youngren [3], or AVL. This tool has been used by the team to model conventional aircraft in the past with great success. The second tool is VORSTAB [4], a quasi-vortex lattice program that uses the Leading-Edge-Suction Analogy to determine total lift from potential flow. The Leading-Edge-Suction Analogy is a theory developed by Edward Polhamus in 1966 to mathematically model vortex lift using lifting surface methods [5]. VORSTAB is capable of analyzing vortex lift resulting from leading edge vortices reattaching to the top of the wing, generating more lift than sole potential flow predictions. VORLAX, developed by Miranda et al. in 1977, is a robust application for modeling traditional vortex lattice theories while also accounting for leading edge suction [6]. Lamar published wind tunnel data of a planform that has an *AR* of 0.84 and Taper Ratio, R_T, of 0.5, very similar values to that of *Trilobuzz* with an *AR* of 0.72 and R_T of 0.62 [7]. This data is shown compared to the analytical tools in Figure 4.5 and Figure 4.6.

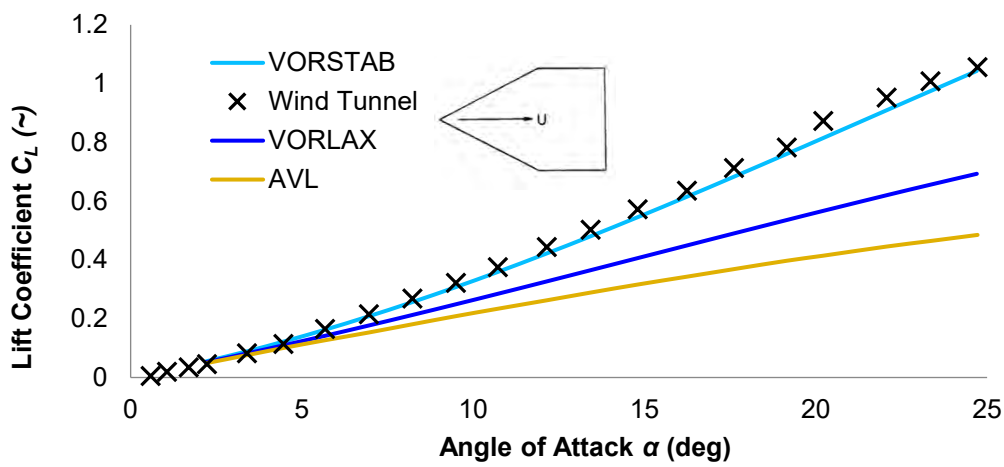

Figure 4.5: Lift estimation for clipped delta planform; wind tunnel data from Lamar [7]

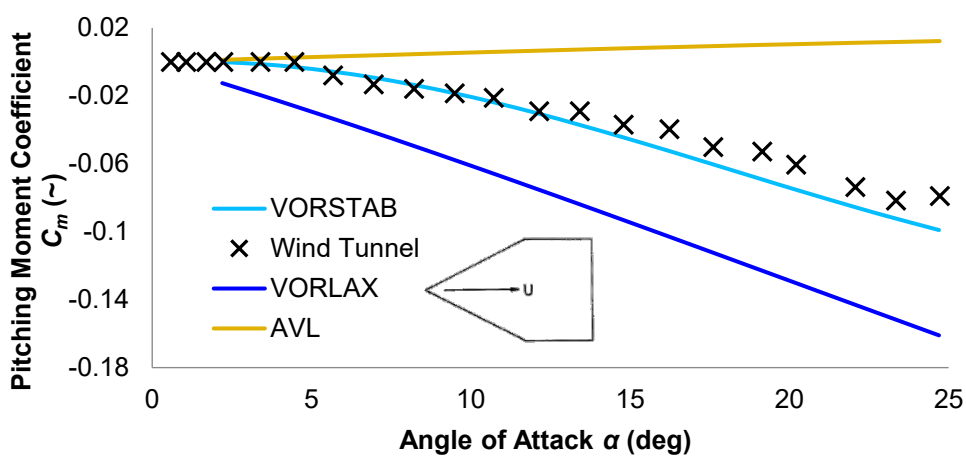

Figure 4.6: Pitching moment estimation for clipped delta planform; wind tunnel data from Lamar [7]

The comparison to wind tunnel results showed that VORLAX and AVL under-predicted the lift, while VORSTAB accounted for the added effect of vortex lift, especially on the sides of the wing. The wind tunnel results in Figure 4.6 show that the slope of the pitching moment curve increases in magnitude as the angle of attack is increased, a well-known feature of vortex lift producing wings. Only VORSTAB succeeded in modeling the nonlinear pitching moment characteristics and matching the wind tunnel data. Thus, VORSTAB was selected for use in all key aerodynamic analysis.

4.4.2 Lifting Surface Analysis

The final design configuration was analyzed with VORSTAB to generate the lift versus angle of attack plot in Figure 4.7 for the clipped delta planform. This method cannot predict stall behavior or stall angle but is suitable for most flight regimes. The results show that vortex lift can make up more than half of the lift contribution at high angles of attack, creating a much more useful lift coefficient.

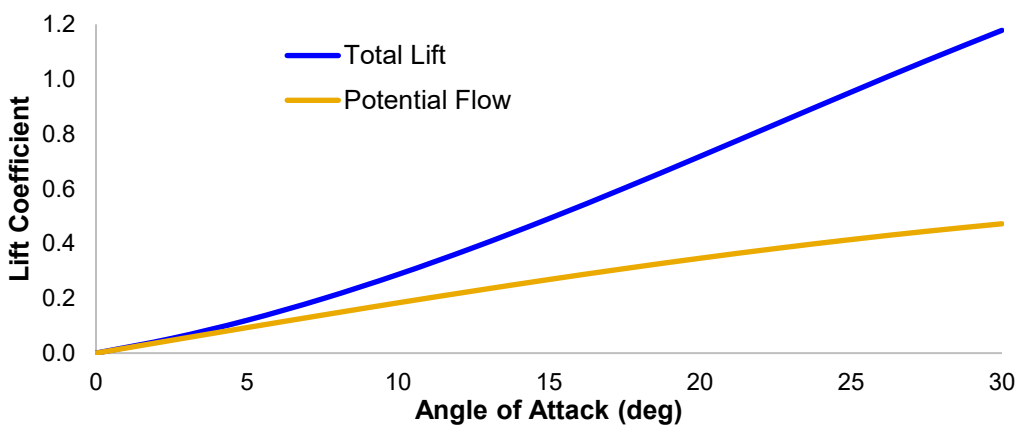

Figure 4.7: Final design VORSTAB lift curve

4.4.3 Drag Analysis

Preliminary parasitic drag estimates were obtained by summing each component's drag contributions, computed using the semi-empirical methods from Hoerner's *Fluid Dynamic Drag* [8], and then normalizing each component according to the wing reference area. Table 4.3 shows the contributions of the major aircraft components, with Figure 4.8 showing the same data as a percentage breakdown at 0 and 10 degrees angle of attack. The relatively large landing gear creates most of the zero-lift drag, though the highly turbulent flow over the wing becomes the largest contributor as the angle of attack is increased.

Table 4.3: Breakdown of various sources of drag

Component	$C_{D,0}$	$C_{D,10°}$
Wing	0.0154	0.0859
Tail	0.00184	0.00184
Landing Gear	0.018	0.018
Total	0.0353	0.106

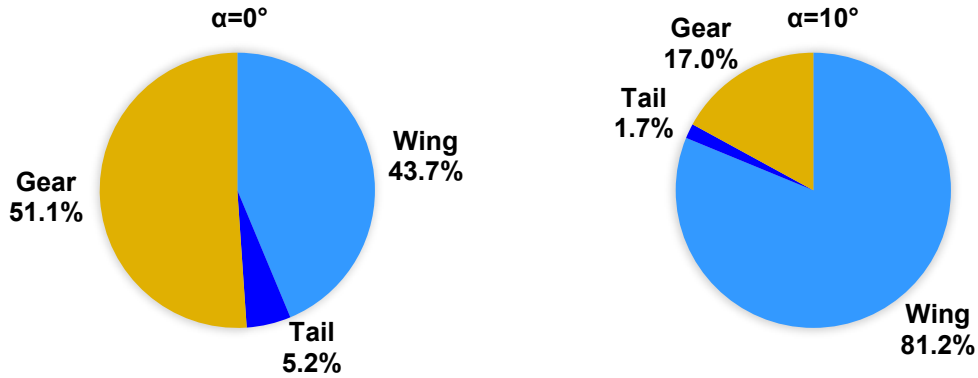

Figure 4.8: Breakdown of various sources of drag

Wing: The zero lift drag coefficient of the wing was found using the semi-empirical Hoerner's method as seen in Equation 4.4:

$$_{,0} = \qquad (1 + \ '(\ / \ ) + 100(\ / \ )^4) \cdot \frac{\quad}{\quad} \tag{4.4}$$

where is the wing fuselage interference factor (assumed to be equal to 1, since the wing is the fuselage), is the lifting surface correction, which is a function of the sweep angle, is the turbulent plate friction coefficient of the wing, which is a function of Reynolds number (R_e), $'$ is the airfoil thickness location factor, $/$ is the thickness-to-chord ratio, is the wetted area of the wing, and is the wing reference area.

Tail: The vertical tail was modeled as a simple wing, and its drag was determined using Hoerner's method. A wing interference factor of 1.04 was used to reflect the perpendicular joint between the tail and the wing.

Landing Gear: The landing gear components are significant contributors to the overall drag of the aircraft. The main gear and nose gear drag contributions were calculated separately, but both were modeled as a wheel and a flat plate.

The drag polar was calculated as the combination of the wing normalized $C_{D,0}$ values estimated using Hoerner's method for each component, and the lift dependent drag predicted by VORSTAB. The drag predicted by VORSTAB corresponds only to the increased drag on the wing, because it was assumed that the drag on other components is independent of angle of attack. Figure 4.9 shows the resulting drag polar.

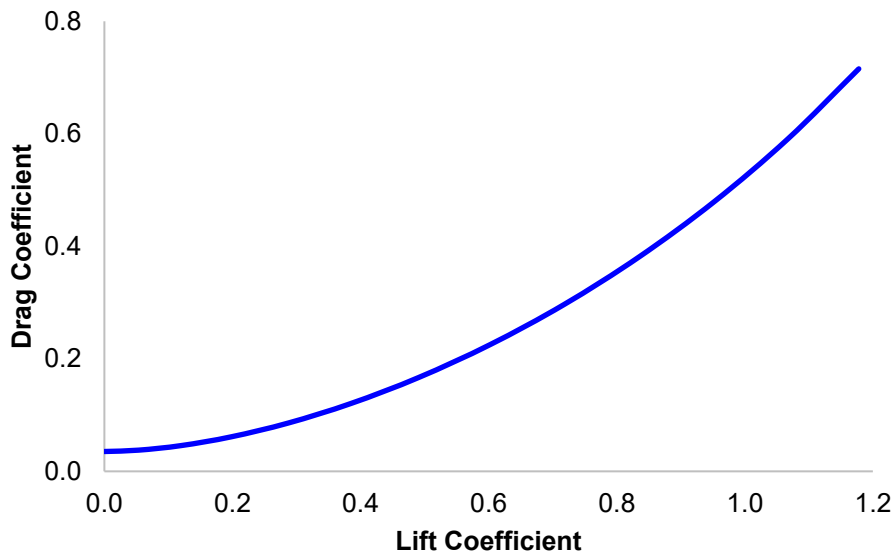

Figure 4.9: Drag coefficient prediction using vortex lift calculation

The wing exhibits a very shallow lift-curve slope due to the 0.72 aspect ratio. The maximum angle of attack and maximum lift coefficient were defined using the drag polar in Figure 4.9**,** above. No distinct upper limit on angle of attack exists for wings taking advantage of vortex lift. However, a combination of flight test results and pilot consultations show that the aircraft is difficult to control at angles of attack above 30°. As a result, the aircraft flight envelope is limited to angles of attack less than 30°.

4.5 Stability and Control

Static and dynamic stability were analyzed to ensure that the aircraft would be able to successfully complete the flight missions. The fastest speeds, slowest speeds, heaviest weights, lightest weights, cruise, climbs, and turns were all considered, with results presented only for the critical flight condition.

4.5.1 Static Stability Analysis

The only condition for static longitudinal stability is for the center of gravity to be located in front of the neutral point. VORSTAB was used to identify the neutral point and calculate stability and damping derivatives. It is a well-known property of vortex lift that the neutral point moves backward as angle of attack increases. This increases the restoring moment, which makes the aircraft very stable at high angles of attack. Figure 4.10 shows the pitching moment derivative curve at the CG, 5.3 inches from the datum.

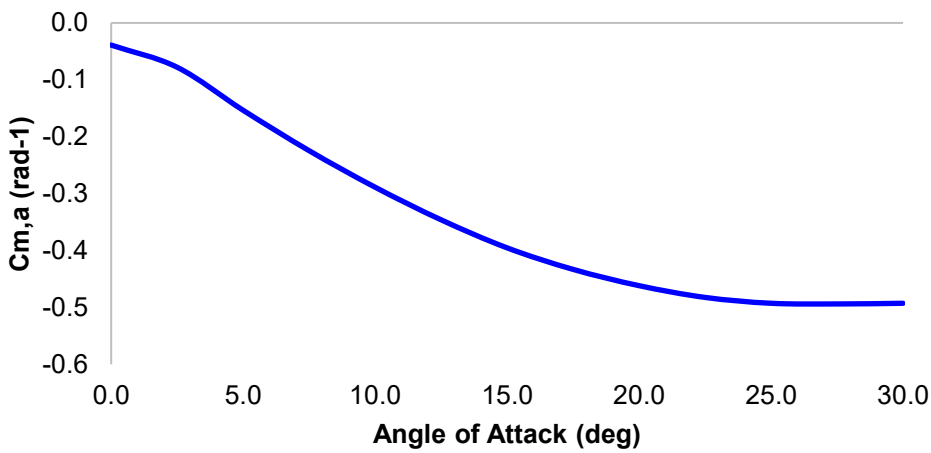

Figure 4.10: Moment coefficient derivative versus angle of attack at the CG

The most demanding flight condition for trim was at the highest weight and lowest speed. Stability derivatives for these flight conditions are given in Table 4.4. The aircraft was designed to be trimmed at this condition with minimal elevon deflection. VORSTAB assumes a symmetric airfoil configuration, and therefore does not consider the moment offset generated by the circulation of flow around what is essentially a negatively cambered fuselage. Flight tests, however revealed that minimal trim is needed when the CG is located 5.3 inches from the datum. The elevon deflection requirements for each case were found to be within acceptable limits, in large due to the sizable elevons which composed 30% of the total wing area. The aircraft was found to be longitudinally, statically stable at all necessary cases, with a static margin of 4.1% at 0° and 17.8% at 20° angle of attack.

Table 4.4: Relevant stability coefficients and derivatives for static stability

Parameter	VORSTAB Results	
Inputs	W_{total} (lbs.)	1.34
	V (ft/s)	40
Aerodynamic Parameters	C_L	0.718
	α (deg.)	20
	β (deg.)	0.0
Stability Derivatives	$C_{l,\beta}$ (rad^{-1})	-0.26
	$C_{L,\alpha}$ (rad^{-1})	2.67
	$C_{m,\alpha}$ (rad^{-1})	-0.38
	$C_{n,\beta}$ (rad^{-1})	0.13
Damping Derivatives	$C_{l,p}$ (rad^{-1})	-0.18
	$C_{m,q}$ (rad^{-1})	-0.87
	$C_{n,r}$ (rad^{-1})	-0.28
Static Margin (α=0°)	% Chord	4.2
Static Margin (α=20°)	% Chord	17.8

4.5.2 Dynamic Stability Analysis

Having found the trim conditions as a part of the static stability analysis, the next step was to take the aerodynamic derivatives about the trim conditions described earlier and investigate the dynamic behavior of the airplane. The stability and control derivatives were obtained from the VORSTAB, the mass properties from the CAD file, and the stability characteristics calculated from the full 12×12 6-DOF linearized differential equations found in Phillips's *Mechanics of Flight,* Section 9.8 [9]. The eigenvalues and eigenvectors of the matrix showed the stability of each of the five dynamic modes, revealing that the aircraft is stable in all dynamic modes, except spiral. The flight conditions used were the same as used in the static stability section, listed in Table 4.4. The dynamic stability characteristics are tabulated in Table 4.5.

Table 4.5: Dynamic stability characteristics

		Longitudinal Modes		Lateral Modes		
	Mode	**Short Period**	**Phugoid**	**Dutch Roll**	**Roll**	**Spiral**
Production Aircraft	Damping Rate (s^{-1})	2.66	0.577	0.357	3.099	-0.451
	Time to double/half (s)	0.261	1.2	1.94	0.224	1.54
	Damping Ratio (~)	0.299	0.271	0.0389	-	-
	Damped Natural Frequency (s^{-1})	8.46	2.05	9.18	-	-
	Undamped Natural Frequency (s^{-1})	8.87	2.13	9.18	-	-

4.6 Mission Performance

Predicting the performance of the aircraft is essential for verifying that the aircraft can complete all missions. Lap trajectories were estimated using the equations listed in Section 4.3, propulsion characteristics from MotoCalc and the aerodynamic properties found using VORSTAB and Hoerner's method. The flight performance was calculated with a 10x7 propeller, a Cobra 2217-12 motor and a 6S 1500 mAh NiMH battery pack. Missions 2 and 3 are virtually identical in single lap performance due to the weight of the payload block being less than 5 grams, and therefore negligible. Therefore, the estimated velocity profile of a single lap of mission 2 or 3 is plotted in Figure 4.11. The performance targets for Mission 1 should also be met for any aircraft capable of completing mission 3, due to the reduced wing loading with no passenger. The maximum velocity when loaded with a passenger was found to be 60.8 mph and the lap time was estimated to be 35.8 seconds. Therefore, the aircraft should be capable of completing all missions in the necessary time. Takeoff distance was estimated to be 14.96 feet.

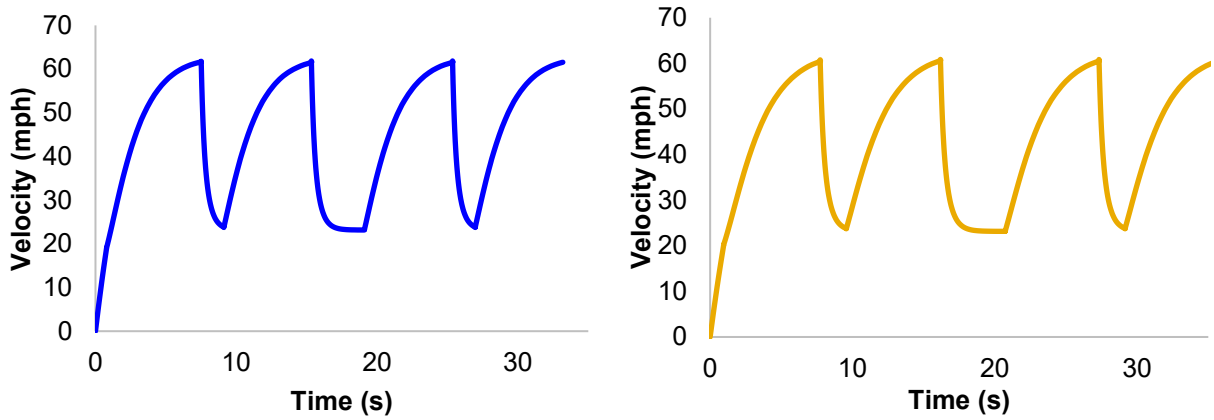

Figure 4.11: Simulation of lap trajectories for M1 (left) and M2/M3 (right)

5 DETAIL DESIGN

5.1 Final Design – Aircraft

Generally, structural analysis, layout, component selection, weight-balance calculations, and flight testing did not indicate major changes were required to the aircraft between preliminary and detailed design stages. Control surfaces were designed to achieve a balance between controllability of the aircraft and size of the surface. These dimensions, along with the dimensions of the rest of the aircraft, are in Table 5.1. The final aircraft was designed for flight stability, simplicity, and structural efficiency.

Table 5.1: Final aircraft dimensions

	Dimension	
Aircraft	Span (in)	11.8
	Mean Chord (in)	16.85
	Root Chord (in)	19.43
	Tip Chord (in)	12.08
	Leading Edge Sweep (deg)	64.5
	Aspect Ratio	0.72
	Wing Area (ft^2)	1.35
	Static Margin (%) at α=0°	4.2
Elevon	Span (in)	11.8
	Chord (in)	5
	Max δ (deg)	35
	Reference Area (in^2)	59
Vertical Stabilizer	Span (in)	3.5
	Chord (in)	5
	Reference Area (in^2)	17.5

5.2 Structural Characteristics

5.2.1 Layout and Design

The structural layout was created to ensure that all loads were accounted for and have an adequate load path to the major load bearing components. The team divided the loads the aircraft would see into three categories.

Thrust Loads: Includes thrust, torque, and sustained vibrations. Components should be made of harder, quasi-isotropic materials such as plywood, and all fasteners must be locked.

Aerodynamic Loads: Includes wing and control-surface lift, drag, and moment, which translate to bending and torsion. Components can be anisotropic for added strength in the load direction.

Ground Loads: Includes aircraft weight and landing impact. Struts should be metal, which sustains impact by bending, not breaking.

The high structural loads on *Trilobuzz* contributed to the short wingspan and highly integrated components. Ground loads and thrust loads are directly transferred into the surrounding main structure. Aerodynamic loads applied to the aircraft by the main control surfaces during maneuvering, such as during takeoff or the turns, are also transferred directly to the main structure. These loads are shown in Figure 5.1.

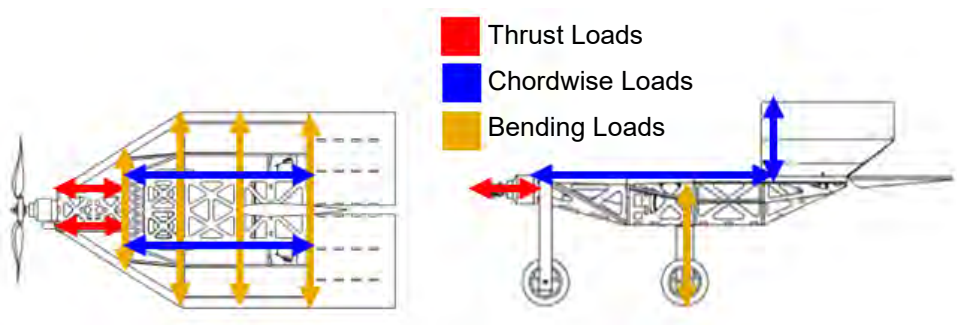

Figure 5.1: Load paths of major forces

5.2.2 Operating Envelope

With the loads mapped and layouts complete, the aircraft structures were designed to withstand the design load of 5g at the maximum gross weight of 1.34 lbs. This translates to a 78.5° bank angle for sustained, level turns. The 5g design load limit at small deflections was retained as the maximum positive load envelope. The negative design loading was designed at a maximum of -3g fully loaded and therefore -3.38g when empty. The defining structural limits were combined with aerodynamic performance limits to construct a V-n diagram, shown in Figure 5.2. The aircrafts weight change between missions 2 and 3 can be assumed negligible and are therefore represented by the same line in the V-n diagram. The 0.15 lbs. weight difference between the unloaded aircraft in mission 1 and the loaded aircraft in mission 2 and 3 results in a slight change in the aircrafts stall limits, structural load limits and max velocity.

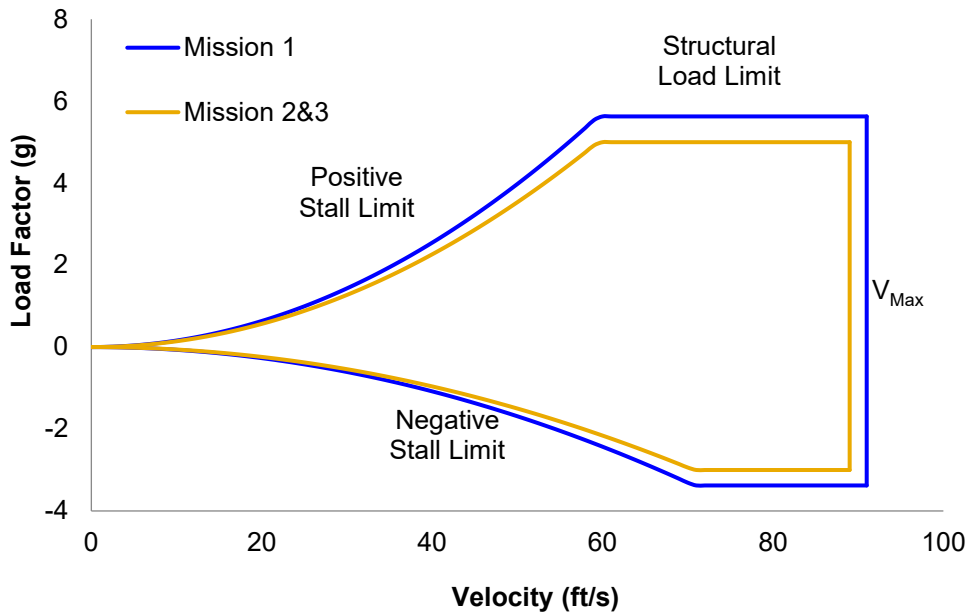

Figure 5.2: V-n diagram showing loading as a function of velocity for all flight missions

5.3 System and Subsystem Design and Implementation

To finalize the aircraft design, the following subsystems were analyzed with greater detail: radio controller, servos, flight surfaces, propulsion system, and landing gear. The structural architecture/assembly for each of these components: wing body and payload bays, wing tips, motor mount, elevons and vertical stabilizer, receiver and transmitter, propulsion, servos, and landing gear was also further examined.

5.3.1 Wing Body and Payload Bays

The wing body and payload bays are primarily made from 1/8” balsa wood running spanwise and chordwise that interconnect in a jigsaw fashion. This method allows for the grain direction of the balsa wood to increase the strength and load transfer across the structure while also leading to efficient manufacturing. Lightening holes were designed to minimize weight, while balsa rods and capping are added to increase strength at high stress areas. The center sections of *Trilobuzz’s* body are hollow to allow for the passenger and payload bays, as well as batteries and other essential parts. These payload bays are fully contained on all sides by the structure of the body, with one side acting as a removable lid designed with a friction fit and secured with adhesive material. The CAD model (Figure 5.3) shows the interconnection of balsa pieces, the hollow passenger and payload bays, as well as the other design choices.

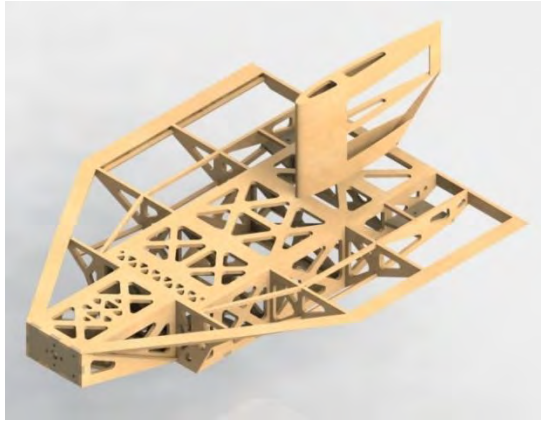

Figure 5.3: Trilobuzz body CAD

5.3.2 Vertical Stabilizer

The vertical stabilizer is attached via an interface spar that meshes with a spanwise rib, with the rib being reinforced by 1/32” pieces of plywood on either side of the balsa rib. The vertical stabilizer has no rudder due to the design of the airplane’s controls. The vertical tail is designed with a typical wing structure including several ribs in the shape of a NACA 0012 airfoil attached to a load bearing spar at the quarter-chord. Additionally, 1/32” balsa sheeting is used along the leading edge to maintain the airfoil shape.

5.3.3 Elevons

The elevons are 3D control surfaces constructed out of laser cut 1/8-inch balsa, reinforced with nylon carbon-fiber for torsional stiffness. The elevons are designed so that their leading edge is the same thickness as the trailing edge of the mean airframe. Hinge tape with lateral and longitudinal threading is implemented to attach the elevons to the airframe, while still allowing the full range of motion necessary for the aircraft to maneuver. Servos mounted near the trailing edge of the main airframe are connected to the elevons by metal wire push-rods. The elevons are the only control surfaces on the aircraft. They allow the aircraft to pitch and roll, but do not directly allow for yawing motion. To change orientation on the inertial XY-plane, the aircraft must perform a combination of pitch and roll. By limiting the aircraft to only two control surfaces, the wingspan and empty weight of the aircraft is minimized. An installed elevon attached is shown in Figure 5.4.

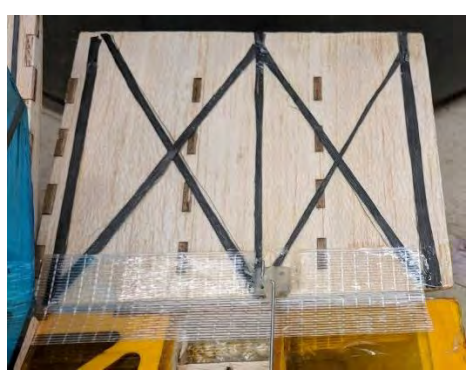

Figure 5.4: Elevon attachment mechanism

To satisfy the Ground Mission LRU requirement for control surfaces, the elevons can be removed by cutting the hinge tape used to attach them, disconnecting the servo pushrod from the now free control surface, and reattaching the pushrod to the replacement elevon, before applying fresh hinge tape.

5.3.4 Receiver and Transmitter Selection

The selected receiver is the OrangeRx GA7003XS, as it provides the required failsafe mechanism with minimum weight. The receiver is securely attached to a plywood plate in a forward electronics bay, where it is easily accessible. The receiver also contains a rate gyro system to provide additional roll damping in which the low aspect ratio configuration is deficient. When the receiver detects an angular velocity along the roll axis of the aircraft, it automatically deflects the elevons to produce a restoring roll moment. The magnitude of this moment can be altered with screws on the top of the receiver. A Futaba T8FG radio controller was used to communicate with the Futaba-compatible receiver. The receiver is accessible through the electronics access panel. Should the receiver be the randomly selected LRU in stage 2 of the Ground Mission, it can be quickly disconnected and replaced within the requisite time.

5.3.5 Propulsion System

A Maxxpacks E1506S-3 1500 mAh NiMH battery pack was selected to minimize weight while maintaining enough power to achieve mission requirements. The Thunderbird 36 speed controller was selected for its light weight and compact form factor. The speed controller connectors were altered to the appropriate size to fit through the airframe. A variety of motors and propellers were analyzed using the MotoCalc program, as described in Section 4.2.2. Two were selected for further testing, as described in Section 8.1.1. The Cobra C-2217/12 1550 kV motor was chosen for its weight, size and static thrust. The Aeronaut 10x7 propeller was chosen for its desired ratio between performance at high speed and ample static thrust. The final selected propulsion system components are listed in Table 5.2. Figure 5.5 shows a CAD rendering of the motor mounted to the airframe. All of the components that make up the propulsion system are candidates to be replaced in the Ground Mission. Each is capable of being replaced within the requisite time period, accessed either externally or by removing the appropriate access panel.

Table 5.2: Selected propulsion and electronics components

Components	Description
Motor	Cobra C-2217/12 1550 kV
Battery	Maxxpacks E1506S-3
Speed Controller	Thunderbird 36
Receiver	OrangeRx GA7003XS
Transmitter	Futaba T8FG
Tail Servos	Futaba 3114
Propeller	Aeronaut 10x7

Figure 5.5: Motor mount

5.3.6 Servo Selection

The Futaba 3114 was selected as the elevon servo. These servos were selected by analyzing hinge-moments for each control surface using VORSTAB and then finding servos that had sufficient control power to handle the calculated moments, with the lightest weight possible.

Servos create a unique challenge, in terms of the Ground Mission. They are Stage 1 Ground Mission candidates, meaning they must be replaceable within three minutes, but they must also be secure enough to reliably manipulate control surfaces. The solution to this design challenge was to create a removable servo and servo platform that is bolted directly to the airframe. Using blind nuts embedded into the airframe structure, each servo can be removed and replaced by removing two bolts. Once the servo platform is disconnected, the entire system can be removed, disconnected from the pushrod, and replaced. This operation is the same method that will be used to replace pushrods. By removing the servo first, the push rod can be detached at one end from the servo, and then is easily removed from the elevon control horn.

Figure 5.6: Removable servo prototype

5.3.7 Landing Gear

The height of the landing gear was chosen to provide enough clearance so that the propeller does not strike the ground. The rear landing gear was sized to be the same width as the payload bay to provide the highest stability through having the mounting points as wide as possible. The rear landing gear was placed at a location behind the CG, but sufficiently close enough to enable takeoff rotation. The front landing gear is attached off to one side of the airplane centerline at the front of the plane and bolted to the same plywood piece that the motor is mounted to. The landing gear is made from 1/8" thick aluminum sheeting bent to the desired shape of straight vertical pieces attached to the wheels. The configuration of the landing gear can be seen in Figure 5.7. The landing gear is attached with external bolts and embedded blind nuts to allow for fast replacement during the Ground Mission. The wheels are secured with lock nuts and washers that can be removed with a ratchet wrench. Landing gear LRUs can be replaced well within the requisite time.

Figure 5.7: Landing gear

5.3.8 Passenger Seat and Payload Blocks

Successful completion of M2 and M3 requires that the chosen number of passengers are secured in individual seats with a 2-inch by 2-inch aisle. *Trilobuzz* is designed to carry a single passenger, so a single seat mechanism is implemented into the aircraft design. A prototype of the passenger seat mechanism is in Figure 5.8. Two elastic bands are attached to the base plate of the mechanism and feed through a top plate. The bands secure the passenger in the lateral and longitudinal direction, and the top plate compresses the passenger, securing it vertically. With this mechanism, a passenger of any size can be secured without making any modifications. The right image in Figure 5.8 shows the largest size passenger in the seat. The base plate of the mechanism and passenger cabin are sized so that the required 2-inch aisle is always available, regardless of passenger size. This mechanism has been integrated into the structure of the airframe to reduce aircraft thickness and passenger loading complexity for competition.

Figure 5.8: Prototype passenger seat with and without a passenger

One payload block was selected as the maximum number of payload blocks for *Trilobuzz* to carry. The dimensions of the block were determined according to the volume available in the airframe after accounting for the fixed volumes of electrical components and the passenger cabin. Since the payload block dimensions may be selected by the team, creating a payload bay and payload block with matching volume dimensions was simple. The single payload block is 3.95 in. by 3.12 in. by 2.05 in. These dimensions satisfy the requirement that all payload dimensions be no less than two inches and sum to at least nine inches.

5.4 Weight and Balances

To maintain stable flight, it is important to know that the center of gravity (CG) is in the correct location. To estimate the CG, component weights and locations were individually measured and entered into a simple spreadsheet calculator. The CAD model was also used to estimate the CG. The predicted location of the CG is shown in Figure 5.9.

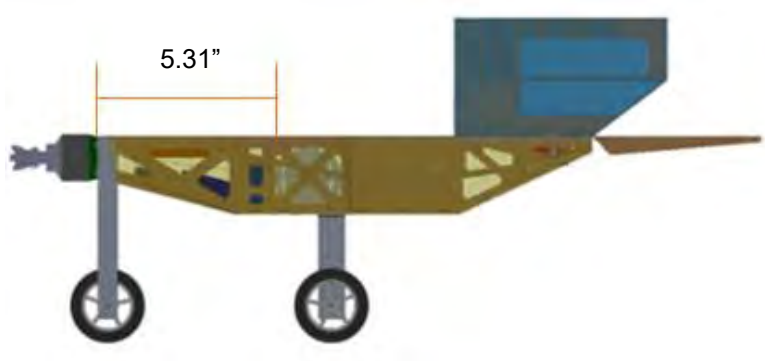

Figure 5.9: CAD Predicted CG Location

Table 5.3 shows the weight and balances of Trilobuzz. X-axis location is measured aft positive relative to the nose, and y-axis location is measured starboard positive.

Table 5.3: Weight and balance

Component	X-CG Location (in)	Weight (lbs)	Moment (in-lb)
Airframe	7.50	0.18	1.36
ESC	2.10	0.07	0.15
Receiver	2.10	0.05	0.11
Propeller	-1.80	0.04	-0.07
Left Elevon Servo	13.15	0.04	0.52
Right Elevon Servo	13.15	0.04	0.52
Motor	-0.78	0.18	-0.14
Main Battery	4.47	0.32	1.44
Receiver Battery	2.10	0.06	0.13
Left Elevon	16.50	0.03	0.55
Right Elevon	16.50	0.03	0.55
Nose Gear	0.25	0.05	0.01
Main Gear	6.80	0.10	0.66
Empty Aircraft	**4.85**	**1.19**	**5.79**
Payload Block	6.12	0.01	0.07
Passenger (max)	8.90	0.15	1.33
Fully Loaded Aircraft	**5.31**	**1.35**	**7.18**

5.5 Performance

5.5.1 Flight Performance

The flight performance of the aircraft is described by the point performance of the vehicle. Key aspects including the velocity envelope, turn performance, and stall speed are given in Table 5.4.

Table 5.4: System flight performance parameters for each mission

Parameter	Mission 1	Mission 2 & 3
Weight (lbs)	1.19	1.34
W/S (psf)	0.878	0.989
V_{min} (ft/sec)	25.52	27.08
V_{max} (ft/sec)	90.72	89.26
Turn Load Factor	5.0	5.0
Turn Radius (ft)	21.37	24.97
Time for 360 (s)	3.93	4.61

Weight represents the gross takeoff weights for each individual mission. Both wing loading and stall speed are calculated at 1g assuming steady level flight while using the VORSTAB prediction for C_L at 30° angle of attack as C_{Lmax}. As mentioned in Section 4.2, this is a desired upper limit, rather than a definite stall point due to the innate characteristics of vortex lift, and the difficulties in predicting the onset of stall. This angle is also larger than the maximum approach angle because higher angles are more tolerable for the pilot during cruise and turn conditions than during landing. Load factor for each mission is the maximum allowable based on the results from the V-n diagram and is found to be 5g's. The turn radius and time to

complete a 360-degree turn were calculated for each mission from expected maximum velocity and allowable load factor. Thrust required is calculated using Equation 5.1(5.1 where $C_{D,0}$ and K_1 were obtained from quadratic regression of the curve in Figure 4.9. The point where thrust available is equal to thrust required corresponds to the maximum velocity of the aircraft.

$$= \frac{1}{2} \quad 2 \quad ,0 + \frac{2 \quad 1}{2} \tag{5.1}$$

Thrust available as a function of velocity was computed using MotoCalc for both propellers considered and plotted in Figure 5.10 along with the thrust required curves in steady-level flight. Note that the 9.5x6 propeller provides greater static thrust, but takeoff is not a driving constraint, as described previously.

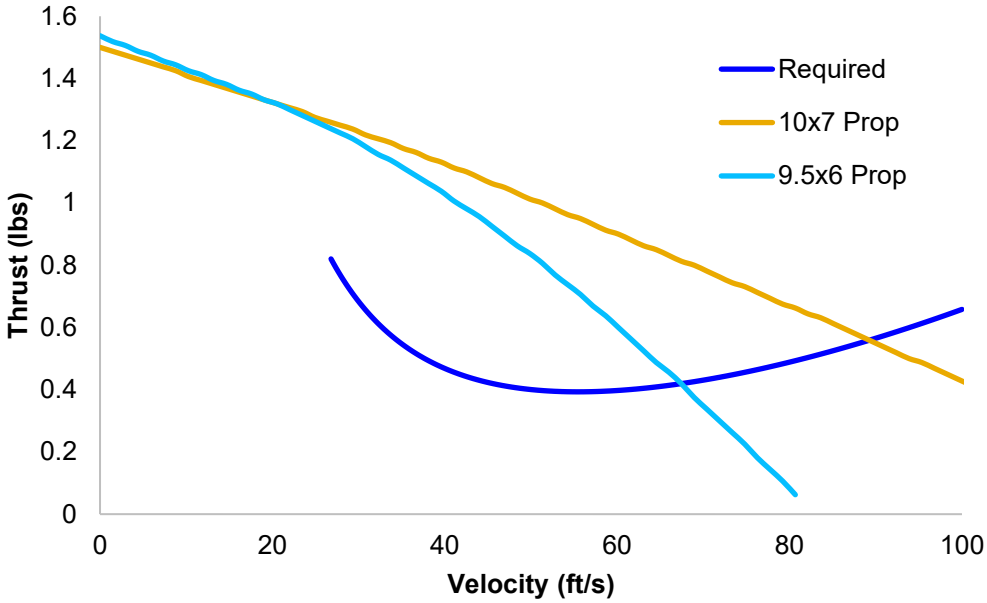

Figure 5.10: Thrust available and thrust required versus velocity

5.5.2 Mission Performance

The final mission performance of the aircraft was estimated using the mission model described in Section 4.3. The lap time estimation was computed by combining aerodynamic analysis, power and current characteristics from MotoCalc, and the physical model of the mission. Figure 5.11 displays the projected first lap trajectories for each mission with an initial ramp-up following takeoff and dips in velocity occurring at the turns. The remaining laps for Missions 1 and 2 are faster because takeoff is not included.

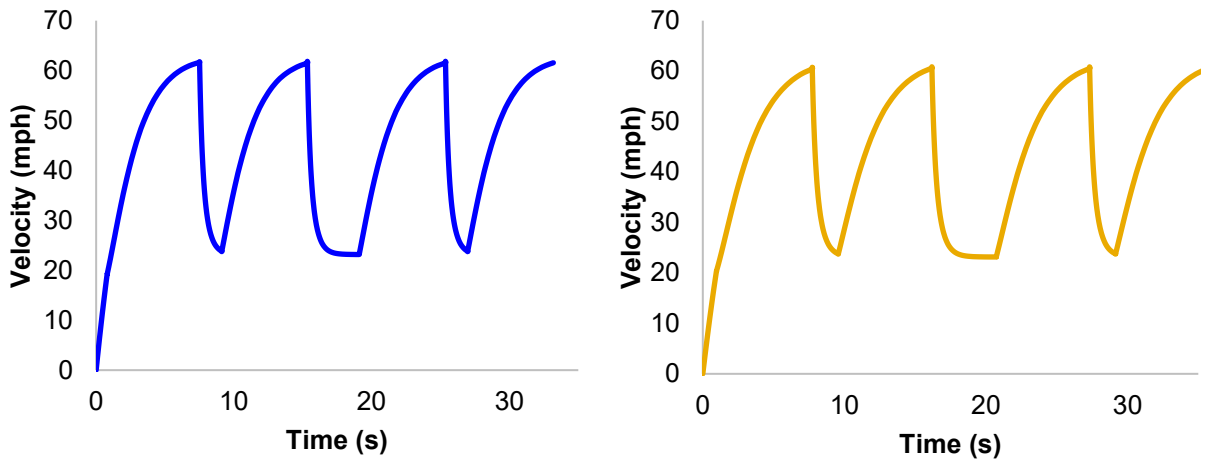

Figure 5.11: Simulation of lap trajectories for M1 (left) and M2/M3 (right)

Table 5.5 shows the resulting estimated performance for each of the three missions with the selected propellers. The table also includes preliminary scoring estimates based on the updated analysis. Due to the fact the missions 2 and 3 are scaled by the results of the highest scoring team, the values in the table are only preliminary scores. If the highest scoring team carries many more passengers than Trilobuzz, as expected, then the scaled part of the mission score will approach zero. The estimated scaled mission score is also shown in Table 5.5.

Table 5.5: Aircraft mission performance parameters

Mission Parameter	Mission 1	Mission 2	Mission 3
W/S (psf)	0.878	0.989	0.989
Propeller Selection	10x7	10x7	10x7
Max Current (Amp)	25	25	25
Static Thrust (lbs)	1.5	1.5	1.5
1st Lap Time (sec)	33.19	35.76	35.76
Mission Performance	3 laps in 5 minutes	3 laps in 5 minutes	1 lap in 10 minutes
Mission Score	1.0	0.0479	2.00003
RAC	14.01	14.01	14.01

5.6 Drawing Package

The following four pages illustrate the detailed CAD of the *Trilobuzz* system. The first sheet contains the three-view diagram with relevant dimensions. The second and third sheets show the structural arrangement of all major components and the systems layout. The fourth sheet displays the payload arrangements for both aircraft.

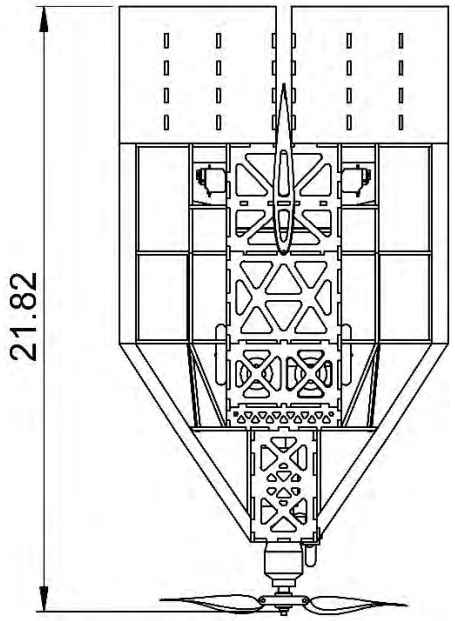

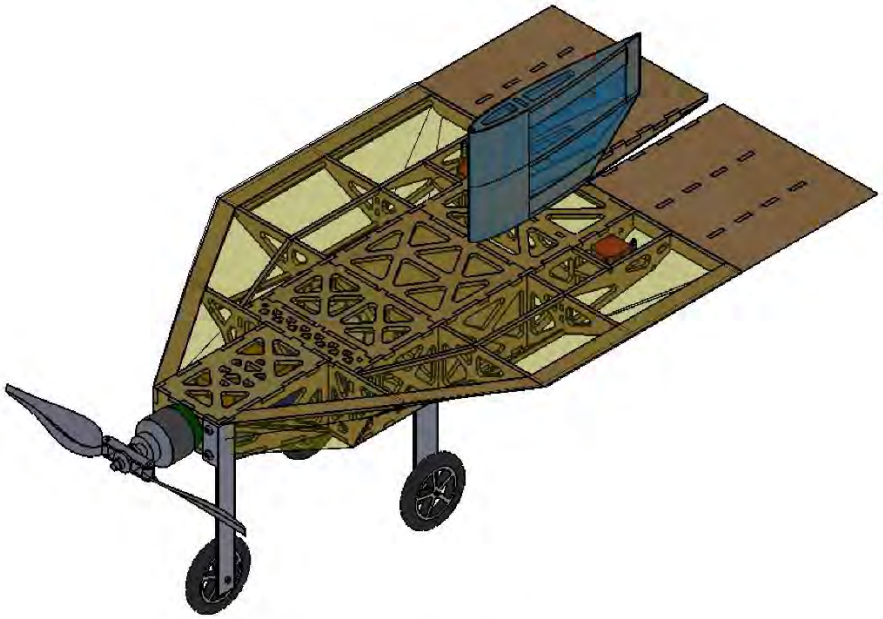

Isometric Scale 1:5

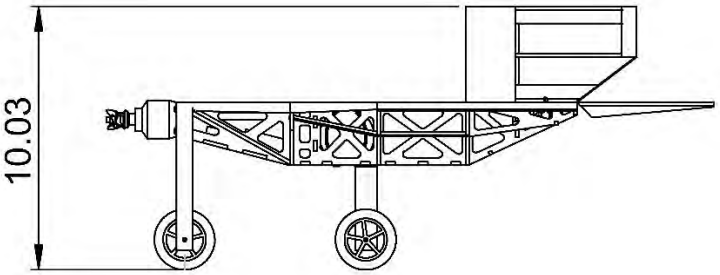

2/20/2018	**Georgia Institute of Technology**	
Drawn by: Daniel Sagan	Trilobuzz	
Checked by: Mitchell Hastings	Size **A**	Aircraft Three-view with Dimensions
Scale 1:7	All Dimensions in inches	Sheet 1 of 4

SOLIDWORKS Educational Product. For Instructional Use Only.

Parts List			
Item No.	Item Name	Qty.	Description
1	Wing/Airframe	1	Balsa
2	Vertical Stabilizer	1	Balsa
3	Elevons	2	Balsa
4	Main Gear	1	Aluminum
5	Nose Gear	1	Aluminum
6	Motor Mount	1	Plywood
7	Passenger Seating Plate	1	Plywood
8	Removable Servo Mount	2	Balsa
9	Electronics Access Panel	1	Plywood
10	Passenger Access Panel	1	Balsa
11	Payload Access Panel	1	Balsa

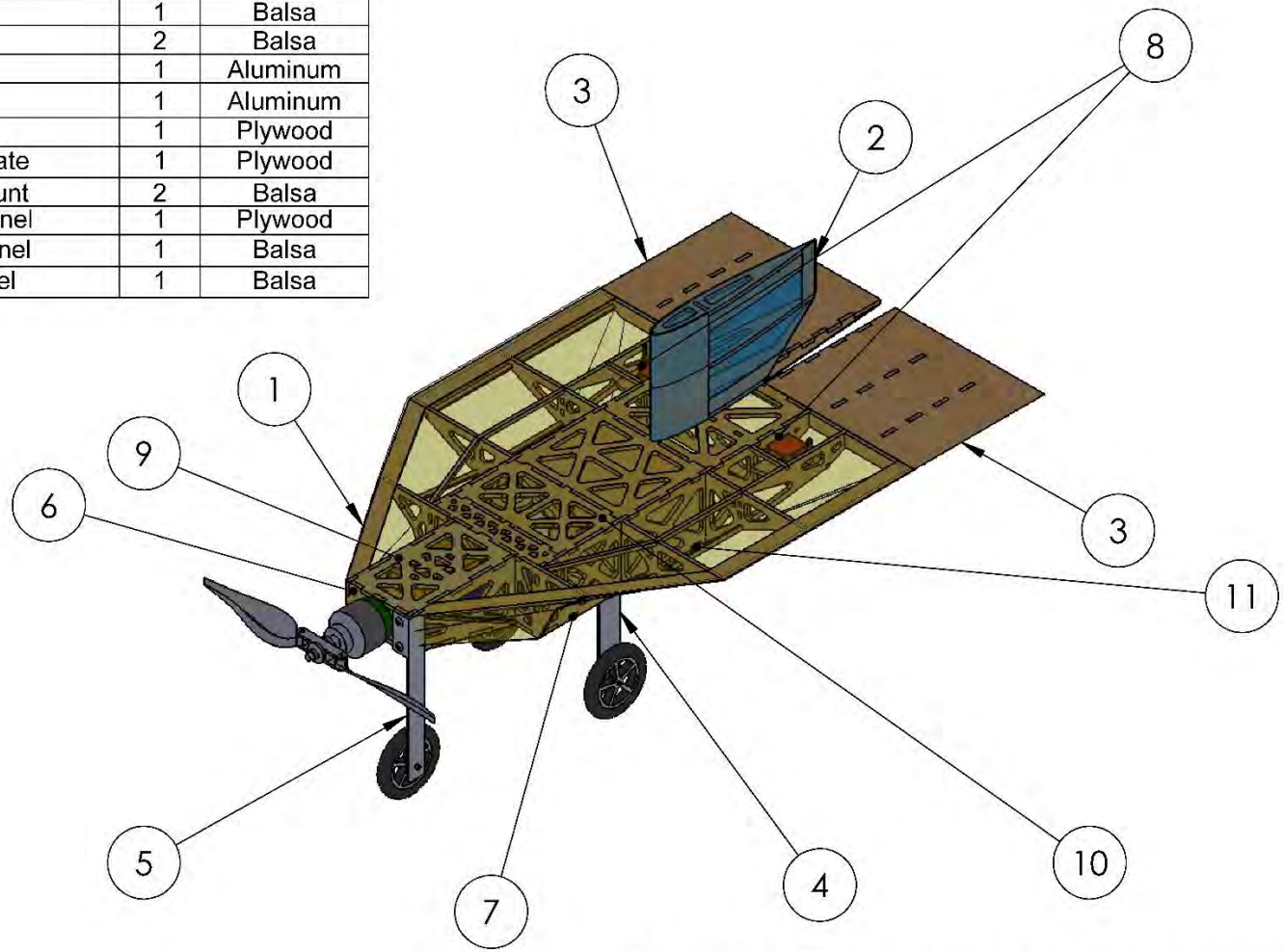

2/20/2018	**Georgia Institute of Technology**	
Drawn by: Daniel Sagan	Trilobuzz	
Checked by: Mitchell Hastings	Size **A**	Aircraft Three-view with Dimensions
Scale 1:5	All Dimensions in inches	Sheet 2 of 4

SOLIDWORKS Educational Product. For Instructional Use Only.

Systems List			
Item No.	Item Name	Qty.	Description
1	Propeller	1	Aeronaut 10 x 7
2	Motor	1	Cobra C-2217/12 1550 Kv
3	Speed Controller	1	Thunderbird 36
4	Receiver	1	OrangeRx GA7003XS
5	Elevon Servos	2	Futaba 3114
6	Main Battery Pack	1	Maxxpacks E1506S-3
7	Reciever Battery Pack	1	NiMh 4 Cell
8	Passenger Seating	1	Rubber bands and Plywood
9	Nose Landing Gear	1	Aluminum
10	Rear Landing Gear	1	Aluminum

Monokote removed for better view

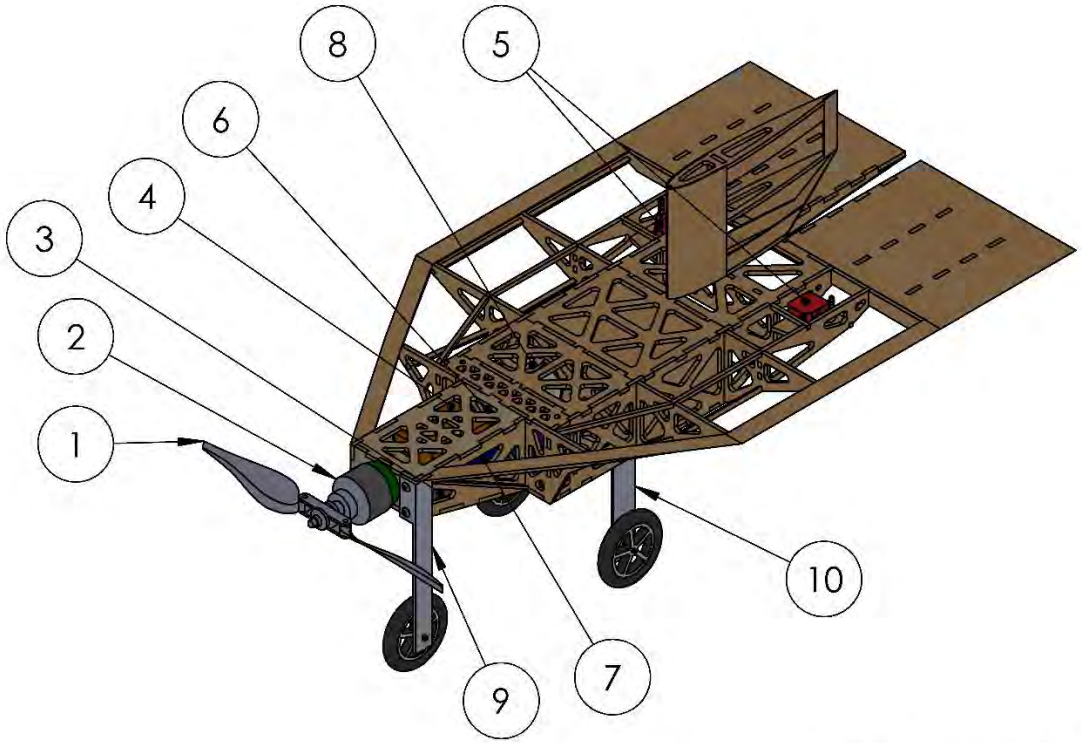

2/20/2018	**Georgia Institute of Technology**	
Drawn by: Daniel Sagan	Trilobuzz	
Checked by: Mitchell Hastings	Size **A**	Aircraft Three-view with Dimensions
Scale 1:5	All Dimensions in inches	Sheet 3 of 4

SOLIDWORKS Educational Product. For Instructional Use Only.

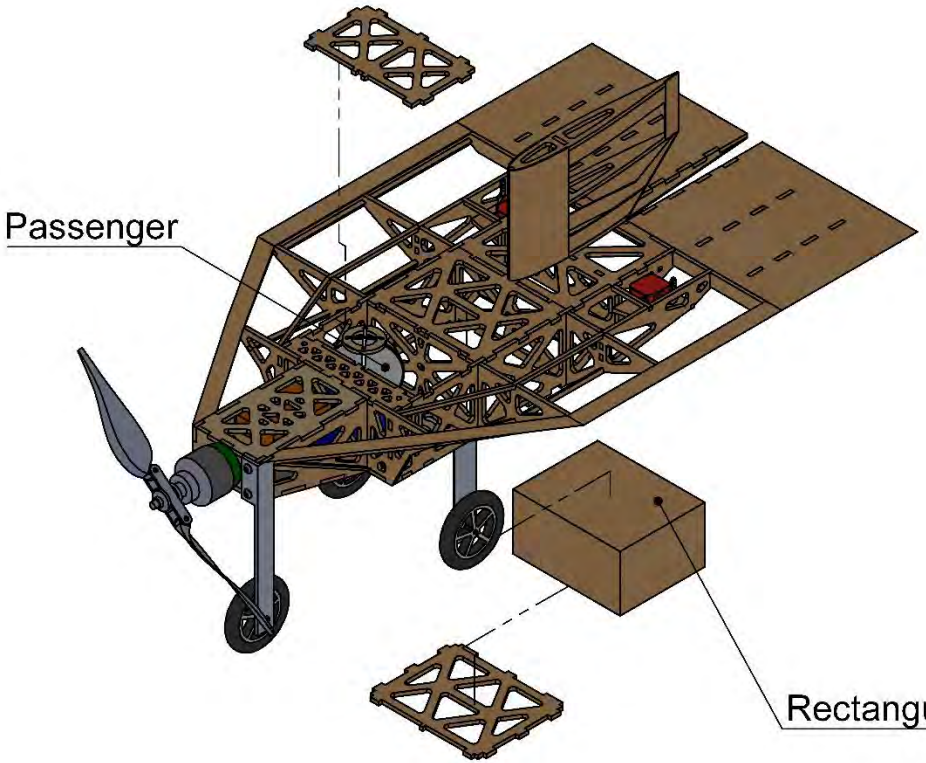

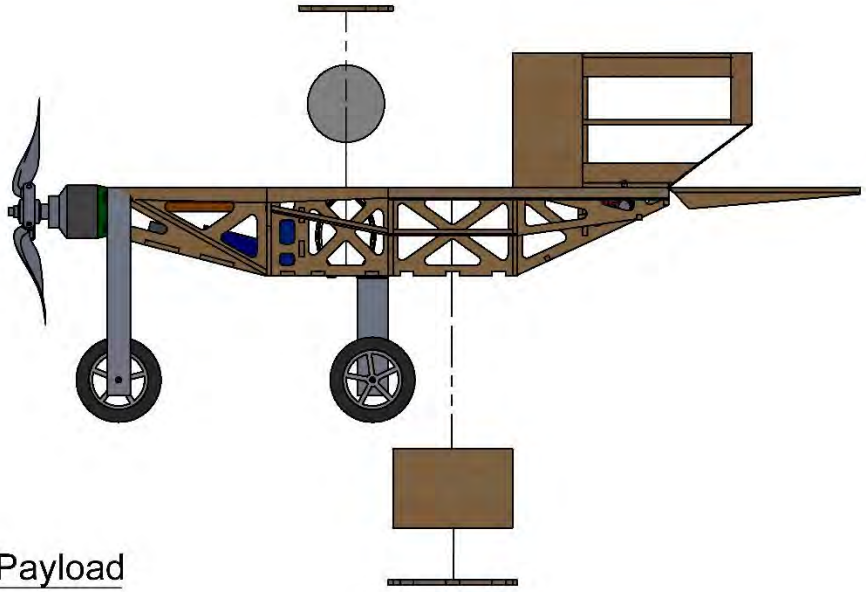

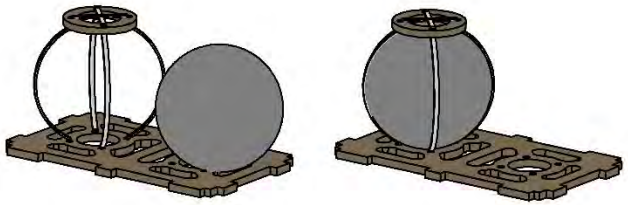

Passenger is inserted horizontally into seat
Scale 1:3

2/20/2018	**Georgia Institute of Technology**	
Drawn by: Daniel Sagan	Trilobuzz	
Checked by: Mitchell Hastings	Size **A**	Aircraft Three-view with Dimensions
Scale 1:5	All Dimensions in inches	Sheet 4 of 4

SOLIDWORKS Educational Product. For Instructional Use Only.

6 MANUFACTURING

The team considered various manufacturing processes and materials to build the aircraft. The manufacturing process selected represented the best combination of weight, reparability, speed of manufacturing, team experience with the process, and cost.

6.1 Processes Investigated

The team had a wealth of experience using the built-up balsa wood manufacturing technique. However, there were other viable manufacturing processes that could be superior. These processes were considered and qualitatively compared to the built-up balsa technique using Figures of Merit, detailed below and summarized in Table 6.1.

Weight: As with conceptual design, weight was still the most important factor for any design decision and was assigned a FOM of 5.

Reparability: Crashing is an inevitable part of the testing process so the ability to quickly repair an aircraft must be accounted for and was assigned a FOM of 2.

Ease of Manufacture: The ability to quickly produce aircraft to specification is critical for rapid prototyping to meet expected performance. It is directly related to Ease of Manufacture and was therefore assigned a FOM of 3.

Experience: The team's knowledge was given some weighting because it relates to the ability of team members to produce quality results, as well as to refine existing techniques. However, since the team is always willing to learn new techniques, experience was only assigned a FOM of 2.

Cost: Keeping in mind that the team had limited resources, cost was added as a FOM. However, since the team emphasizes winning above all, cost was assigned a FOM of 1.

Table 6.1: Manufacturing FOM Weighting

Figure of Merit	0	1	2	3	4	5
Weight						5
Ease of Manufacture				3		
Reparability			2			
Experience			2			
Cost		1				

These Figures of Merit were used to investigate the manufacturing processes and materials common to remote control aircraft construction. The processes to manufacture the airframe were investigated in detail below.

Built-up Balsa: Pieces made of competition grade balsa wood are laser cut from CAD models and glued together using cyanoacrylate (CA) adhesive to form the airframe and the tail surfaces of the aircraft. Plywood is used in key areas when required. The aircraft components are then covered with Monokote heat shrink film.

Fiber Reinforced Plastic (FRP): Foam molds are created based on the outer-mold line of the aircraft. A fiberglass-epoxy layup or carbon fiber-epoxy layup is then made within a vacuum bag, and the system sealed for 24 hours to allow for a full cure. The molds are then removed and the reinforced plastic acts as the primary structure.

3D Printed ABS: CAD models are printed using professional grade 3D printers. Print time increases proportionally with the volume of the aircraft.

Foam Core Composite: Large blocks of foam are cut with a hot-wire or CNC router to form the basic shape of the aircraft. Structural reinforcements are locally added if needed, and the entire foam-core is coated in fiberglass or carbon fiber, adding strength as a monocoque.

The processes were evaluated against each other by assigning each one a FOM score, with a score of five indicating a superior choice, three an average choice, and one equaling an inferior choice. All methods were assumed to result in an aircraft designed for an identical load. The results of the comparison are summarized in Table 6.2.

Table 6.2: Example airframe manufacturing process selection

		Manufacturing Process			
FOM	**Value**	**Built-up Balsa**	**Fiberglass**	**3D Printing**	**Foam Core Composites**
Weight	**5**	5	4	2	3
Ease of Manufacture	**3**	3	2	4	3
Reparability	**2**	3	4	1	1
Experience	**2**	5	2	4	3
Cost	**1**	5	3	2	3
Total	13	55	41	34	35

Based on the Figures of Merit, built-up balsa was considered the best method for the major airframe and empennage structure. However, the team determined that different elements of the design could use different manufacturing processes to create a more harmonious whole.

6.2 Processes Selected

The team used the above comparison to optimize the built-up balsa and ply technique to achieve the most competitive aircraft by having the lightest structure possible in accordance with competition rules without sacrificing structural integrity. Of the many ways to apply built-up balsa and ply, the team chose specific techniques and materials that would minimize the aircraft structural weight without compromising its strength. These strategies are as follows.

Selective Material Use: Since wood can vary significantly in density and strength, the team sorted its entire stock of balsa and ply by weight. The lightest pieces were selected for construction and were cut using the team's laser cutter, with the lightest of the cut parts reserved for the final competition aircraft.

Local Reinforcements: Due to the very low density of balsa used, several inherently problematic locations could potentially fracture during normal operations. Rather than compensate by over-building the entire aircraft, these locations were reinforced with composite or additional balsa, increasing strength with minimal penalty in weight.

Lightening Holes: An efficient structural design eliminated significant loading from most structural members. Lightening holes were integrated into the airframe to reduce weight without reducing the overall stiffness and strength of the aircraft.

Covering: The aircraft was coated with a heat shrink adhesive infused plastic covering material called Monokote.

Nylon Carbon-fiber: Rip stop nylon was chosen for reinforcement to provide torsional stiffness to the control surfaces.

6.2.1 Airframe Structure

The airframe was constructed using the balsa build-up method to minimize weight. Jigsaw-like parts were laser cut, fit together, and bonded with cyanoacrylate (CA). The center plate was made using ply as it was determined that using a balsa sheet for this part would compromise the structural integrity of the plane. Additional balsa sheeting and sticks were cut and bonded on to reinforce and complete the structure.

Figure 6.1: Airframe during construction

6.2.2 Control Surfaces and Vertical Tail

The control surfaces and vertical tail were constructed using the balsa build up method to minimize weight. Ribs and spars were laser cut with fitting slots. Carbon-fiber tow was applied in a cross pattern on one side for a lightweight solution to stiffen the control surface.

6.2.3 Rapid Prototyping

Due to the small size of the aircraft and delicateness of materials used, it was determined that it would be more beneficial to continuously manufacture prototypes rather than attempting to test and constantly repair a single aircraft. Manufacturing techniques were refined, and manufacturing duties were assigned to individuals to develop specialization and ensure the most efficient production possible. This allowed for multiple aircraft modifications to be tested individually in a short period of time. After design considerations

were finalized, a rate of production of one aircraft every 1 to 2 weeks was achieved. Expensive parts such as servos, motors, and landing gear were salvaged from previous prototypes for use in the next iteration.

Figure 6.2: Multiple prototype aircraft before a flight test

6.3 Manufacturing Milestones

A Gantt chart containing manufacturing milestones was established prior to initial prototype manufacturing to ensure a logical, consistent order was followed during construction. Progress was recorded and monitored by the team leader to ensure all major milestones were met. The Gantt chart is shown in Figure 6.3, capturing the planned and actual timing of manufacturing steps. The team constructed many prototypes, so Figure 6.3 describes the typical manufacturing timeline for a single aircraft.

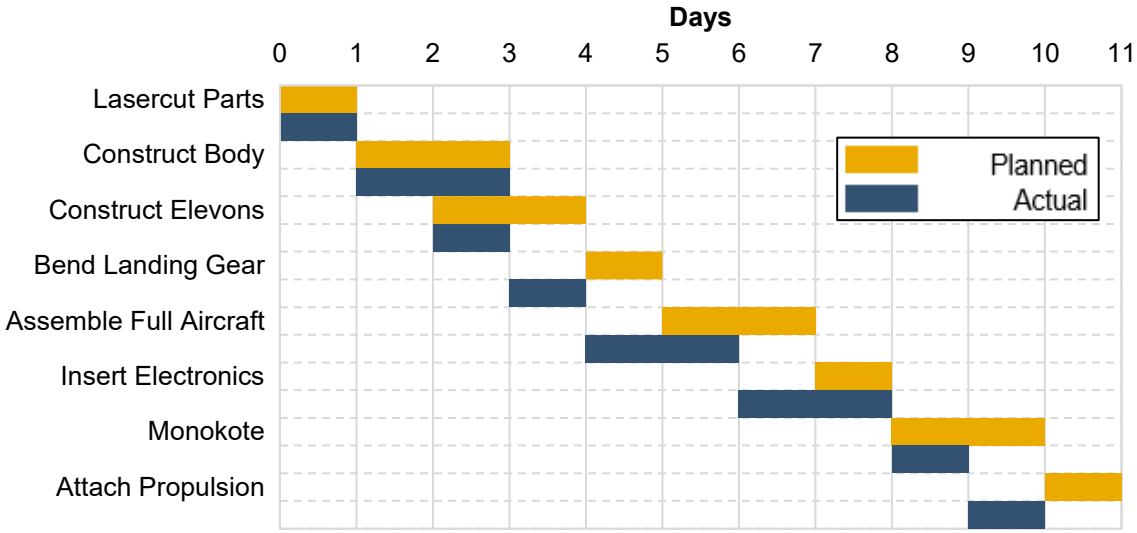

Figure 6.3: Aircraft manufacturing milestone chart showing planned and actual timing of objectives

7 TESTING PLAN

A plan for an extensive testing campaign to validate the aircraft, and its components, was created to determine what configurations would be the most capable. Testing culminates in test flying a full round of competition flights on the final competition airframe.

7.1 Objectives and Schedule

The testing was broken up into three main categories: propulsion, structures, and performance. The propulsion and structures subsystems were tested before flying the whole aircraft to gain knowledge and set realistic and useful objectives at each test flight. A breakdown of the testing schedule is displayed in the following Gantt chart, shown in Figure 7.1.

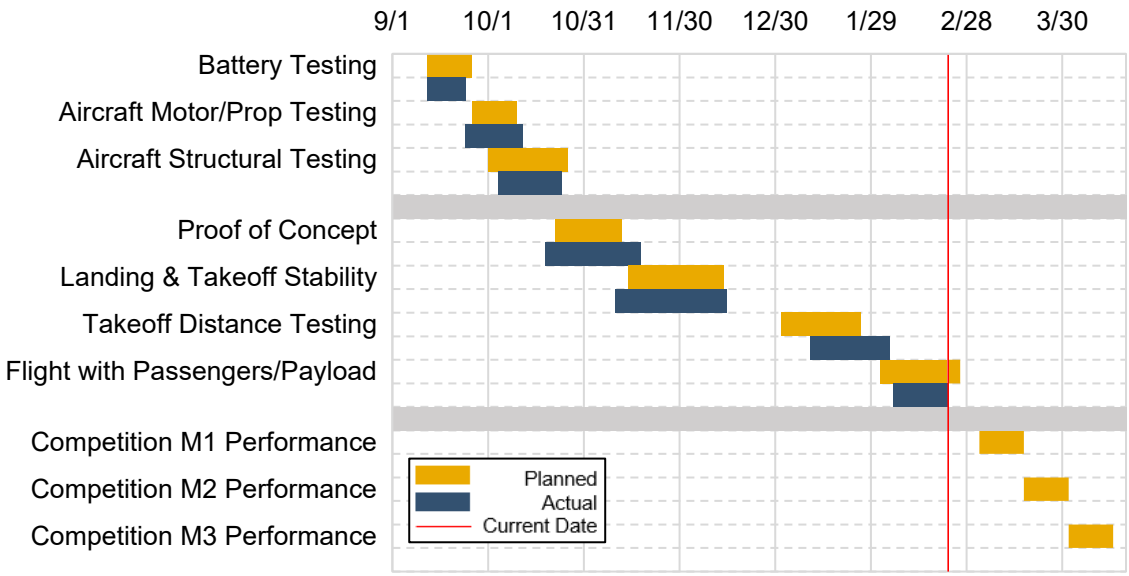

Figure 7.1: Aircraft and subsystem testing milestone chart with planned and actual timing of objectives

The objectives for the propulsion testing were to determine which motors would work best for the aircraft. The motors and propellers tested were based on MotoCalc predictions as expressed in Section 4.2.2. Thrust versus velocity for vehicle performance and power draw for motor performance for each motor propeller combination were determined using measurements of thrust, torque, RPM, voltage, and current draw. Using data obtained from testing, the team was able to compare the actual performance of the motors to the MotoCalc predictions in order to gather a better estimate of actual performance. This information allowed the team to select the best propulsion system to achieve the best score possible.

A rig that included load cells to calculate thrust and torque as well as an electric motor measurement system was constructed as shown in Figure 7.2. The team used the rig to perform static thrust tests and used the data to compare it with MotoCalc predictions. The electric motor parameters were monitored with an

EagleTree system that records the RPM, voltage, and current draw of the motor. Custom written software was used to collect the torque and thrust values as well as to remotely control the motor for 30-second intervals with 10-second full thrust intervals and 10-second acceleration and deceleration intervals. The results of the static thrust tests are described in Section 8.1.1.

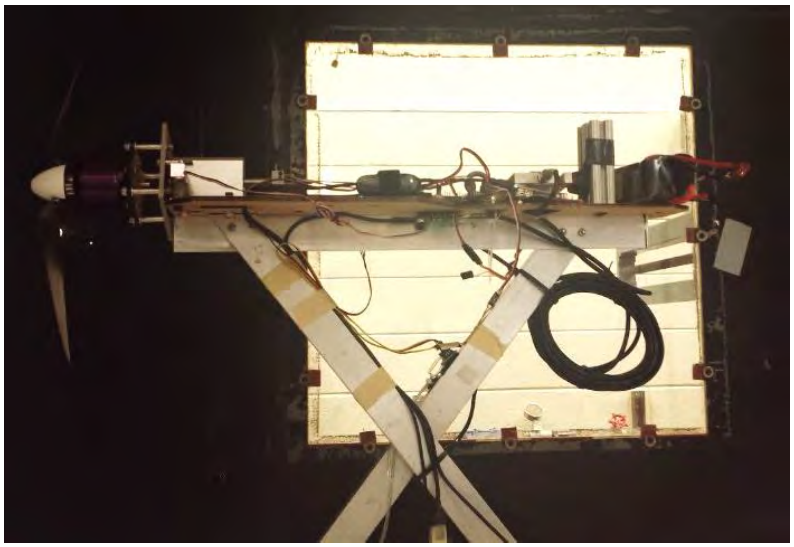

Figure 7.2: Thrust test rig

7.2 Structural Testing

Wingtip tests were conducted to validate the structural integrity of the design. A wingtip test simulates the maximum loading the wings would experience in flight by loading the payload bay with the maximum weight and lifting the plane by the wing tip, which simulates a root bending moment of 2.5g. Figure 8.3 shows wingtip test being performed. A team member holds the aircraft at the forward most point where the wing span is maximum. Since the wing planform is a delta wing, its center of gravity is far forward of this point and so if the plane is simply held up there it would tip over forwards. Therefore, the team member must additionally apply a torque to keep the aircraft level.

LRU testing was performed by simulating the individual Ground Mission stages with two crew members and a timer. The crew members conducted the test multiple times for each LRU, verifying that the designed method of replacement was sufficient for competition.

7.3 Flight Testing

Flight testing was conducted across many iterations, with a final aircraft planned as the competition design. Initial iterations were used to determine the flying qualities of the aircraft designs. After this step, the structural layout was verified through simulated mission flights. These test results then were used to determine necessary design modifications.

Intermediate iterations are currently being used as testing platforms, with changes being implemented based on feedback from assembly teams and the pilot. These include increasing the main landing gear width to prevent tip-over during harsh landings, wing sizing modifications to increase roll stability, and increasing vertical stabilizer aspect ratio to improve effectiveness.

The current iteration of *Trilobuzz* is being used to verify the required battery size to complete M3. Experience and data gained from all iterations will be used to generate a final design that will go to competition. The final iteration will fly simulations of the flight missions to verify and validate the aircraft's capabilities.

7.4 Checklists

Various tests have specific procedures which must be followed accurately to produce the desired objectives and ensure safety. This section lists the checklists utilized by *Trilobuzz* while conducting tests that required a significant number of steps, such as propulsion and flight testing.

7.4.1 Propulsion Test Checklist

The checklist in Table 7.1 was created to ensure safety while dealing with propellers and electrical equipment, and to make sure the test is not wasted due to some mistake in preparation. This checklist was used in the testing of all motor, battery, and propeller combinations.

Table 7.1: Propulsion testing checklist

Propulsion Test Checklist					
1. Propeller secured?	☐	2. Motor mount secured?	☐	3. All plugs secured?	☐
4. Batteries peaked?	☐	5. Throttle down?	☐	6. Data system on?	☐
7. Custom code running?	☐	8. All clear of testing rig?	☐		

7.4.2 Flight Test Checklist

The checklist in Table 7.2 was created with the important goal of preventing any system from malfunctioning in mid-air, which could lead to the aircraft crashing; its thorough execution is paramount to the team's success, and it will be used at the DBF event as well.

Table 7.2: Pre-flight checklist

General System Checks					
Structural Integrity			Time		Date
Center of Gravity Location					
X			Y		
Payload			**Passengers**		
Laterally Secure?			Laterally Secure?		
Longitudinally Secure?			Longitudinally Secure?		
Bay Door Secure?			Bay Door Secure?		
Control Surfaces					
Left Elevon			Right Elevon		
Deflects?	Glued?	Slop?	Deflects?	Glued?	Slop?
Electronics and Propulsion					
Receiver Battery Charged?		Receiver Battery Secure?		Wires Secure?	
Primary Battery Charged?		Primary Battery Hot?		Primary Battery Secure?	
Receiver/Transmitter GO?		Prop Secure?		Prop Direction?	
Weather					
V_{wind}		Θ_{wind}		Temperature	
Initials for Approval					
Chief Engineer		Pilot		Advisor	

8 PERFORMANCE RESULTS

8.1 Component and Subsystem Performance

8.1.1 Propulsion

Batteries: A 6-cell, 1500 mAh NiMH battery pack was discharged at 5 amps (3.3 times its capacity) and at 15 amps (10 times its capacity) to characterize the discharge capabilities of the NiMH batteries. The resulting data is shown in Figure 8.1 on a per cell basis. NiMH battery cells have a nominal voltage of 1.2V, and the 5-amp discharge curve can maintain this voltage. At 15 amps, the cell voltage continuously drops, resulting in a small decrease in the available effective power. The higher current draw of the 15-amp discharge is necessary to achieve the power required for the aircraft.

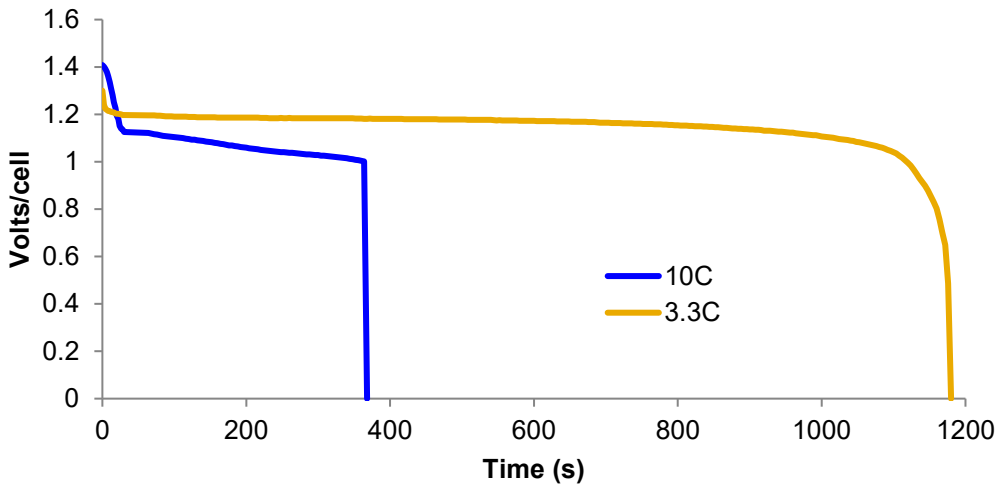

Figure 8.1: Battery discharge rates

Motors and Propellers: Using MotoCalc software, several motor and propeller combinations were theoretically computed. The Scorpion SII-2212-18 and Cobra 2217-12 motors provided the best combination of thrust and performance at different aircraft velocities, as well as a realistic current draw to reduce the size of the battery pack. The team tested the motors and propellers using the test stand shown in Section 7.1 in static conditions. Figure 8.2 shows the difference between the experimental and theoretical results predicted by the MotoCalc program for the best two propellers per engine with regards to their thrust. The Cobra 2217-12 with a 10x7 propeller was selected based on its superior thrust output.

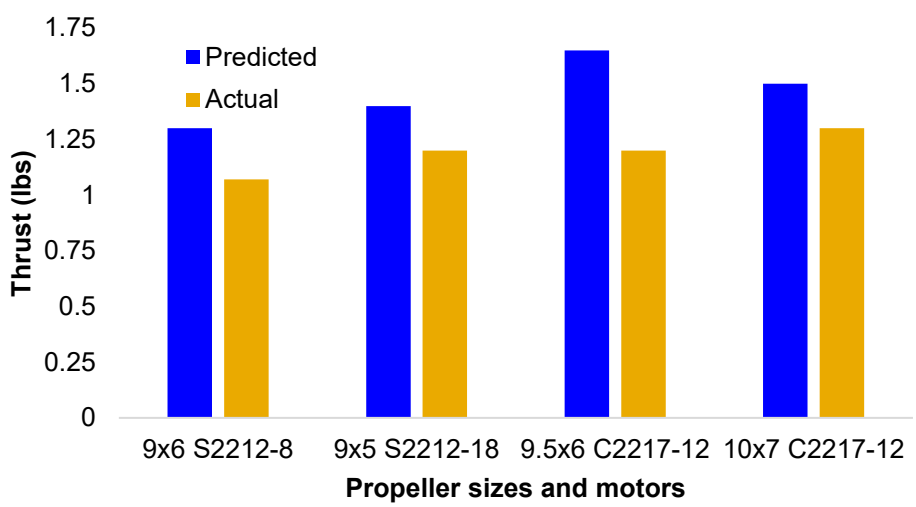

Figure 8.2: Predicted thrust versus actual thrust for different propellers

8.1.2 Structural Tests

Wing Testing Results: The full-size airplane was subjected to the required wing tip testing specified in the rules as part of the technical inspection process. This was done by loading the passenger and payload and then lifting the airplane by the wing tips. Figure 8.3 shows the successful wingtip test.

Figure 8.3: Wingtip test

Line-Replaceable Units: All required LRU replacements necessary for the Ground Mission were tested and timed. Based on the results, any combination of Stage 1 and Stage 2 LRUs can be replaced within the prescribed mission time with time to spare in the event a replacement takes longer than anticipated at competition.

Table 8.1: LRU replacement times

Stage 1 LRU	Replacement Time (s)	Stage 2 LRU	Replacement Time (s)
Servo	57	ESC	31
Rx Battery	14	Left Elevon	116
Main Battery	28	Right Elevon	116
Servo pushrod	25	Rx-Receiver	44
Landing Gear wheel	75	Main Landing Gear	132
Propeller	26	Motor	85

8.2 System Performance

Flight tests of *Trilobuzz* were performed to evaluate the performance of the aircraft and validate performance predictions. To this end, the team equipped the aircraft with a data collection system that could be used to compare to the estimated mission performance in Section 4.6. The team purpose-built an Arduino-based telemetry system with a live data feed. On a number of test flights, the Arduino was mounted to the aircraft and recorded GPS at 1 Hz to yield trajectory data. An example of a full lap trajectory is displayed in Figure 8.6 superimposed on satellite imagery using Google Earth.

Figure 8.4: Trajectory of aircraft during competition laps from GPS data

The results of flight testing are shown in Table 8.2. They indicate the performance predictions were optimistic. Further optimization and increasing pilot familiarity with the system should improve system performance to meet or exceed the predicted performance.

Table 8.2: Comparison of predicted and actual performance averages

	1st Lap Time (s)		Time for 360 (s)		Laps Flown		Max. Speed (mph)	
	Pred.	**Act.**	**Pred.**	**Act.**	**Pred.**	**Act.**	**Pred.**	**Act.**
M1	33.19	31	3.93	3.5	3	3	61.85	55
M2/M3	35.76	33	4.61	3.9	3	3	60.86	54

The lap times and metrics for M1 and M2/M3 shown in Table 8.2 match well between the predicted and tested values. The flight test data does not match perfectly, however; *Trilobuzz* consistently performed better than expected. These differences can be explained by the uncertainties in the predictions as described in Section 4.3.2. Namely, the mathematical models lack a vertical dimension and any wind model. When turning, the model assumes the aircraft will drop speed to maintain altitude, an assumption that appears to correspond well with the flight test data. The offset for when the turns are initiated can be explained by pilot response to changes in wind direction. Predicted and actual times for a 360-degree turn are fairly variable, again due to pilot behavior. In all cases, time for a 360-degree turn was predicted assuming maximum velocity. However, during testing, the pilot tended to reduce speed significantly when going into a turn, which reduced the turn radius. Regardless, the turning performance obtained from the test data exists within the envelope predicted by the simulations, verifying that the aircraft is operating as expected by its design.

In conclusion, the concept of a low aspect ratio, clipped delta wing design allows for a compact form factor and empty weight that minimized RAC. In combination with the optimal propulsion system and internal store layout, the design optimizes TMS over RAC, resulting in maximum overall score. The research, component selection, and testing that fed into the design process resulted in a lightweight aircraft capable of successfully flying all three missions.

9 BIBLIOGRAPHY

[1] Anderson, J. D., *Fundamentals of Aerodynamics,* 4th ed., McGraw Hill, 2004.

[2] Tosti, L. P., "Low-speed static stability and damping-in-roll characteristics of some swept and unswept low-aspect-ratio wings," NACA-TN-1468*,* October 1947.

[3] Drela, M., and Youngren, H., "AVL Overview", *Massachusetts Institute of Technology* [online]*,* 2008, http://web.mit.edu/drela/Public/web/avl/. [retrieved 21 February 2018],

[4] Edward, L. C., "VORSTAB – A computer program for calculating lateral-directional stability derivatives with vortex flow effect," NASA-CR-172501, January 1985.

[5] Polhamus, E. C., "A concept of the vortex lift of sharp-edge delta wings based on a leading-edge-suction analogy*"*, NASA-TN-D-3767, December 1966.

[6] Miranda, L. R., Elliot, R. D., and Baker, W. M., "A generalized vortex lattice method for subsonic and supersonic flow applications," NASA-CR-2865, December 1977.

[7] Lamar, J. E. "Extension of leading-edge-suction analogy to wings with separated flow around the side edges at subsonic speeds," NASA-TR-R-428, October 1974.

[8] Hoerner, S. F., *Fluid Dynamic Drag*, 2nd ed., Published by author, 1992.

[9] Phillips, W. F., *Mechanics of Flight*, 1st ed., Wiley, Hoboken, NJ, 2004.